DECEMBER 1, 1989

Analytical CHEMISTRY

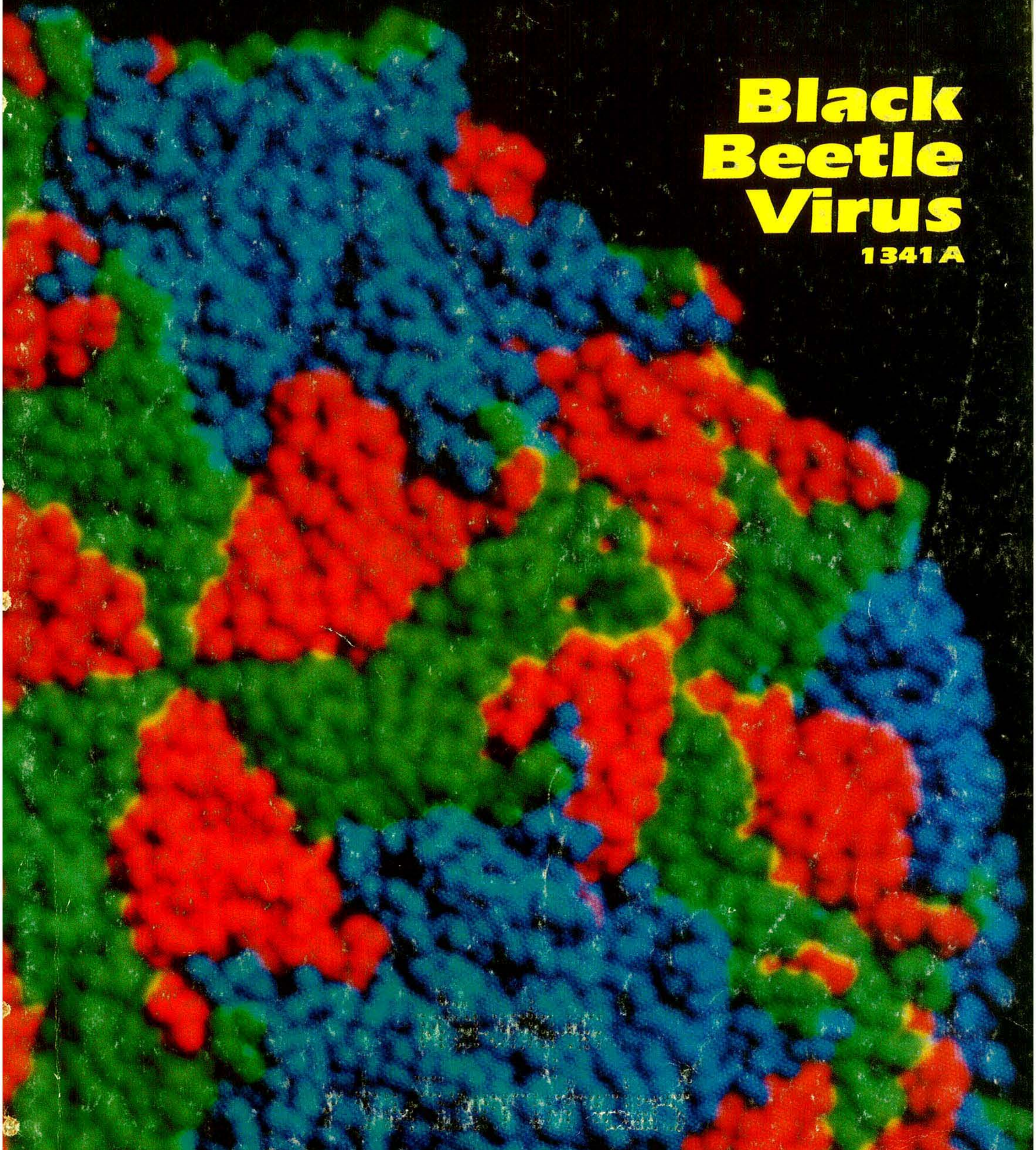

Black Beetle Virus

1341 A

We Take Great Ideas… & Make Them Even Better.™

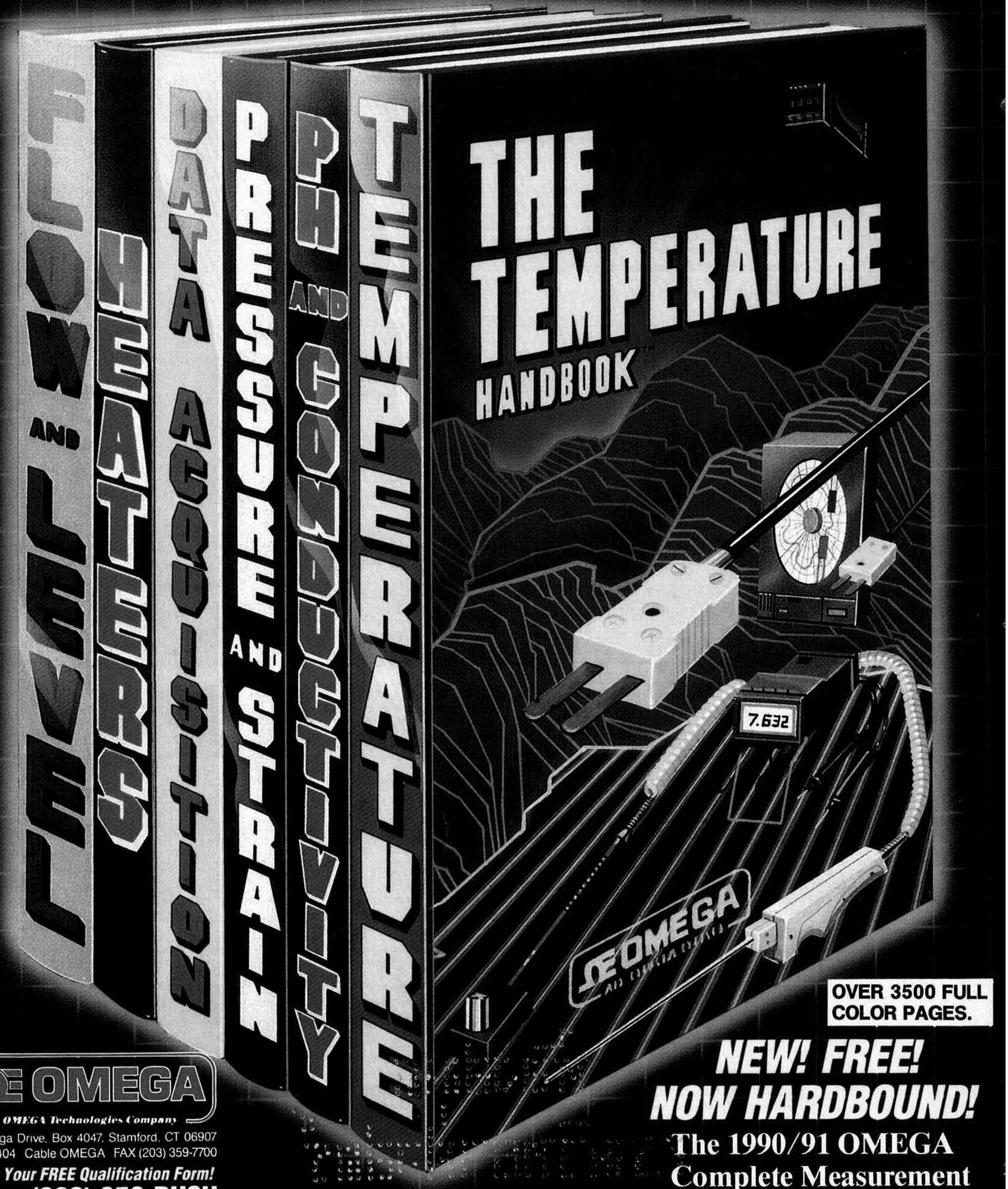
FLOW AND LEVEL
HEATERS
DATA ACQUISITION
PRESSURE AND STRAIN
PH AND CONDUCTIVITY
TEMPERATURE
THE TEMPERATURE HANDBOOK™
7.632
OMEGA

OVER 3500 FULL COLOR PAGES.

NEW! FREE! NOW HARDBOUND!

The 1990/91 OMEGA Complete Measurement and Control Handbooks & Encyclopedias®

OMEGA®

An OMEGA Technologies Company

One Omega Drive, Box 4047, Stamford, CT 06907
Telex 996404 Cable OMEGA FAX (203) 359-7700

Ask For Your FREE Qualification Form!

DIAL (203) 359-RUSH
(203) 359-7874

COPYRIGHT 1989, OMEGA ENGINEERING, INC., ALL RIGHTS RESERVED

CIRCLE 120 ON READER SERVICE CARD

Finally, a real GC/MS for under $50,000!

HP 5890 Series II GC sets new industry standards with high temperature operation, cool-on-column injection and pressure programming.

MS ChemStation (DOS series) is 386-based to provide speed and multi-tasking for highest lab productivity.

Sensitive, universal and specific, the HP 5971A MSD produces true EI spectra even from dirty, complex matrices.

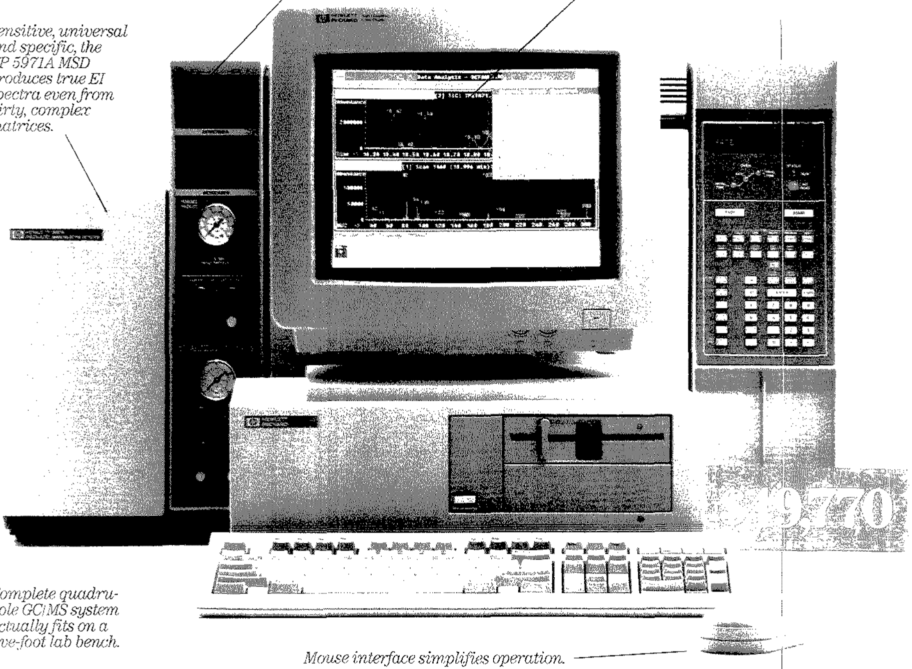

Complete quadrupole GC/MS system actually fits on a five-foot lab bench.

Mouse interface simplifies operation.

Now any lab can afford a GC/MS with an HP mass selective detector (MSD). Our new PC-controlled system costs only $49,770,* yet gives you high performance.

There's multitasking for acquiring and analyzing data simultaneously. There's true, classical EI spectra that stand up to challenge. There's Microsoft® Windows software for ease of use. Plus access to PC word processing, spreadsheets and desktop publishing. And for total automation, you can add an optional autosampler and bar-code reader.

Put the system to work in *any* size laboratory. Even network it to other vendors' data systems. Then enjoy the highest uptime in the industry because HP is consistently rated number 1 for reliability, service and support. For more, call **1 800 556-1234, Ext. 10218.** In CA, **1 800 441-2345, Ext. 10218.**

*U.S. list price.
Microsoft® is a U.S. registered trademark of Microsoft Corporation.

HEWLETT PACKARD

© 1989 The Hewlett-Packard Company
AG-04910

CIRCLE 65 ON READER SERVICE CARD

COMPARE FTIR PERFORMANCE & PRICE

Mattson's Galaxy 6020® FTIR System offers you more.

Proof that a better-run company can afford to develop innovative products and competitive prices.

Features & Capability	**Mattson 6020**	Perkin Elmer 1760	Nicolet 510	Nicolet 800	Digilab FTS-40
Cube Corner Interferometer	**Yes**	No	No	No	No
Modern User Interface including mouse	**Yes**	No	No	No	No
High Precision 96 bit FFT	**Yes**	No (32 Bit)	No (20 Bit)	No (20 Bit)	No (32 Bit)
Macros	**Yes**	?	Yes	Yes	?
Precision Scan Reference (quadrature)	**Yes**	Yes	No	Yes	No
Sealed Interferometer	**Yes**	Yes	No	No	No
19 Bit ADC	**Yes**	No (16 Bit)	?	No (18 Bit)	Yes
Multi-Component Quantitative Analysis	**Yes**	Yes	Yes	Yes	Yes
Sadtler Libraries	**Yes**	Yes	No	No	Yes
MS-DOS Compatibility †	**Yes**	Third Party	No	No	No
UNIX Compatibility †	**Yes**	No	No	No	Third Party
Macintosh Compatibility †	**Yes**	No	No	No	No
Price	**$27,000**	$45,000*	$30,000*	$80,000*	$40,000*

* Product Comparisons are based on sales information and competitive bid situations. Prices and features may vary significantly with individual negotiations. Please contact vendors directly for more specific information.

† Compatibility meaning primary spectrometer control and data acquisition without intermediate data conversions or alternate operating systems.

See for yourself the extraordinary performance of the Mattson 6020 FTIR System. Call us for a demo. We'll have a Galaxy 6020 up and running in your lab in 5 minutes.

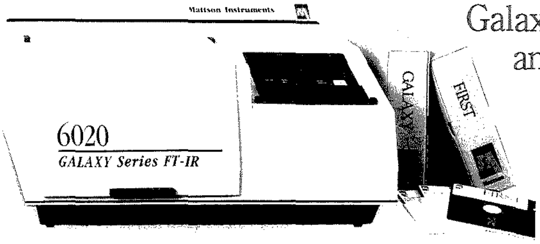

Mattson

Mattson Instruments, Inc.
1001 Fourier Drive
Madison, WI 53717 U.S.A.
Tel. (608) 831-5515
Fax: (608) 831-2093

Mattson Instruments, Ltd.
Green Farm Road
Newport Pagnell
Bucks MK16 0AL
England
Tel. (44) 908 211414
Fax: (44) 908 618292
Telex: 82304 FORUM G

CIRCLE 94 ON READER SERVICE CARD

DECEMBER 1, 1989
VOLUME 61
NUMBER 23

The Audit Bureau
ANCHAM
61(23) 1301A–1352A/2593–2688 (1989)
ISSN 0003-2700

Registered in U.S. Patent and Trademark Office; Copyright 1989 by the American Chemical Society

ANALYTICAL CHEMISTRY (ISSN 0003-2700) is published semimonthly by the American Chemical Society at 1155 16th St., N.W., Washington, DC 20036. Editorial offices are located at the same ACS address (202-872-4570; FAX 202-872-6325; TDD 202-872-8733). Second-class postage paid at Washington, DC, and additional mailing offices. Postmaster: Send address changes to ANALYTICAL CHEMISTRY Member & Subscriber Services, P.O. Box 3337, Columbus, OH 43210.

Claims for missing numbers will not be allowed if loss was due to failure of notice of change of address to be received in the time specified; if claim is dated (a) North America: more than 90 days beyond issue date, (b) all other foreign: more than one year beyond issue date, or if the reason given is "missing from files."

Copyright Permission: An individual may make a single reprographic copy of an article in this publication for personal use. Reprographic copying beyond that permitted by Section 107 or 108 of the U.S. Copyright Law is allowed, provided that the appropriate per-copy fee is paid through the Copyright Clearance Center, Inc., 27 Congress St., Salem, MA 01970. For reprint permission, write Copyright Administrator, Publications Division, ACS, 1155 16th St., N.W., Washington, DC 20036.

Registered names and trademarks, etc., used in this publication, even without specific indication thereof, are not to be considered unprotected by law.

Advertising Management: Centcom, Ltd., 500 Post Rd. East, Westport, CT 06880 (203-226-7131)

1989 subscription rates include air delivery outside the U.S., Canada, and Mexico

	1 yr	2 yr
Members		
Domestic	$ 27	$ 45
Canada and Mexico	56	103
Europe	83	157
All Other Countries	120	231
Nonmembers		
Domestic	49	83
Canada and Mexico	78	141
Europe	155	280
All Other Countries	192	354

Three-year and other rates contact: Member & Subscriber Services, ACS, P.O. Box 3337, Columbus, OH 43210 (614-447-3776 or 800-333-9511).

Subscription orders by phone may be charged to VISA, MasterCard, Barclay card, Access, or American Express. Call toll free 800-ACS-5558 in the continental United States; in the Washington, DC, metropolitan area and outside the continental United States, call 202-872-8065. Mail orders for new and renewal subscriptions should be sent with payment to the Business Management Division, ACS, P.O. Box 57136, West End Station, Washington, DC 20037.

Subscription service inquiries and changes of address (include both old and new addresses with ZIP code and *recent mailing label*) should be directed to the ACS Columbus address noted above. Please allow six weeks for change of address to become effective.

ACS membership information: Lorraine Bowlin (202-872-4567)

Single issues, current year, $7.00 except review issue and LabGuide, $12.00; **back issues and volumes and microform editions** available by single volume or back issue collection. For information or to order, call 800-ACS-5558 or write the Microform & Back Issues Office at the Washington address.

Nonmembers rates in Japan: Rates above do not apply to nonmember subscribers in Japan, who must enter subscription orders with Maruzen Company Ltd., 3-10 Nihonbashi 2-chome, Chuo-ku, Tokyo 103, Japan. Tel: (03) 272-7211.

Analytical Chemistry

REPORT **1315 A**

László Zechmeister. 1989 marks the centenary of the birth of László Zechmeister, one of the most important pioneers of classical column chromatography. Leslie S. Ettre of the Perkin-Elmer Corporation looks back on his life, activities, and scientific achievements

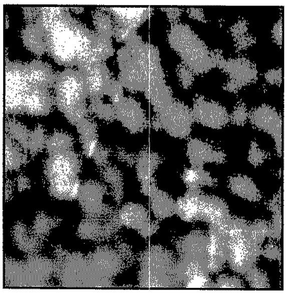

ANALYTICAL APPROACH **1341 A**

***On the cover.* Insect viruses** are well-defined systems for studying structural biology at near-atomic resolution. John E. Johnson and Jean-Pierre Wery of Purdue University discuss the X-ray structure of black beetle virus and how this information aids scientists in understanding the biochemistry of viruses

BRIEFS **1304 A**

EDITORIAL **1311 A**

SIMS VII. More than 400 researchers from academia, government, and industry gathered at the Seventh International Conference on Secondary Ion Mass Spectrometry in Monterey, CA, in September. Among the topics discussed were instrument development, applications to geology and metallurgy, the use of static SIMS to provide molecular information about polymer and biological surfaces, and imaging

NEWS **1313 A**

Nominations sought for 1991 **ACS awards.** ▶ Lloyd Snyder elected subdivision head

FOCUS **1329 A and 1333 A**

In **The First International Symposium on Field-Flow Fractionation** (p. 1329 A), researchers from around the world gathered this past summer in Park City, UT, to discuss new techniques and ideas in the developing area of FFF. Participant Sharon Kraus of Rohm and Haas highlights many of the presentations and discussions at this first-ever meeting of FFF experts. In **Surface Science in Analytical Chemistry** (p. 1333 A), Fred M. Hawkridge and Joseph A. Gardella, Jr., visiting scientists at NSF, recount the 42nd Annual Summer Symposium of the ACS Division of Analytical Chemistry, held July 23–26 at Virginia Tech

NEW PRODUCTS & MANUFACTURERS' LITERATURE **1336 A**

AUTHOR INDEX **2593**

BRIEFS

Articles

Amperometric Detection of Nonelectroactive Cations in Flow Systems at a Cupric Hexacyanoferrate Electrode 2594

Submicromolar levels of potassium and ammonium ions are determined indirectly by their ability to enhance the electroreduction of a cupric hexacyanoferrate film coated onto glassy carbon. These electrodes provide stable and reproducible performance in flow-injection and ion chromatography systems.

Karsten N. Thomsen and Richard P. Baldwin*, Department of Chemistry, University of Louisville, Louisville, KY 40292

Electroanalysis of Aromatic Aldehydes with Modified Carbon Paste Electrodes 2599

The utility of carbon paste electrodes modified with aniline, 4-aminobenzoic acid, or $[Fe(CN)_5 4\text{-aminopyridine}]^{-3}$ for the determination of aldehydes in solution is demonstrated. Submicromolar sensitivity is obtained with electrodes modified with $[Fe(CN)_5 4\text{-aminopyridine}]^{-3}$.

Katherine E. Liu and Héctor D. Abruña*, Department of Chemistry, Baker Laboratory, Cornell University, Ithaca, NY 14853-1301

Electrochemical Activation of Carbon Electrodes in Base: Minimization of Dopamine Adsorption and Electrode Capacitance 2603

The electrode is activated at 1.2 V(SCE) in a pH 13 solution for 5 min. Compared with previous methods, this activation lowers capacitance and dopamine adsorption. The method is applied to four types of glassy carbon and to a pyrolytic carbon film electrode.

Dennis M. Anjo*, Michael Kahr, M. M. Khodabakhsh, Stuart Nowinski, and Michael Wanger, Department of Chemistry and Biochemistry, California State University, Long Beach, CA 90840

Effects of Background Electrolyte and Oxygen on Trace Analysis for Lead and Cadmium by Anodic Stripping Voltammetry 2609

The determination of lead and cadmium at ppb levels by DPASV in acidic aqueous media is affected by the presence of chloride ion and dissolved oxygen. The dissolved oxygen affects only the stripping step as molecular oxygen rather than H_2O_2.

Angelo R. Fernando and James A. Plambeck*, Department of Chemistry, University of Alberta, Edmonton, Alberta, Canada T6G 2G2

Optimization of Signal-to-Noise Ratios in Time-Filtered Fluorescence Detection 2611

Numerical algorithms are used to optimize quantification by fluorometry. The calculations are based on nanosecond temporal behavior differences between sample and blank emissions.

Newton K. Seitzinger, Kenneth D. Hughes, and Fred E. Lytle*, Department of Chemistry, Purdue University, West Lafayette, IN 47907

Supercritical Fluid Chromatography/Flame Photometric Detection: Determination of High Molecular Weight Compounds 2616

SFC with flame photometric detection is used to determine sulfur in high molecular weight compounds. For capillary SFC/FPD, the predominant noise source is shot noise.

Lars A. Pekay and Susan V. Olesik*, Department of Chemistry, The Ohio State University, 120 West 18th Avenue, Columbus, OH 43210

Whole Column Detection: Application to High-Performance Liquid Chromatography 2624

Information contained in the three-dimensional data set of peak intensity, position, and time can be used to enhance quantitation and speed of analysis.

Kathy L. Rowlen, Kenneth A. Duell, James P. Avery, and John W. Birks*, Department of Chemistry and Biochemistry and Cooperative Institute for Research in Environmental Sciences (CIRES), University of Colorado, Boulder, CO 80309

Rota-Microspeciation of Aspartic Acid and Asparagine 2631

Methods and results for the analytical determination of 9 and 15 differently protonated, coexisting rotamers are given for asparagine and aspartic acid, respectively. The relevant equilibrium constants are also determined.

Béla Noszál*, Department of Inorganic and Analytical Chemistry, L. Eötvös University, Muzeum krt. 4/B, Budapest H-1088, Hungary and **Péter Sándor**, Central Research Institute of Chemistry, Pf. 17, Budapest H-1575, Hungary

Chemical Acoustic Emission Analysis in the Frequency Domain 2638

Information available in the frequency domain representation of chemical acoustic emission signals is investigated by studying several chemical processes, including dissolution, hydration, effervescence, and solid–liquid and solid–solid phase transitions.

Peter D. Wentzell and Adrian P. Wade*, Laboratory for Automated Chemical Analysis, Department of Chemistry, University of British Columbia, Vancouver, British Columbia, Canada V6T 1Y6

---

* Corresponding author

DIALOG INTRODUCES ANOTHER TABLE OF BASIC ELEMENTS FOR YOUR LAB.

There's no symbol for *information* in the Periodic Table. Yet nothing could be more crucial to your research than complete, accurate technical and business information.

That's why many chemists consider DIALOG an essential element in the modern lab.

As the world's largest online knowledgebank, DIALOG gives you access to a whole world of critical information. Right in your own lab.

For starters, you can tap into the crucial scientific data. DIALOG has detailed information on everything from compound identification to chemical safety data, property data, substance and substructure.

Then you can expand your focus by accessing important, related data that will enable you to look at your work in a broader context.

For example, you can investigate patents, competitive projects, new product markets, and worldwide industry trends. In fact, you can investigate any topic, anytime.

And you won't have to sacrifice depth for the sake of breadth. DIALOG is updated continuously, so the data is always comprehensive and current. And many citations can be conveniently retrieved in full text.

Call today for more information and a free Periodic Table Reference Card. Once you've examined them, you'll see how DIALOG can become a basic element of all your research.

Call us toll free at 800-3-DIALOG, (800-334-2564). Or request information by Fax at 415-858-7069.

DIALOG INFORMATION SERVICES, INC
A Knight-Ridder Company KR

The world's largest online knowledgebank.

© 1989 Dialog Information Services, Inc., 3460 Hillview Avenue, Palo Alto, California 94304. All rights reserved. DIALOG is a servicemark of Dialog Information Services, Inc. Registered U.S. Patent and Trademark Office.

CIRCLE 34 ON READER SERVICE CARD

Econo-Cap from Alltech
$300.00
$149.95

Cuts Your GC Capillary Costs in Half - Without Compromising Results

Flexible capillary columns are manufactured under license granted by Hewlett-Packard Company

Request Bulletin #172 for more information

Alltech Associates, Inc.
2051 Waukegan Road • Deerfield, IL 60015
Phone: 708-948-8600 • FAX: 708-948-1078

CIRCLE 1 ON READER SERVICE CARD

RENT
Analytical Instruments
lease or rent-to-own

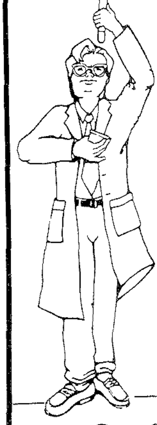

✓ Free Instrument delivery & setup in selected areas.
✓ GC•MSD•FTIR•AA•ICP•LC•IR
✓ Choose from many major manufacturers
✓ Hewlett-Packard GC•MSD Systems in stock
✓ New Catalog of Chromatography Supplies.

1-800-551-2783

On-Site Instruments®
ENVIRORENTAL®
689 North James Road Columbus Ohio 43219-1837
(614) 237-3022

CIRCLE 122 ON READER SERVICE CARD

BRIEFS

Analytical Characteristics of β-Cyclodextrin/Salt Mixtures in Room-Temperature Solid-Surface Luminescence Analysis 2643

A 30% β-cyclodextrin mixture produces strong luminescence signals from adsorbed compounds without the need for a heavy atom. Linear ranges, reproducibility, and detection limits for *p*-aminobenzoic acid and phenanthrene are presented.

Marsha D. Richmond and Robert J. Hurtubise*, Chemistry Department, University of Wyoming, Laramie, WY 82071-3838

Evaluation of a Diode Laser/Charge Coupled Device Spectrometer for Near-Infrared Raman Spectroscopy 2647

Millimolar detection limits and effective fluorescence reduction are achieved with a low-power diode laser operating at 782 and 830 nm. The approach affords many of the advantages of FT-Raman spectroscopy with significantly higher sensitivity.

Yan Wang and Richard L. McCreery*, Department of Chemistry, The Ohio State University, Columbus, OH 43210

Copper Atomization Mechanisms in Graphite Furnace Atomizers 2652

The copper atomization mechanism for an aqueous solution is $Cu(NO_3)_{2(s)} \rightarrow CuO_{(ads)} \rightarrow Cu_{(ads)} \rightarrow Cu_{(g)}$. The first-order desorption of copper atoms from the graphite surface at individual active sites is the rate-limiting step. MS, AA, and computational techniques are used.

Pingxin Wang, Vahid Majidi, and James A. Holcombe*, Department of Chemistry, The University of Texas at Austin, Austin, TX 78712

Simulation of Carbon-13 Nuclear Magnetic Resonance Spectra of Linear Cyclic Aromatic Compounds 2658

Electronic parameters are devised for use in simulating ^{13}C NMR chemical shifts in linear cyclic aromatic systems. Employing Hückel molecular orbital theory and molecular mechanics calculations, it is possible to simulate spectra to an average error of 0.509 ppm.

Abigail S. Barber and Gary W. Small*, Department of Chemistry, The University of Iowa, Iowa City, IA 52242

Electrochemical Detection of Peptides 2664

Postcolumn addition of biuret reagent to LC effluent creates electrochemically active species from most peptides. Selectivity over nonelectroactive amino acids is 10^3–10^4.

Anne M. Warner and Stephen G. Weber*, Department of Chemistry, University of Pittsburgh, Pittsburgh, PA 15260

Determination of Polycyclic Aromatic Hydrocarbons Using Gas Chromatography/Laser Ionization Mass Spectrometry with Picosecond and Nanosecond Light Pulses 2669

Laser ionization GC/MS with nanosecond and picosecond pulses is used to investigate the relative ionization efficiencies of polycyclic aromatic hydrocarbons. Molecules that undergo rapid excited-state relaxation demonstrate higher ionization efficiency in the short-pulse experiment.

Charles W. Wilkerson, Jr., Steven M. Colby, and James P. Reilly*, Department of Chemistry, Indiana University, Bloomington, IN 47405

Amazing Reproducibility:

New B&J Columns for Size Exclusion GPC

Your search for a superior GPC column is over. The new Burdick & Jackson GPC Column delivers exceptional reproducibility and long-term, cost-efficient life for analysis across a wide range of polymers. With maximum pore volume and high resolution, the packings provide wider solvent compatibility, higher tolerance to water, and better temperature stability. For added assurance, *every* B&J column is performance tested. Go to the source for all your analytical GPC needs, from columns to standards to high purity solvents.

Contact
Baxter Healthcare Corporation
Burdick & Jackson Division
1953 South Harvey Street
Muskegon, MI 49442 USA.

For technical assistance, call us toll-free at 800.368.0050.

Distributed by
Baxter Healthcare Corporation
Scientific Products Division

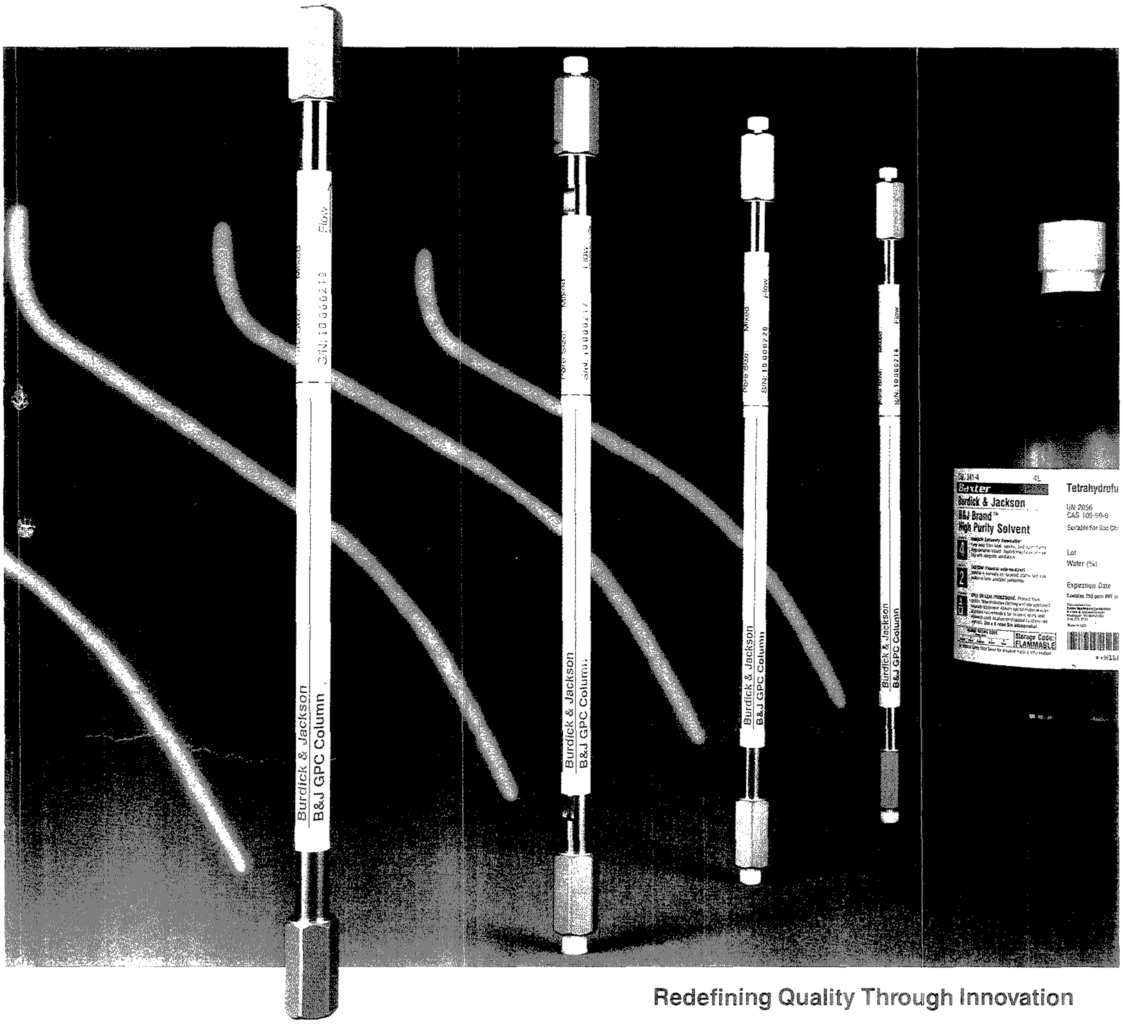
Burdick & Jackson
B&J GPC Column
Flow
Pore Size: Mixed
Baxter
Burdick & Jackson
B&J Brand
High Purity Solvent
Tetrahydrofu
Storage Code: FLAMMABLE

Redefining Quality Through Innovation

Baxter

© Copyright 1989. Baxter Healthcare Corporation. All rights reserved.

CIRCLE 20 ON READER SERVICE CARD

MAXIMIZE YOUR SENSITIVITY...
for Volatile Organic Compounds by Dynamic Headspace Concentration

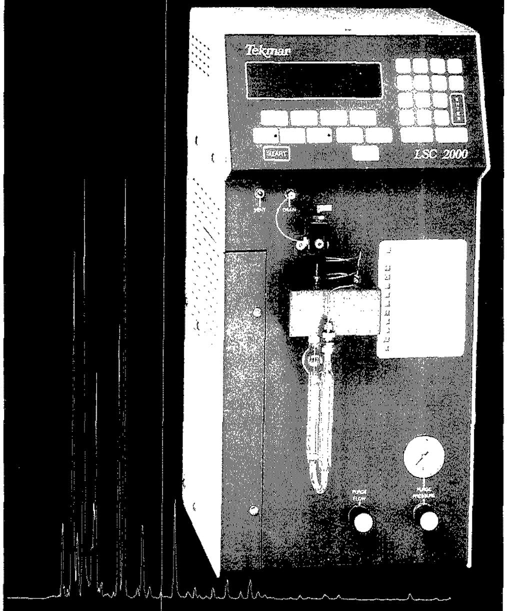

*5 ml **Coffee** on Tekmar's LSC 2000 and Capillary Interface*

Flavor/Fragrance
Competitive Analysis
Off Flavor/Odor Analysis
Packaging Materials
Pharmaceuticals/Residual Solvents
Building Products/Outgassing Studies
Polymers
Residual Monomers/Solvents

Ask for our FREE bibliography of reprints on a wide range of applications

P.O. Box 371856 • Cincinnati, OH 45222-1856
(800) 543-4461 Sales • (800) 874-2004 Service
Fax (513) 761-5183 • Telex 21-4221

CIRCLE 158 ON READER SERVICE CARD

BRIEFS

Influence of the Ratio of Matrix to Analyte on the Fast Atom Bombardment Mass Spectrometric Response of Peptides Sampled from Aqueous Glycerol 2674

A systematic manipulation of sample composition (analyte, glycerol, and water) with five different peptides shows the potential for significant mass spectral enhancement. A model emphasizing surface effects is proposed.

C. E. Heine, J. F. Holland, and J. T. Watson*, Departments of Chemistry and Biochemistry, Michigan State University, East Lansing, MI 48824

Comparison of Screening Techniques for Polychlorinated Biphenyls in Waste Oils 2682

The accuracy, precision, and interference susceptibility of colorimetric kits and neutron activation analysis for screening PCBs in oils are reported.

Carol R. Sutcliffe, Ernest S. Gladney*, Deanna M. Seitz, and George H. Brooks, Health and Environmental Chemistry, Group HSE-9, Mail Stop K-484, Los Alamos National Laboratory, Los Alamos, NM 87545

Correspondence

Assessing Heterogeneity of the High-Mannose Glycopeptide gp432 on the Variant Surface Glycoprotein of Trypanosomes: A Comparison of Plasma Desorption Mass Spectrometry and Radiolabeling Techniques 2686

Mark F. Bean, James D. Bangs, Tamara L. Doering, Paul T. Englund, Gerald W. Hart, Catherine Fenselau, and Robert J. Cotter*, Department of Pharmacology and Molecular Sciences and Department of Biological Chemistry, Johns Hopkins University School of Medicine, Baltimore, MD 21205

Correction. Effect of Apolar Diluents on the Behavior of Chiral Stationary Phases in Gas Chromatography. Binary Mixtures of *N*-Lauroyl-L-valine-*tert*-butylamide with Squalane and *n*-Tetracosane 2688

Katsunori Watabe and Emanuel Gil-Av*, Department of Organic Chemistry, The Weizmann Institute of Science, Rehovot, Israel and **Toshiyuki Hobo* and Shigetaka Suzuki**, Department of Industrial Chemistry, Faculty of Technology, Tokyo Metropolitan University, Fukasawa, Setagaya-ku, Tokyo 158, Japan

SIEMENS

Your choice in a high performance x-ray spectrometer - the SRS 303

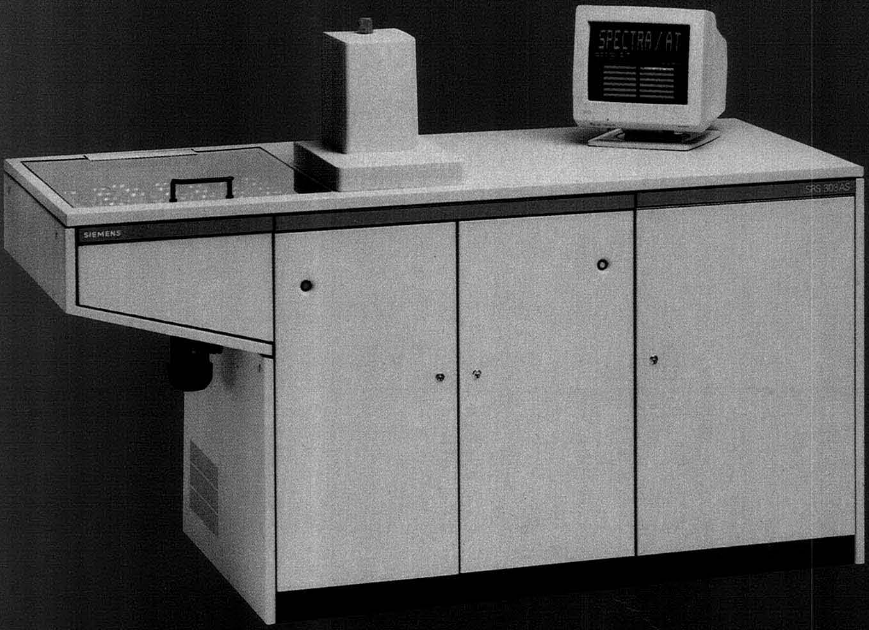

- **Wavelength dispersive sequential design** for flexibility in analysis with a high degree of accuracy.
- **SPECTRA AT software** with PC-compatible computer that supports simultaneous data collection while running *any other task* on the PC.
- **Microprocessor controller** monitors the instrument and displays complete status information at all times.
- **Choice of 10-position or 72-position sample changers** for batch or continuous operation.
- **6-position crystal changer** permits configuration for a wide range of applications.
- **Rh end-window tube** for improved light element sensitivity.
- **Compact 3.0 kW x-ray generator** with efficient medium-frequency design to reduce operating costs.

Your Solution is Siemens

In USA & Canada contact: Siemens Analytical X-Ray Instruments, Inc. • 6300 Enterprise Lane • Madison, WI 53719 • (608) 276-3000 • FAX (608) 276-3015
Worldwide contact: Siemens AG, Analytical Systems V 353 • D 7500 Karlsruhe 21 P.O. Box 21 1262 Federal Republic of Germany • Tel. (0721) 595-4295

CIRCLE 150 ON READER SERVICE CARD

RF POWER

As You Like It.

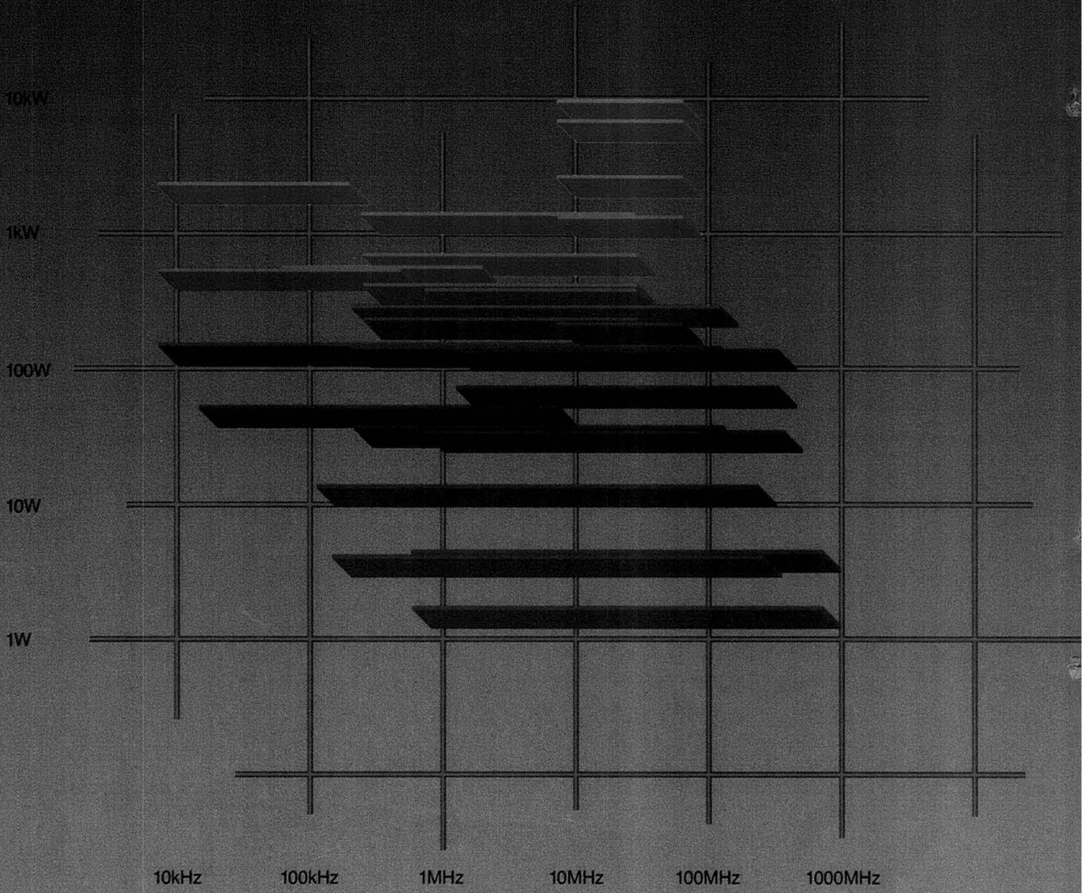

All solid state. Unconditionally stable. Compact. Tremendously versatile. Whatever your need for RF Power, ENI offers you a choice of Class A power amplifiers unsurpassed in quality. Our wide line spans a frequency spectrum from 10kHz to 1GHz with power outputs that range from 300 milliwatts to over 4000 watts.

These units can be driven by virtually any signal source. They're completely broadband and untuned, amplifying inputs of AM, FM, TV, SSB, and pulse modulations with minimum distortion. Their unconditional stability and fail-safe design make them impervious to severe mismatch conditions, and capable of delivering rated power to any load impedance from an open to a closed circuit.

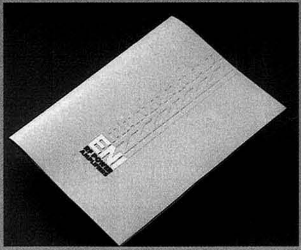

For our latest catalog, please contact us at any of the offices listed below.

ENI

U.S. HEADQUARTERS: ENI, 100 Highpower Road, Rochester, NY 14623-3498 USA,
Tel: (716) 427-8300, Tlx: 671 1542 ENI UW, Fax: (716) 427-7839
SANTA CLARA, CA: Tel: (408) 727-0993, Fax: (408) 727-1352
TOKYO, JAPAN: Tel: 0425 229011, Fax: 0425 222636
OSAKA, JAPAN: Tel: 06 367-0823, Fax: 06 367-0827
WELWYN GARDEN CITY, UK: Tel: (0707) 371558, Fax: (0707) 339286
STUTTGART, WEST GERMANY: Tel: 7156-2 10 95, Fax: 7165-4 9372

CIRCLE 44 ON READER SERVICE CARD

EDITORIAL

Secondary Ion Mass Spectrometry—SIMS VII

One of the most well-established and yet rapidly developing areas of surface analysis is secondary ion mass spectrometry (SIMS), which provides qualitative and quantitative information about the chemical composition of inorganic and organic materials. The broad scope and powerful capabilities of this technique were highlighted at the Seventh International Conference on Secondary Ion Mass Spectrometry (SIMS VII), held last September in Monterey, CA. The chairman of the local organizing committee was Charles A. Evans, Jr., of Charles Evans and Associates. Howard A. Storms of General Electric Co., Vallecitos, served as chairman of the program committee. More than 400 scientists from around the world attended and learned about the latest advances in this important surface analytical technique.

Twelve years ago, at SIMS I, the significant instrumentation and methodologies were still in their infancy, but many basic themes and goals expressed at that conference remain valid today. These include improved understanding of the physical processes involved in the technique, improved quantitation, increased use of computer-aided analysis, improved instrument performance, and application of the technique to solve problems in new and exciting areas. The most recent conference dedicated a full day to the area of Fundamentals and included a session honoring the late Don E. Harrison of the Naval Postgraduate School. Other areas that remain vital parts of the SIMS discipline include the analysis of semiconductors, instrumentation development, and the application of the technique to geology and metallurgy.

The use of the technique for organic and biological analysis was in most cases an untapped resource at the first SIMS meeting; today, some of the most intriguing and significant advances are in these two areas. Static SIMS, which can provide molecular information about polymer and biological surfaces, is a rapidly advancing technique. The analysis of biologically important systems with SIMS garnered a great deal of attention at the latest meeting. The quantitative imaging of diffusible elements in cells and the high-resolution imaging of ^{14}C-labeled chromosomes were just some of the highlights. The entire area of imaging was also covered in detail, illustrating the increasing significance of spatially resolved analysis.

The format of the SIMS meeting was also significant. Researchers from universities, national laboratories, and leading industrial labs met with the common interest of improving their field. This broad base of interest is important in ensuring scientific integrity and general applicability. Both oral and poster presentations were made, the latter allowing for significant exchange and discussion of ideas. In addition, contributions from student participants are particularly noteworthy, for the youngest members of any field represent that field's future.

The nature and progress of the SIMS field mirrors the entire area of analytical chemistry. Analytical techniques must remain based on sound science, yet prove themselves in practical applications. As techniques emerge, the sophistication and complexity of the methods will increase, but so will the quality of the results—providing solutions to problems previously considered impossible to solve.

G. H. Morrison

varian
9010
Solvent Delivery System

ONLY THE BEST FOR THE BEST.

Can your HPLC system pump champagne? Can your HPLC system reliably pump ANY solvent without costly, time consuming degassing procedures?

Only one HPLC pump can — the Varian LC Star 9010. Our 9010 can pump ANY HPLC solvent, without prior preparation, with reliable results, everytime.

Let's face it. If you can't count on your pump, it doesn't matter how well the other parts of your HPLC system work. High performance isn't enough when one tiny bubble can shut down your whole operation.

The unique, patented design of the Star 9010 delivers high performance and dependability with any mobile phase. It eliminates pump cavitation, so your HPLC system can operate for hours on end, even overnight, unattended.

The net result is that, over the long run, you can have more analyses completed in less time, and with greater confidence.

Let us show you how dependable and productive a pump can be. For more information on the Star 9010 Pump and the entire Varian LC Star System, call **800-231-8134**. In Canada, call **416-457-4130**.

CIRCLE 170 ON READER SERVICE CARD

LC WITH A FUTURE

Nominations Sought for 1991 ACS Awards

Nominations are being sought for the 1991 American Chemical Society Awards. Several of these awards are of interest to the analytical community: the Award in Analytical Chemistry, the Award in Chromatography, the Award in Separations Science and Technology, the Frank H. Field and Joe L. Franklin Award for Outstanding Achievement in Mass Spectrometry, the Award for Computers in Chemistry, and the Garvan Medal.

Established in 1947 by Fisher Scientific Company, the ACS Award in Analytical Chemistry consists of $5000 and an etching. The award honors contributions to pure or applied analytical chemistry by a Canadian or U.S. scientist. The selection committee gives special consideration to "the independence of thought and originality shown, or to the importance of the work when applied to public welfare, economics, or the needs and desires of humanity."

Sponsored by Supelco, Inc., since 1970, the ACS Award in Chromatography is given to a scientist who has made an exceptional contribution to the field of chromatography, with particular emphasis on the development of new methods. The winner receives $5000 and a certificate.

The ACS Award in Separations Science and Technology, sponsored by Rohm and Haas Company, recognizes extraordinary accomplishments in either fundamental or applied areas of separations science and technology. The award, established in 1982, covers all fields in which separations science and technology are practiced, including chemistry, biology, engineering, geology, and medicine. The awardee is honored with $5000 and a plaque.

Established one year later, the Frank H. Field and Joe L. Franklin Award for Outstanding Achievement in Mass Spectrometry will in 1991 recognize advances in techniques or fundamental processes in MS. The award is sponsored by Extrel Corporation and consists of $3000 and a certificate.

The ACS Award for Computers in Chemistry, established to recognize and encourage the use of computers for the advancement of chemical science, is sponsored by Digital Equipment Corporation. The awardee receives $3000 and a certificate.

The Garvan Medal, sponsored by Olin Corporation since 1984, recognizes distinguished service to chemistry by women who are U.S. citizens. Established in 1936 through a donation from Francis P. Garvan, the award consists of $4500, an inscribed gold medal, and a bronze replica of the medal.

Individuals (except nominating committee members) may submit one nomination for each award. Nominations should be accompanied by a biographical sketch, a list of publications and patents, and a letter of 1000 words or less describing the nominee's accomplishments and the work to be recognized. Seconding letters are optional, and no more than two of these—containing information not provided in the nomination letter—may be submitted. Six copies of each nomination should be mailed to the Awards Office, ACS, 1155 16th St., N.W., Washington, DC 20036.

Materials must be postmarked by Feb. 1, 1990. For further information, see "Awards Administered by the ACS" (Bulletin 7), available through the Awards Office.

Snyder Elected Subdivision Head

The ACS Division of Analytical Chemistry's Subdivision on Chromatography and Separations Science has chosen Lloyd Snyder as chairman-elect for 1991–93. Snyder is an expert on liquid chromatography and a pioneer in the development and application of high-performance liquid chromatography.

He received both his B.S. degree (1952) and Ph.D. (1954) from the University of California at Berkeley. From there he entered industry, working for Shell Oil; Technicolor, Inc.; Union Oil; and Technicon Corporation. Since 1985 he has managed his own consulting firm, LC Resources Incorporated.

Snyder has served on the editorial boards of several journals, including ANALYTICAL CHEMISTRY (1971–73). He has also authored or co-authored six books dealing with various aspects of chromatography.

Peter Carr of the University of Minnesota will continue until 1991 as chair of the Chromatography and Separations Science Subdivision, and John Nikelly of the Philadelphia College of Pharmacy and Science will serve as secretary until 1993.

For Your Information

Travis Ganunis, a chemistry major from Franklin and Marshall College, **has won the Association of Official Analytical Chemists' Harvey W. Wiley Scholarship Award.** The two-year scholarship is awarded annually to a promising junior-year student studying a subject important to public health and agriculture.

The National Institute of Standards and Technology (NIST) has revised its ***Directory of International and Regional Organizations Conducting Standards-Related Activities.*** The directory now contains listings on 338 groups that conduct standardization, certification, and laboratory accreditation. For more information on this and related documents, contact the Office of Standards Code and Information, A629 Administration Bldg., NIST, Gaithersburg, MD 20899 (301-975-4031).

The National Institute of Standards and Technology (NIST) **is offering a reference material for determining cholesterol in eggs.** The standard consists of dried whole egg powder certified to contain 19.0 ± 0.2 mg cholesterol/g. For more information, contact the Office of Standard Reference Materials, NIST, B311 Chemistry Bldg., Gaithersburg, MD 20899 (301-975-6776).

The National Science Foundation has funded the development of science and technology exhibits at eight U.S. science museums. Among the projects in preparation is the Lansing, MI, **Impression 5 Museum's exhibit on the role of chemistry in everyday life.**

THE INTEGRATOR YOU'VE BEEN ASKING FOR...

Inkjet printer with easily readable printing and plotting.

Convenient Z-fold paper.

Baselines are drawn in —automatically!

Backlit supertwist display for real-time information.

Low ink supply indication.

128K memory, expandable to 512K.

A real PC-style keyboard.

Add a second channel— any time.

IS HERE.

ChromJet, the new integrator from Spectra-Physics. Everything you want in an integrator. And more.

For complete information, call toll free: **800-424-7666.**

Spectra-Physics Autolab, 3333 North First Street, San Jose, CA 95134.

Spectra-Physics

Discover the Quality

Circle 154 for Sales Rep. Circle 155 for Information.

László Zechmeister: A Pioneer of Chromatography

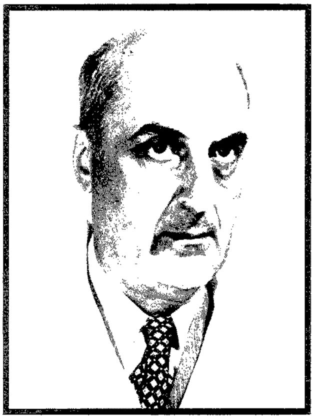

Leslie S. Ettre
Advanced Analytical Technology
The Perkin-Elmer Corporation
Norwalk, CT 06859-0284

This year we are commemorating the centenary of the birth of László Zechmeister, one of the most important pioneers of classical column chromatography. Many scientists today know little about him or his work, yet his books and scholarly publications were widely read from the 1930s to the 1950s. He was one of the generation of scientists who rediscovered chromatography and demonstrated its use for separating and isolating complex natural pigments. Therefore, it is appropriate that we look back on his life, activities, and achievements.

László Zechmeister was born on May 14, 1889, in Györ, Hungary. He received his primary education in Györ, and after finishing high school, enrolled at the Eidgenössische Technische Hochschule (ETH), the Federal Technical University, in Zurich, Switzerland, graduating in 1911 as a chemical engineer. He continued his graduate studies there under Richard Willstätter, one of the foremost organic chemists of that period. In 1912 Willstätter moved to Berlin-Dahlem as the director of the Kaiser Wilhelm Institut für Chemie, and Zechmeister went with him as an assistant, receiving his technical doctorate from the ETH in 1913.

Wanderjahre

Willstätter is usually identified with his research on chlorophyll, for which he received the Nobel prize for chemistry in 1915. Zechmeister's doctoral thesis, however, dealt with another of Willstätter's pet projects: the investigation of the cellulose and lignin of trees (*1*, *2*). Zechmeister continued his research in this area at Pécs, collaborating with Willstätter (*3*).

Another early project on which Zechmeister worked in Berlin-Dahlem dealt with anthocyanes. At the July 30, 1914, session of the Royal Prussian Academy of Sciences (of which Willstätter was a member) they reported on the first synthesis of pelargonidin (*4*). In 1919 they published this work in a Hungarian scientific journal (*5*).

At the outbreak of World War I, Zechmeister joined the Hungarian Army. He was wounded and became a prisoner of war in Russia, returning via Sweden in 1919 (*6*). He then became associated with the Chinoin Pharmaceutical Company in Budapest, becoming head of the research group, and was also involved in various research projects at the Hungarian Veterinary Medicine College and the Technical University.

His cooperation with George von Hevesy during this period is particularly interesting. Von Hevesy was doing research in Budapest on isotope separation, and Zechmeister worked with him on this project. The first report of their work was published in Hungarian (*7*), followed by two publications in leading German journals (*8*, *9*). Von Hevesy then moved to Copenhagen to work with Niels Bohr and Johannes Brönsted at the Institute of Physics. Within a year Zechmeister also went to Copenhagen, where he was associated with Professor Niels Bjerrum at the Royal Danish Veterinary Agricultural Academy. It was in Copenhagen that, in 1922, von Hevesy discovered the element hafnium, and Zechmeister hastened to report this discovery to his Hungarian colleagues (*10*).

Professor at the University of Pécs

Although Zechmeister enjoyed his stay in Denmark, he returned to Hungary in 1923 when the Hungarian government reestablished the University of Pozsony (which, as a result of the peace treaties following the war, became part of the newly formed Czechoslovakia) in the city of Pécs in southern Hungary. Zechmeister was appointed a full professor and head of the Chemical Institute within the faculty of medicine. This appointment was a great honor for Zechmeister: He was only 33 years old, and such a young person seldom received a cathedra. His new job was not, however, an easy one for a number of reasons.

REPORT

First, the whole country and, conse-

0003-2700/A361-1315/$01.50/0
© 1989 American Chemical Society

quently, the new university, was very poor. The university was relocated in name only; everything else remained in Bratislava (the Slovak name for Pozsony), and the university continued to function there, as a Slovak university. Buildings had to be erected, laboratories established, and equipment purchased. This took a long time. In addition, the whole curriculum had to be reestablished or, better stated, set up from scratch. Zechmeister did an excellent job and even wrote three textbooks for his students. The first was a book translated as *Chemical (Laboratory) Practice*, which he coauthored with two Danish scientists, Carl Faurholt and J. K. Gjaldbaek (*11*). The book was dedicated to Professor Niels Bjerrum. One chapter was also published as a separate book translated as *Introduction to Titrimetry* (*12*). Zechmeister's most important textbook from this period was a two-volume monograph on organic chemistry (*13*) published in 1930–32 and dedicated to Richard Willstätter, his former mentor. This book was the first of its kind in Hungarian and was widely used for almost a decade.

These books show how seriously Zechmeister regarded his teaching duties. Indeed, he was well known for the excellence of his lectures; a eulogy published in the Pécs University yearbook (*14*) mentions that his lectures created a "unique impression" for the students; they were "carefully prepared and excellently presented," and he always had a large audience.

Teaching is, however, only part of a university professor's job: He must also perform meaningful research and attract good collaborators. Zechmeister was particularly successful at this. After accepting the position at Pécs, one of the first things he did was to look for a good assistant. On the advice of Géza Zemplén, an internationally known organic chemist at the Technical University Budapest and former pupil of Emil Fischer, he invited László Cholnoky to become his assistant. Cholnoky was 10 years younger than Zechmeister and a pharmacist by training. He became Zechmeister's closest collaborator and eventually his successor. Zechmeister also succeeded in recruiting excellent graduate students such as Pál Tuzson and Géza Tóth, who later acquired important positions in Hungary.

Lâszlô Cholnoky, Zechmeister's assistant, deputy, and successor. (Courtesy of Mrs. Cholnoky.)

For his research, Zechmeister selected fields with which he became familiar while associated with Willstätter. In addition to continuing his work with cellulose, he began to investigate the chromatographic separation of enzymes, collaborating with Wolfgang Grassmann, then in Willstätter's laboratory in Munich. After moving to the United States, Zechmeister collaborated with Margarete Rohdewald, who for many years had served as Willstätter's primary assistant and who continued to work at the University of Munich even after Willstätter's departure.

Investigations of carotenoids

Although these investigations are noteworthy, without doubt the most important work of Zechmeister and his group is related to the investigations of carotenoids and other natural pigments. His interest in this area most likely originated in Willstätter's laboratory, but although Willstätter carefully followed Tswett's activities, he did not consider chromatography an important method. In fact, he called it "an odd way" to obtain pure compounds.

Of the wide range of activities of Zechmeister's group related to carotenoids, two are of particular interest: the investigation of the pigments of various fruits and of red paprika. Zechmeister published 10 papers on the latter, all coauthored with Cholnoky and published in the journal *Liebig's Annalen der Chemie*—the first in 1927 (*15*) and the last in 1937 (*16*). His involvement in chromatography was also a result of his investigations of carotenoids.

We know that the "rebirth" of chromatography occurred in 1931, in the laboratory of Richard Kuhn in Heidelberg, where Edgar Lederer first applied it to the separation of xanthophylls (*17*). We also know (*18, 19*) that one of the sources from which Lederer learned about chromatography was the

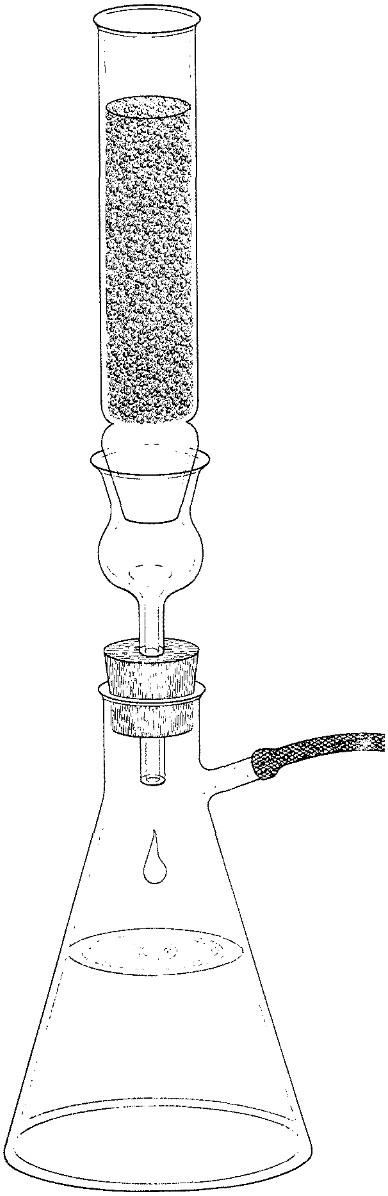

Figure 1. A "conventional laboratory chromatography system" described by Zechmeister and Cholnoky in their book on chromatography (*25*).

The packing in the vertical tube is held in place with the help of a glass filter plate or small cotton wad. Typical dimensions of the vertical glass column are 20 × 2 cm, 23 × 3.5 cm, 25 × 4.5 cm, 30 × 6 cm, or 35 × 8 cm.

German translation of Tswett's 1910 book (*20*). This was actually a private translation prepared specially for Willstätter, who then gave it to Kuhn. Because Zechmeister had been with Willstätter in the years following the publication of Tswett's original Russian book, a logical question may be raised: Did Zechmeister actually learn about chromatography from Willstätter? And was there any connection between Kuhn and Zechmeister, the two Willstätter pupils?

After a careful study of all the available information, my answer to both questions is no. There was no direct connection between Zechmeister and Kuhn (who was 11 years younger); in fact, there was fierce competition between them. Most likely, Zechmeister's knowledge about chromatography originated from Leroy Palmer's book on carotenoids published in the United States in 1922 (*21*). Palmer graduated from the University of Missouri in 1913 with a Ph.D. in dairy chemistry, and his thesis dealt with the pigments in milk and milk products. In this work he successfully used Tswett's method; and in his book on carotenoids, published about 10 years later while he was professor at the University of Minnesota, Palmer elaborated in even more detail on the advantages of chromatography for the investigations of carotenoids and other plant and animal pigments. Obviously, Zechmeister was familiar with Palmer's work, and in his own chromatographic investigations he used similar systems (Figure 1).

Zechmeister's first paper on carotenoids was published in 1927, and in a few years his familiarity with this field was so well known that he was asked to contribute a chapter entitled "Carotenoids of Higher Plants: Polyene Pigments" to the *Handbook of Plant Analysis*, published in 1932 (*22*), which he soon expanded into a 340-page monograph on carotenoids published in 1934 (*23*). In both books he discusses the chromatographic technique and its possible use for such investigations, although he wrote these books before his own first publication on the use of chromatography!

The use of chromatography was first reported by Zechmeister and Cholnoky in Part VII of their series on the pigments of paprika, published in 1934 (*24*). Figure 2 shows one of their "chromatograms" (*25*). Why then did Zechmeister not immediately apply chromatography to the investigation of plant pigments that he had started as early as 1927? In my opinion this could be because the instrumentation available at that time in Pécs was inadequate. During that time, the identification of pure compounds always had to be corroborated by elemental analysis. In the 1920s Zechmeister did not yet have the proper equipment (a microbalance, in particular) to perform such determinations from the very small chromatographic fractions. Thus, although his group was aware of chromatography and most likely had already experimented with it, they did not report on its use until 1934, when the proper equipment finally became available.

In 1938 the European scientific community was surprised by a major book, written by Zechmeister and Cholnoky, describing the "chromatographic adsorption method" (*25*). This was the right book published by the right people at the right time, and it became an instant best-seller. In fact, it was such a success that within one year a second, greatly enlarged edition was published. About one-third of the text dealt with fundamentals and methodology while about two-thirds of it discussed applications. It is amazing to realize how widely chromatography was already being used just seven years after its "rediscovery." This book became Zechmeister's greatest contribution to chromatography; through it, he taught a whole generation of chemists.

Immigration to the United States

By the end of the 1930s, Zechmeister was well established and respected both at home and abroad. He was already a member of the Hungarian Academy of Sciences, receiving its Grand Prize in 1937, and he was also elected a foreign member of the Royal Danish Academy of Sciences. In 1934 he received the prestigious Pasteur Medal of the French Société de Chimie Biologique, and his book on chromatography became the standard textbook in the field. He had been invited a number of times to give lecture tours in Europe and even in the United States. At that time this was a special distinction, particularly for someone from a small Central European country. He was at the height of his scientific career, and he could approach his 50th birthday with satisfaction and look forward to some relaxation. But fate decided otherwise, and politics interfered with these plans.

By 1938–39, it was obvious that the peaceful conditions in Europe were over. Hitler was preparing for war, and Hungary could not stay out of the conflict. Zechmeister was primarily a scientist and not a politician, but he was also a person to whom violence and racial discrimination were simply unacceptable. After much soul-searching, he and his wife decided to leave Hungary to accept an invitation to join the faculty of the California Institute of Technology that had been extended to Zechmeister following his visit to the United States. There was, however, one serious problem: His wife had tuberculosis and her immigration to the United States was prohibited.

According to the original plans, Zechmeister was to arrive in Pasadena in the summer of 1939 prior to the start of the new academic year, but this became impossible. Finally it was decided that Zechmeister would leave alone, and his wife would follow in a few months after her health improved. Zechmeister finally sailed in February 1940, from Genoa, Italy, arriving in New York on February 29, 1940. Andor

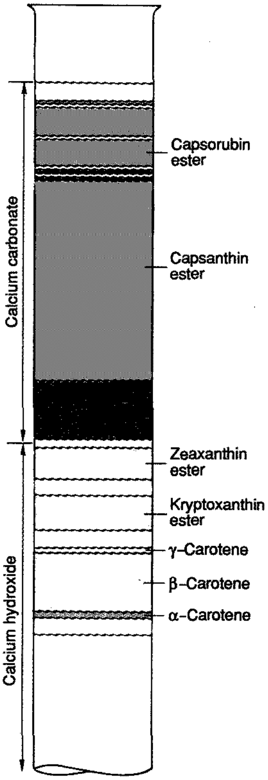

Figure 2. Separation of the pigments present in Hungarian paprika (*25*).
The 20 × 4.5-cm glass column was packed with two adsorbents, as indicated. Paprika skin was extracted with a low-boiling petroleum fraction and the "chromatogram" developed with the same solvent.

Polgár, who had received his Ph.D. a few months earlier in Zechmeister's laboratory, traveled with him. Polgár remained with Zechmeister at Pasadena until the fall of 1944 when he joined Shell Development Company, where he was a distinguished scientist until his retirement in 1972.

Incidentally, the delay in Zechmeister's immigration had an interesting consequence (*26*). In 1939 a young scientist named Justus Kirchner was hired to be Zechmeister's assistant, but because of the immigration delay, Kirchner temporarily joined A. J. Haagen-Smit, another Caltech professor, and became involved in investigations of the aroma and flavor of pineapples. When Zechmeister finally arrived, Kirchner decided to remain in this field rather than work with Zechmeister. In 1945 Kirchner joined the United States Department of Agriculture's Fruit and Vegetable Laboratory in Los Angeles, where he developed thin-layer chromatography in 1951.

Like every immigrant, Zechmeister had to start anew. It was particularly difficult for him because of his wife's illness. Their hope was that she would join him in Pasadena, but her condition worsened and she died in Hungary on July 7, 1941. Soon after, Zechmeister's connections with home were severed because of the war. He returned to Hungary for a brief visit in 1946 but did not stay; he had decided to spend the rest of his life in the United States, and he officially resigned his position at the University of Pécs. In 1947 he remarried and he remained at CalTech until 1959, when be became professor emeritus. On this occasion, Springer Verlag published a bibliography of his literary activities, listing a total of 257 publications (*27*).

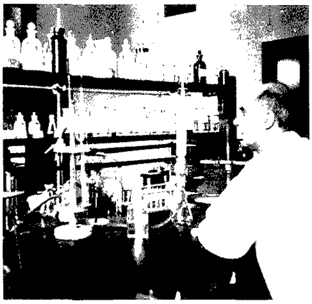

Zechmeister's laboratory in Pasadena, April 1940. Polgár is shown with the first chromatographic setup, analyzing a carrot extract. (*Courtesy of A. Polgár.*)

Soon after his arrival in the United States, the English translation of his chromatography book—already in preparation for some time—was published (*28*). Professor Heilbron of Imperial College, London, wrote the foreword to the book, emphasizing its outstanding merits. According to Heilbron, the book was "invaluable not only to those who themselves propose to make use of chromatographic methods, but also to all interested in the sparsely explored territory that lies between the domains of physical and organic chemistry."

Heilbron correctly pointed out Zechmeister's main characteristic: He never considered chromatography as the ultimate subject of his work; it represented only the means to achieve his goals as an organic chemist studying complex natural products. For example, at a lecture at the 1950 meeting of the Southern California Section of the American Chemical Society, Zechmeister said: "Recently chromatography became so popular that the English language has been enriched by a new noun, 'the chromatographer'. I would protest against such a label. In research, chromatography should be considered first of all a tool, like, for example, fractional distillation, and those of our colleagues who have achieved success by using distillation methods should certainly not be named distillers."

To illustrate that Zechmeister considered the investigation of complex natural products his main activity, I should mention that in 1938 he initiated a book series entitled *Fortschritte der Chemie organischer Naturstoffe*. Publication of the series was discontinued during the war, but was continued afterward, with the English title *Progress in the Chemistry of Organic Natural Products*. Zechmeister edited the series until his death.

In November 1946 the New York Academy of Sciences organized the first major postwar chromatography conference, to which two important European scientists—Claesson from the University of Uppsala and A.J.P. Martin from England—were invited. Zechmeister was asked to give the introductory lecture on the history, scope, and methods of chromatography (*29*).

In Pasadena, Zechmeister continued to collect the literature of chromatography and critically evaluate the new results, with the idea of publishing this as a supplement to his original chroma-

OUR STANDARDS ENDURE THE TEST OF TIME.

Conostan oil-based calibration standards combine the convenience of blended standards and exceptional stability for the analysis of metals in oil. These metallo-organic sulfonates remain stable in liquid form for more than a year—and individual concentrates have exhibited even longer shelf lives. For a complete list of single and multi-element standards that endure the test of time, write or call for our free brochure.

Standards to Burn
CONOSTAN®

Conostan Division
Conoco Specialty Products Inc
P.O. Box 1267
Ponca City, OK 74603
Phone: (405) 767-3078
Fax: (405) 767-5843

CIRCLE 30 ON READER SERVICE CARD

tography book. The manuscript of this new book, entitled *Progress in Chromatography 1938–1947* (*30*) was finished in early 1948, but its publication took two years. This book received excellent reviews; for example, a review in the journal *Enzymologia* (*31*) stated that "the author has been known as a master in the application of chromatography to many biochemical and especially enzymatic problems for many years. . . . He gives us in this book the benefit of his practical experience in this field and makes chromatography interesting and easy to use for every biochemist."

The main subject of his research during his two decades at CalTech was the study of stereoisomers, and he used chromatography primarily for the separation of these compounds. In fact, during the last two decades of his scientific activities he considered this application as his most important achievement. This is best illustrated by some of the lectures he presented at major meetings. The first such occasion was the 1946 meeting of the New York Academy of Sciences mentioned above, where Zechmeister presented a second lecture entitled "Stereochemistry and Chromatography" (*32*).

In September 1949 the (British) Faraday Society organized a General Discussion on Chromatographic Analysis, undoubtedly one of the best and most important scientific meetings of the early postwar period. Naturally, Zechmeister participated, presenting a lecture on Adsorption and Some Constitutional and Steric Properties (*33*).

Further evidence of his emphasis on the application of chromatography to the separation of stereoisomers is the lecture he presented in 1962, upon receiving the ACS Award in Chromatography and Electrophoresis. It is customary for the award winner to give a major lecture at the meeting where the award is presented, and Zechmeister selected Column Chromatography and Geometrical Isomerism as the subject of his lecture, describing the development of the technique together with one of its most important applications: the separation of certain cis and trans isomers. His book *Cis-Trans Isomeric Carotenoids, Vitamin A, and Arylpolyenes* (*34*), published in 1962, together with his ACS lecture, represent the swan song of his scientific career.

Zechmeister the person

Finally, I would like to deal with László Zechmeister, the person. I have already referred a number of times to his integrity and honesty, and I would like to illustrate these with two examples. The

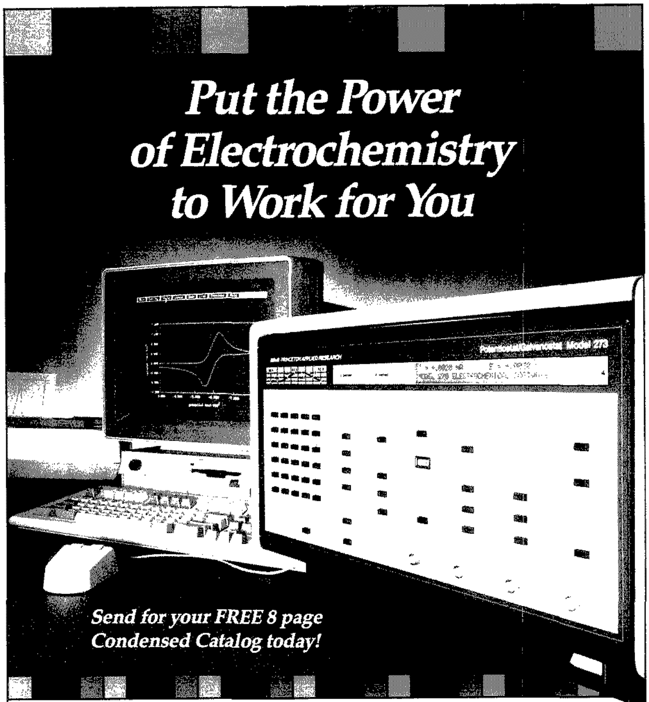
Put the Power of Electrochemistry to Work for You
Send for your FREE 8 page Condensed Catalog today!

Whether you're involved in ground-breaking research, product development, or QC, you can count on electrochemistry for precise answers—and you can depend on EG&G PARC for the right combination of instruments, technical support and applications know-how.

Gain the Power of a Computer-Assisted Laboratory

Streamline your compound characterizations, analytical measurements, biological investigations, process development, mechanistic studies, and more. The Model 270 Electrochemical Analysis System is fast, precise, and easy to use. Select **Standard** or **Expert** mode, and make use of more than 20 basic electrochemical techniques. Plus, you can cost-effectively expand into corrosion, impedance, and customized electrochemical measurements.

Detect a Wide Variety of Compounds

The Model 384B Voltammetric Analyzer is extremely versatile—enabling you to automatically determine trace concentrations of ions, metals, and inorganics. Accuracy and repeatability are assured through low noise electronics and microprocessor-controlled operation.

Analyze the Most Complex Compounds

The Model 400, LCEC detector offers femtogram sensitivity providing state-of-the-art technology for your catecholamine analyses. Pulse mode lets you detect compounds such as carbohydrates. Your methods development is streamlined with the prescan feature.

EG&G
PRINCETON APPLIED RESEARCH

CN 5206 • PRINCETON, NJ 08543-5206 • (609) 895-0100 • (800) 274-PARC • TELEX: 8543409 • FAX: (609) 895-0063

270-2

Circle 46 for literature. Circle 47 to have a representative call.

first is related to the 1950 publication of his book *Progress in Chromatography.* At that time Zechmeister was already established in the United States, and the Cold War was under way. Thus, it seemed logical that in publicity material only Zechmeister's name be used when mentioning his major chromatography book, of which this was considered a continuation. However, in an August 1950 letter to the publisher, he insisted that "Cholnoky's name should appear in the same manner as mine."

The second example is related to the English translation of the chromatography book he wrote with Cholnoky. Soon after its publication, one of the major laboratory supply houses reproduced a figure from the book in its newsletter (distributed free of charge to many thousands of laboratories). The caption, however, had been changed, so as to be incorrect and misleading. Zechmeister immediately wrote to the publisher requesting correction, but was told that it was a small item not worthy of bother and that use of a figure from a book in a publication with such a wide circulation represented good publicity for the book itself. Zechmeister immediately replied, stating that "... my duty as a scientist is to fight against any distortion of scientific truth.... If you say that the article in question represents 'precisely the sort of publicity which we solicit,' I may remark that the distortion of scientific facts, established by long years of effort, is just the sort of publicity which no scientist can desire."

The last decade of Zechmeister's life was not a happy one. The ACS Award in Chromatography and Electrophoresis pleased him very much, and he understood the inevitability of obtaining emeritus status. However, he felt that he could do more than the circumstances at CalTech permitted. At the same time, he realized that chromatography as a technique was starting to outgrow him. Chromatography went through an exponential growth during this period; Zechmeister followed it carefully but could not become a part of it anymore.

Another sad experience had to do with his recognition in Hungary. In 1949, using trumped-up political charges, his membership in the Hungarian Academy of Sciences was terminated. In 1967, the 78-year-old Zechmeister participated in the celebration of the 600th anniversary of the predecessor of Pécs University, and expected that this unjustice would be corrected, at least by bestowing upon him an honorary doctorate. This, however, did not happen, and he was given an honorary doctorate only in 1971, a few months before his death. The Academy of Sciences did not officially acknowledge the error it made in 1949 until 1989, when the membership of Zechmeister and his colleagues was reinstated.

Zechmeister died in Pasadena on February 28, 1972. As he requested, his ashes were scattered into the ocean near Los Angeles.

Today, chromatography is a mature field, and we are again studying the interrelationship of the various disciplines. We are looking back to the pioneers, investigating their activities, and trying to find out what can we learn from their work. It is most proper to honor the memory of Zechmeister, teacher of a generation of chromatographers, and preserve it for future generations.

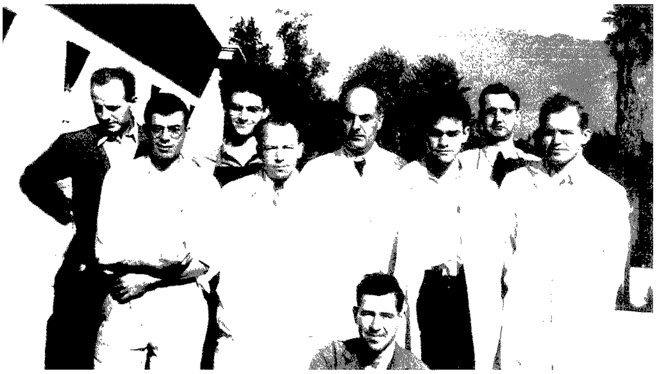

The early days in Pasadena, February 1941. Standing right to left: W. H. McNeeley, W. A. Schroeder, A. L. LeRosen, Zechmeister, and Polgâr. W. T. Stewart is on the far left, and R. B. Escue is in the front. The two unidentified persons were technicians in the laboratory. (Courtesy of A. Polgâr.)

Sample preparation for XRF-AA-ICP-CHEM.

PEAK QUALITY with Claisse Fluxes

(Borates and Phosphates)

Get a new perspective on analysis and better results. The CLAISSE FLUXES have exceptional qualities due to their PURITY and COARSE texture. Claisse Fluxes are Tip-Top.

FEATURES
- free-flowing crystals
- low surface area
- high density
- fused, not mixed
- popular and special compositions

CONSEQUENT ADVANTAGES
- no loss from static electricity
- no loss by splattering or foaming on heating
- very low water absorption
- no uncertainty on quantity weighed
- no segregation in containers
- FREE SAMPLE upon request

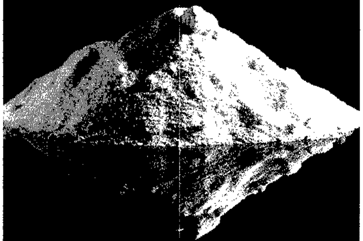

For world-wide sales, address of local agents and service information please call or write to:

corporation scientifique claisse inc.

2522, chemin Sainte-Foy
Sainte-Foy (Québec)
Canada G1V 1T5
Tel: (418) 656-6453
Fax: (418) 656-1169
Telex: 051-31731

The First and Finest in Fusion.

CIRCLE 28 ON READER SERVICE CARD

MODEL 305

Modular HPLC Pump

305 PUMP
1
2
3
4
5
6
7
8
9
0
PRIME
HELP
CANCEL
ENTER
GILSON

The new Gilson Model 305 Master Pump. For analytical or preparative HPLC in the isocratic, binary or ternary modes.

The Pump.

Now you can program gradients without a computer. Upgrade your isocratic system without major expense. Switch from analytical to preparative and back again. Use the special dispense mode for repetitive injection in automatic preparative systems.

The heads.

For micro-analytical up to laboratory preparative scale (0.025 - 200 mL/min). For aqueous or salt-concentrated solutions. In titanium for ion-free work. All completely interchangeable so you can choose the optimum combination for your separation.

This compact new pump (only 32 cm wide) can handle any HPLC application.

To find out more about Gilson's new Master Pump, please contact your nearest Gilson representative.

THE MASTER PUMP

with built-in gradient controller

GILSON

U.S.A. - Box 27, 3000 West Beltline Hwy - Middleton, WI 53562 - Tel. : 608-836-1551
Tlx : 26-5478 - Fax : 608-831-4451 - FRANCE - BP 45 - 95400 Villiers-le-Bel - Tel. : (1) 34 29 50 00
Tlx : 606 682 - Fax : (1) 39 94 51 83

CIRCLE 61 ON READER SERVICE CARD

JUST
WHAT YOU
NEED
WHEN
YOU WANT IT
[illegible]
WHAT
YOU NEED.

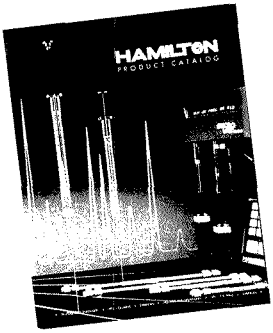

Hamilton's 1990 Product Catalog has been completely redesigned to help you select exactly what you need — syringes, diluters/dispensers and polymeric HPLC columns. Using a combination of product photos, illustrations and application charts, the catalog guides you to the right choice... precisely and accurately. To get what you need for free, call (800) 648-5950.

HAMILTON
The measure of excellence.

For a free copy of this catalog, circle No. 57

This article is based on plenary lectures presented at the Seventh Danube Symposium on Chromatography (Leipzig, G.D.R., August 21–25, 1989) and at the Second Scientific Meeting on the Role of Hungarians in the Scientific and Technical Progress of the World (Budapest, August 21–25, 1989).

Most of my research into Zechmeister's life and activities was done in the mid-1970s. I had the opportunity to check the Zechmeister Files at the Archives of the R.A. Millikan Memorial Library at CalTech, and to examine many of the original publications and books in the Kline Science Library at Yale University. As always, Eleanor Dempsey of Perkin-Elmer's library was of great help to me in clearing up dubious references and getting copies of some obscure papers. Additional information was obtained through personal discussions and correspondence with Elisabeth Zechmeister, Mrs. László Cholnoky, Géza Tóth, and Andor Polgár. I also obtained information from my brother, Csongor Olajos, a reporter and editor for Hungarian television. I would like to express my gratitude to all of them.

References

(1) Zechmeister, L. *Zur Kenntnis der Cellulose und des Lignins*; Doctoral thesis, E. T. H.: Zurich, Switzerland, 1913.
(2) Willstätter, R.; Zechmeister, L. *Ber. dtsch. chem. Ges.* **1913,** *46*, 2401–12.
(3) Willstätter, R.; Zechmeister, L. *Ber. dtsch. chem. Ges.* **1929,** *62*, 722–25.
(4) Willstätter, R.; Zechmeister, L. *Sitzungsber. kgl. preuss. Akad. Wiss.* **1914,** *34*, 866–93.
(5) Willstätter, R.; Zechmeister, L. *Magy. Chem. Foly.* **1919,** *25*, 1–8.
(6) Willstätter, R. *Aus meinem Leben*, 2nd ed.; Verlag Chemie: Weinheim, 1958; pp. 220, 223.
(7) von Hevesy, G.; Zechmeister, L. *Magy. Chem. Foly.* **1920,** *26*, 58–64.
(8) von Hevesy, G.; Zechmeister, L. *Z. Elektrochem.* **1920,** *20*, 151–53.
(9) von Hevesy, G.; Zechmeister, L. *Ber. dtsch. chem. Ges.* **1920,** *53*, 410–15.
(10) Zechmeister, L. *Magy. Chem. Foly.* **1923,** *29*, 1.
(11) Faurholt, C.; Gjaldbaek, J. K.; Zechmeister, L. *Chemiai gyakorlatok* (Chemical Practice), 2nd ed.; Egyetemi Kiadó és Nyomda: Pécs, Hungary, 1932.
(12) Zechmeister, L. *Bevezetés a titrimetriába* (Introduction to Titrimetry); Dunántul Könyvkiadó RT: Pécs, Hungary, 1925.
(13) Zechmeister, L. *Organikus chemia, I-II* (Organic Chemistry); Sylvester Irodalmi és Nyomdai Intézet RT: Budapest, I: 1930, II: 1932.
(14) *Pécsi Orvostudományi Egyetem Évkönyve* (Yearbook of Pécs Medical University); 1971–72; pp. 38–40.
(15) Zechmeister, L.; Cholnoky, L. *Liebig's Ann. Chem.* **1927,** *454*, 54–71.
(16) Zechmeister, L.; Cholnoky, L. *Liebig's Ann. Chem.* **1937,** *530*, 291–300.
(17) Ettre, L. S. In *HPLC—Advances and Perspectives, Vol. 1*; Horváth, C., Ed.; Academic Press: New York, 1980, pp. 1–74.
(18) Lederer, E. *J. Chromatogr.* **1972,** *73*, 261–66.
(19) Lederer, E. In *75 Years of Chromatography—A Historical Dialogue*; Ettre, L. S.; Zlatkis, A., Eds.; Elsevier: Amsterdam, 1979, pp. 237–45.
(20) Tswett, M. S. *Khromofilly v Rastitel'nom i Zhivotnom Mire* (Chromophylls in the Plant and Animal World); Izd. Karbasnikov: Warsaw, 1910.
(21) Palmer, L. S. *Carotenoids and Related Pigments: The Chromolipids*; American Chemical Society Monograph Series; Chemical Catalog Co.: New York, 1922.
(22) Zechmeister, L. In *Handbuch der Pflanzenanalyse*; Klein, G., Ed.; Springer Verlag: Vienna, 1932; Vol. 3, pp. 1239–1350.
(23) Zechmeister, L. *Carotinoide. Ein biochemischer Bericht über pflanzliche und tierische Polyenfarbstoffe*; Springer Verlag: Berlin, 1934.
(24) Zechmeister, L.; Cholnoky, L. *Liebig's Ann. Chem.* **1934,** *509*, 269–87.
(25) Zechmeister, L.; Cholnoky, L. *Die chromatographische Adsorptionsmethode. Grundlagen, Methodik, Anwendungen*; Springer Verlag: Vienna, 1938.
(26) Kirchner, J. G. In *75 Years of Chromatography—A Historical Dialogue*; Ettre, L. S.; Zlatkis, A., Eds.; Elsevier: Amsterdam, 1979, pp. 201–8.
(27) *Bibliography of Papers Published by L. Zechmeister and Co-Authors in the Fields of Chemistry and Biochemistry 1913–1958*; Springer Verlag: Vienna, 1958.
(28) Zechmeister, L.; Cholnoky, L. *Principles and Practice of Chromatography*; translated by Bacharach, A. L. and Robinson, F. A.; Chapman & Hall: London; J. Wiley & Sons: New York, 1941.
(29) Zechmeister, L. *Ann N.Y. Acad. Sci.* **1948,** *49*, 145–60.
(30) Zechmeister, L. *Progress in Chromatography 1938–1947*; Chapman & Hall: London; J. Wiley & Sons: New York, 1950.
(31) *Enzymologia* **1951,** 324.
(32) Zechmeister, L. *Ann. N.Y. Acad. Sci.* **1948,** *49*, 220–34.
(33) Zechmeister, L. *Disc. Faraday Soc.* **1949,** *7*, 54–57.
(34) Zechmeister, L. *Cis-trans Isomeric Carotenoids, Vitamin A and Arylpolyenes*; Springer Verlag: Vienna, 1962.

Leslie S. Ettre received his technical doctorate from the Technical University Budapest. He immigrated to the United States in 1958 and since then, except for a four-year period when he served as the executive editor of the Encyclopedia of Industrial Chemical Analysis, *he has been associated with the Perkin-Elmer Corporation, where he is a senior scientist. He has been active in chromatography since 1957 and is primarily known for his contributions to the development of open-tubular (capillary) columns. He is a recipient of the ACS Award in Chromatography and of the A.J.P. Martin Award of the (British) Chromatography Society.*

TASK MASTER.

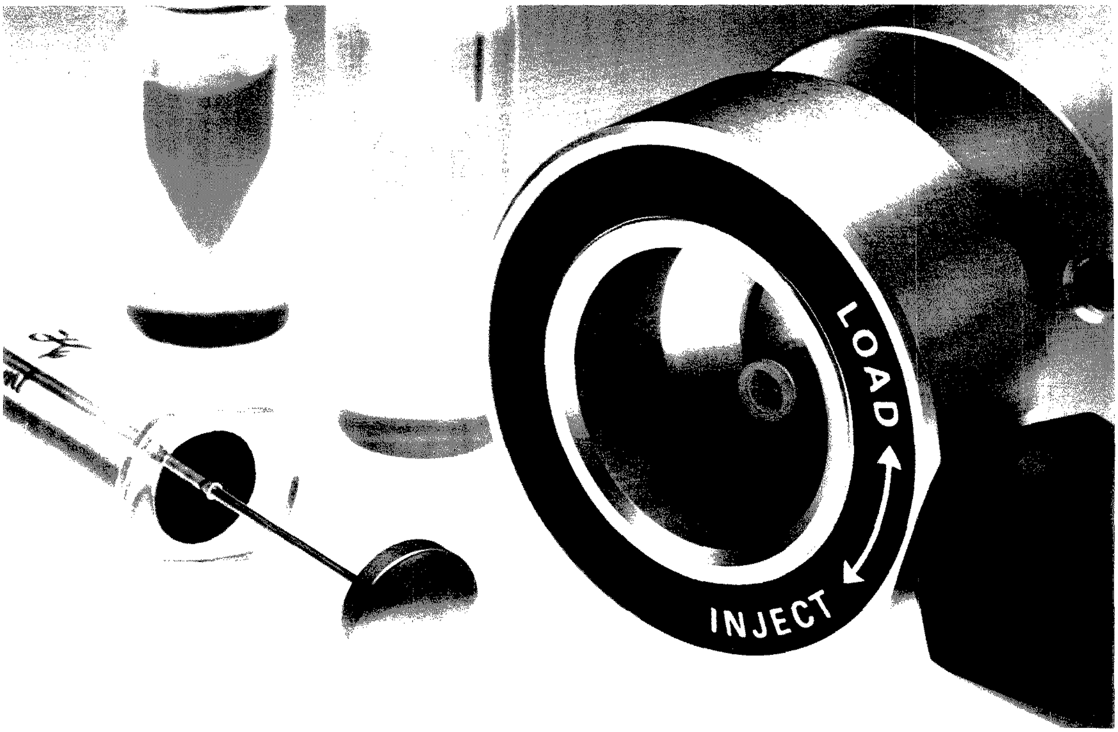

The Rheodyne 7125 LC sample injector is equipped with two operating modes to master every injection task.

In the "partial-fill" mode, the sample from a syringe fills a sample loop only partially. No sample is lost. The amount injected is the exact volume dispensed from the syringe.

You use this mode when you need to conserve sample or change sample volume frequently. You can inject from 1 μL to 2.5 mL with a precision of 1%.

In the "complete-fill" mode, sample from a syringe fills the loop completely–using excess sample. The amount injected is the exact volume of the loop.

You use this mode when you need the maximum volumetric precision of 0.1%, or you wish to load sample without having to read syringe calibrations carefully. You can inject from 5 μL to 5 mL using one of ten interchangeable sample loops.

Variations of the Model 7125 perform yet other tasks. Model 8125 minimizes sample dispersion with micro columns. And Model 9125 uses inert plastic flow passages to prevent the mobile phase from contacting metal.

For more information about these versatile injectors, phone your Rheodyne dealer. Or contact Rheodyne, Inc., P.O. Box 996, Cotati, California, 94931, U.S.A. Phone (707) 664-9050.

CIRCLE 140 ON READER SERVICE CARD

RHEODYNE
THE LC CONNECTION COMPANY

LC/MS Systems for those who hunger to know all they can

EXTREL advanced LC/MS systems technology is satisfying the appetites of scientists, worldwide, whose very existences depend upon their need to know.

These are men and women who, like you, have a deep, abiding concern about how their analyses impact the marketplace, the environment and the world. And they look to EXTREL for answers.

Leaders in LC/MS systems

Here and now in our twenty-fifth year, EXTREL's commitment to solutions has made us a leader in LC/MS systems technology.

In 1986, we proposed an EI LC/MS method to EPA. In 1987, we introduced our ThermaBeam™ LC/MS — the first commercially available particle-beam interface. In 1988, ThermaBeam SFC/MS debuted along with our improved Thermospray design.

And for '89? We're unveiling API LC/MS for ultra-low detection levels and ThermaBeam FAB for ultra-soft ionization at practical LC flow rates.

Solving real-world problems

Who can you ask about EXTREL LC/MS?

People like the R&D director of a major fabric manufacturer who has been solving real-world problems for the past two years with a ThermaBeam LC/MS system. With the wealth of information from his system, he knows more about his products (and his competitors') than ever before.

Backed by the inventors

Those who are faced with the seemingly unanswerable turn to us for answers.

They know that no other manufacturer of LC/MS systems offers scientists such a complete menu of inlet choices as EXTREL. They know that we're the only manufacturer that provides systems which are truly upgradable. They also know that the ThermaBeam Team who invented our LC/MS technology is behind them with technical support.

Whet your appetite. Circle the number below to receive important information which highlights our latest developments and how an EXTREL LC/MS system can satisfy your need to know.

EXTREL

Manufacturers of Mass Spectrometers for 25 Years

240 Alpha Drive, P.O Box 11512, Pittsburgh, PA 15238 USA
Tel: (412) 963-7530 Telex: 812 316 EXTRALAB Fax: (412) 963-6578

ThermaBeam is a trademark of Extrel Corporation.

CIRCLE 50 ON READER SERVICE CARD

PHILIPS

Philips – analytical solutions worldwide

Philips Analytical

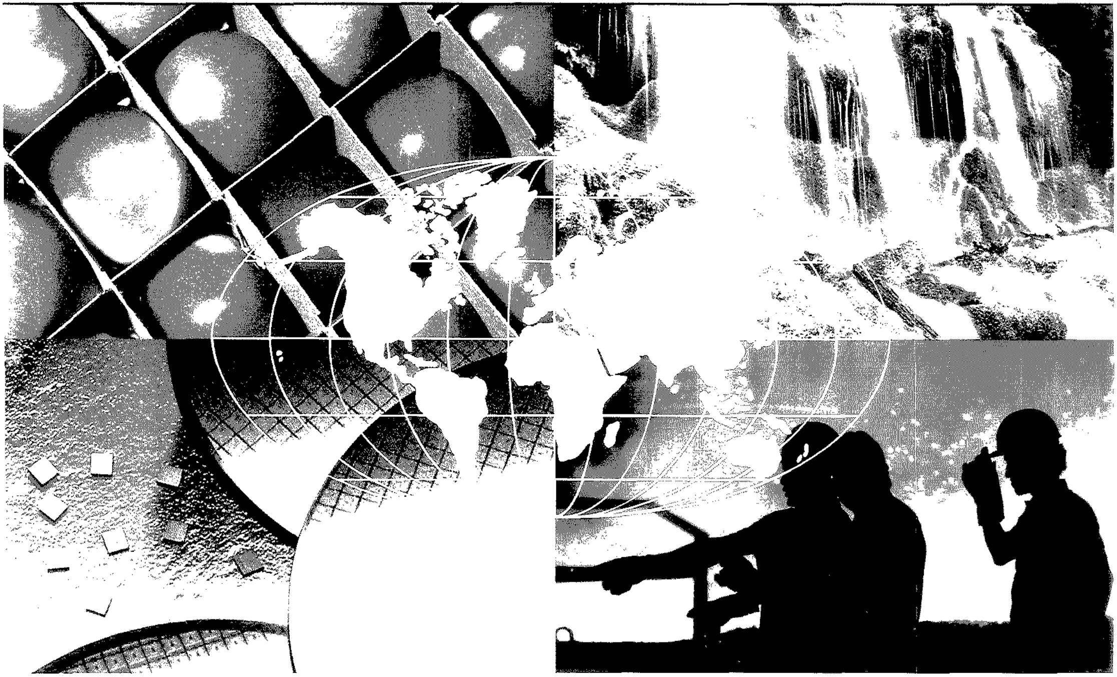

Philips Analytical is accustomed to providing solutions. We've been doing it for a great many years. And today, more than ever before, our wide range of analytical products (in fact, the widest of any manufacturer) offers solutions to the most difficult problems; in materials research, in life sciences – in a whole range of other industries – worldwide from Stockholm to Sydney and Toronto to Tokyo.

Beyond our instruments we care for our customers with after-sales service and support, training facilities and a presence in 55 countries. This unique global network enables us to provide comprehensive applications advice, rapid on-site maintenance and superb technical back-up.

For more information on our complete range of instrumentation and other analytical services use the reader reply service or contact us at the address below.

X-ray fluorescence spectrometry (Simultaneous/Sequential)

Optical emission spectrometry (Arc Spark/ICP – Simultaneous/Sequential)

Spectrometry (AA/UV-vis/IR)

Chromatography (LC/GC)

Electron microscopy (SEM/TEM/STEM)

X-ray diffraction

Electrochemistry

EDAX (Integrated Microanalysis Systems)

So when *you* need a complete analytical solution – call Philips.

PHILIPS ANALYTICAL - *BIGGER IDEAS FOR BETTER ANALYSIS*

Philips Analytical, I&E Department, Building HKF (Room 53), Eindhoven, The Netherlands Tel +31 40 785213

CIRCLE 125 ON READER SERVICE CARD

CA01a

Here's Why Two Esteemed, Technical Societies Want *Your* Expertise...

The American Chemical Society & American Institute of Chemical Engineers
Announce their 1990 co-publication of

BIOTECHNOLOGY PROGRESS

Editor, Jerome S. Schultz, *University of Pittsburgh*

SUBMIT YOUR PAPERS NOW TO THIS IMPORTANT "NEW" PUBLISHING MEDIUM

Beginning January 1990 BIOTECHNOLOGY PROGRESS, a well-established journal of the American Institute of Chemical Engineers, will become a joint publication of the American Chemical Society and AIChE. As a collaborative effort, several significant changes will occur, ***providing enhanced editorial coverage and expanded readership.*** These include:

- **Accelerated frequency** — from quarterly to bimonthly issues!
- **A redesigned format** which will better meet the needs of both new and current subscribers.
- **A redefined editorial focus** guaranteed to attract:
  1) additional topical papers and primary research findings
  2) an audience comprising the very experts ***you*** want to reach!

ATTENTION CHEMISTS, LIFE SCIENTISTS, AND ENGINEERS!

In bimonthly issues, BIOTECHNOLOGY PROGRESS will provide the latest concepts — in genetics...microbiology and biochemistry...molecular and cellular biology...chemistry and chemical engineering — as they apply to the development of processes, products, and devices. Emphasis will be placed on the ***application of fundamental engineering principles*** to the ***analysis*** of biological phenomena involved.

BIOTECHNOLOGY PROGRESS will be of particular interest to ***practitioners of R&D in process development, product development, and equipment/instrumentation design for the biotechnology/bioprocess industry.*** Its coverage will encompass food, pharmaceutical, and biomedical arenas.

LOOK FOR HIGHLY TARGETED TOPICS LIKE THESE

- **Applied Biochemistry:** Equilibrium data, protein conformations in solution, mapping of molecular surfaces.
- **Applied Molecular Biology***:* Cell physiology, gene expression, protein transport, metabolic engineering.
- **Bioreactor Technology:** Reactor engineering, mechanical engineering, materials science, process control, biosensors.
- **Biocatalytic Processes:** Site specific mutagenesis, enzyme minetics, cofactor regeneration, applied pharmaceutical minetics.
- **Formulation and Product Delivery.**
- **Bioanalysis:** Online monitoring, containment, containment monitoring, offline analysis, statistical analysis (nonlinear regression, multifactor analysis).
- **Bioseparations.**

ADDRESS YOUR MANUSCRIPT SUBMISSIONS & AUTHOR INQUIRIES TO:

Jerome S. Schultz
Editor, BIOTECHNOLOGY PROGRESS
Center for Biotechnology and Bioengineering
University of Pittsburgh
911 William Pitt Union
Pittsburgh, PA 15260
Telephone: 412/648-7956 Fax: 412/624-7145

To receive editorial updates please write:
American Chemical Society, Marketing,
BIOTECHNOLOGY PROGRESS, Room 609,
1155 Sixteenth St., N.W., Washington, D.C. 20036
FAX: 202/872-6005
Telex: 440159 ACSP UI or 89 2582 ACSPUBS

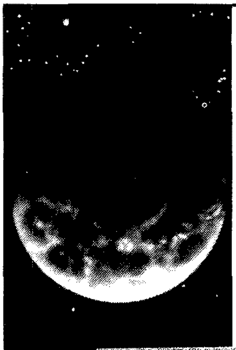

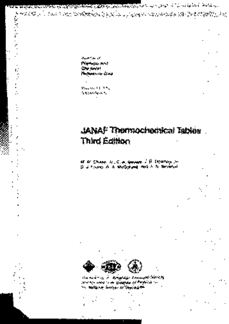
JANAF Thermochemical Tables
Third Edition

JANAF THERMOCHEMICAL TABLES

Third Edition

A Major Supplement from JOURNAL OF PHYSICAL AND CHEMICAL REFERENCE DATA

Presenting Reliable Data Utilized by Chemists, Chemical Engineers, and Materials Scientists from Around the World for Over 25 Years

JOURNAL OF PHYSICAL AND CHEMICAL REFERENCE DATA is very pleased to publish the Third Edition of the JANAF THERMOCHEMICAL TABLES.

Since the first version appeared 25 years ago, the JANAF THERMOCHEMICAL TABLES have been among the most widely used data tables in science and engineering. You'll find:

- Reliable tables of thermodynamic properties of substances of wide interest
- A highly professional approach with critical evaluations of the world's thermochemical and spectroscopic literature
- A concise and easy-to-use format

This Third Edition presents an extensive set of tables including thermodynamic properties of more than 1800 substances, expressed in SI units. The notation has been made consistent with current international recommendations.

There is no other reference source of thermodynamic data that satisfies the needs of such a broad base of users.

Order your 2-volume set of the JANAF THERMOCHEMICAL TABLES today! You'll get over 1890 pages of valuable information that is crucial to your research—in two hardback volumes.

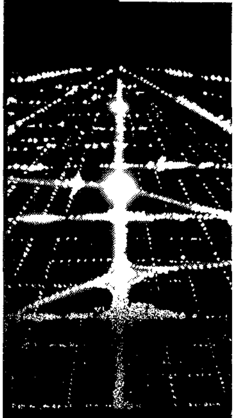

Editors:
M.W. Chase, Jr.
National Institute of Standards and Technology
C.A. Davies
Dow Chemical U.S.A.
J.R. Downey, Jr.
Dow Chemical U.S.A.
D.J. Frurip
Dow Chemical U.S.A.
R.A. McDonald
Dow Chemical U.S.A.
A.N. Syverud
Dow Chemical U.S.A.

SUBSCRIPTION INFORMATION

The JANAF THERMOCHEMICAL TABLES, THIRD EDITION is a two-volume supplement of *Journal of Physical and Chemical Reference Data.*

1896 pages, 2 volumes, hardcover
ISBN 0-88318-473-7
Supplement Number 1 to Volume 14, 1985

U.S. & Canada	$130.00
All Other Countries	$156.00
(Postage included.)	

All orders for supplements must be prepaid.

Foreign payment must be made in U.S. currency by international money order, UNESCO coupons, U.S. bank draft, or order through your subscription agency. For rates in Japan, contact Maruzen Co., Ltd. Please allow four to six weeks for your copy to be mailed.

For more information, write **American Chemical Society**, Marketing Communications Department, 1155 Sixteenth Street, NW, Washington, DC 20036.

In a hurry? Call TOLL FREE 800-227-5558 and charge your order!

Published by the **American Chemical Society** and the **American Institute of Physics** for the **National Institute of Standards and Technology**

NUPRO Valves and Filters for Analytical Applications

NUPRO Valves and Filters offer these design and performance choices:

- **End Connections:** SWAGELOK® Tube Fittings, NPT, Tube Stub, Weld, CAJON VCO® & VCR®
- **Service Ratings:** vacuum to 6000 psi; temperatures to 900°F

STOCKED FOR IMMEDIATE DELIVERY BY AUTHORIZED SALES AND SERVICE REPRESENTATIVES.

Nupro Company, 4800 East 345th St.,
Willoughby, OH 44094

NUPRO®
A SWAGELOK COMPANY

SWAGELOK — TM Crawford Fitting Company
CAJON, VCO & VCR — TM Cajon Company
© 1986 Swagelok Co., all rights reserved N-56

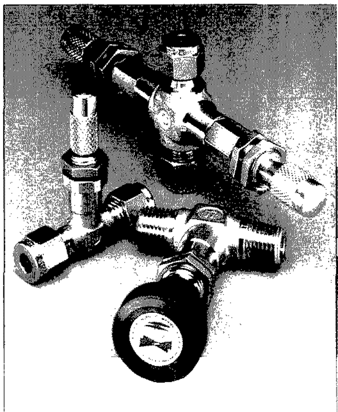

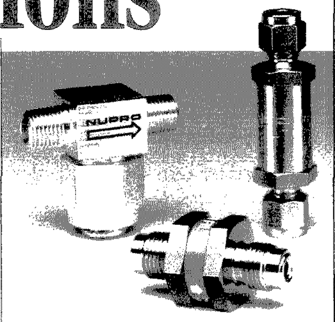

FILTRATION

Inline and tee type filters to protect instruments by removing hard particle contamination from fluid lines

- choice of sintered and wire mesh elements from 0.5 to 440 microns
- compact designs
- all metal construction

METERING

Valves for precise flow control in laboratory and instrument systems

- accurate, repeatable flow adjustment with no initial surge
- compact, low dead space
- stem threads removed from system

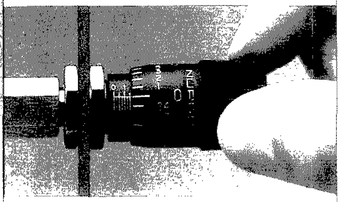

SHUT OFF

Compact valves for reliable flow regulation and shut off

- stem threads removed from system fluid
- compact designs
- ball tip or regulating stems

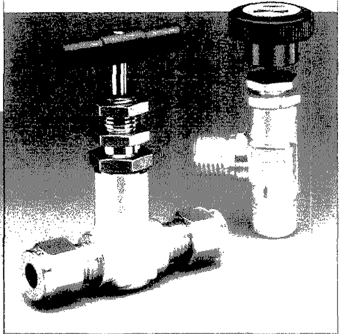

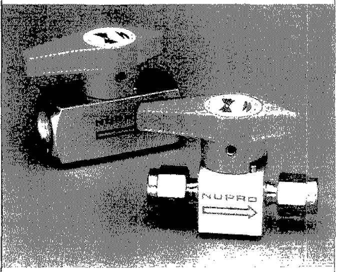

- quick-acting, 1/4 turn
- full flow
- easy maintenance

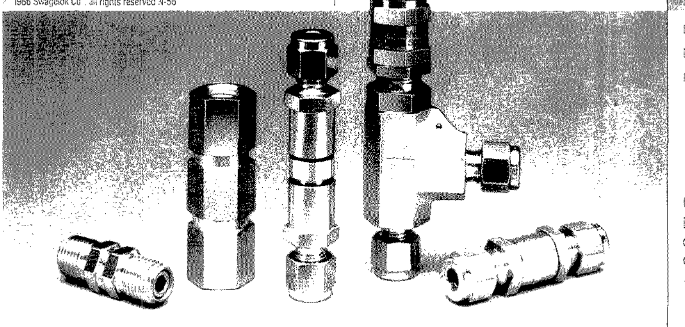

CHECK & RELIEF

Relief valves open at pre-set pressure; check valves allow unidirectional flow control

- cracking pressures 1/3 to 6000 psi
- smooth floating poppet
- positive back stop

CIRCLE 152 ON READER SERVICE CARD

The First International Symposium on Field-Flow Fractionation

Sharon Kraus
Rohm and Haas Company Research Laboratories
727 Norristown Road
Spring House, PA 19477

The First International Symposium on Field-Flow Fractionation (FFF), sponsored by the University of Utah's Field-Flow Fractionation Research Center, convened June 15 and 16 in Park City, UT. The meeting attracted 80 academic and industrial scientists from Europe, Asia, Australia, and the United States. Representing diverse interests in FFF technology, the group ranged from researchers working on the theory and fundamental development of techniques to those applying FFF to the characterization and separation of polymers, biological materials, and particulates.

During these busy two days, the mood of the participants reflected the excitement of being involved in an emerging technology. According to Jack Kirkland of Du Pont, the current state of FFF development is comparable to the early days of high-performance liquid chromatography. Coincidentally, the 23 papers presented at this symposium equaled the number presented at the First International Symposium on Chromatography in 1963.

Reports on the theoretical developments and applications of sedimentation field-flow fractionation (SdFFF) predictably were most abundant, because SdFFF is the best understood of all the FFF techniques and is commercially available. Mark Schure of Rohm and Haas presented an elaborate computer modeling of secondary flow in the SdFFF channel. This secondary flow is the result of the Coriolis Force, which arises when a fluid flows relative to a rotating frame of reference. He described the effect as a wave in the flow stream, which causes a dispersion of the zones. The result is that some of the retained material elutes too soon. Schure suggested that experimentalists look for solute in the void volume peak. As his model confirmed and experimentalists determined, this effect can be minimized by using thin rectangular separation channels with high-aspect ratios.

In another session devoted to wall effects and perturbations at the accumulation wall, Dominique Maes, from Limburgs Universitair Centrum in Diepenbeek, Belgium, described theoretically the fundamental characteristics of particles flowing in an FFF channel. Edward Schmauch of Du Pont, focusing on an application, provided an analytical solution for steric relaxation effects for TiO_2 particles in a SdFFF channel.

Nonideal retention behavior in SdFFF from particle wall interactions was discussed by Marcia Hansen of Procter & Gamble. She showed that the electrostatic interactions between sample particles and the FFF channel wall were a function of carrier strength and sample size as well as other parameters such as field strength and the channel wall material. Perturbations to standard retention behavior were theoretically treated by including the electrostatic forces in the retention equation. Peak shape in SdFFF as a function of various experimental parameters was studied by Francesco Dondi of the University of Ferrara, Italy. Dondi used peak shape analysis to quantify overloading effects and to discriminate between overloading and other nonideal effects.

Applications of SdFFF continue to become more diverse. For instance, FFF is finding a special niche in environmental studies. Methodologies to fractionate and size colloidal particles extracted from river waters using SdFFF were presented by Ron Beckett of the Chisholm Institute of Technology in Australia and Pierluigi Reschiglian of the University of Ferrara. Howard Taylor, from the U.S. Geological Survey in Denver, CO, used inductively coupled plasma mass spectrometry as a detector for inorganic materials separated by SdFFF. Although this particular system is expensive, the idea of connecting various detectors to an FFF system could greatly extend the applications. In general, environmental analyses present some difficult applications for which the separation capabilities of FFF methods—both SdFFF and flow FFF—are shown to be uniquely suited.

FOCUS

0003-2700/89/A361-1329/$01.50/0
© 1989 American Chemical Society

Applying FFF to latex and other emulsion polymers involves much more than just determining particle size distributions. Bhajendra Barman of Utah's FFF Center used SdFFF to identify aggregated latex particulates. John Ho of the University of Utah presented methods for estimating the thickness of an adsorbed layer on colloidal particles. Ho—along with Dennis Nagy from Air Products & Chemicals—applied SdFFF to the determination of the densities of materials, whereas Milton McDonnell from Allied-Signal used SdFFF to characterize the size and density of a complex polyethylene copolymer wax emulsion.

One area of active interest is the use of thermal FFF (TFFF) for characterizing polymers. This powerful new method for quantifying the molecular weight distribution of soluble organic polymers extends to a higher molecular weight range than do more conventional methods. Retention in TFFF is believed to be dependent on the ordinary diffusion coefficient D as well as the thermal diffusion coefficient D_T. D_T is a difficult parameter to assess, and the physicochemical parameters governing the thermal diffusion of polymers in solution are not well understood. Without an understanding or knowledge of D_T for various polymer systems, it is difficult to predict retention in TFFF experiments under a variety of operating conditions.

In an empirical approach to this problem, Kirkland studied retention effects in TFFF over a range of experimental conditions and offered better definitions of the limitations of the method. He also presented techniques for conducting more effective TFFF experiments. Kirkland suggested that TFFF has other potential applications that follow from determining Mark–Howink constants for calculating the radius of gyration of molecules and intrinsic viscosity distributions.

For polymers with a known value of D_T, Yushu Gao of Academia Sinica in Beijing, China, described a universal calibration procedure that holds for a single set of experimental conditions. Martin Schimpf, Bend Research, used TFFF as a method for determining D_T of polymers, and Marcus Meyers of Utah's FFF Center pointed out that large errors in determined molecular weights can arise from inexact D and D_T values.

Many researchers believe that applications for biological materials will be important to the future success of commercial SdFFF instrumentation because the number of potential users in this market could be greater than those for industrial applications. In one example, Samuel Mozersky of the U.S. Department of Agriculture used SdFFF to determine the effect of sucrose and lactose on the size of casein micelles. Most of the other biological applications rely on alternate fields or hybrid techniques. Examples include fractionation of living blood cells by gravitational FFF, reported by Michel Martin from Ecole Supérieure de Physique et Chimie Industrielles in Paris, and the separation of B and T immune system cells using a hybrid of cellular adhesion chromatography and FFF, presented by James Bigelow from the University of Vermont.

Flow FFF appears to be another promising subtechnique with a broad range of applications. Kim Ratanathanawongs of Utah's FFF Research Center described the development and applications of flow FFF in particle characterization. Separation of particles is based on size and is independent of density,

THE UNIVERSITY OF DAYTON RESEARCH INSTITUTE
ENVIRONMENTAL SCIENCES

- TOXIC WASTE INCINERATION
  - INCINERABILITY TESTING
  - BY-PRODUCT IDENTIFICATION
  - TRIAL BURN SUPPORT
- THERMAL STABILITY
  - FIRE SAFETY
  - EVOLVED GAS ANALYSIS
  - LAB-SCALE PROCESS SIMULATION
- ANALYTICAL SERVICES
  - GC-FID/MS/FTIR
  - CUSTOM ANALYSIS
  - TGA

The University of Dayton
ENVIRONMENTAL SCIENCES GROUP
RESEARCH INSTITUTE
300 College Park
Dayton, Ohio 45469-0001
(513) 229-2846

CIRCLE 32 ON READER SERVICE CARD

Pyrolysis Oils from Biomass
Producing, Analyzing, and Upgrading

Provides a timely and necessary update on the latest research—from feedstock to upgraded liquid fuels suitable as replacements for petroleum-derived fuels. Looks at the state of the science in the complete fuel cycle. Discusses biomass pyrolysis and its place in a renewable fuel economy. Presents the technology of pyrolysis oil production. Also offers analysis of the oils. With 27 chapters, coverage includes topics on • characterization • kinetics • chromatographic techniques and more. Concludes with seven chapters on upgrading pyrolysis oils to liquid fuels.

Serves as a collaborative effort to combat the long-term rise in CO_2 levels resulting from deforestation and the burning of fossil fuels. Specialists from five countries contributed the results of their research. A must for anyone interested in the progress in pyrolysis oil production as a long-term solution to the need for a renewable source of liquid transportation fuels.

Ed J. Soltes, *Editor*, Texas A&M University
Thomas A. Milne, *Editor*, Solar Energy Research Institute
Developed from a symposium sponsored by the Cellulose, Paper, and Textile Division and the Division of Fuel Chemistry of the American Chemical Society

ACS Symposium Series No. 376
ISBN 0-8412-1536-7 LC 88-24172
353 pages (1988) Clothbound
US & Canada $74.95 Export$89.95

Order from: American Chemical Society, Distribution Office, Dept. 03
1155 Sixteenth St., N.W., Washington, DC 20036
or CALL TOLL FREE 800-227-5558
(in Washington, D.C. 872-4363) and use your credit card!

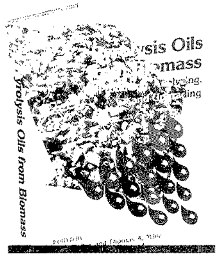

which has potential advantages over sedimentation-based techniques. A novel approach to solving the problem of channel deformation in flow FFF was described by Karl-Gustav Wahlund of Sweden's Uppsala University Biomedical Center. He used an asymmetrical flow FFF channel with a single permeable wall. For the other wall, Wahlund replaced the porous plate—used in a normal symmetrical flow FFF channel—with a glass plate. This approach yielded rapid separations for a broad range of biological samples including proteins, viruses, plasmids, and plasmid fractions. Particularly significant was the separation of plasmids within minutes rather than the hours required for standard gel electrophoresis. Finally, Alf Carlshaf from the University of Lund in Sweden successfully substituted a circular geometry (small porous capillaries) for the usual rectangular shape in flow FFF.

Talks focusing on new technologies offered a valuable opportunity for researchers to interact and exchange ideas on experimental strategies and the characteristics of the technology. Two papers that prompted much discussion were Karin Caldwell's description of a useful experimental approach using SdFFF for the analysis of colloids with very broad distributions and J. C. Giddings' consideration of techniques to optimize the performance of FFF. Both researchers are associated with the University of Utah.

Optimization of FFF is a broad topic. Giddings' objective was to outline some global optima, discuss how they could be achieved, and describe the associated trade-offs. He targeted three main criteria for choosing an FFF technique: applicability, instrument availability, and selectivity (basis of technique and magnitude). As an example, Giddings compared SdFFF with flow FFF. SdFFF is useful for particles $< 1\ \mu m$ and is sensitive to particle density, whereas flow FFF is applied to particles $> 1\ \mu m$ and is independent of particle density. Various forms of field programming, including the time-delayed exponential decay used by Du Pont and the power program developed at the University of Utah, were included in the discussion. The flexibility of FFF techniques, and the wide variety of experimental parameters that can be altered within techniques, leads to many choices and, consequently, researchers must make many compromises.

The recent Park City FFF symposium and possible future symposia may contribute to worldwide progress in FFF theory, instrumentation, and applications. In addition, they should assist the important transfer of FFF technology to the international, academic, and industrial communities.

Sharon Kraus is a scientist with the research laboratories of Rohm and Haas, Springhouse, PA. She was formerly with the analytical research department. Her interests include developing methods for particle characterization using SdFFF. She received her B.A. degree in chemistry from Temple University in Philadelphia.

PROGRAMMING/DIGITAL/ANALOG
TEMPUNIT® & TEMPETTE®

Bath/Circulators

THE *ORIGINALS* AND STILL THE BEST

Once you buy a Techne Bath/Circulator, either an original Tempunit or the Tempette, you'll never want to own any other. Reports from our own customers prove that over 98% recommend our circulators to their colleagues. That's why we sell the same customers over and over again and why our customer base is continuously expanding. The reason? In two words: Reliability and Performance. When you receive our catalog, check the specification *and price* with the leading competition and talk to your colleagues. Then your choice will be 'no choice'. Because the Tempunit and Tempette Bath/Circulators are clearly the best.

TRANSFORM YOUR BATH INTO A PRECISE THERMOSTATIC SYSTEM

AT CONSTANT TEMPERATURE

Techne
Tempette TE-8D
RB-12
Techne
TU-16D
Techne

TECHNE INC./3700 Brunswick Pike, Princeton, NJ 08540/Phone (609) 452-9275/Fax (609) 987-8177/Telex 4971718

CIRCLE 156 ON READER SERVICE CARD

NEW

THE MERCK INDEX Eleventh Edition

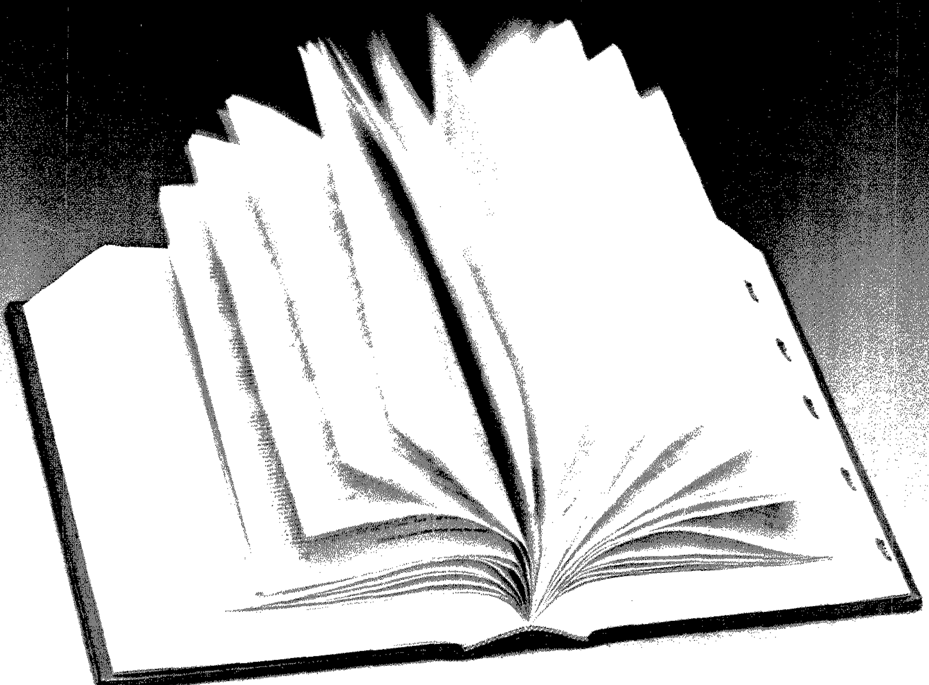

Keeping pace with chemistry and biochemistry...
for over 100 years

Since 1889, *The Merck Index* has provided pertinent, authoritative information of interest to scientists the world over. Now we are pleased to present the newly published Eleventh/Centennial Edition. This special leather-bound edition provides expanded coverage of therapeutically important biotechnology products, agriculturals and compounds of environmental impact, and features an entirely new therapeutic category/bioactivity index as well as CAS Registry Number indices. And you'll find information on more than 10,000 significant drugs, chemicals, and natural substances.

To order, call toll-free 1-800-999-3633, extension 750 (VISA or MasterCard only) or complete the coupon.

NEW

THE
CENTENNIAL
EDITION

THE
MERCK
INDEX

Merck & Co., Inc., a research-intensive company, publishes *The Merck Index* as a non-profit service to the scientific and medical communities.

CIRCLE 98 ON READER SERVICE CARD

Enclosed is my payment for $35.00 for the Eleventh/Centennial Edition of THE MERCK INDEX. I will not be charged for shipping.

☐ Check enclosed. Make check payable to Merck & Co., Inc.　☐ VISA　☐ MasterCard

Card No.　Exp. Date

Signature

Name

Address

City

State　Zip

Please allow four to six weeks for delivery.

Merck & Co., Inc.
Professional Handbooks
Department 750
P.O. Box 2000
Rahway, NJ 07065-0901

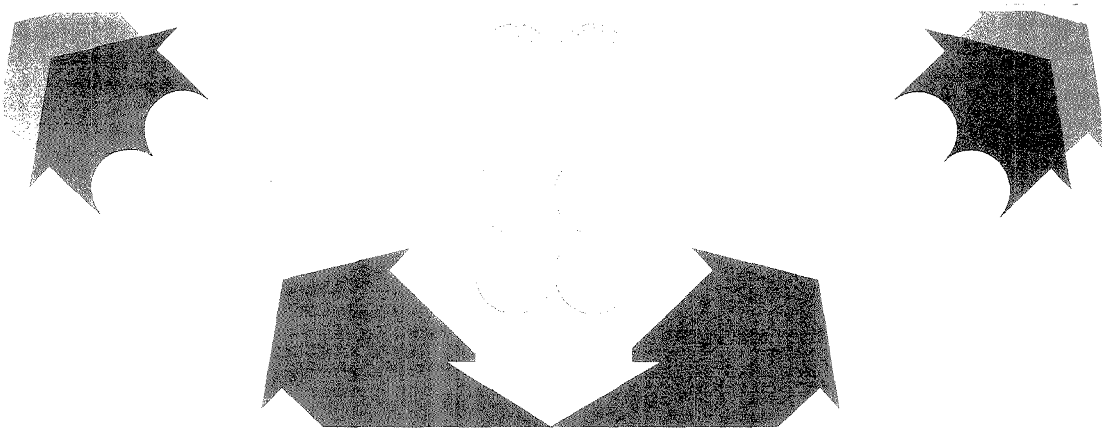

SURFACE SCIENCE IN ANALYTICAL CHEMISTRY

Fred M. Hawkridge and Joseph A. Gardella, Jr.
Chemistry Division
National Science Foundation
Washington, DC 20550

The 42nd Annual Summer Symposium of the ACS Division of Analytical Chemistry was held July 23–26 at Virginia Polytechnic Institute and State University in Blacksburg, VA. According to general chairman Harold M. McNair of Virginia Tech and program chairman Richard W. Linton of the University of North Carolina at Chapel Hill, the topic was chosen to bring together leaders in the traditional subdisciplines of analytical chemistry (electrochemistry, spectroscopy, and separations) through their common interests in surface science.

In opening the two-and-one-half-day symposium, Rich Linton and his program committee co-chairman Paul W. Bohn of the University of Illinois pointed out that the invited speakers were chosen to illustrate the exciting science being done by both the younger and the more established investigators in the discipline. The high level of creativity and innovation evident in the research described in this program was clearly and forcefully conveyed. Everyone shared the sense of excitement about the present and future of analytical chemistry that has become the hallmark of the Division's summer symposia. We strongly encourage graduate students and other scientists to plan now to attend next year's summer symposium on mass spectrometry, which will be held July 24–27 in Oak Ridge, TN. The summer symposium is a marvelous opportunity to learn about a topical area in analytical chemistry at a very informal, yet intensive, meeting.

The aims of the conference chairmen were successfully met by four invited lecture sessions and a contributed poster session. The first session, chaired by Joe Gordon of IBM's Almaden Research Center, covered the topic "Surface Science of Electrochemistry," including basic work on metal surface structure as well as modifications and in situ probes of electrode structure. Alan Campion of the University of Texas chaired the next session on "Optical Probes of Surfaces." Methods discussed included the use of nonlinear optics, real-time ellipsometry, optical waveguides, Raman spectroscopy, and quantitative IR reflection spectroscopy.

FOCUS

A session on "Electron and Ion Spectroscopy/Microscopy of Surfaces" was chaired by Joe Gardella and Rich Linton. Talks emphasized the quantification and improved spatial resolution aspects of the exciting techniques in chemical and structural analysis that are either now available or are on the horizon. The final session, chaired by John Dorsey of the University of Cincinnati, covered "Surfaces in Separations Science" and included a host of novel developments in the ability to design, characterize, and use chromatographic interfaces.

Topics covered in the contributed poster session complemented the invited papers. Harold McNair and Rich Linton chaired this session, which was held Monday evening in conjunction with a wine and cheese reception.

Surface science of electrochemistry

Opening the Monday morning session was Wayne Goodman of Texas A&M University. He talked about the extraordinary differences in surface chemistry and catalytic reactions that can be realized by preparing controlled monolayer and submonolayer structures of one metal on a different bulk metal substrate. For example, decreasing surface coverage of Ni on a W(110) metal substrate increases the rate of ethane hydrogenolysis as more single-nickel low-coordination sites are prepared.

Andrew Gewirth of the University of Illinois described dynamic in situ scanning tunneling microscopic studies of electrode surfaces during electrochemical reactions. Data can be acquired at a rate greater than 20 Hz in the constant height mode, but problems of thermal drift in aqueous samples must be considered. The exciting possibilities of following structural changes in situ during electrode reactions were tempered by a discussion of the details needed to develop the STM experiment. These experiments are neither as easy as they seem nor as conceptually simple to interpret as the images may appear.

Next, Joe Gordon described in situ results from fluorescence-detected surface-extended X-ray absorption fine structure (EXAFS) and grazing incidence X-ray scattering spectroscopic studies of surfaces prepared by underpotential deposition (UPD) (e.g., ad-

0003-2700/A361-1333/$01.50/0
© 1989 American Chemical Society

layers on Au(111)). Predicted hexagonal two-dimensional structures are found for thallium and lead adlayers; adsorbed bromides reveal a more complicated structure, and a UPD monolayer of Ag shows perchlorate ion and water molecule decorations.

Jacek Lipkowski of the University of Guelph then talked about the structure of adsorbed organic molecules at polycrystalline and low-angle, single-crystal gold surfaces. Using concepts such as traditional surface excess, Lipkowski discussed the relationship between the number of voltammetric cycles applied to an electrode and adsorption coverage. As surface roughness increases, the range of potential over which adsorption occurs increases.

The morning session concluded with a talk by Rick McCreery of The Ohio State University on the use of in situ spectroscopic probes for examining and controlling the surface microstructure of carbon electrodes. In situ laser activation of carbon surfaces has been shown to increase rates of heterogeneous electron transfer by up to 7 orders of magnitude for a variety of model redox couples. The surface structure of carbon—specifically, edge plane density, surface roughness, and surface cleanliness—contributes to this remarkable alteration in rates of heterogeneous electron transfer. Understanding of these mechanisms has led to models of glassy carbon surface structure in relation to highly ordered pyrolytic graphite and to subsequent laser surface treatments.

Optical probes of surfaces

Monday afternoon's session began with Geraldine Richmond of the University of Oregon. Her talk, "Nonlinear Optics and the Single-Crystal Electrode Surface," described the nonlinear optical properties, potential dependent surface stabilities, and structure of single-crystal silver, copper, and gold electrodes. Sorting out these structural effects on the time-domain measurements involved in the use of second-harmonic generation (SHG) must be done before chemical interrogation can be accomplished with SHG. Real-time measurements of thin-film growth were discussed.

Robert Collins of The Pennsylvania State University then spoke about the use of spectroscopic ellipsometry (SE) as a real-time probe for surfaces and thin-film growth. Details of the necessary signal processing and instrumentation were described. For example, incorporation of optical multichannel detection in SE allows the acquisition of measurements with a time resolution of 50 ms. The approach was illustrated by Collins' work on amorphous silicon formation.

The next talk, by Paul Bohn, described approaches for determining the tilt angle of uniaxially bound adsorbates on dielectric optical waveguides using linear dichroism measurements and on sputtered oxide surfaces using internal-reflection excited Raman scattering. Complementary information on the orientation of the electron transition moment obtained from the former method and the molecular polarizability ellipsoid data from the latter method were described.

Alan Campion then described the use of Raman spectroscopy in studies of molecular adsorbates at surfaces. The utility of the unenhanced Raman signal in heterogeneous catalysis, electrochemistry, and thin organic polymeric films was presented.

The final talk, by Dave Allara of The Pennsylvania State University, concerned his use of IR wavelength reflection spectroscopy for the quantitative analysis of organic interfaces. Allara detailed some of the theoretical approaches that have allowed quantitative determination of structure in films. Results of his careful experiments of anisotropic films on nonmetallic substrates were presented, and the development of physical models for quantifying the structure of films with biaxial symmetry (e.g., single-crystal Langmuir–Blodgett films) was introduced. Applications to possible problems in glass surface chemistry were projected.

Electron and ion spectroscopy/microscopy of surfaces

Neal Armstrong of the University of Arizona opened the Tuesday morning session with a talk on quantification using Auger electron and X-ray photoelectron spectroscopies, the subject of a recent A-page article (*Anal. Chem.* **1989**, *61*, 469 A). Armstrong discussed the difficulties in determining the necessary instrumental and system parameters when one attempts to quantify surfaces by these methods alone. One approach, developed in Armstrong's laboratories, involves the determination of band shapes for quantitative ESCA curve resolution derived from electron energy loss spectroscopy using an external beam of electrons. The limits of quantification of ESCA and Auger spectroscopies were explored with examples from metal and oxide surface chemistry. New approaches to describing layered chalcogenide material surfaces and their use as standard materials were also described.

Jean-Jacques Pireaux of the Facultés Universitaire Notre-Dame de la Paix in Namur, Belgium, has long been concerned with the study of organic and polymeric surfaces by electron spectroscopy. He described, with examples, the types of qualitative and quantitative information available from ESCA analysis of polymer surfaces and the possibility of electron-induced vibrational spectroscopy (HREELS) of such samples.

Joe Gardella's talk on ion spectroscopy of organic and polymeric surfaces followed. The application of secondary ion mass spectrometry (SIMS) to the study of Langmuir–Blodgett monolayers and multilayers has revealed that the common molecular ion formation mechanisms at these surfaces may involve simple proton transfer in structured systems. New developments in the quantification of molecular ions from static SIMS were illustrated using LB film model systems. Orientation of polymer surface functional groups can also be ascertained using ion scattering spectrometry (ISS).

Christopher Becker of Stanford Research Institute International described a new time-of-flight MS surface analysis technique using laser-based photoionization of sputtered neutrals (surface analysis by laser ionization, SALI). Because most of the species sputtered or desorbed from a surface are neutral, ion formation using laser ionization affords a means of producing gas-phase ions for mass analysis. Single-photon ionization of organic molecules using a 118-nm UV laser is more desirable for organic and polymeric surfaces than nonresonant multiphoton ionization schemes developed previously for atomic species. Applications include catalytic systems and polymers, which show fragmentation directly related to monomer structure.

Rich Linton discussed the three-dimensional imaging of the near-surface chemical composition with high-resolution ion microscopy-based SIMS. In addition to the important applications in electronic materials characterization, emerging applications include the characterization of entire microelectronic devices, polymeric fibers, and composites. Linton described the analytical limits of small-area imaging in terms of signal-to-noise ratio and ion yield, and he discussed possible new developments in instrumentation and post-ionization as well as their effects on ion microscopy.

Michael Kersker of JEOL U.S.A., Inc., concluded the afternoon session with a paper on "Electron Microscopy in Surface Analysis." He described the special problems encountered in obtaining high-resolution (i.e., atomic scale) images of small areas in transmission electron microscopy. Ultra high vacuum and the use of reflection imaging and through-surface imaging have served to meet some of these requirements.

Surfaces in separations science

Leading off the final session on Wednesday morning was Sarah Rutan of Virginia Commonwealth University, who spoke about the use of UV–vis and fluorescence solvatochromic methods for characterizing TLC and HPLC stationary phases. Multiple internal-reflection spectroscopy is being used to sample only the near-surface region of approximately 100–200 μm.

Harold McNair presented the next paper on surface effects of capillary GC performance. Use of silanol-deactivating reagents such as chlorosilanes, disilazanes, cyclic siloxanes, and pyrolyzed polyethylene glycols produces capillary columns that can be used to determine trace levels of amines. He illustrated the use of classical surface energy/tension methods (i.e., the Zisman contact angle approach) to determine the surface characteristics of stationary-phase materials.

William Cooper of Florida State University then discussed the use of inverse, heterogeneous gas–solid chromatography for characterizing LC-bonded phases. Adsorbate–adsorbent interaction energies are calculated from the pressure dependence of retention volumes. A surface polarity scale and a surface selectivity triangle have been developed that are analogous to the Rohrschneider scale and the Snyder solvent selectivity scheme, respectively.

"Derivatization and Characterization of Chromatographic Surfaces" was the topic of the next presentation, by John Dorsey. By using ultrasound to derivatize silica surfaces, higher chain-packing densities have been achieved. Dill's theoretical predictions for reversed-phase retention show good agreement with the results obtained at these chromatographic surfaces.

The final paper was given by Roger Gilpin of Kent State University on the use of NMR techniques to characterize bonded phases and retention mechanisms. Results from wide-line deuterium NMR provide information on the chemical and structural nature of these surfaces, uniformity of surface coverage, modes of motion for the immobilized stationary-phase molecules, and retention mechanisms.

The organizing committee should be congratulated for preparing a strong technical program and a pleasant environment in which to learn. The informal and formal social portions were also well done, and symposium participants had an opportunity to enjoy the sights and scenery of the Blue Ridge region. Both the technical program and the local arrangements were excellent. The excitement and enthusiasm evident at Virginia Tech will surely be part of next summer's symposium at Oak Ridge National Laboratories, and we look forward to seeing you in Tennessee next July.

Fred M. Hawkridge is professor of chemistry at Virginia Commonwealth University in Richmond, VA. Joseph A. Gardella, Jr., is associate professor of chemistry and codirector of the Industry University Center for Biosurfaces at the State University of New York at Buffalo. Both are currently visiting scientists in the analytical and surface chemistry program of the chemistry division at the National Science Foundation.

WIN A STATE-OF-THE-ART

PTI®

FLUOROMETER

ABSOLUTELY FREE!

Guess the total number of years of experience that the professionals at PHOTON TECHNOLOGY INTERNATIONAL have in fluorescence.

The winner will have a choice of either an ALPHASCAN or the R&D 100 winner LS-100.

Over $30,000 value — complete with installation and warranty.

This promotion is undertaken to celebrate the introduction of the new line of fluorescence instrumentation for virtually every need or budget. We would also like to make you aware of our experience and to demonstrate our commitment and ability to provide you with the best customer service and applications support.

To obtain an application form and the contest rules, please write or call:

In the United States:
Photon Technology International Inc.
1 Deerpark Drive, Suite F
Monmouth Junction, New Jersey 08852
Phone: (201) 329-0910
Fax: (201) 329-9069

In Western Europe:
Photon Technology International Inc.
11 Well Lane
East Sheen, London, England SW14 7AE
Phone: (01) 878-7928
Fax: (01) 876-6495

In Canada:
Photon Technology International (Canada) Inc.
347 Consortium Court
London, Ontario, Canada N6E 2S8
Phone: (519) 668-1256
Fax: (519) 668-8437

Contest will close May 1, 1990.
Winner to be announced shortly afterward.
The free offer applies to the United States and Canada; other countries will be charged for installation, duties, taxes, etc.
Offer void where prohibited.

CIRCLE 127 ON READER SERVICE CARD

NEW PRODUCTS

Electrophoresis. Probe Tech Basic system combines gel electrophoresis and vacuum transfer in a single integrated chamber. The system includes a vacuum regulator, a waste container, and a choice of three electrophoresis/vacuum transfer cartridges. Oncor 404

MS. QX 2000 quadrupole mass spectrometer, designed for process and residual gas analysis, is menu driven via an integrated touch-sensitive screen and includes an IBM/AT-compatible computer with 640 kB RAM. Applications include semiconductor fabrication and materials research. Leybold AG 405

Proteins. Model 473A protein system is capable of sequencing a low-picomole sample load with femtomole detection. The Macintosh-based data system provides amino acid histogram plots, multiple cycle comparisons, cycle yield plots, and repetitive yield plots. Applied Biosystems 406

Oxygen. Model 308WA on-line trace oxygen analyzer detects O_2 contamination in hydrogen, nitrogen, ethylene, propylene, butadiene, and other high-purity gases. Oxygen levels as low as 0–500 ppb can be determined with an accuracy of ±1%. Teledyne Analytical Instruments 407

Detector. Model 1433 Cryo-CCD detector is a cryogenically cooled, two-dimensional, multichannel area detector designed for low-light-level spectroscopic imaging. The detector can be used for Raman, fluorescence, and emission spectroscopy. EG&G Princeton Applied Research 408

FT-IR. DA8 research-grade FT-IR spectrometer features a built-in array processor that presents fully computed spectra to an Ethernet link. The host computer can be any VAX system with workstation graphics or VT240 and mouse. Bomem 409

Sample preparation. Maxidigest is a modular high-production microwave digester designed for food and environmental applications. The system, which can run up to four samples simultaneously, features a 250-mL capacity digestion vessel. Questron 412

SEM. Model 1860 FE digital imaging field emission SEM features spatial resolution of 8 nm at 1 kV and 2 nm at 10 kV. The system, which can accommodate a full 8-in. wafer, has a magnification range of 25× to 400,000× at a 12-mm working distance. Amray 413

Liquid scintillation. LS 6000SE liquid scintillation counter incorporates built-in help screens, preset counting regions, and quench curve setup parameters. Included with the system are an 80-column printer, sample racks, and electrostatic controller. Beckman Instruments 410

Surface analysis. TFS surface analyzer, an ion-imaging time-of-flight secondary ion mass spectrometer, features stigmatic ion optics that allow the entire analytical area to be bombarded and the secondary ions from each image point to be simultaneously mass analyzed and detected. Charles Evans & Associates 411

Software

Mathematics. Maple is an interactive computer algebra system that features a source code library of more than 2000 mathematical functions. Capabilities include linear algebra, calculus, trigonometry, differential equations, modeling, and statistics. Waterloo Maple Software 415

LIMS. EasyLIMS is designed to streamline the recording and transcription of laboratory test results and the preparation of reports. The software package includes database, word processing, spreadsheet, and statistical analysis capabilities. Beckman Instruments 416

Manufacturers' Literature

Peptides. Technical bulletin discusses the LC-based peptide-mapping system, which is capable of routine peptide mapping at the 5–10-pmol level

For more information on listed items, circle the appropriate numbers on one of our Readers' Service Cards

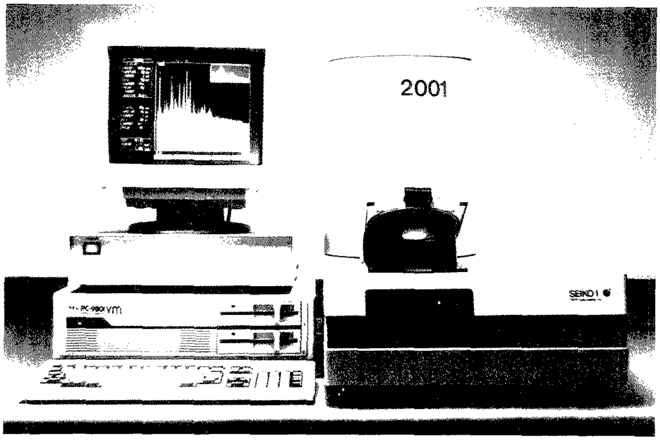

X-ray fluorescent SEA2001 element and composition analyzer system determines the presence and compositional percentage of up to 20 elements in an unknown homogeneous sample. Seiko Instruments 401

Don't inject variables into your chromatography. Use Millex® filter units.

© 1986 Millipore Corporation

Use Millex HPLC filters, and put an end to particle contamination problems. Maximize column life while improving the consistency of your chromatographic results.

Designed for fast, reliable sample clarification, Millex units remove all particulate contaminants down to the rated pore size. Devices are available in 4 mm, 13 mm, and 25 mm configurations, for sample volumes ranging from less than 1 ml up to 100 ml, and offer these advantages:

Maximum sample recovery. Hold-up volume of 4 mm Millex units is less than 10 μl after air purge. For 13 mm units, less than 50 μl. For 25 mm units, less than 0.1 ml.

Ultraclean design. Membranes are incorporated into solvent-resistant housings. There are no glues, binders, or dyes to add unwelcome extractables to your analyses.

Wide chemical compatibility. Millipore's unique Durapore® membrane is non protein-binding, and compatible with most organic, aqueous, or isocratic solutions. Other membrane types are available to clarify a broad range of samples and solvents.

Try Millex HPLC filters in your lab—free. We'll send you a free prep kit and a brochure on sample management and reagent purification. Call (800) 225-1380. In Massachusetts, (617) 275-9200. Or write Millipore Corporation,
80 Ashby Rd.,
Bedford,
MA 01730.

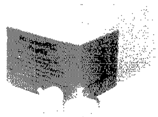

CIRCLE 96 ON READER SERVICE CARD

and is compatible with high-speed and narrow-bore peptide columns. Perkin-Elmer 418

Electron spectroscopy. Brochure highlights the VSW Scientific Instruments CLASS range of hemispherical analyzers for electron spectroscopy. The analyzers are available in 100- and 150-mm sizes. 4 pp. Microscience 419

Newsletter. *Chromatogram*, Vol. 10, No. 2, contains articles on drug monitoring, amino acids, nucleic acids, quality control, and chromatography instrumentation. 12 pp. Beckman Instruments 420

Blotting. Bulletin discusses equipment, detection systems, and reagents for Western blotting. A comparative guide to semi-dry and tank blotting is provided. 6 pp. Bio-Rad Laboratories 421

LC. Guide provides information on the selection of polymeric HPLC columns for analysis of biological, pharmaceutical, industrial, and environmental compounds. Eighty-four chromatograms are included. EM Science 423

Gases. Brochure describes high-purity hydrocarbon gases, including 1,3-butadiene, *n*-butane, ethane, carbon monoxide, methane, isobutylene, and propylene. Airgas 422

IR. *Scan Time*, No. 16, includes articles on applications of reflectance FT-IR microspectroscopy and diffuse reflectance spectroscopy. 6 pp. Spectra-Tech 425

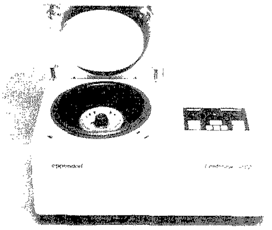

Eppendorf Model 5402 refrigerated microcentrifuge features a temperature range of −9 to 40°C, maximum rotational speed of 14,000 rpm, and maximum spin time of 99 min. Brinkmann Instruments 402

DNA. Brochure highlights the PCR-Mate EP DNA synthesizer. The system includes high-quality reagents, specialty cartridges for one-step purification, and sequence information management software. Applied Biosystems 424

Chromatography. Brochure discusses the separation of saccharides by size-exclusion and ion-exchange chromatography using Toyopearl resins. 14 pp. TosoHaas 426

Catalogs

Chromatography. Catalog contains analytical and preparative columns and cartridges, gel permeation chromatography columns, bioseparations and application-specific columns and products, and sample preparation products. 38 pp. Waters Chromatography Division of Millipore 430

Chemicals/separations. Catalog lists specialty biochemicals, peptides, proteins, ion-exchange resins, and products for electrophoresis, GC, and LC. 432 pp. Serva Biochemicals 431

Reaching Perfection in MS and SEM.
"A man's reach should exceed his grasp..."
Robert Browning

Galileo detectors for Mass Spectrometry and Electron Microscopy.

What silicon chips did for computers, Galileo high-performance detectors are doing for GC/MS, MS and SEM analysis.

Whether your projects involve environmental or pharmaceutical analysis, analysis of organic compounds or general spectroscopy applications, a Galileo detector will speed sample identification while providing accurate and precise analysis.

When research projects require frequent sample analysis over a long period of time, you'll want the latest and best technology backing you up. Galileo is the innovator in analytical instrument detectors. If you demand high performance and are concerned about down time, rapid analysis, dynamic range and cost, insist on Galileo scientific detectors. You'll wonder how you ever got along without us.

Write us and ask how to ensure that your instruments have Galileo scientific detectors.

Galileo Electro-Optics Corp.
Scientific Detector Products Group
P.O. Box 550, Dept. AA
Sturbridge, MA 01566
(508) 347-9191

GALILEO
Galileo Electro-Optics Corp.

CIRCLE 58 ON READER SERVICE CARD

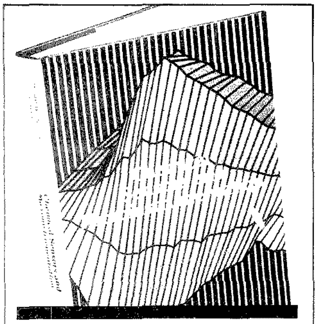

Chemical Sensors and Microinstrumentation

New! A revealing look at how developments in the technology of miniaturization are resulting in the design of more sensitive and more selective measurement systems. Presents state-of-the-art approaches that demonstrate fundamental principles, incorporating new chemical and physical concepts into the basis for making chemical measurements.

Offers contributions by more than eighty leading scholars that represent a true cross-section of the most significant international research activities in chemical sensors today. Presents basic applications of electrical, optical, mass, and thermal phenomena to sensor design. Features recent developments in electrochemical sensing:

- potentiometric sensors for gases and anions
- light addressable potentiometric sensors
- polymer immobilization techniques for selectivity
- miniaturization of sensors
- mediated enzyme sensors
- opto-electrochemical sensors

Three major sections cover

- sensors based on electrical measurements
- sensors based on mass or thermal measurements
- sensors based on optical measurements

Also covers a wide range of methods, equipment and phenomena-trace analysis, electrochemistry, spectrophotometry, optical fibers, piezoelectric phenomena, biosensors, enzyme- and immunoanalysis.

Royce W. Murray, *Editor*, University of North Carolina

Raymond E. Dessy, *Editor*, Virginia Polytechnic Institute and State University

William R. Heineman, *Editor*, University of Cincinnati

Jiri Janata, *Editor*, University of Utah

W. Rudolf Seitz, *Editor*, University of New Hampshire

Developed from a symposium sponsored by the Division of Analytical Chemistry of the American Chemical Society

ACS Symposium Series No. 403
551 pages (1989) Clothbound
ISBN 0-8412-1661-4 LC 89-15149
U.S. & Canada $89.95 Export $107.95

ORDER FROM

American Chemical Society
Distribution Office, Dept. 39
1155 Sixteenth St., N.W.
Washington, DC 20036
or CALL TOLL FREE

800-227-5558

(in Washington, D.C. 872-4363) and use your credit card!

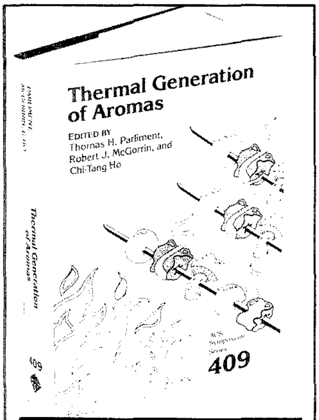
Thermal Generation of Aromas
EDITED BY Thomas H. Parliment, Robert J. McGorrin, and Chi-Tang Ho
409

Thermal Generation of Aromas

The process of cooking plays an important role in imparting many desirable aromas to foods. In this new volume, the chemical aspects of thermally processed aromas are reviewed and recent research in this area is examined. This book offers an overview of relevant aroma isolation and identification techniques and describes recent advances in the thermal, microwave, and extruded generation of aromas.

Fifty chapters, written by internationally recognized experts provide extensive coverage in the following areas:

- analytical methodology
- lipid-derived aromas
- mechanistic studies
- generation of selected aromas
- generation of meat aromas
- extrusion and microwave

The first section contains four comprehensive reviews of thermal generation of aromas, written from four different perspectives. This section alone makes this book invaluable as a basic reference for students and experienced flavor chemists. Also included are historical perspectives and regulatory viewpoints.

Thomas H. Parliment, *Editor*, General Foods USA

Robert J. McGorrin, *Editor*, Kraft USA

Chi-Tang Ho, *Editor*, Rutgers University

Developed from a symposium sponsored by the Division of Agricultural and Food Chemistry of the American Chemical Society

ACS Symposium Series No. 409
560 pages (1989) Clothbound
ISBN: 0-8412-1682-7 LC:89-17796
US & Canada $109.95 Export $131.95

ORDER FROM

American Chemical Society
Distribution Office, Dept. 48
1155 Sixteenth St., N.W.
Washington, DC 20036
or CALL TOLL FREE

800-227-5558

(in Washington, D.C. 872-4363) and use your credit card!

About Your

Polymer Branching

Absolute Molecular Weight

Why worry about polymers refractive index increment and 2nd viral coefficient required by laser light scattering techniques?

Using Viscotek's new dual detector (a Differential Refractometer combined with Viscotek's patented Viscometer) coupled on-line with your present GPC equipment provides continuous measurement of intrinsic viscosity of the polymer across the entire chromatogram without the use of expensive laser light scattering equipment.

The results: The ability to determine molecular weight distribution, radius of gyration, and, branching frequency, with a sensitivity to molecular weights as low as 100.

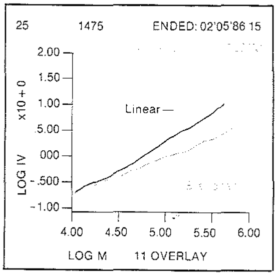

Overlay of Mark-Houwink Plot gives a direct visual indication of branching based on the slope of the plot.

1032 Russell Dr.
Porter, Texas 77365
(713) 359-5966
Telex: 9102400852

CIRCLE 172 ON READER SERVICE CARD

If your job involves process measurement, here's an opportunity to make an investment in your career....

PROCESS MEASUREMENT AND CONTROL

A New Audio Course from the American Chemical Society

Special 30-day free examination offer for ACS members!

Process Measurement and Control offers you a complete background in every aspect of this area—from understanding the principles fundamental to making these measurements. . .deciding on your application. . .to selecting the equipment to best do it. . .to running your application. Here's what you'll be able to do after taking this course:

- Choose the right equipment for your application
- Obtain better on-line process control
- Optimize the selection of equipment and controller
- Understand process and engineering instrument drawings
- Comprehend manufacturers' literature, including accuracy and sensitivity specifications
- Know how to obtain the proper accuracy of your instrument to meet requirements

In addition, you'll learn about the practical side of equipment selection.....how to:

- Speak the language you need to communicate with equipment vendors
- Protect yourself from over-enthusiastic vendor claims
- Look for the right components when selecting equipment

All in all, this course gives you a complete overview of the theories, instrumentation, and applications of process measurement and control.

Who Should Take This Course

You should, if you are a:

- Scientist or engineer who has just been assigned to do process measurement—to get the background you need
- Manager that has just been given responsibility for a process measurement area—to direct, understand, and communicate with your staff who perform this function
- Manager responsible for training new personnel to perform process measurement—for use in group or self-paced individual learning
- Salesperson for an instrumentation company—to see how your product fits in with the competition and to learn the vocabulary to communicate with your customers

Brief Course Outline

- Introduction
- Measurement—Instrumentation
- Pressure Measurement
- Temperature Measurement
- Flow Measurement
- Control Valves
- Level Measurement
- On-Line Physical Property Measurement
- Analysis Instrumentation—On-Line Chemical Composition Measurement
- Control Instrumentation

The Instructor

Marvin D. Weiss is retired after thirty years of experience in a variety of areas: development for a major instrument company, instrument applications in major chemical companies, academic teaching and consulting, and management of instrument divisions of major design and construction companies.

The Unit

Process Measurement and Control consists of four cassettes (five hours of taped instruction) and a 280-page manual. It comes in one compact package, so that you can keep it with you to study when you want—at work, at home, or even while traveling.

Order your course today! Use the coupon below or call 1-800-227-5558.

Order Form

Please send me **Process Measurement and Control** (Catalog No. A8):

	Qty.	*US & Canada*	*Export*	*Total*
Complete Course	_____	$435	$522	_____
Additional Manuals	_____	$42	$50	_____
		Total order		_____

Payment Options:

1. Payment enclosed (make check payable to American Chemical Society).
2. Purchase order enclosed.
   P.O. # ____________________
3. Charge my ☐ MasterCard/VISA
   ☐ AMEX ☐ Diners Club/Carte Blanche.

Account No. ____________________

Name of cardholder ____________________

Expires ____________________

Signature ____________________

4. Send me my course to examine free for 30 days. I am an ACS member.
ACS membership no. (above your name on your C&EN mailing label): __________

Signature ____________________

Ship to:

Name ____________________

Address ____________________

City, ____________________

State, ZIP ____________________

Phone ____________________

Please allow 3-4 weeks for delivery. Prices quoted in U.S. dollars. Foreign payment must be in U.S. currency by international money order, UNESCO coupons, or U.S. bank draft.

Mail this order form to **American Chemical Society, Distribution Office Dept. 17, P.O. Box 57136, West End Station, Washington, DC 20037.** 17

ANALYTICAL APPROACH

MOLECULAR BIOLOGY AT ATOMIC RESOLUTION

The Structure of an Insect Virus and its Functional Implications

Jean-Pierre Wery and John E. Johnson
Department of Biological Sciences
Purdue University
West Lafayette, IN 47907

Viruses provide well-defined systems for studying structural biology at near-atomic resolution. They are nucleoprotein particles designed to transport specific genes between cells of a host and between hosts. Depending on the virus type, the genetic information may be coded on either RNA or DNA, which may be single stranded or double stranded. The nucleic acid is packaged in a capsid or shell composed of either protein (nonenveloped virus) or of a lipid membrane and protein (enveloped virus).

The size and complexity of virus capsids and the availability of substantial quantities of virus have largely dictated the early course of high-resolution X-ray crystallographic studies (*1*). Small, nonenveloped, single-stranded RNA plant viruses were the first spherical viruses to be studied because it is relatively easy to obtain gram quantities. Mammalian and insect viruses can be isolated only in milligram quantities; therefore, their high-resolution structures have been elucidated only recently. Larger, more complex virus structures have been determined at moderate resolution by image analysis of electron micrographs and X-ray diffraction. Enveloped viruses have been difficult to study because, in general, their flexible, nonsymmetric capsids prevent crystallization. High-resolution studies of the components of an enveloped virus (e.g., influenza virus) have been successful. Two components of the influenza virus, the hemagglutinin and neuraminidase protein structures, have been determined by first removing them from the membrane by proteolytic cleavage, then crystallizing the isolated proteins. Similarly, the hexon units of adenovirus, a virus without a lipid coat but with spikes (protruding columns of protein) that inhibit crystallization, have been studied. Virus structures that have been determined by X-ray crystallography are listed in Table I.

In this article we will discuss the structure determination of an insect virus at atomic resolution. This information along with biochemical and molecular genetics data can improve our understanding of the biochemistry of viruses at the molecular level.

Black beetle virus and the nodavirus family

Black beetle virus (BBV), the first insect virus to be determined at atomic resolution, was originally isolated (*3, 4*) from the New Zealand black beetle (*Heteronychus arator*). BBV is an isometric virion 30 nm in diameter (a virion is a complete virus particle with its outer coat intact) composed of 180 copies of a coat protein subunit and two RNA molecules, one coding for the RNA-directed RNA polymerase and another coding for the coat protein. These properties classify BBV as a member of a group of small divided genome riboviruses (RNA viruses), the *Nodaviridae* family (*5–7*). Members of this family are among the simplest reproducing objects in nature. BBV is ideal for studying assembly and is also a useful model for examining how

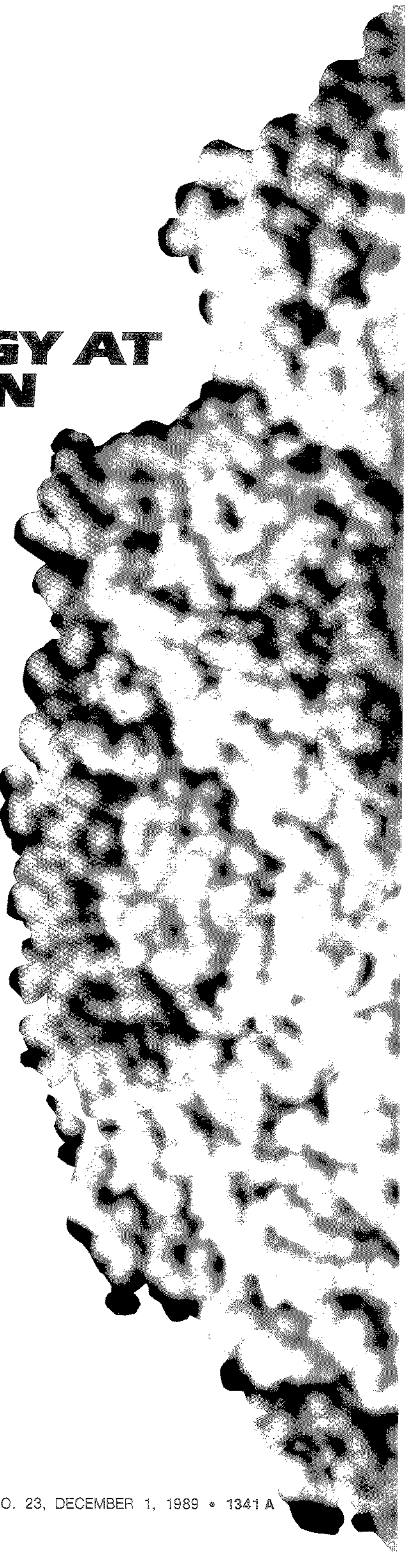

0003-2700/A361-1341/$01.50/0
© 1989 American Chemical Society

Table I. Virus structures determined by X-ray crystallography (*2*)

Virus	Capsid type[a]	Resolution
Plant viruses		
TBSV	$T = 3$	2.9 Å
Swollen TBSV	$T = 3$	8.0 Å
TCV	$T = 3$	3.2 Å
SBMV	$T = 3$	2.9 Å
CPMV	Como	3.0 Å
AMV Reassembled protein	$T = 1$	4.5 Å
SBMV Reassembled protein	$T = 1$	7.5 Å
STNV	$T = 1$	2.5 Å
Animal viruses		
Rhinovirus 14	Picorna	3.0 Å
Poliovirus Mahoney 1	Picorna	2.9 Å
Poliovirus Sabin 3	Picorna	2.4 Å
Mengo virus	Picorna	3.0 Å
FMDV	Picorna	2.9 Å
Polyomavirus	$T = 7$	22.5 Å
Black beetle virus	$T = 3$	3.0 Å
Virus components		
Influenza virus, hemagglutinin component		3.0 Å
Influenza virus, neuraminidase component		2.9 Å
Adenovirus hexon		2.9 Å

Abbreviations: TBSV—tomato bushy stunt virus; TCV—turnip crinkle virus; SBMV—southern bean mosaic virus; CPMV—cowpea mosaic virus; AMV—alfalfa mosaic virus; STNV—satellite tobacco necrosis virus; FMDV—foot-and-mouth disease virus.

[a] Capsid type describes the number of subunits and subunit types in the protein shell of a virus particle. A particle with one subunit type contains 60T subunits in its shell (e.g., BBV has a $T = 3$ shell and contains 180 subunits). A picorna capsid contains 60 copies each of three different subunit types; a como capsid contains 60 copies each of two different subunit types.

structure is related to a virus's ability to infect certain insect species. This is because the three-dimensional structure of BBV is known and nodavirus structures are relatively simple. Understanding these factors may prove useful in identifying, or perhaps in eventually genetically engineering, viruses suitable for use in biological pest control as an alternative to chemical poisons. For example, naturally occurring viruses are already being used in efforts to eradicate the gypsy moth (*8*).

Nodaviruses undergo a novel maturation process (*9*). The RNA 2 molecule is translated into a coat protein α that contains 407 amino acids. This α coat protein is rapidly assembled into a provirion (immature virion, Figure 1) that becomes a mature particle only after it cleaves into β (363 amino acids) and γ (44 amino acids) proteins. Roughly 80% of the coat proteins in a mature particle are in the cleaved form. This cleavage dramatically alters the virion stability, and the proteolysis (hydrolysis of proteins) is autocatalytic and occurs only after virion assembly (*9*). One of our objectives was to use the three-dimensional structure of BBV to understand the cleavage mechanism and the relation between this cleavage and the alteration in particle stability. In this work, we used the coat protein sequences of BBV and three other nodaviruses: flockhouse virus (FHV), boolarra virus (BOV), and nodamura virus (NOV) (*10–12*).

Three-dimensional structure determination

High-resolution structures of biological macromolecules can be determined using NMR spectroscopy (*13*) and X-ray crystallography. Only crystallography can be used to study structures as large as viruses. Molecular imaging using X-ray crystallography is analogous to the formation of an image in an optical microscope. However, the electromagnetic radiation used has a wavelength of 1 Å instead of 5000 Å. Collecting X-ray data from single crystals is equivalent to recording light scattered by an object on the microscope slide before it enters the objective lens. Crystals, containing roughly 10^{13} virus particles, produce scattered radiation that is readily interpreted as if it came from a single copy of the virus particle. Although the objective lens in a light microscope properly combines the scattered radiation to form a magnified image, there is no direct physical method to focus X-rays because of their short wavelength. The phase or focusing problem is solved computationally by the crystallographer, and the image formed is a three-dimensional electron density map of the crystalline molecule. X-ray crystallography is now a routine method for studying small molecules and a well-established technique for studying proteins. It is, however, still a challenging problem to solve the structure of a virus using this method.

Crystallographic analysis of a virus requires at least 10–20 mg of material, and often quantities in excess of 100 mg are needed. Production of such quantities of an animal virus is difficult and costly. Plant viruses are particularly attractive subjects for crystallography because they can often be prepared in large quantities at relatively low cost. BBV is grown in culture using *Drosophila* gut cells where it typically constitutes 20% of the cell mass 48 h after infection. The most critical step in a crystallographic analysis is the production of large (0.3–0.8 mm) well-ordered single crystals. This is achieved by slowly precipitating the virus over the course of days, weeks, or even months. A particularly effective method for doing this is vapor diffusion. Typically conditions need to be found in which the virus is insoluble. This is achieved by varying pH, buffer, polyethylene glycol concentration, or salt concentration. The solution, without virus, is called the reservoir solution, and about 1 mL is present in the crystallization chamber. Approximately 5 µL of the reservoir solution is mixed 1:1 with a dilute buffer containing virus at a concentration of 7–10 mg/mL or higher. This is called the drop. The 10-µL drop is placed in vapor equilibrium with the reservoir, and the solution in the drop approaches a state in which the virus is insoluble, leading to crystallization. Other methods for crystallizing proteins and viruses have been reported by McPherson (*14*).

Single-crystal data collection is normally performed using a synchrotron X-ray source. The high-intensity parallel radiation is ideal for rapid collection of high-quality data. Each diffraction photograph contains 8000–10,000 diffraction maxima (spots) that are densely spaced because virus crystal unit cells are in excess of 300 Å. Currently, only photographic film permits diffraction maxima to be spatially resolved at high resolution. Normally a new crystal specimen is needed for each exposure because biological molecules are damaged by X-rays, and the crystals are destroyed. Depending on the symmetry, 50–400 individual photographs may be required to complete a three-dimensional data set. The optical densities of these observations are measured using a densitometer, and the integrated intensities of each reflection are determined using a sophisticated processing procedure (*15*). Supercomputers are needed for processing the large quantity of single-crystal data from viruses. Because the quantity of data is proportional to the volume of the crystalline unit cell, data sets from virus crystals will generally be more than a thousand times larger than a small-molecule data set.

Icosahedral (20 sided) RNA viruses have been studied with considerable success. The symmetric shell of the virus has 532-point group symmetry (*16*). We have found that 180 copies of one type of protein subunit form the protein shell of BBV, and it packages and protects the RNA. The symmetry of the protein shell has played a crucial role in all the structures determined to date (*17*). Isomorphous replacement, coupled with averaging the electron density over the symmetry of the shell, has proven to be a very powerful method for determining the phases for the measured structure amplitudes. (This will be explained in more detail below.) These calculations involve the Fourier transformation of maps containing from 10^7 to 10^8 grid points. The averaging procedures may involve up to 10^9 linear transformations. Electron density maps of extraordinary quality have been obtained using these methods. In all cases to date, the known amino acid sequence of the protein subunits has permitted construction of chemical models that accurately fit the electron density maps. These models are then refined to produce the smallest difference between the experimentally measured structure amplitudes and those calculated based on the model. This least-squares refinement typically includes 20,000–25,000 variables per icosahedral asymmetric unit as well as restraints that are based on the stereochemistry of amino acid structures determined using small-molecule crystallography.

X-ray analysis of BBV

Single crystals of BBV, suitable for X-ray analysis, were grown using vapor diffusion (*18*). The crystals were cubic and belonged to the space group $P4_232$. The cell parameter was a = 362 Å and there were two particles per cell. Diffraction patterns to a resolution of 2.8 Å were obtained using a high-intensity X-ray beam generated by a synchrotron. The diffraction patterns were recorded on X-ray films and 130,273 unique diffraction maxima were measured.

To compute the high-resolution electron density map, both the amplitude (square root of the diffraction maxima) and the phase of the diffracted beams were needed. The phases cannot be measured experimentally. Thus a first estimate of the phases was obtained by using multiple isomorphous replacement. In this technique, heavy atoms such as mercury or platinum are bound to each molecule in the crystal. This produces a change in the intensity of each diffraction maxima that depends on its phase. It is somewhat like placing the lens of a microscope inside the object to be imaged. At least two heavy-atom derivatives are needed if this method alone is used for phase determination.

In the case of BBV, the application of this technique allowed calculation of an electron density map at 5.0-Å resolution. This density was not accurate enough to build a model for BBV, but it was suitable to initiate phase improvement by using the symmetry of the capsid. This procedure eventually resulted in an electron density map at 3.0-Å resolution in which the first model of BBV was built (*19*) using the known amino acid sequence of the capsid protein (*10*).

The RNA core is not visible in the electron density map because it lacks the symmetry necessary for detection by the crystallography method. Only a model of high accuracy is useful in explaining, at the molecular level, the biochemistry of the virus. Thus the model was subjected to the restrained least-squares refinement method (*20*). This refinement resulted in the model described below.

Three-dimensional structure of BBV

The shell of the virus is composed of 60 triangular units arranged with icosahedral symmetry (the icosahedron is one

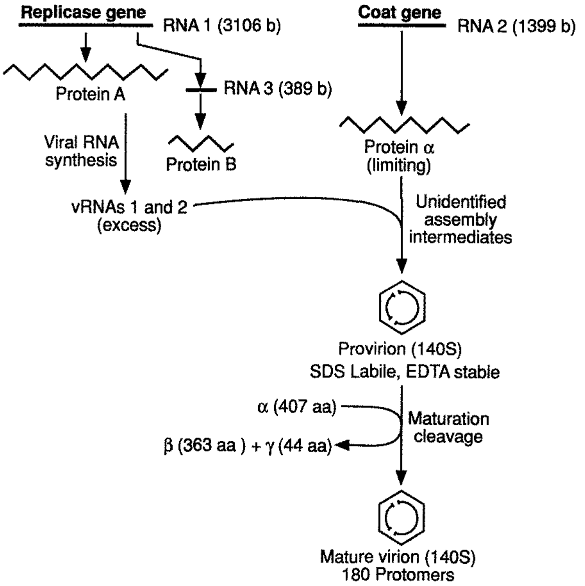

Figure 1. Schematic representation illustrating the current understanding of nodavirus morphogenesis.

The two RNA molecules comprising the genome (RNA 1 left and RNA 2 right) are translated into protein molecules. Protein A and protein B catalyze the synthesis of more copies of the viral RNAs 1 and 2 (left), which then assemble with the protein α synthesized from RNA 2 to form the provirion (immature virion). Protein α undergoes cleavage to $\beta + \gamma$, leading to the mature infectious virion.

of the five platonic solids [*21*]) (Figure 2). Each triangular unit consists of three identical polypeptide chains (protomers) arranged with approximately threefold symmetry to form the icosahedral asymmetric unit characteristic of a $T = 3$ surface lattice (*22*). The quasi-equivalent positions of the three chains that make up the asymmetric unit are distinguished by color and letter codes: blue (A), red (B), and green (C). The three subunits form a prominent, terraced pyramid that rises to a peak.

Figure 2d illustrates a cross section of the shell from the inside (bottom) to the outside (top). In the electron density map, each subunit appears to be in the cleaved form ($\beta + \gamma$). The fold of one subunit and the cleavage site are shown in Figure 2a. We have been able to build the β-chain from residue 44 to residue 363. The first 43 residues were invisible in the electron density map, indicating that this portion of the chain is disordered. This invisible portion, which contains 17 basic residues capable of neutralizing the negatively charged phosphate groups of the nucleic acid, probably adapts to the various conformations of the RNA.

Apart from the disordered amino terminus, the polypeptide β (residues 1–363) consists of an eight-stranded antiparallel β-barrel as seen in other animal and plant viruses, an outer protrusion composed predominantly of β-sheets and formed by the three large insertions between the strands of the β-barrel, and a carboxy terminal domain composed of two α-helices lying inside the shell. For each protomer, the cleavage site between residue 363 (Asn) and 364 (Ala) and the first 16 residues of γ (364–379) have been built in the electron density.

In addition, a polypeptide of about 10 residues was located in a groove at the twofold joint between two icosahedral asymmetric units (Figure 3). This peptide may correspond to a portion of the γ peptide, although part of γ is disordered, making it impossible to determine unequivocally the position of this polypeptide in the primary structure. The side chain electron density map and other evidence suggest that these are the carboxy terminal residues of γ (i.e., residues 398–407). The significance of this inserted polypeptide and its location in the primary sequence will be discussed below.

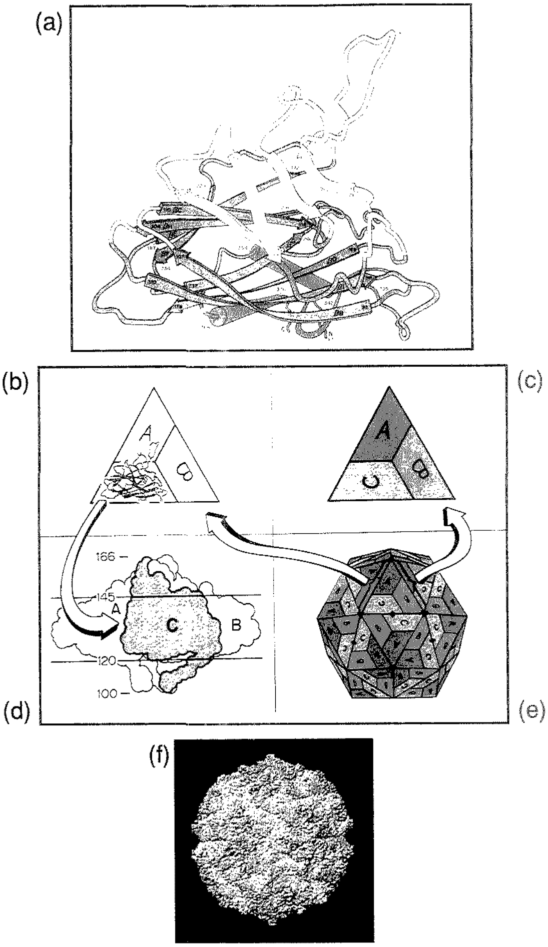

Figure 2. Organization of black beetle virus established from the 2.8-Å electron density map.

Different portions of the subunit structure (a) are colored according to their distance from the center of the particle. Essentially, the lower part (red, 100–120 Å) lies inside of the particle; the middle part (blue, 120–145 Å) forms the contiguous shell of the virion; and the outer part (yellow, 145–166 Å) forms one-third of the pyramidal protrusion on the surface of the capsid (see also c and d). Sixty trimeric clusters (c) arranged with icosahedral symmetry form the intact capsid (e, f), which encapsulates both parts of the bipartite genome. The space-filling representation (f) was generated by placing a sphere of 3.0-Å diameter at each C_α position.

Results of the sequence comparison

The amino acid sequences of BBV, FHV, BOV, and NOV have been aligned (*11*) using algorithms in the Wisconsin Genetic Package (*23*). The sequence comparisons gain in functional significance when the tertiary structure of BBV is used as a reference for analyzing variations in the primary structures of the four viruses. Differences in amino acid sequences will affect the particular environment of a residue, but the level of sequence similarity indicates that the overall fold of the subunit structure for all four nodaviruses must be closely similar. The comparison shows that most of the sequence changes occur on the subunit outer surface (yellow part of the protomer in Figure 2a).

It is well established that changes in surface regions of mammalian picornaviruses (small, single-stranded, RNA-containing animal viruses, including the human common cold virus, poliovirus, and foot-and-mouth disease virus) and influenza virus are largely responsible for their success in avoiding the immune system. Although insect viruses are not challenged by such an immune system, the outer portion of the virus tolerates amino acid variations more readily than the interior of the subunit. Changes in surface residues of nodaviruses may be important in developing receptor binding sites, thereby changing host specificity. The portion of the protomer located inside the particle (red part of the protomer in Figure 2a) is the most conserved region of the protein among all four viruses. This is the region where the subunit cleavage occurs and, like active sites in enzymes, amino acid changes that affect the chemistry of this activity cannot be tolerated.

Cleavage and its implication

The refined structure shows that the subunit cleavage sites display threefold quasi-equivalence, as do the first resi-

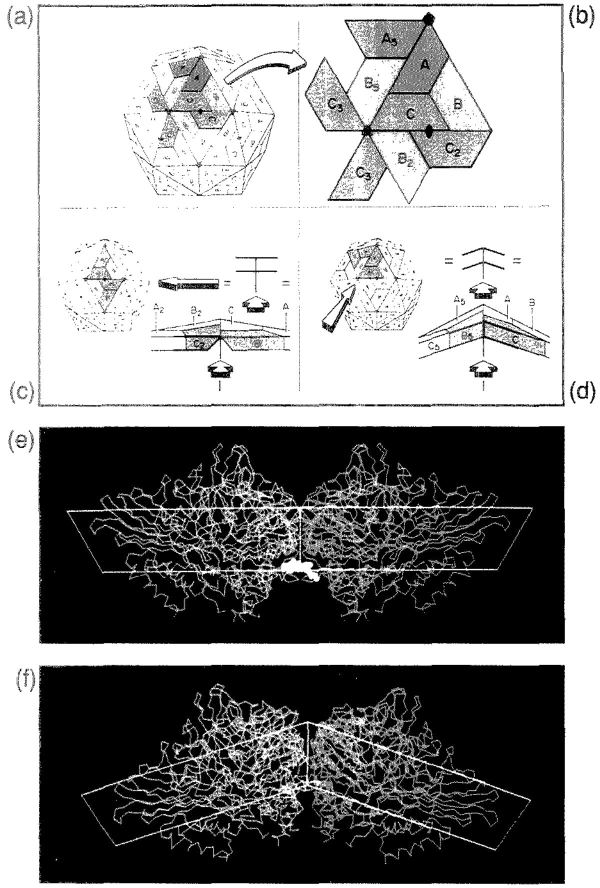

Figure 3. Geometric requirements to form a shell, with icosahedral symmetry, composed of 180 chemically identical subunits (a, b).

Two different contacts between icosahedral asymmetric units are required (c, d). Icosahedral twofold interactions (C-C_2) are flat (c) and quasi-twofold interactions (A-B_5) are bent (d). The molecular structure shows that the flat contacts result from the insertion of a 10-amino acid polypeptide at the C-C_2 contact (e), whereas the subunits interact directly at the bent A-B_5 contact (f).

Still using these tools

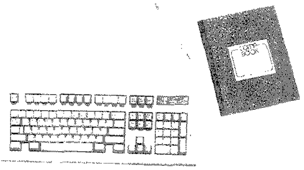

to enter your
analytical/laboratory
data into a
spreadsheet?

If so, you need...

MEASURE

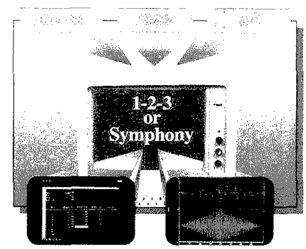

Measure is the *only* package that stores engineering and scientific data directly to either a Lotus 1-2-3 or Symphony spreadsheet where it is ready for immediate analysis, storage, or display. Measure accepts data from IEEE-488 and RS-232 instruments and plug-in data acquisition boards for IBM PC/XT/AT and PS/2 computers.

Now supports new Lab-PC data acquisition board—high performance at a low cost.

Call for *Free* Catalog
(800) IEEE-488 • (512) 794-0100

NATIONAL INSTRUMENTS®
The Software is the Instrument™
12109 Technology Blvd.
Austin, Texas 78727-6204

JAPAN (3) 788-1922 • FRANCE (1) 48 65 33 70
UNITED KINGDOM (06) 523-545 • WEST GERMANY (89) 80 7081
ITALY (2) 4830-1892 • THE NETHERLANDS (7) 099-6360

CIRCLE 110 ON READER SERVICE CARD

GOOD NEWS FOR ATOMIC ABSORPTION SPECTROSCOPY

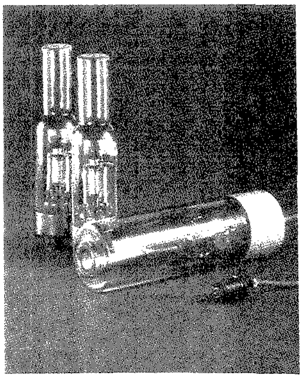

Hamamatsu Hollow Cathode Lamps are now available from major lab suppliers.

Hamamatsu single and multi-element Hollow Cathode Lamps offer superior stability, spectral purity and output intensity, even for such elements as arsenic and selenium. They are compatible with most commercial spectrophotometers, including Beckman, Zeiss and Perkin-Elmer. And best of all, they're available from your local lab supplier.

For Application Information, Call 1-800-524-0504
1-201-231-0960 in New Jersey

HAMAMATSU

HAMAMATSU CORPORATION
360 FOOTHILL ROAD
P. O. BOX 6910
BRIDGEWATER, NJ 08807
PHONE: 201/231-0960
International Offices in Major Countries of Europe and Asia.

© Hamamatsu Photonics, 1986

CIRCLE 63 ON READER SERVICE CARD

dues of the cleavage product (the γ peptide). A proposal for the active site for the autocatalytic cleavage has been made by using the sequence comparison described and by analyzing the distribution of potentially important residues in the vicinity of the cleavage site. Important residues for the proteolysis mechanism should be conserved among the four sequences, given that all nodaviruses demonstrate the cleavage. These data and the three-dimensional structure of BBV have helped us to identify several residues probably involved in the cleavage mechanism (Cys 69, Asp 75, Tyr 176, and Lys 192). One of these residues (Asp 75) is very close to the cleavage site (Figure 4).

The role of cleavage in the maturation of the particle is not clear. Capsid structures with $T = 3$ symmetry display two types of twofold joints (Figure 3). Although the subunits involved in the molecular contacts are identical, the nature of these contacts is different. Those occurring at the quasi-twofold axes have direct interactions between the subunits (Figure 3f). Contacts occurring at the icosahedral twofold axes are mediated by a polypeptide lying in a groove just inside the surface of the particle (Figure 3e). The cleavage may permit the full insertion of the polypeptide into the groove.

Future directions

This work is the first step in understanding the detailed chemistry of a relatively simple biological process. Crystallographic studies of other members of the nodavirus family (FHV and NOV) are in progress. In these studies, the known three-dimensional structure of BBV is used to generate a first set of low-resolution phases; noncrystallographic symmetry techniques are then used to generate an accurate high-resolution electron density map. At the same time, more detailed studies of the cleavage kinetics, the pH optimum of the cleavage, and the relation between cleavage and infectivity are under way (*24*). Finally, specific residues probably involved in the cleavage are being altered by molecular genetics methods to test their role in catalysis (*25*).

This work was possible because we had access to X-ray synchrotron sources for data collection (at LURE, Orsay, France, and at CHESS, Cornell University, Ithaca, NY) and to a supercomputer (the Cyber 205 at Purdue University) for all of our calculations.

We thank Paul Kaesberg, Roland Rueckert, and their colleagues at the Institute for Molecular Virology, University of Wisconsin—Madison for results prior to publication and helpful discussions. We thank Tom Gallagher and Roland Rueckert for permission to use Figure 1. We thank Sharon Fateley for help in preparing this manuscript.

References

(1) Johnson, J. E. In *Crystallography in North America;* McLachlan, D., Jr.; Glusker, J. P., Eds.; American Crystallographic Association: Lansing, MI, 1983; pp. 410–14.
(2) Rossmann, M. G.; Johnson, J. E. *Ann. Rev. Biochem.* **1989,** *58,* 533–73.
(3) Longworth, J. F.; Archibald, R. D. *N. Z. J. Zool.* **1975,** *2,* 233–36.

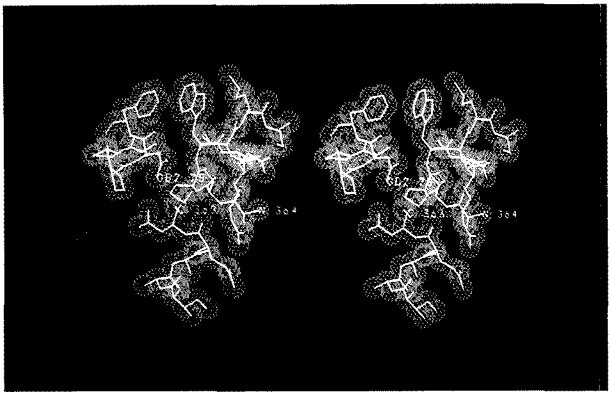

Figure 4. Stereoview of the region near the cleavage site in the capsid subunit.
Colored spheres 1 Å in radius have been superimposed on each atom. Asparagine 363 is the carboxy terminus of protein β and alanine 364 (8 Å from 363) is the amino terminus of protein γ. Residue 75 (OD2 75) in β is an aspartic acid that is hydrogen bonded to 363 (Asn) and may play a role in the cleavage reaction.

Choosing a graduate school?

Need to know who's doing research critical to yours?

New edition just published!

The ACS Directory of Graduate Research 1989

All the information you need on chemical research and researchers at universities in the U.S. and Canada . . . in a single source.

Includes listings for chemistry, chemical engineering, biochemistry, pharmaceutical/medicinal chemistry, clinical chemistry, and polymer science.

Lists universities with names and biographical information for all faculty members, their areas of specialization, titles of all papers published within the last two years, and individual telephone numbers, FAX numbers, and computer addresses.

Provides a statistical summary of academic chemical research—with information by department on numbers of full- and part-time faculty, postdoctoral appointments, graduate students, and M.S. and Ph.D. degrees granted.

What you'll find inside . . .

Information on . . .
- 683 academic departments
- 11,936 faculty members
- 68,276 publication citations

Listings for . . .
- chemistry
- chemical engineering
- biochemistry
- pharmaceutical/medicinal chemistry
- clinical chemistry
- polymer science

1436 pages (1989) Clothbound
Price:
US & Canada **$55.00**
Export **$66.00**

No academic institution or chemically oriented business can afford to be without the ACS Directory of Graduate Research 1989! Order today by calling TOLL FREE (800) 227-5558. In Washington, D.C., call 872-4363. Or use the coupon below.

Please send me ______copy(ies) of the ACS Directory of Graduate Research 1989. Price: US & Canada $55.00 Export $66.00.

☐ Payment enclosed (make checks payable to American Chemical Society).

☐ Purchase order enclosed. P.O.# ________________

Charge my: ☐ MasterCard/VISA ☐ American Express ☐ Diners Club/Carte Blanche

Account # ________________ Expires ________

Signature ________________

Phone ________________

Ship books to:

Name ________________

Address ________________

City, State, ZIP ________________

ORDERS FROM INDIVIDUALS MUST BE PREPAID. Please allow 4-6 weeks for delivery. Prices are quoted in U.S. dollars. Mail this order form with your payment or purchase order to:

American Chemical Society, Distribution Office Dept. 705,
P.O. Box 57136, West End Station, Washington, D.C. 20037.

705

(4) Friesen, P.; Scotti, P.; Longworth, J.; Rueckert, R. R. *J. Virol.* 1980, *35*, 741–47.

(5) Murphy, F. A.; Scherer, W. F.; Harrison, A. K; Dunne, W. G.; Carey, G. W. *Virology* **1970**, *40*, 1008–21.

(6) Kaesberg, P. *Molecular Organization of Positive Strand Viruses*; Academic Press: London, 1987, pp. 207–18.

(7) Dasmahaptra, B.; Dasgupta, R.; Ghosh, A.; Kaesberg, P. *J. Mol. Biol.* **1985**, *182*, 183–89.

(8) Podgwaite, J. D. In *Viral Insecticides for Biological Control*; Maramorosch, K.; Sherman, K., Eds.; Academic Press: New York, 1985; pp. 775–97.

(9) Gallagher, T. M.; Rueckert, R. R. *J. Virol.* **1988**, *62*, 3399–406.

(10) Dasgupta, R.; Ghosh, A.; Dasmahaptra, B.; Guarino, L.; Kaesberg, P. *Nucl. Acid Res.* **1984**, *12*, 7215–23.

(11) Kaesberg, P.; Dasgupta, R.; Sgro, J. Y.; Wery, J. P.; Selling, B.; Hosur, M. V.; Schmidt, T.; Johnson, J. E., submitted for publication in *J. Mol. Biol.*

(12) Dasgupta, R.; Sgro, J. Y. *Nucl. Acids Res.*, in press.

(13) Wuthrich, K. *NMR of Proteins and Nucleic Acids*; Wiley & Sons: New York, 1986.

(14) McPherson, A. *Preparation and Analysis of Protein Crystals*; Wiley & Sons: New York, 1982.

(15) Rossmann, M. G. *J. Appl. Crystallogr.* **1979**, *12*, 225–38.

(16) Cotton, F. A. *Chemical Applications of Group Theory*, 2nd ed.; Wiley Interscience: New York, 1971; pp. 40–45.

(17) Rossmann, M. G. *The Molecular Replacement Method;* Gordon & Bresch: New York, 1972.

(18) Hosur, M. V.; Schmidt, T.; Tucker, R. C.; Johnson, J. E.; Selling, B. H.; Rueckert, R. R. *Virology* **1984**, *133*, 119–27.

(19) Hosur, M. V.; Schmidt, T.; Tucker, R. C.; Johnson, J. E.; Gallagher, T. M.; Selling, B. H.; Rueckert, R. R. *Proteins* **1987**, *2*, 167–76.

(20) Hendrickson, W. A.; Konnert, J. H. In *Biomolecular Structure, Function, Conformation and Evolution*; Srinivasan, R., Ed.; Pergamon Press: Oxford, U.K., 1980, pp. 43–57.

(21) Williams, R. *The Geometrical Foundation of Natural Structure*; Dover Publications: New York, 1972; p. 67.

(22) Caspar, D.L.D.; Klug, A. *Cold Spring Harbor Symp. Quant. Biol.* 1962, *27*, 1–24.

(23) Devereaux, J.; Haeberli, P.; Smithies, O. *Nucl. Acids Res.* **1984**, *12*, 387–95.

(24) Rueckert, R. R., University of Wisconsin—Madison, personal communication, 1989.

(25) Kaesberg, P., University of Wisconsin—Madison, personal communication, 1989.

John E. Johnson, professor of biological sciences at Purdue University, received a Ph.D. in physical chemistry in 1972 from Iowa State University. His research interests include the use of physical and chemical methods for studying virus structure.

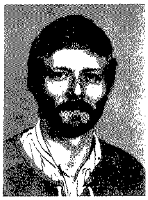

Jean-Pierre Wery, a postdoctoral research associate at Purdue University, is working on the structure determination of four serologically related viruses in the nodavirus group. He received a Ph.D. from the University of Liège, Belgium, in 1987.

LABORATORY SERVICE CENTER

NMR ANALYSIS

MULTINUCLEAR LIQUID or
MULTIFIELD SOLID STATE
SPECTRAL DATA SERVICES, INC.
818 Pioneer
Champaign, IL 61820
(217) 352-7084

HELP WANTED ADS

ROP display at ROP rates. Rate based on number of insertions within contract year. Cannot be combined for frequency.

Unit	1-Ti	6-Ti	12-Ti
1″ (25 mm)	$190	$170	$160
	24-Ti	48-Ti	72-Ti
	$150	$140	$130

CALL OR WRITE JANE GATENBY

ANALYTICAL CHEMISTRY
500 Post Road East
P.O. Box 231
Westport, CT 06880
203-226-7131
FAX: 203-454-9939

Laboratory Service Center (Equipment, Materials, Services, Instruments for Leasing), Maximum space — 4 inches per advertisement. Column width, 2-3/16″; two column width, 4-9/16″. Artwork accepted. No combination of directory rates with ROP advertising. Rates based on number of inches used within **12** months from first date of first insertion. Per inch: 1″ **— $165; 12″ — $160; 24″ — $155; 36″ — $150; 48″ — $145.**

CALL OR WRITE JANE GATENBY

ANALYTICAL CHEMISTRY
500 Post Road East
P.O. Box 231
Westport, CT 06880
203-226-7131/FAX: 203-454-9939

FREE DATA, FAST

To quickly amass data on all of the products you need, consult the Lab Data Service section on our *Analytical Chemistry* reader reply card insert.

USE LABORATORY SERVICE CENTER

INDEX TO ADVERTISERS IN THIS ISSUE

CIRCLE INQUIRY NO.	ADVERTISERS	PAGE NO.
1	*Alltech Chromad	1306A
20	Burdick & Jackson Division/Baxter Nordstrom/Cox Marketing	1307A
30	*Conostan Division/Conoco Specialty Products Robert Lamons & Associates	1318A
28	Corporation Scientifique Claisse, Inc.	1320A
34	*Dialog Information Services, Inc. Humpal, Leftwich & Sinn, Inc.	1305A
46, 47	*EG&G Princeton Applied Research Market Force	1319A
44	ENI Quinlan Foels & Company	1310A
50	Extrel Blattner/Brunner, Inc.	1324A
58	*Galileo Electro-Optics Corp. Legasse Associates Advertising Inc.	1338A
60	*Gilson Medical Electronics, Inc.	1321A
61	**Gilson Medical Electronics, SA	1321A
63	Hamamatsu Corporation Ketchum/Mandabach & Simms	1348A
67	*Hamilton Company Robert E. LaPointe & Company	1322A
65	*Hewlett-Packard Company Brooks Communications	1301A
90	*Leco Corporation	OBC
94	*Mattson Instruments, Inc. Cunningham & Welch Design Group	1302A
98	Merck & Company, Inc. William Douglas McAdams, Inc.	1332A
96	*Millipore Corporation Mintz & Hoke	1337A
110	*National Instruments	1347A
152	*Nupro Company/A Swagelok Company Falls Advertising Company	1328A
120	*Omega Engineering, Inc. Media Business House	IFC
122	*On-Site Instruments	1306A
125	**Philips Analytical	1326B
127	*Photon Technology International, Inc.	1335A
140	Rheodyne, Inc. Bonfield Associates	1323A
150	Siemens Analytical X-Ray Instruments, Inc.	1309A
154, 155	*Spectra-Physics	1314A
156	*Techne, Inc. Brunswick Advertising	1331A
158	*Tekmar Company Kenyon Hoag Associates	1308A
32	The University of Dayton Research Institute	1330A
170	*Varian Lanig Associates	1312A
172	Viscotek Corporation	1339A

Directory section, see page 1350A.
** See ad in ACS Laboratory Guide.*
*** Company so marked has advertisement in Foreign Regional edition only.*
Advertising Management for the American Chemical Society Publications

CENTCOM, LTD

President
Thomas N. J. Koerwer
Executive Vice President *Senior Vice President*
James A. Byrne **Benjamin W. Jones**
Clay S. Holden, *Vice President*
Robert L. Voepel, *Vice President*
Joseph P. Stenza, *Production Director*

500 Post Road East
P.O. Box 231
Westport, Connecticut 06880
(Area Code 203) 226-7131
Telex No.643310
FAX: 203-454-9939

ADVERTISING SALES MANAGER
Bruce E. Poorman

ADVERTISING PRODUCTION MANAGER
Jane F. Gatenby

SALES REPRESENTATIVES

Philadelphia, PA . . . Patricia O'Donnell, CENTCOM, LTD., GSB Building, Suite 405, 1 Belmont Avenue, Bala Cynwyd, Pa. 19004. Telephone: 215-667-9666, FAX: 215-667-9353

New York, NY . . . John F. Raftery, CENTCOM, LTD., 60 East 42nd St., New York, N.Y. 10165. Telephone: 212-972-9660

Westport, CT . . . Edward M. Black, CENTCOM, LTD., 500 Post Road East, P.O. Box 231, Westport, Ct. 06880. Telephone: 203-226-7131, Telex 643310, FAX: 203-454-9939

Cleveland, OH . . . Bruce E. Poorman, John C. Guyot, CENTCOM, LTD., 325 Front St., Suite 2, Berea, Ohio 44017. Telephone: 216-234-1333, FAX: 216-234-3425

Chicago, IL . . . Michael J. Pak, CENTCOM, LTD., 540 Frontage Rd., Northfield, Ill. 60093. Telephone: 708-441-6383, FAX: 708-441-6382

Houston, TX . . . Michael J. Pak, CENTCOM, LTD. Telephone: 708-441-6383

San Francisco, CA . . . Paul M. Butts, CENTCOM, LTD., Suite 1070, 2672 Bayshore Frontage Road, Mountain View, CA 94043. Telephone: 415-969-4604

Los Angeles, CA . . . Clay S. Holden, CENTCOM, LTD., Newton Pacific Center, 3142 Pacific Coast Highway, Suite 200, Torrance, CA 90505. Telephone: 213-325-1903

Boston, MA . . . Edward M. Black, CENTCOM, LTD. Telephone: 203-226-7131

Atlanta, GA . . . John F. Raftery, CENTCOM, LTD. Telephone: 212-972-9660

Denver, CO . . . Paul M. Butts, CENTCOM, LTD. Telephone: 415-969-4604

United Kingdom

Reading, England . . . Malcolm Thiele, Technomedia Ltd., Wood Cottage, Shurlock Row, Reading RG10 OQE, Berkshire, England. Telephone: 073-434-3302, Telex #848800, FAX: 073-434-3848

Lancashire, England . . . Technomedia Ltd., c/o Meconomics Ltd., Meconomics House, 31 Old Street, Ashton Under Lyne, Lancashire, England. Telephone: 061-308-3025

Continental Europe . . . Andre Jamar, International Communications, Inc., Rue Mallar 1, 4800 Verviers, Belgium. Telephone: (087) 22-53-85, FAX: (087) 23-03-29

Tokyo, Japan . . . Sumio Oka, International Media Representatives Ltd., 2-29 Toranomon, 1-Chome Minato-ku Tokyo 105 Japan. Telephone: 502-0656, Telex #22633, FAX: 591-2530

BESTSELLING BOOKS

FROM THE AMERICAN CHEMICAL SOCIETY

The ACS Style Guide: A Manual for Authors and Editors

The essential desk reference for authors, editors and publishers of scientific research is here! *The ACS Style Guide* is a complete stylistic handbook for the scientist, covering all phases of publishing and presenting scientific information. Includes in-depth information on grammar, style and usage; illustrations, chemical structures, tables, and lists; copyright and permissions; how to submit papers electronically; and how to give effective oral presentations. From start to finish, this handbook will help you make the most effective written and oral presentations possible. Greatly expands and updates the *ACS Handbook for Authors.*

Janet S. Dodd, Editor
200 pages (1985)
Clothbound: US & Can. **$24.95** Export **$29.95**
Paperbound: US & Can. **$14.95** Export **$17.95**

Biotechnology and Materials Science: Chemistry for the Future

Now you can get a better understanding of biotechnology and materials science and their tremendous impact on technology. Written in nontechnical language, this new book presents discussions of exciting advances by outstanding researchers in these pivotal fields. See how chemists, through their ability to manipulate chemical structures, will significantly influence our national economic vitality. Learn the history behind present-day biotechnology and see where advances are predicted.

***Mary L. Good, Editor,** and*
Jacqueline K. Barton, Associate Editor
144 pages (1988)
Clothbound: US & Can. **$24.95** Export **$29.95**
Paperbound: US & Can. **$14.95** Export **$17.95**

Chemical Demonstrations: A Sourcebook for Teachers — Volume 1, 2nd Edition and Volume 2, 2nd Edition

These two volumes offer hundreds of demonstrations suitable for introductory chemistry programs. You'll find the clear, concise text will tell you what each demonstration does, how to do it, what the reactions are, and how to prepare materials and solutions. You and your students will both benefit from the teaching tips included with the demonstrations. Safety precautions are also discussed in each volume.

Vol. 1 ***Lee R. Summerlin** and **James L. Ealy***
200 pages (1988)
Spiralbound: US & Can. **$19.95** Export **$23.95**

Vol. 2 ***Lee R. Summerlin, Christie L. Borgford,** and **Julie B. Ealy***
244 pages (1988)
Spiralbound: US & Can. **$19.95** Export **$23.95**
Order both volumes and save!
US & Can. **$34.95** Export **$41.95**

Chemical Activities

This new volume offers over 100 chemical activities that are simple, safe, and FUN! You and your students both will benefit from this sourcebook— the activities are designed for use by the student to introduce or reinforce the chemical topics you're teaching and will help your students better comprehend the experimental nature of chemistry. Offered in both a Teacher and Student edition; the Teacher Edition includes a background section for each activity.

Christie L. Borgford** and **Lee R. Summerlin
244 pages (1988) Spiralbound
Teacher Edition: US & Can. **$19.95** Export **$23.95**
Student Edition: US & Can. **$12.95** Export **$15.95**

The Language of Biotechnology: A Dictionary of Terms

If you're involved in any area of biotechnology, you must understand the jargon of related fields in order to integrate your research successfully. This book can help you do just that. It's all here in a single easy-to-use reference—specialized terms in the various areas of biotechnology arranged in dictionary format for speedy look-up. The definitions are short, just one sentence, and are followed by expanded definitions that explain the usage of each word with examples.

John M. Walker** and **Michael E. Cox
274 pages (1988)
Clothbound: US & Can. **$49.95** Export **$59.95**
Paperbound: US & Can. **$39.95** Export **$47.95**

Writing the Laboratory Notebook

Learn to increase your effectiveness on the job by using a notebook for planning, observation, and analysis of experiments. Goes far beyond mechanics of simply filling in notebook pages to show you how to plan and record with the clarity and detail you need for a successful experiment . . . and a successful career. Gives examples of notebook entries and an overview of current standards for universities, industrial labs, and government research centers. Nowhere else will you find a book on this important topic!

Howard M. Kanare
150 pages (1985)
Clothbound: US & Can. **$19.95** Export **$23.95**
Paperbound: US & Can. **$12.95** Export **$15.95**

Polymeric Materials: Chemistry for the Future

This new volume examines the growth of the polymer industry over the past 50 years. Covers the basics, including what they are; how they are made, modified, and processed; how and why they were developed; and what factors account for their varied physical properties. Examines the foreign market and need for increased research. Fully illustrated.

Joseph Alper** and **Gordon L. Nelson
112 pages (1989)
Clothbound: US & Can. **$24.95** Export **$29.95**
Paperbound: US & Can. **$14.95** Export **$17.95**

Order from: The American Chemical Society, Distribution Office, Dept. # 24, P.O. Box 57136, West End Station, Washington, DC 20037
or call toll-free 1-800-227-5558. In Washington, DC, call 872-4363.
All prices quoted in US dollars and subject to change without notice.

Analytical
CHEMISTRY

EDITOR: **GEORGE H. MORRISON**

ASSOCIATE EDITORS: **Klaus Biemann, Georges Guiochon, Walter C. Herlihy, Robert A. Osteryoung, Edward S. Yeung**

Editorial Headquarters
1155 Sixteenth St., N.W.
Washington, DC 20036
Phone: 202-872-4570
Telefax: 202-872-6325

Managing Editor: Sharon G. Boots

Associate Editors: Louise Voress, Mary Warner

Assistant Editors: Grace K. Lee, Alan R. Newman

Editorial Assistant: Felicia Wach

Director, Operational Support: C. Michael Phillippe

Production Manager: Leroy L. Corcoran

Art Director: Alan Kahan

Designer: Amy Meyer Phifer

Production Editor: Elizabeth E. Wood

Circulation: Claud Robinson

Editorial Assistant, LabGuide: Joanne Mullican

Journals Dept., Columbus, Ohio

Associate Head: Marianne Brogan

Journals Editing Manager: Joseph E. Yurvati

Associate Editor: Rodney L. Temos

Staff Editor: Sharon K. Hatfield

Advisory Board: Bernard J. Bulkin, Michael S. Epstein, Renaat Gijbels, Peter R. Griffiths, Thomas L. Isenhour, Nobuhiko Ishibashi, James W. Jorgenson, Peter C. Jurs, Mary A. Kaiser, David L. Nelson, Lawrence A. Pachla, Ralph E. Sturgeon, George S. Wilson, Mary J. Wirth, Andrew T. Zander, Richard N. Zare
Ex Officio: Sam P. Perone

Instrumentation Advisory Panel: James B. Callis, Bruce Chase, R. Graham Cooks, L. J. Cline Love, Sanford P. Markey, Ronald E. Majors, Linda B. McGown, Gary W. Small, R. Mark Wightman

Published by the
AMERICAN CHEMICAL SOCIETY
1155 16th Street, N.W.
Washington, DC 20036

Publications Division

Director: Robert H. Marks

Journals: Charles R. Bertsch

Special Publications: Randall E. Wedin

Manuscript requirements are published in the January 1, 1989 issue, page 91. Manuscripts for publication (4 copies) should be submitted to ANALYTICAL CHEMISTRY at the ACS Washington address.

The American Chemical Society and its editors assume no responsibility for the statements and opinions advanced by contributors. Views expressed in the editorials are those of the editors and do not necessarily represent the official position of the American Chemical Society.

AUTHOR INDEX

Abruña, H. D., 2599
Anjo, D. M., 2603
Avery, J. P., 2624

Baldwin, R. P., 2594
Bangs, J. D., 2686
Barber, A. S., 2658
Bean, M. F., 2686
Birks, J. W., 2624
Brooks, G. H., 2682

Colby, S. M., 2669
Cotter, R. J., 2686

Doering, T. L., 2686
Duell, K. A., 2624

Englund, P. T., 2686

Fenselau, C., 2686
Fernando, A. R., 2609

Gil-Av, E., 2688
Gladney, E. S., 2682

Hart, G. W., 2686
Heine, C. E., 2674
Hobo, T., 2688
Holcombe, J. A., 2652
Holland, J. F., 2674
Hughes, K. D., 2611
Hurtubise, R. J., 2643

Kahr, M., 2603
Khodabakhsh, M. M., 2603

Liu, K. E., 2599

Lytle, F. E., 2611

Majidi, V., 2652
McCreery, R. L., 2647

Noszál, B., 2631
Nowinski, S., 2603

Olesik, S. V., 2616

Pekay, L. A., 2616
Plambeck, J. A., 2609

Reilly, J. P., 2669
Richmond, M. D., 2643
Rowlen, K. L., 2624

Sándor, P., 2631
Seitz, D. M., 2682
Seitzinger, N. K., 2611
Small, G. W., 2658
Sutcliffe, C. R., 2682
Suzuki, S., 2688

Thomsen, K. N., 2594

Wade, A. P., 2638
Wang, P., 2652
Wang, Y., 2647
Wanger, M., 2603
Warner, A. M., 2664
Watabe, K., 2688
Watson, J. T., 2674
Weber, S. G., 2664
Wentzell, P. D., 2638
Wilkerson, C. W., Jr., 2669

Amperometric Detection of Nonelectroactive Cations in Flow Systems at a Cupric Hexacyanoferrate Electrode

Karsten N. Thomsen[1] **and Richard P. Baldwin***

Department of Chemistry, University of Louisville, Louisville, Kentucky 40292

A glassy carbon electrode coated with an electrodeposited film of cupric hexacyanoferrate (CuHCF) was evaluated as a sensor for nonelectroactive cations in flow injection and ion chromatography systems. In general, the activity of the CuHCF electrode in the flow environment was found to be similar to that seen for static solutions in that reduction of the film was selectively enhanced by potassium and ammonium ions. Consequently, these ions were able to be detected indirectly as cathodic peaks due to CuHCF reduction as sample plugs containing potassium or ammonium passed the electrode surface. Chromatographic detection limits at the submicromolar level and dynamic ranges extending over 3 orders of magnitude were obtained at an applied potential of +0.45 V vs Ag/AgCl. Coating the electrode with a supporting overlayer made of Nafion improved the stability and reproducibility in the flowstream to the extent that repetitive sample injections produced relative standard deviations of 1–5% over several hours of operation.

INTRODUCTION

Recently it has been demonstrated that electrodes modified with an electroactive polymer coating can be used as sensors for nonelectroactive anions in flow injection analysis and high performance liquid chromatography (HPLC) (*1–3*). In all cases, the polymers employed contained oxidizable groups that form positively charged sites in the film upon electrooxidation. Appreciable current can occur for these systems only if anions capable of penetrating the polymer and counterbalancing the positive charge generated in the film are present at the polymer–solution interface. Therefore, anion detection can be accomplished by placing the polymer electrode in the flowstream, poising the potential at a sufficiently positive value to effect oxidation of the polymer, and waiting for a sample plug containing such anions to arrive. When this occurs, there is a transient current flow which, although due to oxidation of the polymer, is proportional in magnitude to the anion concentration in the plug. By means of this approach, subnanomole amounts of anions such as NO_3^- and ClO_4^- were able to be detected in flow injection experiments (*3*).

Naturally, this raised the question whether nonelectroactive cations could be detected by an analogous scheme utilizing a reducible polymer in which the formation of negative sites upon reduction is accompanied by the transport of cations into the film. Our attention in this endeavor was focused on the class of insoluble mixed valence transition-metal hexacyanometalate polymers which are readily formed on a variety of electrode materials. The prototype of these compounds is Prussian Blue (iron(III) hexacyanoferrate(II)), whose incorporation onto carbon, gold, and platinum surfaces has been studied by Neff (*4, 5*) and Itaya (*6*). In addition, related compounds involving other metals such as nickel (*7, 8*), copper (*9, 10*), and ruthenium (*5, 11–13*) have also been investigated, and the resulting class of electrodes has recently been reviewed (*14*).

The three-dimensional network formed by the mixed valence hexacyanometalate polymers is zeolitic in nature and can readily exchange group 1A cations in aqueous solution (*13*). The peak potentials and shapes of the redox waves seen at the coated electrode are highly dependent on the nature of the electrolyte cation—with electroactivity persisting for long times only if hydrated cations small enough to be accommodated within the pores of the network are available in solution. Furthermore, for ions of different size, incorporation into the polymer produces structural changes in the film that alter its redox potential to different extents. The presence of ions possessing a relatively small hydrated radius causes film reduction to be favored and to occur at more positive potentials (*8*). Thus, for the nickel hexacyanoferrate electrode, stable electroactivity has been shown to occur over a 500-mV range, depending on the cation present in solution during voltammetric scanning (*7*). Because of size considerations, the redox process, which occurs at +0.6 V vs SCE with Cs^+, is shifted to +0.1 V with Li^+.

Several applications of these electrodes as analytical sensors have been reported in the literature. Cox applied a ruthenium oxide–ruthenium cyanide electrode for the electrocatalytic determination of As(III) (*12*) and thiocyanate (*15*). For As(III), sensitivities in the micromolar range were obtained in batch experiments (*12*), while thiocyanate could be detected at 2×10^{-7} M in a flow injection setup (*15*). Bocarsly showed that minute concentrations—10^{-8} M—of Cs^+ could be sensed in the presence of a large excess of Na^+ with the nickel hexacyanoferrate electrode (*8*). This was done indirectly in a batch experiment by measuring the decrease in the voltammetric wave associated with Na^+ incorporation caused by the presence of small quantities of Cs^+. Very recently—after this project was initiated—Deakin and Byrd showed that a Prussian Blue film electrodeposited on a quartz crystal microbalance could be used to detect the incorporation of nonelectroactive cations in a flow injection experiment (*16*). The cations were detected both by the frequency change of the microbalance and by the current transients from the Prussian Blue reduction. A detection limit of 10^{-4} M K^+ was reported for the microbalance approach. One of the most important characteristics of many of these electrodes was their impressive stability, typically extending over thousands of voltammetric cycles and hundreds of injections (*7, 9, 15*).

In this paper, we demonstrate that a cuprihexacyanoferrate (CuHCF) film electrodeposited onto glassy carbon can be utilized as a sensor for potassium and ammonium ions in flowing solutions. In the presence of potassium ions, the redox process involved in the electrode activity can formally be represented as (*9*)

$$Cu^{II}_3(Fe^{III}(CN)_6)_2 + 2e^- + 2K^+ = K_2Cu^{II}_3(Fe^{II}(CN)_6)_2$$

The behavior of the electrode has been characterized with respect to several experimental parameters in flow injection, and the application of the electrode for the detection of K^+ and NH_4^+ following cation-exchange HPLC is demonstrated.

EXPERIMENTAL SECTION

Reagents. Concentrated stock solutions of cations were prepared from the reagent grade nitrate, chloride, or sulfate salts and were diluted to the desired concentration just prior to use.

---

[1] Permanent address: Kemisk Institut, Aarhus University, DK-8000 Aarhus C, Denmark.

0003-2700/89/0361-2594$01.50/0 © 1989 American Chemical Society

Dilute nitric acid solutions were prepared from reagent grade concentrated nitric acid. Nafion polymer solutions, obtained at 5 wt % from Aldrich, were diluted to 0.45 wt % with ethanol before use.

Electrode Preparation. The procedure used here for modification of glassy carbon electrodes was essentially the same as that developed by Siperko and Kuwana (*9*). A glassy carbon electrode, freshly polished with 0.05-μm alumina, was placed in a 4×10^{-3} M solution of $Cu(NO_3)_2$ in 0.05 M $KClO_4$ and cycled between +0.5 and −0.5 V vs Ag/AgCl at 50 mV/s until reproducible plating/stripping signals were observed (five to eight cycles). After the electrode was scanned to −0.5 V with the solution stirred, an amount of $K_4Fe(CN)_6$ equivalent to the $Cu(NO_3)_2$ was injected into the cell with a syringe. A red-brown sol was immediately formed, and after the reduction current faded away, the electrode was removed from the cell and flushed with deionized water. At this point, a red-brown layer was clearly visible on the electrode surface which was allowed to air-dry and then was coated with a 2-μL droplet of Nafion solution. Following evaporation of the residual solvent, the electrode was scanned in 1.0 M KCl between +0.4 V and +1.0 V until a steady-state current–voltage profile was obtained. The resulting voltammogram showed a pair of very symmetrical peaks from the iron redox couple at +0.75 V. Last, the cycling was stopped at +0.4 V—i.e., with the film fully reduced—and the electrode could be transferred to the flow cell for use. When nitric acid was employed as the mobile phase, the potential applied to the electrode in the flow system could be changed anodically (i.e., ion outflow) with no difficulty. However, once the film had been so oxidized, subsequent shifts to reducing potentials (i.e., ion uptake) caused the electrode performance to deteriorate unless a sample of a strong potassium solution (e.g., 0.1 M KCl) was first injected and the flow was stopped when the K^+ plug reached the electrode. This allowed the film to be reduced with a cation present that was well suited to penetrate the film and balance the negative charge generated during film reduction.

Evaluation of Electrode Response. The responses in flow injection and HPLC experiments were quantified either by measuring the height of the peak corresponding to CuHCF reduction upon analyte elution or by measuring the difference between the maximum current in the reduction of the film and the minimum current in the following reoxidation. Both quantities appeared to yield equally reproducible results, and calibration curves constructed from the two approaches differed only by a scale factor. Because the difference between maximum and minimum currents afforded the most reliable quantification of partly overlapping responses in HPLC, this approach was used in all HPLC experiments. Simple peak height was used in flow injection experiments.

Apparatus. Cyclic voltammetry was performed with either a Bioanalytical Systems Model CV-1B or an IBM EC/225 potentiostat. A Bioanalytical Systems Model MF1000 glassy carbon electrode (modified or unmodified) was used in conjunction with an Ag/AgCl (saturated KCl) reference electrode and a platinum wire auxiliary electrode. Flow injection and HPLC experiments were carried out with a Perkin-Elmer Series 10 pump, a Rheodyne (Berkeley, CA) Model 7125 injector with a 20-μL sample loop, and a Bioanalytical Systems Model LC-3 amperometric detector. Furthermore, an SSI Model LP-21 pulse dampener was inserted between the pump and injector for flow injection experiments. A Bioanalytical Systems Model MF2020 Ag/AgCl (saturated KCl) reference electrode and a stainless steel auxiliary electrode were employed in the flow system. All chromatographic separations were performed at room temperature with one or two 5 cm long, 4.6 mm i.d. Vydac 400-IC405 cation-exchange columns (Rainin Co., Woburn, MA).

RESULTS AND DISCUSSION

Characterization in Flow Injection. To demonstrate that the CuHCF-coated glassy carbon electrode was sensitive to cations in a flow system, its response was compared to that of a plain, freshly polished glassy carbon electrode in a flow injection experiment. Figure 1a shows the response at the plain electrode held at +0.40 V when a sample, 0.010 M in KNO_3 and 0.090 M in HNO_3, was injected into a carrier stream of 0.10 M HNO_3. No significant change in the electrode response was observed in this case. Figure 1b shows the behavior observed for the CuHCF-coated electrode when a sample of 0.0010 M KNO_3 and 0.099 M HNO_3 was injected into the same mobile phase. (Note that, although the potassium concentration in the latter experiment was only one-tenth of the previous concentration, the current scale used was 10 times larger.) Here, each injection gave rise to a current transient corresponding to a reduction of the film as the plug of potassium ions reached the electrode. As the cations left the electrode again, a slower reoxidation of the film was seen. The electrode potential in both these experiments was +0.40 V, but similar behavior was observed for other potentials in the +0.40 to +0.60 V range. The comparison with the unmodified glassy carbon electrode showed clearly that the current transients observed with the polymer-modified electrode resulted from the specific activity of the film and not from changes in physical properties of the mobile phase (such as conductivity) as the sample plug passed the electrode.

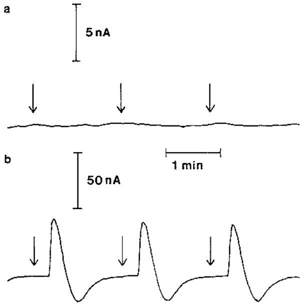

Figure 1. Flow injection responses obtained at (a) an unmodified glassy carbon electrode and (b) the CuHCF electrode: injection of (a) 0.01 M KNO_3 and (b) 0.001 M KNO_3 into 0.10 M nitric acid; injections are marked with arrows; potential, +0.40 V; flow rate, 1.0 mL/min.

When the experiment in Figure 1b was performed with an electrode coated only with the CuHCF film, the response decreased appreciably on repeated injections of identical samples. This effect, which can even be noted in the figure, was attributed to mechanical erosion of the film upon exposure to the flowing solution. To overcome this problem, a film of the perfluorosulfonic acid polymer Nafion was coated on top of the CuHCF film. Thick Nafion films used in this manner were found to hinder diffusion of cations to and from the CuHCF layer somewhat and produced very broad responses as a result. However, thinner films formed by depositing only a 2-μL droplet of a 0.45 wt % Nafion solution onto the chemically modified electrode (CME) allowed rapid diffusion and response and still imparted improved mechanical stability to the CuHCF layer. The extent of the improvement is illustrated in Table I for periodic injections of a potassium standard at four different electrodes. The standards summarized in the table were injected interspersed with other samples to verify the electrode stability even while other experiments were being performed. Also, it was found that electrode activity could be conserved from day to day, either by allowing the mobile phase to continue to flow by the electrode at a low rate (0.1 mL/min) with the working potential applied or by disconnecting the cell and allowing the electrode to air-dry after it had been flushed thoroughly with deionized water.

Initially, three different mobile phases were tested in flow injection experiments: diluted nitric acid, sodium chloride, and lithium perchlorate. The largest reduction response and fastest reoxidation of the electrode were found for the nitric

Table I. Reproducibilities for the CuHCF Electrode

$[K^+]$/M	n^a	RSD/%	time period/h
10^{-4}	9	0.8	0.5
10^{-4}	12	1.9	0.8
10^{-4}	21	2.8	1.5
10^{-5}	45	4.7	3.8

[a] n = number of sample injections.

Table II. Relative Response of CuHCF Electrode for Various Cations

ion	rel peak height	ion	rel peak height
K^+	1.0	Na^+	0.07
NH_4^+	1.7	Mg^{2+}	0.03
Li^+	0.05	Ca^{2+}	0.12

acid and lithium perchlorate media. The former was investigated most thoroughly because this medium was known to be suitable for the intended application of the electrode in HPLC.

The sensitivity of the CuHCF electrode toward other cations besides potassium was studied by comparing the response for samples containing 1.0×10^{-3} M of the cation under study to that for 1.0×10^{-3} M potassium ion. The samples were injected into a 0.10 M nitric acid mobile phase, and the potential of the electrode was held at +0.45 V. The responses for NH_4^+, Li^+, Na^+, Mg^{2+}, and Ca^{2+} are summarized in Table II where the peak heights so obtained are given relative to the potassium peak height. Clearly, the electrode showed selectivity toward potassium and ammonium ions compared to the other cations. This was expected from the earlier work by Siperko and Kuwana (*9, 10*) who found that the CuHCF film activity was stable in the presence of either one of these ions while deterioration of the electrode's activity was observed in the presence of sodium and lithium. This preference was explained by the good match of the ionic radii of the hydrated potassium and ammonium cations with the pore size of the zeolitic channels in the CuHCF film. Thus, penetration of these cations into the film was relatively facile. As seen in Table II, the film did show some activity in the presence of other cations, most notably sodium and calcium. Therefore, either of these ions could be possible interferents in the determination of potassium or ammonium by flow injection. This was investigated more closely by observing the effect of 10^{-4} M, 10^{-3} M, and 10^{-2} M Na^+ on the signal obtained for 10^{-4} M K^+ standard. The resulting increases in peak height relative to the standard were 0, 7, and 110%, respectively. This shows that sodium in approximately equal amounts can be tolerated in flow injection determinations of potassium, but if sodium is much in excess of the potassium, a serious interference should be expected.

It should be noted that injection of cations other than potassium and ammonium had no deleterious effect on the film as the response from a potassium standard in a nitric acid medium could in all cases be reproduced nicely when the standard was injected intermittently with samples containing other cations. This is in contrast with cyclic voltammetric experiments where activity ceased or decreased drastically if the electrode was cycled in electrolytes without potassium or ammonium.

Hydrodynamic voltammograms (HDV's) for the CuHCF electrode were obtained for potassium and ammonium in three different nitric acid media. The samples, 10^{-4} M in one of the two ions, were dissolved in nitric acid of the same concentration as the mobile phase under investigation, and the potential was gradually changed in the anodic direction. Parts a–c of Figure 2 show the HDV's obtained in 0.10, 0.020, and 0.0050 M nitric acid, respectively. There are several things to notice in these figures. First, the interval over which the film showed maximum activity in flow injection occurred at modest potentials for both ions. The +0.35 to +0.50 V range seen here was somewhat lower than that which has been reported in cyclic voltammetry studies (*9*), but the much lower potassium and ammonium concentrations in effect here could well account for this difference. Second, the preference for ammonium ions over potassium was evident both from the larger peak currents and from the more positive peak potentials observed for ammonium in all three media. Third, there was only a slight dependence of the peak potential on the nitric acid concentration, with the 20-fold decrease in acid content employed producing a positive shift of only about 50 mV for both ions. Last, the reoxidation of the film following a cathodic peak was influenced both by the potential and the nitric acid concentration. The reoxidation was slowest by far at more negative potentials and in less concentrated acid solutions.

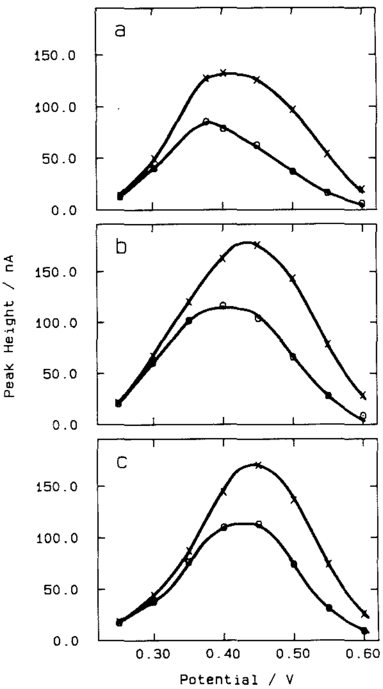

Figure 2. Hydrodynamic voltammograms for 1×10^{-4} M K^+ (O) and 1×10^{-4} M NH_4^+ (X) at the CuHCF electrode: mobile phases, (a) 0.10 M HNO_3, (b) 0.020 M HNO_3, (c) 0.0050 M HNO_3; flow rate, 2.0 mL/min.

The dependence of the potassium signal on nitric acid concentration is further illustrated in Figure 3a where the largest responses were clearly obtained in the less concentrated media. Most likely, this effect was due to the decreased competition from the protons for the exchange of the potassium ion into the film. At the same time, it was again observed that the time necessary to recover after a peak increased at lower acid concentrations; for instance, the recovery time from the beginning of a peak to the return to base line increased 55% (from 0.74 to 1.15 min) in going from 0.10 to 0.0050 M nitric acid. Over the same range, the peak height increased 6-fold.

The peak height was also influenced by the flow rate of the mobile phase. This is shown in Figure 3b for a 10^{-3} M po-

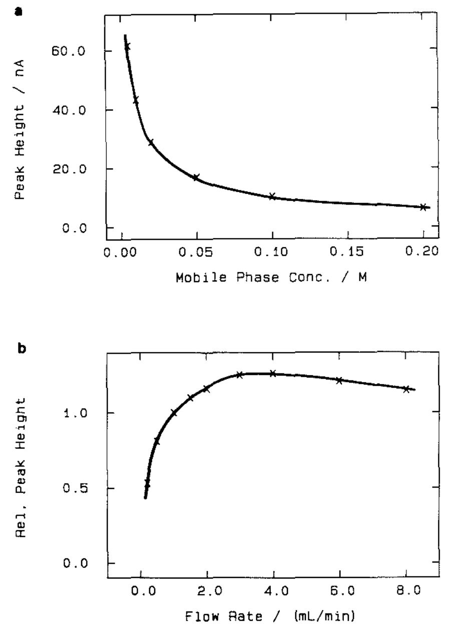

Figure 3. (a) Dependence of flow injection response on concentration of HNO_3 in mobile phase: sample, 1.0×10^{-4} M KNO_3; potential, +0.45 V; flow rate, 2.0 mL/min. (b) Dependence of flow injection response on flow rate: sample, 1.0×10^{-3} M KNO_3; mobile phase, 0.10 M HNO_3; potential, +0.40 V.

tassium sample, a mobile phase of 0.10 M nitric acid, and a potential of +0.40 V. Overall, the peak height increased dramatically with flow rate in the range from 0.2 to 3.0 mL/min and then leveled off and even decreased slightly at rates higher than 4.0 mL/min. This behavior might be rationalized in terms of the diffusion of cations through the Nafion coating and into the film. If, at lower flow rates, diffusion is rapid compared to the residence time of the sample plug in the cell, the peak height is determined by the degree of dispersion of the sample on the way to the cell. Thus, larger signals would be observed at higher flow rates. But if the diffusion in the film becomes the limiting factor at very high flow rates, a decrease in signal should start to be seen as fewer cations are able to penetrate the film during the shorter residence time afforded to the sample plug in the cell. The variation in CME recovery time with flow rate was also consistent with this explanation. Recovery times became shorter as the flow rate was increased up to 4.0 mL/min and did not change significantly at higher values.

With all these experiments in mind, calibration curves were able to be obtained for potassium and ammonium under roughly optimized conditions: 0.0050 M nitric acid mobile phase, a flow rate of 2.0 mL/min, and a potential of +0.45 V. A typical set of curves corresponding to these conditions is shown in Figure 4 for the 10^{-6} to 10^{-4} M concentration range. A 10^{-5} M potassium standard was injected intermittently with the other samples, and the peak heights are given relative to the mean of the peak heights for this standard. Nonlinear calibration plots were obtained for both analytes, again with a larger response seen for ammonium. For both ions, well-defined peaks could be obtained even at concentrations of 10^{-6} M (or 20 pmol injected). Good sensitivity was also observed in stronger nitric acid mobile phases; for example, a calibration curve extending over potassium concentrations from 10^{-6} to 10^{-3} M could be obtained in 0.10 M nitric acid.

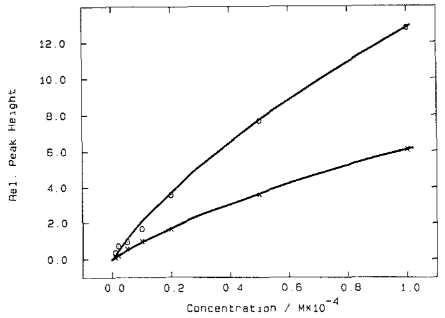

Figure 4. Calibration curves obtained in flow injection for K^+ (X) and NH_4^+ (O) ions: mobile phase, 0.0050 M HNO_3; potential, +0.45 V; flow rate, 2.0 mL/min. Each data point represents the average of three separate injections.

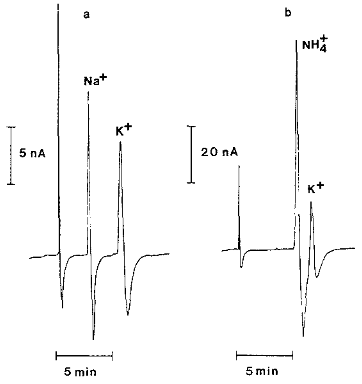

Figure 5. Chromatograms of mixtures containing (a) 1.0×10^{-3} M Na^+ and 5.0×10^{-5} M K^+ and (b) 1.0×10^{-4} M NH_4^+ and 1.0×10^{-4} M K^+: mobile phase, 0.0025 M HNO_3; potential, +0.45 V; flow rate, 2.0 mL/min.

Application in HPLC. After characterization of the CuHCF electrode in flow injection, it was applied as the detector in an HPLC system with a cation exchange column. Two examples of this application are illustrated in Figure 5. First, the chromatogram for a sample containing 10^{-3} M sodium and 5×10^{-5} M potassium is shown in Figure 5a. With a 0.0025 M nitric acid mobile phase, the two cations were base line resolved, with Na^+ eluting first. Obviously, it would present no problem to quantify potassium in the presence of excess sodium by this approach. In Figure 5b, a similar chromatogram of a sample containing 10^{-4} M of both potassium and ammonium ions is shown. In this case, the two cations were not able to be fully resolved as the electrode had not completely recovered from the ammonium peak when the potassium band arrived at the electrode. Because the film was not fully reoxidized under these conditions, a somewhat smaller potassium signal was obtained for the mixture than for a pure potassium sample. This was confirmed in an experiment where a 5×10^{-5} M potassium standard was compared with samples containing the same amount of potassium and varying amounts of ammonium. For ratios of ammonium to potassium concentration of 0.1, 1.0, and 2.0, signals of 0.96, 0.67, and 0.51 relative to the response for the pure standard were found. The responses were evaluated as the difference between the maximum peak current and the minimum trough

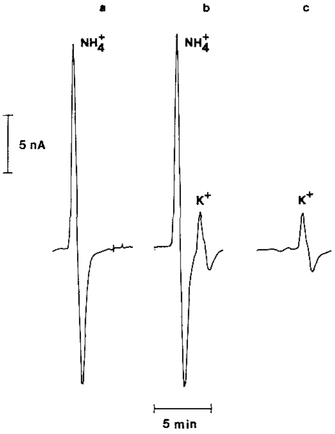

Figure 6. Chromatograms of (a) 1.0 × 10^{-4} M NH_4^+, (b) 1.0 × 10^{-4} M NH_4^+ and 1.0 × 10^{-4} M K^+, (c) 1.0 × 10^{-4} M K^+ with two columns. Other conditions are given in Figure 5.

current in the following reoxidation. Because even small amounts of ammonium ions in the sample influenced the potassium signal, it was apparent that only the former could be reliably determined in a mixture by this approach.

However, by combination of two columns in series and otherwise keeping the conditions the same as above, it was possible to separate potassium and ammonium sufficiently well that ammonium no longer interfered with the potassium signal. This is illustrated in Figure 6, where Figure 6a shows part of a chromatogram of a sample 10^{-4} M in ammonium only, Figure 6b illustrates a sample 10^{-4} M in both potassium and ammonium, and Figure 6c shows the signal from a sample 10^{-4} M in potassium only. Compared to the pure potassium sample, the corresponding peak in the mixture showed no attenuation. This was further demonstrated by injection of a number of samples containing the same amount of potassium and varying amounts of ammonium. For example, for samples containing 10^{-4} M potassium (two injections), 10^{-4} M potassium and 5 × 10^{-5} M ammonium (two injections), and 10^{-4} M potassium and ammonium ions (three injections), the potassium signal for all seven injections was reproduced with a relative standard deviation of only 2.0%. At lower concentrations of the two ions, the interference was even less than this.

The HPLC detection limits (signal/noise = 3) for potassium and ammonium ions were estimated under the conditions of Figure 5. A series of chromatograms for samples containing 5 × 10^{-6}, 2 × 10^{-6}, 1 × 10^{-6}, and 5 × 10^{-7} M potassium and ammonium ions are shown in Figure 7. The inset shows the calibration curves constructed from these chromatograms. As seen in the figure, detection limits of 5 × 10^{-7} M, corresponding to 10 pmol injected, for both potassium and ammonium were realistic. Furthermore, under these chromatographic conditions, the potassium response was somewhat decreased by the ammonium (as demonstrated above); so injection of pure potassium samples would give somewhat larger responses.

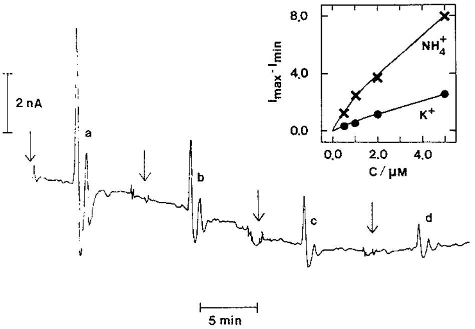

Figure 7. Chromatograms of samples containing (a) 5.0 × 10^{-6} M, (b) 2.0 × 10^{-6} M, (c) 1.0 × 10^{-6} M, and (d) 5.0 × 10^{-7} M of both NH_4^+ and K^+. Injections are marked with arrows. The inset shows the corresponding calibration curves. Conditions are the same as those given in Figure 5.

CONCLUSION

Several previous studies have demonstrated that electrodes coated with transition-metal hexacyanoferrates offer the possibility for detection of nonelectroactive cations such as the group 1A metals. Nearly all of these investigations, however, have employed the electrodes in cyclic voltammetry experiments performed in static solution. In this work, we have explored the suitability of these electrodes—in particular, that formed with cuprihexacyanoferrate—as sensors for these analytes in flow injection and ion chromatography systems. With the CuHCF electrode, selective, but not specific, response for potassium and ammonium was obtained at modest values of applied potential, with detection limits in the submicromolar range. In addition, when the electrode was coated with a supporting Nafion layer, its stability, reproducibility, and dynamic range toward these two ions were attractive for potential applications in flow detection. Most importantly, the electrode operation was compatible with the low ionic strength mobile phases typically employed in modern ion chromatography. Though not attempted in this work, use of the CuHCF electrode for the analysis of real samples appears promising, with the determination of potassium in the presence of sodium in clinical samples as the most obvious application. In such applications, another aspect of the Nafion coating may be advantageous, namely that the surface-active constituents of the samples are prevented from reaching the CuHCF layer.

ACKNOWLEDGMENT

We thank Dr. Robert Buchanan for very helpful discussions.

LITERATURE CITED

(1) Ikariyama, Y.; Heineman, W. R. *Anal. Chem.* **1986**, *58*, 1803–1806.
(2) Ikariyama, Y.; Galiatsatos, C.; Heineman, W. R.; Yamauchi, S. *Sens. Actuators* **1987**, *12*, 455.
(3) Ye, J.; Baldwin, R. P. *Anal. Chem.* **1988**, *60*, 1979–1982.
(4) Ellis, D.; Eckhoff, M.; Neff, V. D. *J. Phys. Chem.* **1981**, *85*, 1225–1231.
(5) Rajan, K. P.; Neff, V. D. *J. Phys. Chem.* **1982**, *86*, 4361–4368.
(6) Itaya, K.; Tatsuaki, A.; Toshima, S. *J. Am. Chem. Soc.* **1982**, *104*, 4767–4772.
(7) Sinha, S.; Humphrey, B. D.; Bocarsly, A. B. *Inorg. Chem.* **1984**, *23*, 203–212.
(8) Amos, L. J.; Duggal, A.; Mirsky, E. J.; Ragonesi, P.; Bocarsly, A. B.; Fitzgerald-Bocarsly, P. A. *Anal. Chem.* **1988**, *60*, 245–249.
(9) Siperko, L. M.; Kuwana, T. *J. Electrochem. Soc.* **1983**, *130*, 396–402.
(10) Siperko, L. M.; Kuwana, T. *Electrochim. Acta* **1987**, *32*, 765–771.
(11) Itaya, K.; Ataka, T.; Toshima, S. *J. Am. Chem. Soc.* **1982**, *104*, 3751–3752.
(12) Cox, J. A.; Kulesza, P. J. *Anal. Chem.* **1984**, *56*, 1021–1025.
(13) Kulesza, P. J. *J. Electroanal. Chem.* **1987**, *220*, 295–309.
(14) Itaya, K.; Uchida, I.; Neff, V. D. *Acc. Chem. Res.* **1986**, *19*, 162–168.
(15) Cox, J. A.; Gray, T.; Kulkarni, K. R. *Anal. Chem.* **1988**, *60*, 1710–1713.
(16) Deakin, M. R.; Byrd, H. *Anal. Chem.* **1989**, *61*, 290–295.

RECEIVED for review June 19, 1989. Accepted September 8, 1989. K.N.T. appreciates financial support from the Danish Natural Science Research Council (Grant No. 11-7145) and the Danish Research Academy (Grant No. F890069). The work was also supported by the College of Arts and Sciences of the University of Louisville.

Anal. Chem. **1989**, *61*, 2599–2602

Electroanalysis of Aromatic Aldehydes with Modified Carbon Paste Electrodes

Katherine E. Liu and Héctor D. Abruña*

Department of Chemistry, Baker Laboratory, Cornell University, Ithaca, New York 14853-1301

The utility of carbon paste electrodes modified with aniline, 4-aminobenzoic acid, or $[Fe(CN)_5L]^{3-}$ (L = 4-aminopyridine) for the determination of aldehydes in solution is demonstrated. The method is based on the reactivity of an immobilized aromatic primary amine toward aldehydes to yield the corresponding imine whose redox response is used as the analytical signal. The effects of paste composition and time of reaction on the analytical signal were assessed for the three modifiers mentioned above. Electrodes modified with $[Fe(CN)_5L]^{3-}$ gave the best results in terms of signal to noise ratio, reproducibility, and electrode stability. Submicromolar amounts of benzaldehyde could be determined by employing this approach. The approach is also applicable to the determination of aliphatic aldehdyes (butyraldehyde) although with diminished sensitivity. The presence of other non-aldehyde carbonyl species (e.g. benzophenone) had no detrimental effects on the analytical signal.

INTRODUCTION

The use of chemically modified electrodes (CME) in analytical applications (*1, 4*) continues to be an area of vigorous research activity. A broad range of approaches has been pursued including electrostatic accumulation (*5–12*), coordination effects (*12–20*), precipitation (*21, 22*), and others (*23–29*). Electrode modification has also been employed to prevent electrode fouling or to enhance selectivity (or both) in analytical determinations of dopamine and related biogenic amines (*30–33*). In addition, many electrode materials have been modified for use in analytical determinations. Of these, the use of carbon paste electrodes (CPE) appears especially advantageous because of the ease of electrode preparation and regeneration as well as low background currents.

In fact a number of studies on the use of CPE for analytical determinations have been previously reported. These include the use of a CPE containing dimethylglyoxime for the determination of nickel (*19*), 1,9-dimethyl-9,10-phenanthroline for the determination of copper (*20*), and 1,10-phenanthroline for the determination of cobalt and iron. Phthalocyanine-modified carbon paste electrodes have also been employed in the determination of sulfhydryl groups (*34*) and α-keto acids (*35, 36*).

We recently demonstrated the utility of chemically modified CPE for the determination of primary amines (*37*). The approach was based on the reaction of the amine with an aromatic aldehyde, incorporated into a polymer film to generate the corresponding imine whose electrochemical response was used as the analytical signal. By use of this approach, submicromolar sensitivity as achieved as well as a dynamic range of about 3 orders of magnitude.

We have extended this approach to the determination of aldehydes by incorporating an aromatic amine group into the carbon paste electrode to make an imine and again use its redox response as the analytical signal.

We present a thorough study of such an analysis system including the use of three different reagents containing the aromatic amine group, carbon paste composition in terms of reagent loading, and preconcentration time.

EXPERIMENTAL SECTION

Reagents. Aniline and benzaldehyde (Aldrich) were vacuum distilled twice and stored under nitrogen in amber bottles. 9-Anthraldehyde, 1-naphthaldehyde, and 4-aminobenzoic acid (Aldrich) were recrystallized from ethanol. 4-Aminopyridine and pentacyanoaminoferroate, $[Fe(CN)_5NH_3]^{3-}$ (Aldrich), were used as received. Water was purified by passing through a Hydro water purification train or a Millipore Milli Q system. Acetonitrile (Burdick and Jackson distilled in glass) was dried over 4-Å molecular sieves. Tetra-*n*-butylammonium perchlorate (TBAP; G. F. Smith) was recrystallized 3 times from ethyl acetate and dried under vacuum for 72 h. $[Fe(CN)_5L]^{3-}$ (L = 4-aminopyridine) referred to in the text as the "iron complex" was prepared by dissolving the ammonium disodium salt of pentacyanoamino ferroate in water and adding (dropwise) a stoichiometric amount of 4-aminopyridine. Substitution of the amino group by the 4-aminopyridine was immediately apparent from the color change (from yellow-green to purple). After being stirred for 30 min at room temperature the solution was filtered. The complex was isolated by removing the water with gentle heating under vacuum. The isolated complex was washed with ether and dried under vacuum overnight.

Instrumentation. Electrochemical experiments were performed on either a BAS 100 electrochemical analyzer or an IBM EC 225 voltammetric analyzer. Data were recorded on a Soltec X-Y recorder. Differential pulse voltammograms (DPV) were obtained by using a 50-mV pulse width and a scan rate of 10 mV/s. Electrochemical cells of conventional design were employed. All potentials are referenced to the sodium-saturated calomel electrode (SSCE) without regards for the liquid junction.

Electrodes. Platinum (sealed in glass) and glassy carbon (sealed in Teflon) disk electrodes were polished with 1-μm diamond paste (Buehler) and rinsed with water and acetone prior to use. Carbon paste electrodes were prepared by mixing graphite powder (Fisher) (typically 1 g) into a solution of ceresin wax (0.1 g) in heptane. The components were thoroughly mixed and the solvent was allowed to evaporate. The amine-containing reagent (i.e. aniline, 4-aminobenzoic acid, or the iron complex) was dissolved (the amine-reagent/graphite powder ratio was varied from 10% to 80%) in ethanol and added to the carbon/wax mixture. It was thoroughly mixed and the solvent was evaporated until a free-flowing powder was obtained. Paraffin oil (0.3–0.4 mL) was added and the mixture was again thoroughly mixed to a smooth consistency paste.

The paste was placed in the cup of a locally designed and built carbon paste electrode assembly made from Kel-F with a platinum wire contact. The body and plunger of the electrode assembly were threaded so that carbon paste could be extruded by simply turning the plunger. The surface of the carbon paste electrode was smoothed by gently rubbing on a piece of filter paper with graphite powder. This procedure was also employed in regenerating the surface of the carbon paste electrode.

Procedures. The carbon paste electrode was immersed in 5 mL of ethanol or 50/50 ethanol/water solution of the aldehyde to be determined (e.g. benzaldehyde) and HCl was added (imine formation is acid catalyzed) to a concentration of 0.02 M. The electrode was allowed to contact the solution for different time periods (vide infra) while stirring. The electrode was rinsed with water and acetone and placed in a degassed (with nitrogen or argon for 20 min) acetonitrile solution/0.1 M TBAP and the redox response of the imine formed was obtained by DPV. The height

0003-2700/89/0361-2599$01.50/0 © 1989 American Chemical Society

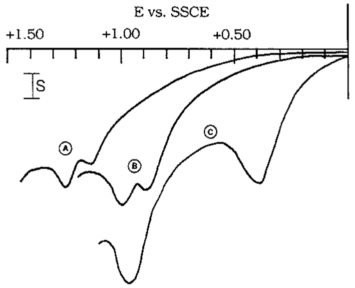

Figure 1. Differential pulse voltammograms in acetonitrile/0.1 M TBAP and in the oxidative region for carbon paste electrodes modified with (A) 4-aminobenzoic acid (35% loading), (B) aniline (50% loading), and (C) the iron complex (10% loading) after imine formation with benzaldehyde at a concentration of 1.0×10^{-3} M. Current scale S = 25 nA for A and B and 50 nA for C.

of this wave was employed in obtaining calibration curves. All analytical measurements represent the average of at least four replicate determinations. The surface of the carbon paste electrode was regenerated prior to each determination.

RESULTS AND DISCUSSION

The effects of a number of parameters on the analytical response were investigated. These included (a) source of incorporated aromatic amine, (b) loading level of reagent into the carbon paste, and (c) incorporation time.

Benzaldehyde was used as a representative analyte in order to determine the optimal conditions for analysis. The results are presented by considering the various reagents and the effects of loading and incorporation time.

Preliminary Voltammetric Characterization. The redox responses of the carbon paste electrodes containing the various amine reagents were obtained after imine formation (with benzaldehyde) in acetonitrile/0.1 M TBAP in order to determine the optimal redox wave to be employed on analytical determinations. Because of the inherent advantage of employing oxidative processes (no degassing is required) in the analytical determination, such processes were investigated first. Figure 1 shows anodic scans (DPV) for the carbon paste electrodes modified with 4-aminobenzoic acid (A), aniline (B), and the iron complex (C) after imine formation with benzaldehyde. For carbon paste electrodes modified with aniline, the peak potentials for oxidation of the amine and the imine were +0.91 and +1.0 V, respectively. For electrodes modified with 4-aminobenzoic acid the corresponding values were +1.23 and +1.13 V. It is clear that in these two cases the large overlap of the two voltammetric waves would make analytical quantification difficult. On the other hand, the redox responses for the amine and imine for carbon paste electrodes modified with the iron complex were very well resolved (Figure 1C).

Because of the significant overlap of voltammetric waves for the amine and imine oxidations for electrodes modified with aniline or 4-aminobenzoic acid, the reduction processes were investigated. We found that whereas the amines did not exhibit any reduction peak in the region from 0.0 to −1.50 V, the imines derived from aniline and 4-aminobenzoic acid with benzaldehyde had very well defined redox responses at −0.83 (Figure 2A) and −0.94 (Figure 2C) V, respectively. An analogous behavior was observed for electrodes modified with the iron complex. In this case in imine had a very well defined reduction at −0.63 V (Figure 2B). The results of these preliminary studies are summarized in Table I.

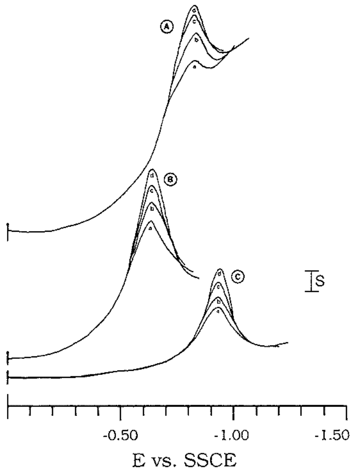

Figure 2. Representative DPV responses for the determination of benzaldehyde with carbon paste modified electrodes. (A) Electrode modified with aniline at 50% loading. Benzaldehyde concentrations: a, 5×10^{-5}; b, 1×10^{-4}; c, 1.5×10^{-4}; d, 1.8×10^{-4}. S = 50 nA. (B) Electrode modified with the iron complex at 10% loading. Benzaldehyde concentrations: a, 5×10^{-5}; b, 1×10^{-4}; c, 1.5×10^{-4}; d, 2.0×10^{-4}. S = 100 nA. (C) Electrode modified with 4-aminobenzoic acid at 35% loading. Benzaldehyde concentrations: a, 1.5×10^{-4}; b, 2.0×10^{-4}; c, 3.0×10^{-4}; d, 4.0×10^{-4}. S = 50 nA.

Table I. Peak Potential Values[a] for the Redox Responses of Amine Containing Reagents and the Imines Derived from Benzaldehyde[b]

	reagent	oxid	red.
1	aniline	+0.91	
	imine	+1.0	−0.83
2	4-aminobenzoic	+1.23	
	imine	+1.13	−0.94
3	$[Fe(CN)_5L]^{-3}$	+0.38	
	imine	+0.95	−0.64

[a] In volts vs SSCE. [b] In acetonitrile/0.1 M TBAP.

For studies with electrodes modified with aniline or 4-aminobenzoic acid, the reduction waves were employed as the analytical signal. For electrodes modified with the iron complex, both the oxidative and the reductive processes were studied and similar results were obtained. However, the use of the oxidative wave is preferred since no degassing is required.

A. Effects of Modifer, Reaction Time, and Reagent Loading. We investigated the effects of using three different sources of the aromatic amine: aniline, 4-aminobenzoic acid, and the iron complex containing coordinated 4-aminopyridine. These were chosen because they represented three different types of interaction with the carbon paste. The aniline was chosen because of its high solubility and partitioning into the pasting medium. The iron complex was chosen as an example of a very highly charged (−3) species and the 4-aminobenzoic acid as representing an intermediate case.

For each of these modifiers we investigated the effects of loading on the carbon paste and time of incorporation on the analytical response.

Our initial studies were with aniline as a modifier followed by 4-aminobenzoic acid and the iron complex.

1. Aniline. From our previous study on the determination of amines with modified carbon paste electrodes (*37*) we had determined that a 50% reagent loading gave optimal results. Thus, our initial investigations with aniline as a modifier were at this loading level. We studied the effect of the time of

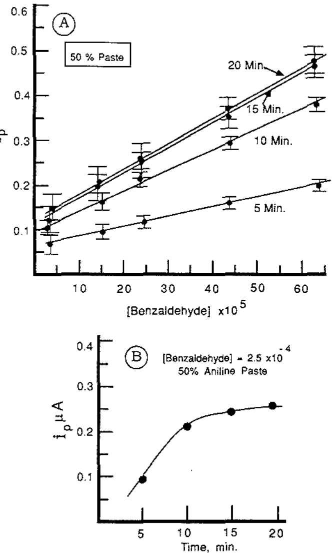

Figure 3. (A) Calibration curves for the determination of benzaldehyde with an aniline modified carbon paste electrode (50% loading) as a function of reaction time. (B) Analytical response for a 50% loading aniline modified carbon paste electrode as a function of time of incorporation for benzaldehyde at a solution concentration of 2.5 × 10^{-4} M.

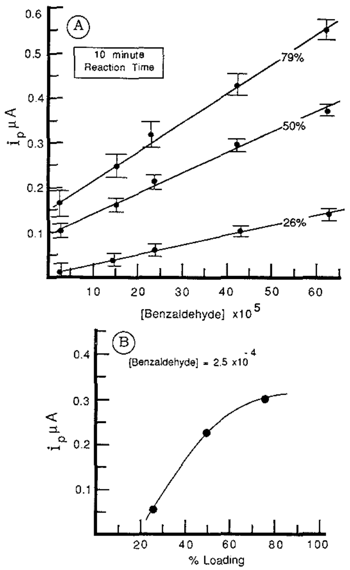

Figure 4. (A) Calibration curves for the determination of benzaldehyde with an aniline modified carbon paste electrode as a function of paste composition using a 10-min reaction time. (B) Analytical response for a 10-min incorporation time for aniline modified carbon paste electrodes as a function of reagent loading for benzaldehyde at a solution concentration of 2.5 × 10^{-4} M.

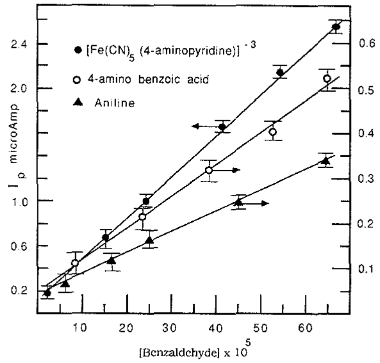

Figure 5. Calibration curves for the determination of benzaldehyde with carbon paste electrodes modified with aniline, 4-aminobenzoic acid, or [Fe(CN)$_5$L]$^{3-}$ under optimal experimental conditions.

reaction for 5, 10, 15, and 20 min. In all cases (Figure 3A) linear calibration curves were obtained with slopes that generally increased with increasing time of reaction. Although the signal amplitude increased with reaction time, the relative increase in the signals at higher exposure times was much smaller than at shorter times of exposure, suggesting a leveling of the response with time. In fact, a plot of peak current vs time at a constant concentration of benzaldehyde exhibited such a trend (Figure 3B). Although the magnitude of the signal was largest at 20 min, there was also an accompanying increase in the background current so that the signal to noise and reproducibility were in fact lower than at 10 min. Although we are not certain as to the origin of the background, we believe that it might be associated with decomposition of the aniline since the background increases further with aging of the paste. Thus, for aniline as a modifier, a 10-min reaction time was considered optimal.

After establishing the optimal reaction time, we studied the effect of reagent loading. In addition to the 50% paste, measurements were carried with pastes at 26%, and 79% loading. The results, shown in Figure 4A, show that for a 10-min reaction time all loadings gave linear calibration curves with slopes (and thus sensitivities) that increased with loading. However, at the 79% loading level, there was a significant increase in the background. At even higher loadings, the background was still higher and, in addition, there were problems with the mechanical integrity of the paste. However, as Figure 4B shows there appears to be an asymptotic response as a function of loading. From these results, a 50% loading was deemed adequate.

Representative responses for the determination of benzaldehyde at various concentrations with aniline modified carbon paste electrodes (at 50% loading) are presented in Figure 2A.

2. 4-Aminobenzoic Acid and [Fe(CN)$_5$L]$^{3-}$ (L = 4-Aminopyridine). Similar experiments were performed for carbon paste electrodes modified with 4-aminobenzoic acid and the iron complex. In the case of 4-aminobenzoic acid, the optimal conditions were a 35% loading level and a 10-min reaction time, whereas for the iron complex these were 25% loading and again a 10-min reaction time. In the case of the iron complex, the 25% loading represented the solubility limit so that higher loadings could not be investigated. In addition, the analtyical responses for the carbon paste electrodes were significantly higher and the background levels much lower than for the other two modifiers.

Representative responses for the determination of benzaldehyde at different concentrations using carbon paste electrodes modified with the iron complex (at 10% loading) or 4-aminobenzoic acid (at 35% loading) are presented in parts B and C, respectively, of Figure 2.

3. Comparison between Modifiers. Figure 5 shows the calibration curves for the determination of benzaldehyde with the three different reagents at the optimal operating conditions. What is immediately apparent is that the response for electrodes modified with the iron complex was about 4 times larger (notice different scales) than those modified with either aniline or 4-aminobenzoic acid. In addition the response of the 4-aminobenzoic acid modified electrodes was about 60% higher than that for the aniline modified electrodes as determined by the ratio of the slopes of the calibration curves.

The reasons for the very large differences in response between electrodes modified with the iron complex and those modified with aniline and 4-aminobenzoic acid are not clear. One could speculate that the iron complex helps in the propagation of charge; however, we have no direct evidence to this effect. Another potential explanation might be the chemical stability of the reactants. For example, electrodes modified with aniline could not be stored (in air) for more than 2 days without severe degradation of performance. Electrodes modified with 4-aminobenzoic acid were stable for about a week and those modified with the iron complex were indefinitely stable. This trend follows the anticipated ease of oxidation of the various reagents and may also pay a role in dictating the observed responses. It is clear that out of the three materials used for modification, the iron complex exhibited the best performance in terms of signal to noise ratio and electrode stability.

Since electrodes modified with the iron complex exhibited the best properties, we have performed some additional studies with it. Specifically, we tried to determine the lower limit of detection and found that even at submicromolar concentration (0.2 μM) a discernible peak, associated with the incorporated imine, could be detected. However, the reproducibility degraded significantly (±30%) over that obtained at 10 μM (±11%). However, these experiments point to the very high sensitivity that can be achieved.

In addition, due to the nature of the chemical reaction involved (only aldehydes will form imines) a very high degree of specificity was obtained. For example, the presence of ketones (e.g. acetophenone) in 100-fold excess did not have any effect on the determination of benzaldehyde.

Although aliphatic aldehydes (butyraldehyde) could also be determined (albeit with diminished sensitivity), the method appears to be most sensitive to aromatic aldehydes. For example the presence of butyraldehyde at 100-fold excess had a relatively small effect on the determination of benzaldehyde, and this probably reflects differences in the rate of imine formation. However, similar detection limits to those obtained for benzaldehyde were obtained for 9-anthraldehyde and 1-naphthaldehyde, consistent with our previous assertion.

It should be mentioned that an analogous analytical scheme had been previously presented by Baldwin and co-workers (*23*) where allylamine was adsorbed onto a platinum electrode and subsequently reacted with ferrocene carboxaldehyde to yield the surface-immobilized ferrocenylimine. The redox response of the surface-immobilized ferrocene was then used as the analytical signal. Although that approach is analogous to the one presented here (both depend on imine formation), we employ a redox process associated with the imine itself as the analytical signal so that our approach would be generally applicable to the determination of aldehydes by imine formation. In addition, most methods for the determination of aldehydes (*38*) are based on the preparation of derivatives suitable for spectrophotometric determination and are generally very time-consuming. There was also a recent report (*39*) on the determination of picolinaldehyde by reduction of its Girard-P derivative at a mercury electrode. The reported limit of detection was 1.5×10^{-5} M and the linear range was found to be from 1.5×10^{-5} to 2.9^{-4} M. Thus, the procedure presented here compares very favorably with these methods.

It is clear that reagents based on the iron complex employed here for the determination of aldehydes and previously for the determination of aromatic amines represent a very versatile group of reagents for the selective and sensitive determination of organic species and we continue to explore their potential analytical applications.

LITERATURE CITED

(1) Murray, R. W. In *Electroanalytical Chemistry*; Bard, A. J., Ed.; Marcel Dekker: New York, 1983; Vol. 13, pp 191–368.
(2) Murray, R. W.; Ewing, A. G.; Durst, R. A. *Anal. Chem.* **1987**, *59*, 379A.
(3) Abruña, H. D. "Electrode Modification with Polymeric Reagents". In *Electroresponsive Molecular and Polymeric Systems*; Skotheim, T. A., Ed.; Marcel Dekker: New York, 1988; Vol. 1, pp 97–171.
(4) Abruña, H. D. *Coord. Chem. Rev.* **1988**, *86*, 135.
(5) Oyama, N.; Anson, F. C. *J. Am. Chem. Soc.* **1979**, *101*, 3450–3456.
(6) Oyama, N.; Anson, F. C. *J. Electrochem. Soc.* **1980**, *127*, 247–248.
(7) Espencheid, M. W.; Ghatak-Roy, A. R.; Moore, R. B., III; Penner, R. M.; Szentirmay, M. N.; Martin, C. R. *J. Chem. Soc., Faraday Trans. 1* **1986**, *82*, 1051–1070.
(8) Whitley, L. D.; Martin, C. R. *Anal. Chem.* **1987**, *59*, 1746.
(9) Cox, J. A.; Kulesza, P. J. *Anal. Chim. Acta* **1983**, *154*, 71.
(10) Wang, J.; Greene, B.; Morgan, C. *Anal. Chim. Acta* **1987**, *158*, 15.
(11) Guadalupe, A. R.; Abruña, H. D. *Anal. Lett.* **1986**, *19*(15&16), 1613–1632.
(12) Guadalupe, A. R.; Abruña, H. D. *Anal. Chem.* **1985**, *57*, 142–149.
(13) Wier, L. M.; Guadalupe, A. R.; Abruña, H. D. *Anal. Chem.* **1985**, *57*, 2009–2011.
(14) Guadalupe, A. R.; Wier, L. M.; Abruña, H. D. *Am. Lab.* **1986**, *18*(8), 102–107.
(15) McCracken, L. L.; Wier, L. M.; Abruña, H. D. *Anal. Lett.* **1987**, *20*, 1521.
(16) Hurrell, H. C.; Abruña, H. D. *Anal. Chem.* **1988**, *60*, 245.
(17) Kasem, K. K.; Abruña, H. D. *J. Electroanal. Chem.* **1988**, *242*, 87.
(18) Gehron, M. J.; Brajter-Toth, A. *Anal. Chem.* **1986**, *58*, 1488–1492.
(19) Baldwin, R. P.; Christensen, J. K.; Kryger, L. *Anal. Chem.* **1980**, *58*, 1790.
(20) Prabhu, S. V.; Baldwin, R. P.; Kryger, L. *Anal. Chem.* **1987**, *59*, 1074.
(21) Cheek, G. T.; Nelson, R. F. *Anal. Lett.* **1978**, *11*, 393–402.
(22) Cox, J. A.; Majda, M. *Anal. Chem.* **1980**, *52*, 861–864.
(23) Price, J. F.; Baldwin, R. P. *Anal. Chem.* **1980**, *52*, 1940–1944.
(24) Pham, M.-C.; Tourillon, G.; Lacaze, P.-C.; Dubois, J.-E. *J. Electroanal. Chem.* **1980**, *111*, 385–390.
(25) Pham, M.-C.; Dubois, J.-E.; Lacaze, P.-C. *J. Electrochem. Soc.* **1983**, *130*, 346–351.
(26) Cox, J. A.; Kulesza, P. J. *J. Electroanal. Chem.* **1983**, *159*, 337–346.
(27) Willman, K. W.; Murray, R. W. *J. Electroanal. Chem.* **1982**, *133*, 211–231.
(28) Lubert, K. H.; Schnurrbush, M.; Thomas, A. *Anal. Chim. Acta* **1982**, *144*, 123–136.
(29) Ikaniyama, Y.; Heineman, W. R. *Anal. Chem.* **1986**, *58*, 1803.
(30) Nagy, F.; Gerhardt, G. A.; Oke, A. F.; Rice, M. E.; Adams, R. N.; Moore, R. B.; Szentirmay, M. N.; Martin, C. R. *J. Electroanal. Chem.* **1985**, *188*, 85.
(31) Gerhardt, G. A.; Oke, A. F.; Nagy, F.; Moghaddam, B.; Adams, R. N. *Brain Res.* **1984**, *290*, 390.
(32) Wang, J.; Tuzhi, P. *Anal. Chem.* **1986**, *58*, 3257.
(33) Wang, J.; Tuzhi, P.; Golden, T. *Anal. Chim. Acta* **1987**, *194*, 129.
(34) Halbert, M. K.; Baldwin, R. P. *Anal. Chem.* **1985**, *57*, 591.
(35) Santos, L. M.; Baldwin, R. P. *Anal. Chem.* **1986**, *58*, 848.
(36) Santos, L. M.; Baldwin, R. P. *J. Chromatogr.* **1987**, *414*, 161.
(37) Guadalupe, A. R.; Jhaveri, S. S.; Liu, K. E.; Abruña, H. D. *Anal. Chem.* **1987**, *59*, 2436.
(38) Siggia, S.; Hanna, J. G. *Quantitative Organic Analysis*, 4th ed.; Wiley: New York, 1979.
(39) Barragán de la Rosa, F. J.; Callejón Mochón, M.; Guiraúm Pérez, A. *Anal. Chim. Acta* **1985**, *172*, 65.

RECEIVED for review July 13, 1989. Accepted September 8, 1989. This work was generously funded by the National Science Foundation. H.D.A. is a recipient of a Presidential Young Investigator Award (1984–1989) and an A. P. Sloan Fellow (1987–1991). K.E.L. acknowledges support by the REU Program at NSF.

Electrochemical Activation of Carbon Electrodes in Base: Minimization of Dopamine Adsorption and Electrode Capacitance

Dennis M. Anjo,* Michael Kahr, M. M. Khodabakhsh, Stuart Nowinski, and Michael Wanger

Department of Chemistry and Biochemistry, California State University, Long Beach, California 90840

A study has been made of the optimum conditions for electrochemical activation of carbon electrodes used in the analysis of dopamine. The conditions optimized were electrolyte pH, activation voltage, and the duration of the activation. The parameters monitored during the optimization were the reversibility of the dopamine couple, electrode capacitance, and dopamine adsorption. It was found that both the capacitance and dopamine adsorption decreased as the pH of the electrolyte was increased. The optimum conditions found for electrochemical activation were a pH of 13, a potential of 1.2 V (SCE) for a duration of 5 min. These activation conditions were then applied to a number of glassy carbons and a pyrolytic carbon film electrode.

INTRODUCTION

Carbon is the most commonly used working electrode in the electrochemical analysis of catecholamines. Numerous forms of carbon are employed, including glassy carbon (*1*), carbon fibers (*2*), carbon films (*3*), and polymer-modified electrodes (*4*). An activation step has been shown to be necessary for a reproducible response at carbon electrodes. Polishing methods (*5, 6*) have been popular, but they have not been effective for a reversible response with catecholamines. Thermal activation (*7–9*) laser methods (*10–13*) and electrochemical activation (*14–20*) have been shown to be effective at inducing reversible behavior with catecholamines. A reversible response is important in multicomponent systems where closely spaced oxidations need to be resolved. Gonon et al. (*2*) have shown that electrochemical activation allows the resolution of ascorbic acid and catecholamine oxidation in vitro with carbon fiber electrodes. Wightman et al. (*14*) have shown that the electrochemical activation of carbon fibers improves the response in many solution mixtures containing biogenic amines. Numerous specific methods for electrochemical carbon electrode activation have been recently published that enhance the sensitivity and selectivity for the biogenic amines for both direct voltammetry and amperometric chromatographic detectors (*2, 14–16*). This paper reports an electrochemical activation method that is an improvement over previously reported procedures.

Two unfortunate side effects of electrochemical activation have been a great increase in the amount of catecholamine accumulated at the electrode surface and an increase in electrode background current. The catecholamine accumulation has been termed adsorption in most recent publications (*2, 12, 13, 15, 17, 19, 21, 22*) although it probably includes absorption, ion exchange, electrostatic uptake, chemisorption, and simple adsorption. It should be noted that the adsorption described in this publication is the total surface accumulation measured by voltammetry. In similar fashion the background current may be composed of double-layer charging, faradaic processes, and ion uptake, but we present the apparent capacitance as a combined measure of the residual current; this allows a comparison with results from other workers in the field who have also summed the background current into a single capacitive value (*8–10, 12, 13, 15, 23*).

The increase in catecholamine adsorption has often been noted, although these results have not been in quantitative agreement between investigators (*2, 15, 17, 19, 21, 22*). All of the reported catecholamine adsorption has occurred after activation in electrolyte from acidic to neutral pH; we have found no report of activation procedures in basic solution for catecholamines. Anecdotal reports of high residual current after electrochemical activation have been made (*3, 15, 24–26*), but only Beilby et al. (*23*) have made a systematic study of the effect of the electrochemical activation conditions on capacitance; this study was limited to optimizing the ferrocyanide couple response and did not investigate conditions for the analysis of catecholamines.

Electrochemical activation of carbon electrodes in neutral to acidic electrolyte has been shown to generate a transparent layer on the electrode surface which refracts light and causes interference colors (*3, 27–29*). This film is composed of carbon oxidation products of the electrode itself and has been termed electrochemical graphite oxide. Kepley and Bard (*28*) have shown that the film layer can grow to a thickness approaching a micrometer. We feel this film is a reservoir for adsorbed catecholamines and other depolarizers and that the film increases the number of charged surface states increasing the capacitance. We present here methods to reduce the level of electrode filming during electrochemical activation, with concomitant improvement in capacitance and lower dopamine adsorption.

Beilby et al. (*23*) found that the ferrocyanide couple approached ideal response kinetics at a carbon electrode anodically activated in basic solution. This method of activation also lowered the electrode capacitance greatly over activation in acidic electrolyte. Because the response of the carbon electrodes improved as the activation solution was changed from acidic to basic, we have carried out a similar study for dopamine response. The response parameters optimized for dopamine analysis were reversibility, dopamine adsorption, and electrode capacitance. We carried out a study of response versus pH from acidic to basic solution, and we determined the optimum potential and duration for activation. We have attempted to keep the activation method simple and accessible to the analyst with standard electrochemical instrumentation.

EXPERIMENTAL SECTION

Apparatus. The experiments were recorded by using either of two Princeton Applied Research instruments, the Model 174A electrochemical analyzer (cyclic voltammetry, constant potential activation, and differential pulse voltammetry) or the Model 362 scanning potentiostat/scanning galvanostat (cyclic voltammetry, constant potential activation, and constant current activation). A Linear strip chart recorder was used to record the chronoamperometry experiments. The reference electrode was the saturated calomel electrode separated from the working cell by a saturated KCl salt bridge; all potentials reported in this publication are relative to the saturated calomel electrode (SCE). The counter electrode was a platinum wire with a 20-mm^2 surface area. The glassy carbon came from the following sources: Bioanalytical

0003-2700/89/0361-2603$01.50/0 © 1989 American Chemical Society

(MF2012), Atomergic Chemetals (V-10 and V-25), and Princeton Applied Research (G0021). The pyrolytic carbon film was prepared from 3,4,9,10-perylenetetracarboxylic dianhydride (Aldrich) by using a previously reported procedure (*3*).

Reagents. The solutions were all prepared with deionized water prepared with a Barnstead Bantam demineralizer with an S-27781 cartridge which was fed distilled water. The sulfuric acid, KCl, hydrochloric acid, K_2HPO_4, NaOH, potassium hydrogen phthalate, sodium bicarbonate, and $K_4Fe(CN)_6$ were of analytical reagent grade from Mallinckrodt. The tris buffer was of analytical reagent grade from Spectrum Chemical Co. Dopamine hydrochloride was from Sigma. The ascorbic acid was of pharmaceutical grade.

Procedure. *Electrode Preparation.* The glassy carbon electrodes were polished by using the standard polishing kit supplied with the Princeton Applied Research (PAR) glassy carbon electrode. The electrodes were polished on a felt polishing mat by using 0.5 μM alumina powder (Raybright A) in water for 5 min. The electrodes were then sonicated for 5 min in deionized water. The Bioanalytical and PAR glassy carbon electrodes are commercial electrodes with cylindrical covers that leave only the circular end contacting the solution; these electrodes were used as is after polishing and sonication. The Atomergic Chemetal glassy carbon and the carbon film electrodes were both 3-mm cylindrical rods. To produce a reproducible circular surface area, the electrodes were lubricated with silicone grease and pressed into 2.5 mm i.d. Tygon tubing. Only the ends of the electrodes were in contact with the solutions. In the past we have used both heat-shrink Teflon tubing and glass tubing with epoxy cement to cover the electrodes, but these seals were not able to withstand the strong base treatment used in these experiments. We found that the basic solution would creep up the sides of the electrodes; this changed the active area when Teflon or epoxy cement was used. (This creeping eventually destroyed the PAR electrode). The Tygon tubing with silicone grease as sealant remained sealed throughout the experiments. An added advantage is that the tubing could be removed during subsequent polishing steps, which prevented the streaking of plastic and cement across the electrode surface. The electrochemical activation procedures are described in detail in the Results section.

Cyclic Voltammetry. Standard cyclic voltammetry experiments were carried out with the two instruments described above. In all experiments, unless otherwise indicated, the scan rate was 10 mV/s over a range from 0.25 to 1.00 V (SCE).

Capacitance Measurement. The apparent electrode capacitance was determined by using the residual current separation between anodic and cathodic sections of cyclic voltagmmograms recorded in background electrolyte. The measurement was made at 0.70 V (SCE), which is a potential approximately equidistant from the faradaic processes at the electrode and from the solvent breakdown potential. The formula used is shown in eq 1, where

$$C = I/(2Av) \qquad (1)$$

C is the capacitance per area, I is the separation between the anodic and cathodic sweep at the chosen voltage, v is the sweep rate in volts per second, and A is the geometric electrode area.

Dopamine Absorption. The total surface accumulation of dopamine on the electrode was determined by using scanning potential voltammetry. The electrode was immersed in the dopamine solution for the time indicated in the specific experiment. The electrode was quickly removed and washed thoroughly with 0.1 M sulfuric acid. The electrode was then placed in an electrochemical cell with 0.1 M sulfuric acid electrolyte, and a voltammogram was immediately recorded between 0.25 and 1.00 V (SCE). The adsorbed dopamine caused a current peak which was integrated to determine the amount of dopamine adsorbed on the electrode.

Electrode Area Determination. The electrode active area was determined by potential step chronoamperometry in 1 mM dopamine with 0.1 M sulfuric acid supporting electrolyte. The potential was stepped from 0.0 to 0.750 V and the current was recorded over a period of 30 s during linear diffusion conditions. Linear regression analysis was used on the Cottrell plot of i vs $t^{-1/2}$. The diffusion coefficients were determined by using the same chronoamperometry procedure with a Beckman platinum button electrode (*30*).

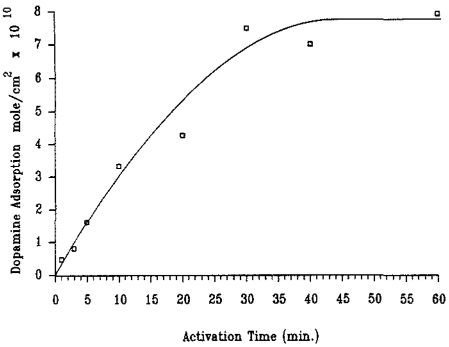

Figure 1. Effect of electrochemical activation period in 0.1 M sulfuric acid on the adsorption of dopamine to an Atomergic V25 glassy carbon electrode.

RESULTS

Our initial studies on carbon electrodes employed activation at voltages around 1.8 V (SCE) in 0.1 M sulfuric acid (*3*). This method was effective at generating near-reversible response with catecholamines, but the activation also greatly increased the residual current and catecholamine adsorption. After an activation period of greater than 10 min, the catecholamine adsorption was great enough to cause the peak separation in cyclic voltammetry to be significantly less than the 29-mV limit. Although the adsorption is apparently strong, the adsorbed catecholamine does not undergo a potential shift to a postwave and actually appears as a prewave; the oxidation and reduction peaks of the adsorbed moieties are almost superimposable, and the response is similar to that in thin-layer voltammetry (*3*). This narrowing artifact in the cyclic voltammetry peak separation made catecholamine electrode kinetic experiments impossible to carry out. The level of catecholamine adsorption was highly variable between electrodes that had been identically treated in 0.1 M sulfuric acid; this variation prevented any method of compensation of background correction with the kinetic experiments. We therefore set out to determine the mechanism of the adsorption and methods to reduce catecholamine adsorption.

We initially studied the effect of acid activation period on dopamine adsorption. The electrode was activated for specific time intervals in 0.1 M sulfuric acid, and then the electrode was placed in 1.00 mM dopamine in 0.1 M sulfuric acid for 30 min. We found that the accumulation step for dopamine took 15–20 min to reach equilibrium, as was found by Gonon et al. (*2*) and by Vasquez and Imai (*17*); the 30-min dip in dopamine was to ensure that complete adsorption equilibrium had been reached. Finally the electrode was placed back in the 0.1 M sulfuric acid, and the accumulated dopamine was anodically stripped by cyclic voltammetry. The amount of dopamine adsorbed was determined by integrating the oxidation peak. The effect of the period of acid activation on the level of dopamine adsorption is shown in Figure 1 for an Atomergic V25 glassy carbon electrode. The level of dopamine adsorption increased monotonically as the electrode was sequentially treated. The absolute level of dopamine adsorption varied from electrode to electrode as mentioned above, but the surface coverage was generally much greater than a simple monolayer; this calculation was based on the maximum surface coverage experiments carried out by Soriaga and Hubbard (*31*) on molecules with dimensions similar to those of dopamine.

The electrode surface often develops a refractive film that varies in color depending on the electrode treatment. We discovered that the film color disappeared when the electrode was washed in 1.0 M NaOH. Our working hypothesis was that

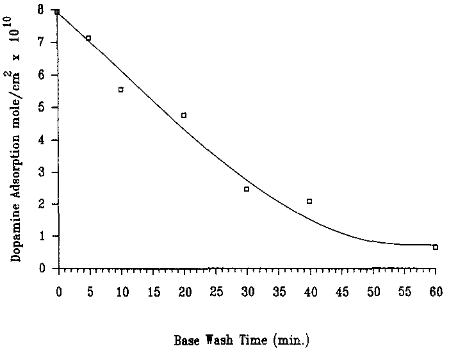

Figure 2. Effect of washing an acid-activated electrode in 1.0 M NaOH. The electrode had previously been electrochemically activated for 60 min in acid solution.

the surface film was responsible for dopamine adsorption, and we then tested on electrode to determine if base washing lowered dopamine adsorption. The results of this experiment are shown in Figure 2. Each point represents a period of 1.0 M NaOH washing of a glassy carbon electrode that had originally been activated in 0.1 M sulfuric acid for 60 min. The electrode was washed in a vigorously stirred solution of 1.0 M NaOH for the time period indicated. At each point the electrode was thoroughly washed with deionized water and placed in a stirred dopamine solution (1.00 mM in 0.1 M sulfuric acid) for 30 min. Finally the electrode was transferred to a solution of 0.1 M sulfuric acid, and the dopamine coverage was determined by scanning voltammetry as described above.

As shown in Figure 2 the level of dopamine adsorption steadily decreased as the electrode was washed in the NaOH solution. The base wash clearly had an effect on the electrode surface, and the capacitance also decreased monotonically. The cyclic voltammetry peak separation of the electrode in 1.00 mM dopamine at each step of the treatment did not significantly change during the entire experiment; this indicates the reversibility was not degraded by the base wash. The level of surface coverage decreased to a level comparable with monolayer coverage after extensive base washing.

During the base wash studies we became aware of the base activation method used by Beilby et al. (*23*), and we carried out an initial activation at 1.8 V (SCE) in 1.0 M NaOH. The activation in base was quite effective at lowering dopamine adsorption; a subsequent wash of the electrode in base did not further lower the dopamine adsorption. We then set out to determine systematically the optimum pH, potential, and duration of carbon electrode activation for dopamine analysis. The responses used to indicate superior response were (a) dopamine adsorption, (b) electrode capacitance, and (c) cyclic voltammetry peak separation in a 1.00 mM dopamine solution. To ensure internal consistency, the optimization was carried out using only Atomergic V-25 glassy carbon. When the method was optimized, it was applied to a number of carbon electrodes.

Activation pH Optimization. To ensure that the response in strong base was not a false minimum on the response curve, we set out to determine the response at pH values from strong acid to strong base. Because the potential for solvent breakdown is pH dependent, activation at a constant potential of 1.8 V (SCE) gives greatly increasing current as the pH is varied from 1 to 14. We therefore carried out the study of activation pH on electrode response at a constant current of 1.5 mA applied for 5 min. This current was more than adequate for activation at all the pH values studied.

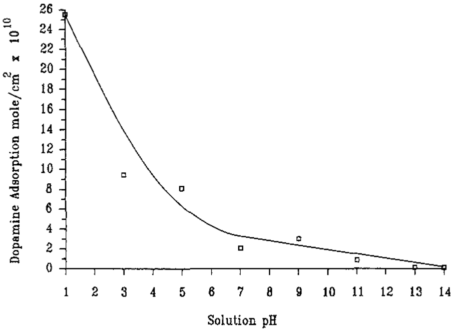

Figure 3. Effect of electrochemical activation pH on dopamine adsorption.

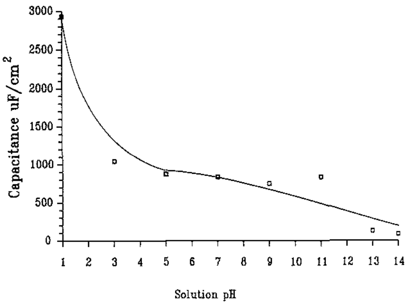

Figure 4. Effect of electrochemical activation pH on electrode capacitance.

The effect of activation pH on dopamine adsorption is shown in Figure 3. As the pH is increased from 1 to 14, there is a decrease in the level of dopamine adsorption. It should be noted that the 1.5-mA current used here is much higher than at the final optimized conditions described at the end of this paper, and the adsorption at the best pH in Figure 3 is much higher than the values at the final optimized conditions. Figure 4 shows the effect of activation pH on electrode capacitance, which also decreases as the pH increases. It is clear from the figures that high pH is not a false minimum and that the optimum pH is the highest value tolerable. We did not use NaOH solutions in excess of 1.0 M for the optimization procedures due to its corrosive effects on glass parts. High concentrations of NaOH had destructive effects on the porous glass junctions of the reference electrodes and corroded the glass sheath on one of the glassy carbon electrodes. The 1.0 M solutions of NaOH should contact "thirsty glass" reference electrode junctions for only the shortest period of time necessary for activation.

The activation pH did not affect the current sensitivity of the electrodes for the analysis of 1.0 mM dopamine in 0.1 M sulfuric acid. The intensity of the oxidation peak in cyclic voltammetry was constant at approximately 200 $\mu A/cm^2$ at all the pH values employed. The value of 200 $\mu A/cm^2$ is the current peak predicted for a reversible cyclic voltammetry peak (*32*) using the diffusion coefficient of dopamine (*30*).

Duration of Activation. The period of activation must be long enough to ensure complete activation of the surface in contact with the solution, but must not be so long that the surface is damaged. The thin carbon film electrodes are especially sensitive, and they are easily destroyed by long periods of anodic activation. We have done studies on the activation of carbon film electrodes in acidic media that in-

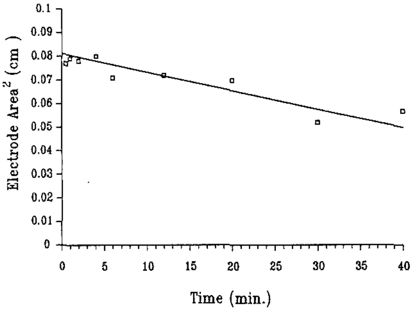

Figure 5. Effect of electrochemical activation period on the active electrode area.

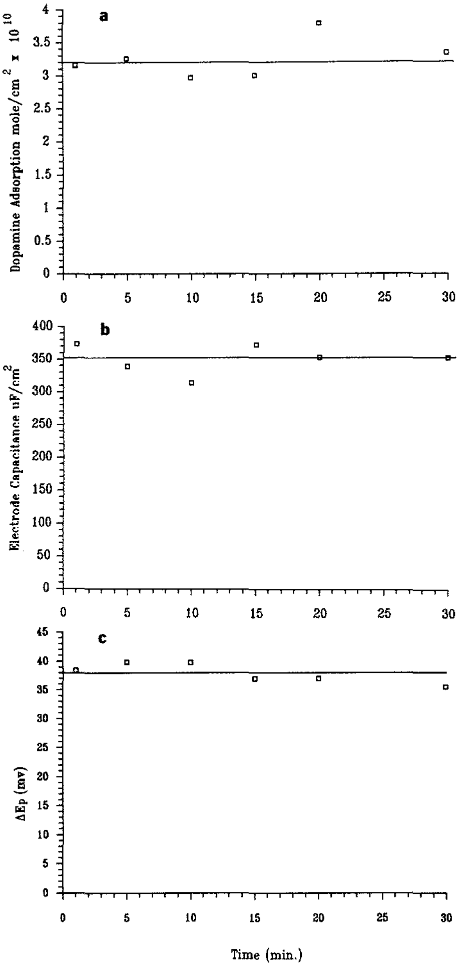

Figure 6. Effect of electrochemical activation period in 1.0 M NaOH at 1.8 V on (a) dopamine adsorption, (b) electrode capacitance, and (c) peak separation.

dicate full activation of electrode area occurs within 5 min. Figure 5 shows the activation time in acid solution versus active electrode area determined by chronoamperometry in

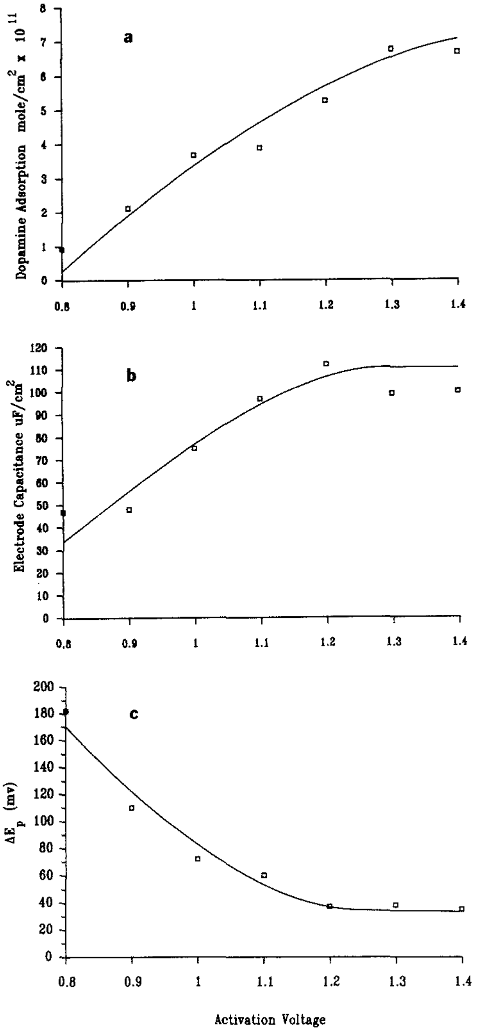

Figure 7. Effect of electrochemical activation voltage on (a) dopamine adsorption, (b) electrode capacitance, and (c) peak separation. The activation was carried out in 1.0 M NaOH for 5 min.

1 mM dopamine. Figure 6 shows the effect of activation time on the following: (1) dopamine adsorption (plot a) (2) electrode capacitance (plot b), and (3) cyclic voltammetry peak separation in 1.00 mM dopamine (plot c), done at 1.8 V in 1.0 M NaOH. These studies indicated that adsorption, peak separation, and capacitance were not greatly affected by the duration of the activation in base solution. There is a slight decrease in the peak separation after 15 min, but this was not considered significantly above experimental uncertainty (±2 mV). We chose an activation period of 5 min to ensure complete surface activation for each procedure below.

Potential of Activation. The potential of activation was varied from 0.8 to 1.4 V, and the following were monitored: (1) the amount of dopamine adsorbed, (2) the electrode capacitance, and (3) the cyclic voltammetry peak separation in 1.0 mM dopamine. The response of each parameter is shown

Table I. Response of the Various Carbon Electrodes

material	capacitance,[a] μF/cm^2	ΔE_p, mV	dopamine adsorption,[b] mol/cm^2 × 10^{-11}
	I. Base Treatment		
glassy carbons			
Atomergic V-25	127 ± 11	35.4 ± 1.0	3.80 ± 0.73
Atomergic V-10	258 ± 11	51.5 ± 2.0	4.07 ± 1.03
Bioanalytical	153 ± 11	34.9 ± 0.5	5.69 ± 1.38
pyrolytic carbon film	35 ± 6.1	74.0 ± 2.6	2.69 ± 0.23
	II. Acid Treatment		
Atomergic V-25	885	35	107
	III. Monolayer Coverage		
			52.5[c]

[a] The measured capacitance is the apparent capcitance including all sources of residual current. [b] The adsorption is the apparent adsorption including all forms of surface accumulation of dopamine. [c] The coverage is based on the work of Soriaga and Hubbard (*31*) using the model compound 4-methylpyrocatechol. The confidence limits listed are standard deviations of the mean.

in Figure 7a–c, respectively. The peak separation experiment indicated that reversibility was not reached until the potential exceeded 1.1 V. Capacitance increased with increasing activation potential, as did the level of dopamine adsorption. We chose 1.2 V as the position of optimum response for the activation. Although the adsorption and capacitance are not fully minimized at this potential, we feel that reversibility is the most important of the three optimization criteria. The electrode must be able to distinguish between closely spaced oxidations in many applications, and reversibility is the parmeter that best indicates selectivity.

The conditions found for optimum electrode activation are (1) a pH value of 14 or higher, (2) a duration of 5 min or greater, and (3) a potential of 1.2 V (SCE). The response of a number of electrodes are summarized in Table I. A number of different glassy carbons and a carbon film electrode are listed. The best capacitance and absorption values were obtained with the carbon film electrode, but it had the least reversible response. The film electrode may be of interest in situations where selectivity is not the most important figure of merit such as an amperometric detector in liquid chromatography. Under these conditions background and response time due to desorption may outweight the disadvantage of poor reversibility. We are working on methods to improve the reversibility of the carbon film electrode with catecholamines.

Of the glassy carbon electrodes we found that the Bioanalytical and the Atomergic V-25 were nearly equivalent in response. The Atomergic V-10 glassy carbon material has been used by other investigators with excellent results, but the batch of rods and plates we received all had severe background current. The V-10 glassy carbon is a low-temperature (1000 °C) pyrolytic carbon, and the material lacks the silver metallic luster typical of the other glassy carbons used. The production tolerances of the V-10 material are unrelated to electrochemistry, and we suspect major variations in electrochemical response could occur. The Atomergic V-25 material is similar in cost but is produced at 2500 °C; three separate lots gave us excellent response. The PAR and Bioanalytical electrodes are commerical electrodes that both initially gave similar responses to the V-25 material. The response of the PAR glassy carbon electrode degraded greatly during these experiments, and the electrode developed both high background and high dopamine adsorption. Microscopic examination indicated that the strong base conditions had attached the epoxy seal between the glassy carbon and the glass electrode body. This occurred during a long-term base wash of over 24 h. We recommend that epoxy-sealed electrodes not be immersed in strong base for longer than the 5-min activation.

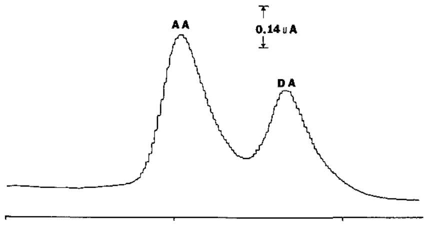

Figure 8. Differential pulse response of base-activated glassy carbon in a solution of 3.4 × 10^{-4} M ascorbic acid (AA) and 4.0 × 10^{-6} M dopamine (DA) in pH 7.4 buffer.

The results with Atomergic V-25 activated in 0.1 M sulfuric acid are shown for comparison; these results are typical of the response of all the glassy carbon electrodes. As mentioned earlier, the level of capacitance and dopamine adsorption varied greatly with acid activation, but the base activation was always at least an order of magnitude lower for capacitance and adsorption. The base activation was also much more reproducible in the three parameters tested: (1) reversibility, (2) dopamine adsorption, and (3) electrode capacitance. The maximum dopamine monolayer coverage predicted frm the data of Soriaga and Hubbard (*31*) is listed at the bottom of Table I; coverage of all the electrodes activated in base was near one-tenth of a monolayer. Acid- and buffer-activated electrodes have varied from 2 to 10 equivalent monolayers of adsorbed dopamine (*2, 13, 15, 17, 19, 21, 22*).

Selectivity of Base-Activated Electrode. The selectivity of the base-activated V-25 for ascorbic acid and dopamine was tested under conditions similar to those used by Gonon et al. (*2*). Figure 8 shows the response of the electrode to ascorbic acid and dopamine at pH 7.4 measured in the differential pulse mode. The figure shows clear separation of ascorbic acid from dopamine at a concentration where ascorbic acid greatly exceeds dopamine. The base-activated electrode behaves as well as a buffer-activated electrode in separating the ascorbic acid signal from that of dopamine.

Surface-State Electrochemistry. The surface electrochemical signal generated by anodic activation has been observed by numerous investigators (*5, 17, 22–24, 28, 33, 34*). The position of the surface signal varies in potential as the solution pH and the activation conditions vary, but Engstrom (*34*) found that the integrated current due to the surface signal exceeds a simple monolayer. The surface signal is greatly decreased by the activation in base solution. Background signals from an acid- and base-activated electrode are shown in Figure 9. The surface signal is reduced by a factor of 5 in going from acid to base activation.

DISCUSSION

The formation of graphite oxide films after electrochemical oxidation of graphite electrodes has been well established, and this topic has been thoroughly reviewed by Besenhard and Fritz (*35*). More recently Kepley and Bard (*28*) and Beilby et al. (*23*) have characterized the anoidic film on glassy carbon as graphite oxide. The structural composition of electrochemical graphite oxide has not been determined; we believe that the material is a complex heterogenous mixture of compounds that range in size from single aromatic rings to large polymers. We also believe that the pH variation in solubility of graphite oxide is due to acidic functional groups on these components. This graphite oxide film probably acts as a reservoir for catecholamines and causes the observed ad-

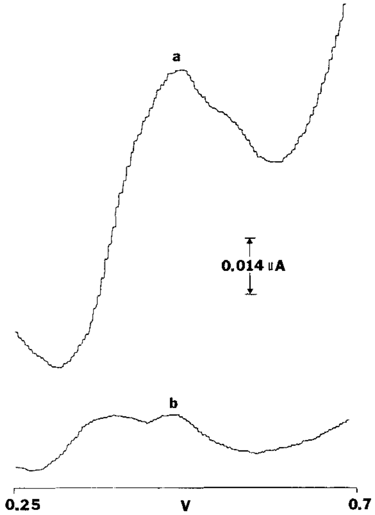

Figure 9. Differential pulse response of the surface states after activation in (a) 0.1 M sulfuric acid and (b) 1.0 M NaOH.

sorption. Following electrochemical activation the carbon electrode surface has been shown to accumulate charged ions following a potential step, and this property may explain the increase in apparent electrode capacitance (*36*). When the electrode is activated in base, the adsorption and capacitance are lowest. We believe this is due to the high solubility of the surface film at this pH. The lowering of the surface redox couple coverage after base activation also argues for the presence of quinone/hydroquinone groups in the surface film.

Kuwana et al. (*8*) have shown that high-vacuum heat treatment can cause carbon electrode activation for organic compounds without an increase in capacitance and adsorption. McCreery et al. (*11*, *12*) and Brajter-Toth et al. (*13*) have also demonstrated that the pulse laser activation can activate carbon for organics without excess adsorption or capacitance. In the case of laser activation, it was found that laser treatment would reverse the high apparent capacitance and adsorption following an initial electrochemical activation (*11*, *12*). Kuwana et al. (*8*), McCreery et al. (*11*, *12*), and Brajter-Toth et al. (*13*) have all stressed that the removal of surface impurities and films is necessary both for carbon electrode activation and for lowering of background and adsorption. We believe that the electrochemical activation of carbon in basic solution is effective at removing the products of the electrode oxidation. Removal of the graphite oxide film during or following electrochemical activation of carbon electrodes is necessary for a reproducible response in the analysis of catecholamines.

CONCLUSIONS

The conditions optimum for anodic activation of the carbon electrodes employed in this work are (1) pH at or above 14, (2) potential at 1.2 V (SCE), and (3) period of activation of 5 min. These conditions generate sufficient surface functionalities to give the catecholamine oxidation a reversible response, but the capacitance and adsorption do not approach the high values observed at acidic and neutral activation conditions. These activation conditions also retain the selectivity of the electrode and lower the surface-state signal of the electrode.

ACKNOWLEDGMENT

We thank M. Steven McDowell for the loan of the Bioanalytical glassy carbon electrode.

Registry No. DA, 51-61-6; AA, 50-81-7; C, 7440-44-0; NaOH, 1310-73-2; sulfuric acid, 7664-93-9.

LITERATURE CITED

(1) Wang, J.; Hutchins, L. *Anal. Chim. Acta* **1985**, *167*, 325.
(2) Gonon, F. G.; Fombarlet, C. M.; Buda, M. J.; Pujol, J. F. *Anal. Chem.* **1981**, *53*, 1386.
(3) Rojo, A.; Rosenstratten, A.; Anjo, D. *Anal. Chem.* **1986**, *58*, 2988.
(4) Gerhardt, G.; Oke, A.; Nagy, G.; Moghaddam, B.; Adams, R. *Brain Res.* **1985**, *340*, 151.
(5) Hu, I.-F.; Karweik, D.; Kuwana, T. *J. Electroanal. Chem. Interfacial Electrochem.* **1985**, *188*, 59.
(6) Rusling, J. *Anal. Chem.* **1984**, *56*, 578.
(7) Stutts, R.; Kovach, P.; Kuhr, W.; Wightman, R. *Anal. Chem.* **1983**, *55*, 1632.
(8) Fagan, D.; Hu, I.-F.; Kuwana, T. *Anal. Chem.* **1985**, *57*, 2759.
(9) Hance, G.; Kuwana, T. *Anal. Chem.* **1987**, *59*, 131.
(10) Poon, M.; McCreery, R. *Anal. Chem.* **1986**, *58*, 2745.
(11) Poon, M.; McCreery, R. *Anal. Chem.* **1987**, *59*, 1615.
(12) Poon, M.; McCreery, R.; Engstrom, R. *Anal. Chem.* **1988**, *60*, 1725.
(13) Bodalbhai, L.; Brajter-Toth, A. *Anal. Chem.* **1988**, *60*, 2557.
(14) Kovach, P.; Ewing, A.; Wilson, R.; Wightman, R. *J. Neurosci. Met.* **1984**, *10*, 215.
(15) Feng, J.; Brazell, M.; Renner, K.; Kasser, R.; Adams, R. *Anal. Chem.* **1987**, *59*, 1863.
(16) Wang, J.; Tuzhi, P. *Anal. Chem.* **1986**, *58*, 1787.
(17) Vasquez, R.; Imai, H. *Bioelectrochem. Bioerg.* **1985**, *14*, 389.
(18) Sujaritvanichpong, S.; Aoki, K.; Tokuda, K.; Matsuda, H. *J. Electroanal. Chem. Interfacial Electrochem.* **1986**, *198*, 195.
(19) Kovach, P.; Deakin, M.; Wightman, R. *J. Phys. Chem.* **1986**, *90*, 4612.
(20) Wang, J.; Tuzhi, P.; Villa, V. *J. Electroanal. Chem. Interfacial Electrochem.* **1987**, *234*, 119.
(21) Michael, A.; Justice, J. *Anal. Chem.* **1987**, *59*, 405.
(22) Nagaoka, T.; Yoshino, T. *Anal. Chem.* **1986**, *58*, 1037.
(23) Beilby, A.; Carlsson, A. *J. Electroanal. Chem. Interfacial Electrochem.* **1988**, *248*, 283.
(24) Engstrom, R.; Strasser, V. *Anal. Chem.* **1984**, *56*, 136.
(25) Hance, G.; Kuwana, T. *Anal. Chem.* **1987**, *59*, 131.
(26) Taylor, R.; Humffray, A. *J. Electroanal. Chem. Interfacial Electrochem.* **1973**, *42*, 347.
(27) Cabaniss, G.; Diamantis, A.; Murphy, W.; Linton, R.; Meyer, T. *J. Am. Chem. Soc.* **1985**, *107*, 1845.
(28) Kepley, L.; Bard, A. *Anal. Chem.* **1988**, *60*, 1459.
(29) Bjelica, L.; Parsons, R.; Reeves, R. *Croat. Chem. Acta* **1980**, *53*, 211.
(30) Nowinski, S.; Anjo, D. *J. Chem. Eng. Data* **1989**, *34*, 265.
(31) Soriaga, M.; Hubbard, A. *J. Am. Chem. Soc.* **1982**, *104*, 2735.
(32) Adams, Ralph N.; *Electrochemistry at Solid Electrodes*; Marcel Dekker, Inc.: New York, 1969; p 124, eq 5–31.
(33) Vasquez, R.; Hono, M.; Kitani, A.; Sasaki, K. *J. Electroanal. Chem. Interfacial Electrochem.* **1985**, *196*, 397.
(34) Engstrom, R. *Anal. Chem.* **1982**, *54*, 2310.
(35) Besenhard, J.; Fritz, H. *Angew. Chem.* (*Int. Ed. Engl.*) **1983**, *22*, 950.
(36) Nagaoka, T.; Fukunaga, T.; Yoshino, T.; Wanatabe, I.; Nakayama, T.; Okazaki, S. *Anal. Chem.* **1988**, *60*, 2766.

RECEIVED for review May 5, 1989. Accepted September 11, 1989. Acknowledgment is made to the donors of the Petroleum Research Fund, administered by the American Chemical Society, for partial support of this research. Acknowledgment is also made to the Office of University Research, California State University, Long Beach, for partial support of this research.

Anal. Chem. **1989,** *61,* 2609–2611

Effects of Background Electrolyte and Oxygen on Trace Analysis for Lead and Cadmium by Anodic Stripping Voltammetry

Angelo R. Fernando and James A. Plambeck*

Department of Chemistry, University of Alberta, Edmonton, Alberta, Canada T6G 2G2

In the analysis for lead and cadmium at parts-per-billion levels by differential pulse anodic stripping voltammetry in acidic aqueous media, the analysis is affected by the presence and amount of chloride ion and by dissolved oxygen. The dissolved oxygen affects only the stripping step and does so as molecular oxygen rather than H_2O_2.

INTRODUCTION

Anodic stripping voltammetry using differential pulse output (DPASV) is now a commonly used electroanalytical technique for determining metals such as lead and cadmium at trace levels. However, recalcitrant real samples such as soils usually require spectroscopic methods of analysis. When complete dissolution of the matrix is difficult, there may be adverse effects of incomplete dissolution products or of reagents on the electroanalytical result. It is the purpose of this paper to examine some of these effects in synthetic samples and to establish a standard DPASV analytical procedure with which various dissolution methods for soil could be tested.

EXPERIMENTAL SECTION

Since the purpose of this study was to vary the sample while holding the analysis methodology constant, commercial automated instrumentation was used. A Model 174A polarographic analyzer (Princeton Applied Research) was used together with a Model 303 static mercury drop electrode (SMDE; also PAR). Both were controlled by a Macsym 150 control microcomputer (Analog Devices) equipped with analog and digital input cards. The operation of the SMDE was controlled by using the digital outputs of the Macsym 150, which also controlled a magnetic stirrer (Fisher Scientific). Analog output was displayed on a 7045A X-Y recorder (Hewlett-Packard) and other printed output on an Imagewriter (Apple Computer). The software programs for the Macsym 150 were written in MACBASIC and are available elsewhere (*1*).

An external saturated calomel electrode (SCE) was used as the reference electrode, connection to the cell being made by a glass salt bridge compartment (Vycor junction) inserted through the side access hole of the Model 303. Some difficulty was encountered maintaining the Model 303 capillaries; keeping the tip immersed in mercury when not in use was found to be the best storage procedure. The apparatus otherwise performed satisfactorily. Reproducibility of drops ranged from 0.8% (large) to 1.7% (small).

Reagents. Distilled water was redistilled from alkaline permanganate at very slow rates (one-half L/h) by using an insulated vertical open column; the lead level after acidification to pH 2 was below 0.03 parts per billion (ppb). All reagents and solutions were prepared from this water.

Aqueous stock solutions of 2 M KNO_3 and of acetate buffer (1 M both in CH_3COONa and CH_3COOH) were prepared from reagent grade materials and further purified by using bulk electrolysis in a large-volume cell with a mercury cathode and a large-volume calomel anode separated from the reduction compartment by glass frits. The potential of the mercury pool was held at −1.4 V against calomel for 1 month while the solution was slowly stirred by bubbling with deoxygenated and water-saturated nitrogen. No detectable concentrations of lead and cadmium remained in these solutions.

Potassium chloride used as salt bridge and calomel electrolyte was reagent grade material, further purified by recrystallization and crystal adsorption (*2*). Triply distilled mercury was purified by anodic oxidation at +0.3 V against SCE under a continuous slow stream of filtered laboratory air obtained by applying a mild vacuum to the cell. Positioning of the air inlet below the mercury surface allowed the air to agitate the mercury as well.

Reagent grade acetic acid was purified by using isopiestic distillation (*3–5*). No lead could be detected in the 1 M acetic acid obtained after 5 days.

High-purity nitrogen was further deoxygenated with acidified vanadium(II) chloride solution/zinc amalgam bubblers (*6*) followed by aqueous washing towers.

Suprapur grade NaOH and HNO_3 were obtained from Merck, high-purity grade HCl was from Fluka, and redistilled grade $HClO_4$ was from G. F. Smith Chemical Co. These reagents were used as received.

Apparatus. Plastic vessels (polyethylene, polypropylene, or Teflon) were used whenever possible and prepared by acid leaching (10% aqueous HNO_3) followed by repeated washings with water. The Teflon Model 303 cells were purchased from Princeton Applied Research. Teflon-covered stirrer bars were also used (care must be taken not to leave these in strongly acidic solutions). Glass containers were found generally unsatisfactory due to adsorption and desorption of lead and cadmium and were never used for storage of solutions to be analyzed or stock reagents.

RESULTS

Calibration runs using both cadmium and lead separately and together at the 1–5 ppb range gave satisfactory results. For a 5-mL sample containing both Cd^{2+} and Pb^{2+} in 0.01 M HNO_3 at these concentrations, the relative standard deviation (RSD) ranged from 2.5% to 5% (Cd) and from 8% to 15% (Pb), which is comparable to the results of others (*7–11*). Repetitive analysis (eight runs each of five determinations) of a standard 100 ppb solution of Cd^{2+} in 0.01 M HNO_3 gave a normal distribution, as indicated by the chi-square test (*12*).

Effects of the Anion. The effect of changing the anion of the analyte was tested by analysis of a standard 100 ppb cadmium solution or lead solution in (a) 0.01 M HNO_3, (b) 0.01 M HCl, and (c) 0.005 M HNO_3 plus 0.005 M HCl. Between analyses (on separate aliquots of the stock solution) the cell and electrodes were washed with water and then rinsed with a 2.5-mL portion of the new solution. The statistical analysis of these results is given elsewhere (*1*). The conclusion is that the sensitivity of DPASV for cadmium is significantly greater in chloride than in nitrate media while the reverse is true for lead. In these experiments the anion concentration ratio in the salt bridge matched that in the analysis cell. Use of a salt bridge that did not match (nitrate in chloride or the reverse) indicated the expected sensitivity change from leakage of the salt bridge anion into the analyte. The presence of chloride leakage into nitrate electrolyte at significant levels (3×10^{-4} M after 60 min) was shown by chloride analysis.

The difference between sensitivities in the presence of chloride and nitrate was not removed by conducting the analysis in pH 3 acetate buffer, despite the fact that acetate is a stronger complexing anion, as tested by the addition of KNO_3 or KCl and by the use of KNO_3 or KCl salt bridges for

0003-2700/89/0361-2609$01.50/0 © 1989 American Chemical Society

Table I. Two-Factor Variance Analysis

sample solution (factor *A*)	
nondeaerated	deaerated
Exchange Solution (Factor *B*) Nondeaerated	
0.439	0.737
0.590	0.635
0.543	0.738
0.680	0.689
0.598	0.684
Exchange Solution (Factor *B*) Deaerated	
0.727	0.721
0.748	0.693
0.720	0.779
0.778	0.725
0.782	0.758

Table II. ANOVA Table for the Effect of Oxygen on Anodic Stripping Analysis

sources	sum of squares	deg of freedom	mean of sum of squares	*F*
between rows (exchange solution)	0.0602	1	0.0602	20.81
between columns (sample solution)	0.0153	1	0.0153	5.29
interactions	0.0255	1	0.0255	8.80
within cells	0.04628	16	2.892	

the reference electrode (*1*). In view of the fact that nitric acid would necessarily be used in the envisaged soil sample dissolutions, the salt bridge employed only KNO_3 and chloride was not added to the analyte.

Effects of Dissolved Oxygen. The effects of dissolved oxygen on anodic stripping voltammetry have been assumed (*13, 14*) to be similar to those observed in classical polarography due to the oxygen reduction waves (at about −0.05 and −0.9 V against SCE). A variety of reasons have been given for this, including an increased background current in linear scan stripping (*15, 16*), reoxidation of plated metal (*17*), and change of solution near the electrode (*18*). It is reported (*15, 19, 20*) that the procedure of matrix exchange, or the exchange of the analytical solution for a deaerated buffer after completion of deposition but prior to stripping, causes disappearance of oxygen interference effects. The use of a flow cell permits one to avoid exposure of the electrode to air and maintain potential control during the exchange process.

Preliminary observations using DPASV on a 50 ppb Pb solution in aqueous nitrate media indicated that 5 min was required to remove all polarographically detectable oxygen and that varying oxygen levels did significantly affect the precision of analysis even though the lead and H_2O_2 peaks were clearly separated. Changes in nitrogen flow, covering of insert holes, and reduction in purge tube diameter could not reduce the time requirement below 4 min.

A matrix-exchange system was constructed by addition of a glass inlet tube (at the top of normal solution level) and a glass outlet tube (at the bottom of the cell) to a Pyrex Model 303 SMDE cell (PAR. GO 057). A metal wire holding a length of poly(vinyl chloride) (PVC) tubing bent into a siphon whose outlet was level with the upper edge of the conical section of the cell and whose highest point was at a level higher than that of the inlet tube completed the drain. The inlet tube was connected to a polythene 500-mL wash bottle that served as a solution reservoir.

This arrangement is superior to the simple drain used by Florence and Mann (*21*) in that their cell does not ensure a constant presence of liquid cover, while their input tube location permits undesirable mixing of solutions. In our arrangement 20 mL of distilled water sufficed to remove all traces of color from 5 mL of $KMnO_4$ solutions contained in the cells.

With this cell, synthetic samples of 50 ppb Pb^{2+} in 0.1 M KNO_3 acidified with HNO_3 to pH 2 were analyzed for lead by DPASV (deposition potential, −0.9 V; modulation, 25 mV; clock, 1 s; scan rate, 5 mV/s; deposition time, 90 s; equilibration time, 30 s). The values of the lead peak height (in microamperes) found for deaerated samples and solutions in a two-factor experiment are shown in Table I. Sample solution deaeration was 5 min/5 mL while the exchange solution was deaerated in the reservoir (1 min/mL). Analysis of variance (Table II) clearly shows that deaeration of the sample solution (factor *A*) has no significant effect while deaeration of the exchange solution (factor *B*) is highly significant ($F(0.01, 1, 16) = 8.53$; $F(0.05, 1, 16) = 4.49$). The dissolved oxygen effect is limited to the stripping step of the analysis.

DISCUSSION

This result is contrary to the published opinion (*13*) that dissolved oxygen interferes with the efficiency of the deposition step. It is in our opinion improbable that such interference would be significant because at a reduction potential of −0.8 V oxygen at the electrode surface must exist as H_2O_2. Reoxidation of reduced lead would require not only loss of the lead from the surface but also its diffusion away from the electrode entirely; the H_2O_2 would be more likely to undergo direct reduction. The effect of pH change due to surface reduction of H_2O_2 should be insignificant in the well-stirred and buffered medium that exists during deposition. Even during the unstirred equilibration period, losses of metal as hydroxy complexes should be insignificant in acidic media.

However, during the stripping step the potential of the electrode is oxidizing relative to Pb^{2+}/Pb but reducing relative to O_2/H_2O_2. It is therefore possible not only that oxygen diffusing to the electrode surface reoxidizes lead, thus producing the observed effect, but that the H_2O_2 produced does so as well. This possibility was tested by using an exchange solution that had been deaerated but to which H_2O_2 had been added. There was no statistically significant difference between results of lead analyses by DPASV using exchange solutions containing H_2O_2 and exchange solutions that were H_2O_2-free. We therefore conclude that the oxygen interference in stripping analysis is limited to the stripping step and arises solely from the reaction of molecular oxygen with the metal being stripped at the electrode surface.

Wang and Dewald (*16*) used linear scan anodic stripping voltammetry (LSASV) with subtraction of stripping curves of background solution from that of the sample and reported that deaeration was unnecessary in such a system. However, oxygen not only affects the base-line current level in a linear sweep stripping situation but also leads to a decrease in the amount of electroactive substance being oxidized during the stripping stage. In LSASV, full correction for both effects may be possible through background subtraction although matching of the dissolved oxygen levels in samples and background electrolytes can be a formidable task. With DPASV, background subtraction may not correct for depletion of the metal due to its reaction with oxygen since in DPASV a constant base line is a zero base line. Our attempts to compare DPASV measurements with background subtraction in deaerated and nondeaerated solutions produced inconsistent data due to the difficulty of matching oxygen levels in background and sample solutions.

ACKNOWLEDGMENT

We are grateful to the Department of Chemistry of the University of Alberta for its support of this work. This paper was taken in part from the thesis of A.R.F., submitted to the

Anal. Chem. **1989**, *61*, 2611–2615

Faculty of Graduate Studies and Research in partial fulfillment of the requirements for the Ph.D. degree.

Registry No. Cd, 7440-43-9; Pb, 7439-92-1; O$_2$, 7782-44-7; chloride, 16887-00-6.

LITERATURE CITED

(1) Fernando, A. R. Ph.D. Thesis, University of Alberta, 1988.

(2) Clem, R. G.; Litton, G.; Ornelas, L. D. *Anal. Chem.* **1973**, *45*, 1306–1317.

(3) Zief, M.; Mitchell, J. W. *Contamination Control in Chemical Analysis*; John Wiley and Sons: New York, 1985.

(4) Mizuike, A. *Enrichment Techniques for Inorganic Trace Analysis*; Springer-Verlag: New York, 1983.

(5) Mitchell, J. W. *Talanta*, **1982**, *29*, 993–1002.

(6) *Deaeration ... Why and How*; Application Note D-2, Princeton Applied Research Corporation, 1980.

(7) Dolezal, J. *J. Electroanal. Chem. Interfacial Electrochem.* **1970**, *25*, 299–306.

(8) Copeland, T. R.; Christie, J. H.; Osteryoung, R. A.; Skogerboe, R. K. *Anal. Chem.* **1973**, *45*, 2171–2174.

(9) Valenta, P.; Rützel, H.; Nürnberg, H. W.; Stoeppler, M. *Z. Anal. Chem.* **1977**, *285*, 25–34.

(10) Valenta, P.; Mart, L.; Rützel, H. *J. Electroanal. Chem. Interfacial Electrochem.* **1977**, *82*, 327–343.

(11) Seelig, P. F.; Blount, H. N. *Anal. Chem.* **1979**, *51*, 1129–1134.

(12) Liteanu, C.; Rica, I. *Statistical Theory and Methodology of Trace Analysis*; John Wiley and Sons: New York, 1980.

(13) Vydra, F.; Stulik, K.; Julakova, E. *Electrochemical Stripping Analysis*; John Wiley and Sons: New York, 1976.

(14) Wang, J. *Stripping Analysis—Principles, Instrumentation and Applications*; VCH Publishers, Inc.: Deerfield Beach, FL, 1985.

(15) Buchanan, E. B., Jr.; Soleta, D. D. *Talanta* **1982**, *29*, 207–211.

(16) Wang, J.; Dewald, H. D. *Anal. Chem.* **1984**, *56*, 156–159.

(17) Sinko, I.; Dolezal, J. *J. Electroanal. Chem. Interfacial Electrochem.* **1970**, *25*, 53–60.

(18) Florence, T. M.; Farrar, Y. J. *J. Electroanal. Chem. Interfacial Electrochem.* **1973**, *41*, 127–133.

(19) Wang, J.; Greene B. *Water Res.* **1983**, *17*, 1635–1638.

(20) Wise, J. A.; Heineman, W. R.; Kissinger, P. T. *Anal. Chim. Acta* **1985**, *172*, 1–12.

(21) Florence, T. M.; Mann, K. J. *Anal. Chim. Acta* **1987**, *200*, 305–312.

RECEIVED for review July 18, 1989. Accepted September 8, 1989.

Optimization of Signal-to-Noise Ratios in Time-Filtered Fluorescence Detection

Newton K. Seitzinger,[1] Kenneth D. Hughes, and Fred E. Lytle*

Department of Chemistry, Purdue University, West Lafayette, Indiana 47907

Subnanosecond, time-filtered detection is achieved by using the technique of time correlated single photon counting. The core of the instrument is a commercial time-to-amplitude converter/multichannel analyzer combination having zero dead time at trigger rates as high as 160 kHz. After data collection, the entire temporal distribution of both blank and signal photons is transferred to a computer for numerical processing. The algorithm optimizes the signal-to-noise ratio by exhaustively computing all possible positions for the leading and trailing edges of a time filter.

INTRODUCTION

Laser-based fluorometry is well noted for being a blank limited technique. To achieve the lower limit of detection implied by the large excitation intensity, ancillary methods have to be utilized to control the level of interferences. Commonly, some property of the sample and/or its environment can be used. As examples, chromatography reduces the effect of sample impurities (*1*), and sheathed flow detection reduces the effect of sample cell related interferences (*2*). On the other hand, properties of the laser itself can be used to improve the detection limit, e.g. both narrow bandwidth site selection (*3*) and subnanosecond, time-resolved spectroscopy (*4*) can be used to reduce the amount of interference observed.

The most common approaches used for fluorometry with time-resolved detection are based upon the measurement of photomultiplier anode current. The two major variants are temporal resolution and gated integration. In temporal resolution a time window shorter than the analyte lifetime is set sufficiently far into the fluorescence decay to minimize detection of photons due to the, most usually, shorter lived blank. In gated integration the period of observation is typically comparable to, or larger than, the lifetime. This allows a greater integrated current, thus a better signal-to-noise ratio (SNR). There are problems associated with both techniques. With temporal resolution methods there is a loss of sensitivity due to excluding all but a small portion of the signal. In gated integration one obtains poor temporal discrimination due to risetime limitations of the electronic gate. In both approaches the stray capacitance of the photomultiplier limits the measured risetime.

To realize the full potential of temporal resolution, an acceptance window must be devised which has photomultiplier transit time-spread limited edges for optimum resolution and samples a large enough period of time to help overcome loss of sensitivity. The goal is to adjust the size and position of the window so that signal is added at a faster rate than interference. In essence, the window acts as a "time filter" (*5*). In this study the filtering is achieved by using the technique of time-correlated single-photon counting due to its excellent (subnanosecond) resolution (*6*). A previous configuration of the instrument used a time-to-amplitude converter (TAC) and a single channel analyzer (SCA) to make up the time filter (*5*). The TAC–SCA combinations was used only because the multichannel analyzers (MCA) available at the time of the first studies could not be triggered as fast as the TAC can output data. Additionally, the TAC–SCA combination requires that the optimum window position be hardware adjusted by the operator for each analytical sample. Recent advances in high-speed electronics have made available MCA's with throughputs slightly greater than the TAC. The instrument for this study utilizes a 175-kHz TAC and a 200-kHz MCA. This allows collection of all of the time-resolved fluorescence and time-resolved blank emission, followed by software maximization of the SNR.

It will be shown through both a computer model and experimental results that with this instrument the SNR is automatically optimized and enhanced for systems where (a) the

---

[1] Present address: Los Alamos National Laboratory, Los Alamos, NM 87545.

0003-2700/89/0361-2611$01.50/0 © 1989 American Chemical Society

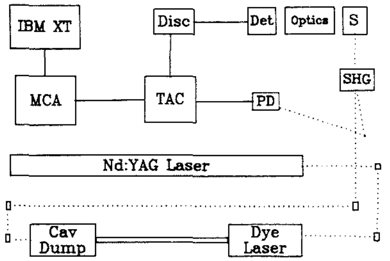

Figure 1. Diagram of the time-filter instrument. The components are described in the text.

blank has a large scatter component, (b) the analyte lifetime is longer than the blank lifetime, and (c) the analyte lifetime is significantly shorter than the blank lifetime. For a 17.6-ns analyte lifetime and an interference dominated by scatter, the experimental result obtained by using time filtering has a SNR improved by a factor of 9 when compared to a steady-state measurement. Data for the same analyte with a 5.1-ns interference is improved by a factor of 2.

EXPERIMENTAL SECTION

Instrumentation. A diagram of the instrument is shown in Figure 1. A synchronously pumped, cavity dumped, frequency doubled dye laser (Spectra-Physics) using rhodamine 6G (Exciton) is driven by a mode-locked Nd:YAG laser (Spectra-Physics Model 3000). This configuration is used to produce the short (picosecond), variable repetition rate (single shot to multiple megahertz) UV pulses needed for this experiment. The detector is an RCA 8850 photomultiplier tube running at −2300 V which is connected to a constant fraction discriminator (Tennelec 455). The heart of the signal processing electronics is an Ortec Model 457 time-to-amplitude converter (TAC). The TAC is run in the conventional configuration with a noninteractive source (*7*). The start signal for the TAC comes from a photodiode (Texas Instruments TIED 56) which is irradiated by the part of the excitation beam back reflected from the second harmonic generator. The repetition rate of the cavity dumper was set to give excitation rates of 150 kHz for the β-naphthylamine samples and 160 kHz for the rhodamine B samples. A frequency doubler (INRAD Model 515) was used to generate 100 μW of 300-nm radiation. The TAC stop signal is provided by the constant fraction discriminator. The sample emission was always attenuated to provide a stop rate less than 10% of the excitation rate so as to keep nonlinearities associated with counting multiple photon events under 5% (*8*). The TAC output is directed to the 1024-channel MCA (Nuclear Data Model 62) which uses a 5-μs fixed conversion time analog to digital converter (ADC). The impulse response of the system was 650 ps full width at half maximum (fwhm). The hardware settings on the electronics gave a time calibration of 80 ps per channel. Data collection time was set at 60 s for all measurements. Once the decay is stored in the memory of the MCA, the data are transferred to an IBM XT for processing.

Materials. The analyte used in this study was β-naphthylamine (BNA) which was obtained from Sigma. A stock solution of 10^{-3} M BNA in methanol (Burdick and Jackson) was kept refrigerated and showed no signs of degradation over the course of the study. A 10^{-5} M solution of BNA in 0.005 M tris(hydroxymethyl)aminomethane (THAM, Fisher), aqueous buffer (pH = 8.0), was prepared from the dilution of the methanolic stock and used for preparation of the other concentrations. Rhodamine B (Exciton) and tris(2,2′-bipyridine)ruthenium(II) dichloride ($\mathrm{Ru(bpy)_3{}^{3+}}$, G.F. Smith), were used without further purification. Solutions of rhodamine B and $\mathrm{Ru(bpy)_3{}^{3+}}$ were made with distilled, deionized water. None of the solutions were degassed.

Procedures. A solution of the analyte having an insignificant blank is first used to determine the fluorescence lifetime and the MCA channel having the maximum counts. An initial window is then defined such that the leading edge is located at the MCA channel having the maximum counts and the trailing edge is at a channel four lifetimes later. Although both of these choices are arbitrary, they are easy to implement and the exclusion of counts outside of the window only degrades sensitivity by a negligible amount. This is the largest window utilized, as any optimization involves moving the leading edge to later channels and/or the trailing edge to earlier channels. The time-resolved counts within the initial window are then used to compute an array of correction factors capable of mapping the signal for any resized window onto a master calibration plot.

When quantifying an unknown, the photons from both the sample solution and the blank solution are counted for the same length of time. The two sets of temporally resolved data from the MCA are transferred to a microcomputer for off-line processing. Software optimization of the window width and position is accomplished by the following algorithm. With the trailing edge fixed, the leading edge is moved one channel at a time toward the trailing edge. This is referred to as a forward search. The SNR is calculated every time the edge is moved by using the equation

$$\mathrm{SNR} = (T - B)/(T + B)^{1/2}$$

where T is the total sample counts in the resultant window, B is the blank counts in the resultant window, and the algebraic form of the denominator is due to the propagation of error. As a result, the window size yielding the best SNR can be determined with a resolution of 80 ps. If the blank is dominated by an impurity having a lifetime greater than the analyte, both the leading and trailing edges can be optimized. This global search is capable of rejecting blank photons occurring after the analyte signal has decayed to a low value.

Several postcomputational performance checks are necessary. The initial window should be used where either search yields a SNR not varying significantly with window size. Any measurement producing an optimum window width of only a few channels should be considered below the lower limit of detection. And if a global search gives a better SNR then a forward search for the case where the blank decays faster the analyte, excessively high dark current may be responsible.

RESULTS AND DISCUSSION

Computer Model. A computer model of the experiment was used to gain insight as to how the temporal behavior of the blank influences the performance of time-filtered detection. The two types of blanks modeled were Gaussian, simulating scatter interference, and exponential, simulating a fluorescent impurity. In all calculations the blank was set to 50 000 counts and the analyte to 1000 counts. Therefore, the SNR obtained for no temporal resolution was 3.1, close to the accepted value for the lower limit of detection. To distribute scatter counts, an 80 ps resolution, variable width Gaussian random number generator was used. To simulate fluorescence, the counts were first distributed into the appropriate Gaussian pulse, then counts in each resolution element were redistributed by an exponential random number generator. This produces a decay convolved with the scatter response. The total sample counts were obtained by adding blank and signal counts for each resolution element. Because of statistical fluctuations in placing the photons in time, the results of five replicate simulations were averaged.

For a Gaussian blank and exponential signal, the time filter should perform well. This is because the blank falls off functionally as $\exp(-t^2)$, whereas the signal decays as $\exp(-t)$. In Figure 2a, the optimum SNR versus analyte lifetime (tau) and blank full width at half maximum (fwhm, gamma) is given, showing that this is indeed the result. Figure 2b shows the fraction of the initial window which yielded the optimum SNR. With a forward search a reduction in size corresponds to the leading edge moving toward the trailing edge. For a lifetime 10 times greater than the fwhm the SNR improves approximately a factor of 9 over the value with no temporal resolution. The leading edge has not moved significantly from its initial position. For the case where the signal is drastically distorted by convolution with the Gaussian, the effect of

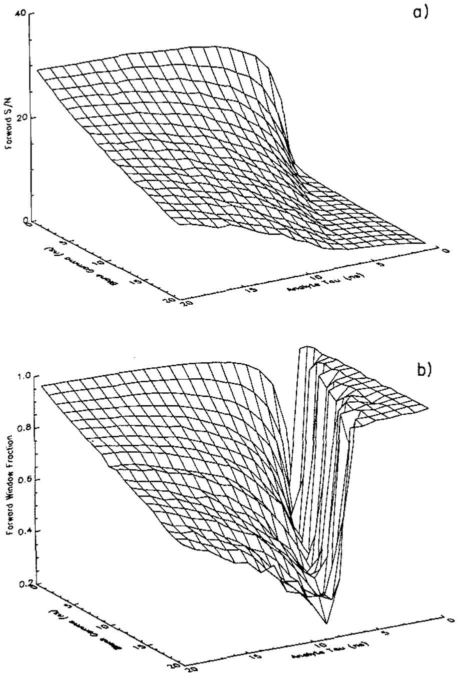

Figure 2. Time-filtered detection for an exponential sample and a Gaussian shaped blank. Tau is the analyte lifetime and gamma is the blank full width at half maximum. The x- and y-axis units are nanoseconds, with the minimum value plotted being 1 ns. (a) Optimum signal-to-noise ratios when performing a forward search. (b) The fraction of the initial window yielding the optimum signal-to-noise ratio.

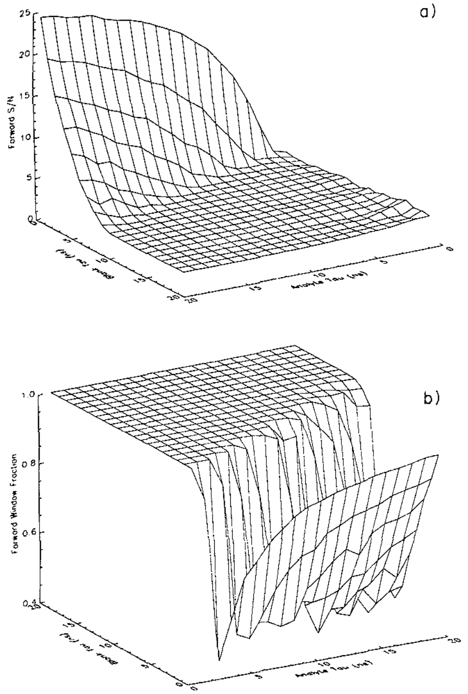

Figure 3. Time-filtered detection for an exponential sample and blank. Tau is the lifetime. The x- and y-axis units are nanoseconds, with the minimum value plotted being 1 ns. (a) Optimum signal-to-noise ratios when performing a forward search. (b) The fraction of the initial window yielding the optimum signal-to-noise ratio.

scatter can still be reduced by a factor of 2 when the signal lifetime is half the fwhm. This information is obtained from Figure 2a for a gamma of 20 ns and a tau of 10 ns, which can be scaled to an impulse response of 650 ps and a fluorescence lifetime of 325 ps for our instrument. Figure 2b shows that this situation is typified by a leading edge which has moved 75% of the way toward the trailing edge in an attempt to isolate the exponential tail of the highly convolved fluorescence. For tau values shorter than about one-fourth gamma, the SNR for time-filtered detection is worse than that obtained from a steady-state measurement. The window also quickly rebounds to its maximum width. On this basis the loss of SNR can be attributed to the initial window including less than half of the signal photons.

Figure 3a shows the optimum SNR for an exponentially distributed blank and analyte. Figure 3b, which has the tau values inverted for graphical clarity, shows the fraction of the initial window which yielded the optimum SNR. When the analyte lifetime is significantly longer than the blank lifetime, the SNR is enhanced due to the front edge of the window moving to longer times. For an analyte lifetime 10 times greater than the blank lifetime, the SNR improves about a factor of 6. The leading edge has moved to yield a window about 80% of the original size. Both the SNR enhancement and the window fraction are smaller than those for a corresponding Gaussian blank. As the two values of tau approach each other, the optimum SNR rapidly degrades. In fact an improvement of a factor of 2 requires that the analyte have a lifetime 3 times that of the blank. For this situation the leading edge has moved about half way toward the trailing edge. When the analyte lifetime is less than twice the blank lifetime, little to no improvement in SNR is obtained by a forward search and the window width has returned to its initial value.

A global search can be used to improve the SNR when the analyte lifetime is significantly less than the blank lifetime. Figure 3a hints at this improvement by the slight ridge at a 1-ns analyte lifetime. Figure 4a shows the SNR difference between the forward and global searches. The difference is due entirely to the trailing edge moving to earlier times. This is dramatically shown by comparing Figure 3b to Figure 4b. As Figure 4a implies, the global search will perform better as the ratio of blank to analyte lifetimes increases beyond the values shown.

The statistical nature of the distribution of the blank and analyte photons prevents the development of an equation relating temporal properties and counts to a SNR enhancement. However, several useful observations can be made from the modeling results. The most important lesson is recognizing that the experimental goal of time resolution is not to totally eliminate the blank counts, but instead reduce the effect that they have on the propagation of error. Thus the leading edge is always positioned well into the blank decay. When the analyte lifetime is a factor of 10 or more longer than the blank decay of fwhm, time resolution can dramatically improve the SNR. When the analyte lifetime is comparable to the blank decay or fwhm, scatter interferences are easier to remove than a background due to fluorescent impurities. When the blank has a decay much longer than the analyte, a global search may still be able to improve the SNR. Temporal resolution works

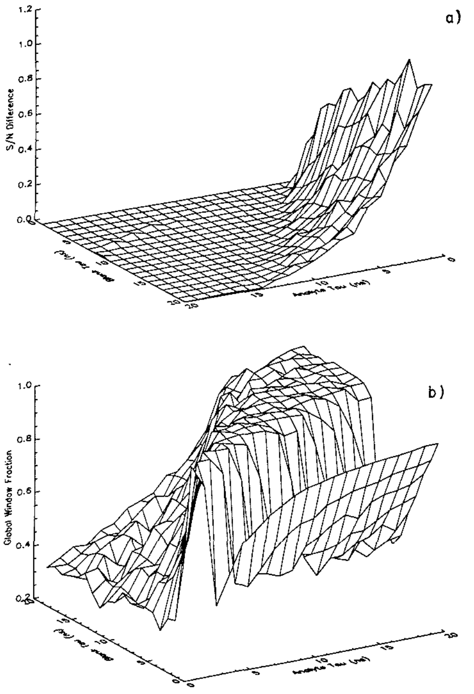

Figure 4. Signal-to-noise ratio improvements with time-filtered detection with a global search which adjusts both the leading and trailing edges. Tau is the lifetime. The x- and y-axis units are nanoseconds, with the minimum value plotted being 1 ns. (a) The difference in improvement between a forward search and a global search. (b) The fraction of the full window used to create the optimum window.

best when steady-state measurements are near or below the limits of detection. For high analyte concentrations where the measured noise is not dominated by the blank, time-filtered detection may reduce sensitivity without significantly enhancing the SNR.

Chemical System. The chemical system employed for most of the studies was β-naphthylamine (BNA) in the sample matrices used in aminopeptidase profiling (*9*). This was done since one of the goals of time-filtered detection is to decrease the detectable concentration of BNA, thus reducing the number of cells necessary for unambiguous identification of bacterial pathogens. In addition, the fluorometric measurement has a blank whose photophysical characteristics vary with the relative concentration of all of the reagents as well as the length of time required to perform the overall microbiological assay (1–4 h of incubation).

A Blank Dominated by Fluorescent Impurities. A 1 $\times$ 10^{-5} M solution of BNA yielded a lifetime of 17.6 ns. The "lifetime" of the fluorescent impurities in the THAM buffer was found to be 5.1 ns. Example data of 5 $\times$ 10^{-10} M BNA in 0.005 M THAM will be given to demonstrate the software optimization. Figure 5a shows the raw data for the sample and the blank with the position of the optimum window superimposed. Since the signal is equal to the sample counts minus the blank counts, it can be seen that the optimum window rejects about 50% of the signal counts and about 90% of the blank counts. Figure 5b shows the computed SNR as the front edge of the window is moved in a forward search from the initial window position. The SNR improves about the factor of 2 predicted from Figure 3a.

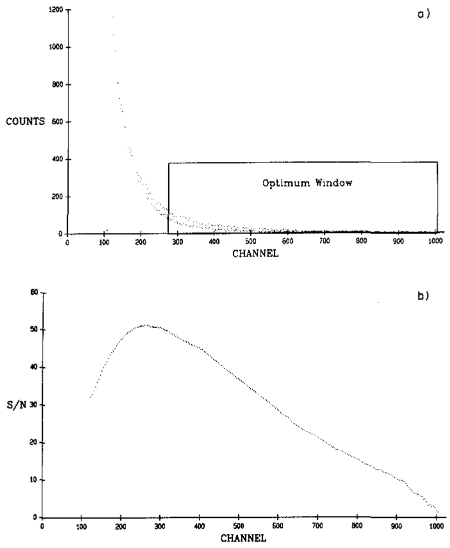

Figure 5. Software optimization of time-filtered detection for 5 $\times$ 10^{-10} M BNA in 0.005 M THAM. (a) The top set of dots corresponds to the sample emission, while the bottom set corresponds to the blank. Each channel has a width of 80 ps. (b) The signal-to-noise ratio produced by moving the leading edge of the time filter to the channel denoted on the x axis. Data were not computed at times prior to the peak of the fluorescence.

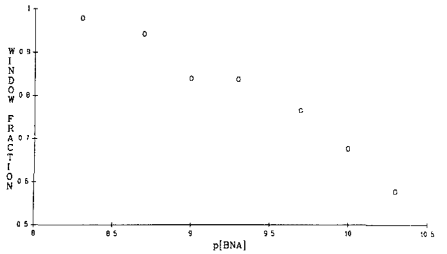

Figure 6. Time filter window fraction as a function of BNA concentration. The solutions are buffered at pH 8 with 0.005 M THAM.

To demonstrate that the correction factors would permit the construction of a calibration graph with time-filtered detection, solutions from 5 $\times$ 10^{-11} to 5 $\times$ 10^{-9} M BNA in 0.005 THAM were examined. A solution of the buffer was used as the blank. The plot was linear with a slope of 5.2 $\times$ 10^{11} cps M^{-1} and a standard deviation of 8.1 $\times$ 10^{9} cps M^{-1}. Figure 6 shows the size of the window as a function of concentration. As expected, the window is large for high concentrations and gradually decreases as the blank begins to dominate the noise. The lower limit of detection (LLD) can only be determined by direct measurement of a solution which gives a SNR of 3. This is because the window size, and consequently the fraction of the blank observed, changes with analyte concentration. The problem is exacerbated by the nonlinear nature of the SNR versus concentration curve at low concentrations. The LLD is estimated to be 6 $\times$ 10^{-11} M. The LLD using the initial window was 1.2 $\times$ 10^{-10} M, while the value with no temporal resolution was 1.6 $\times$ 10^{-10} M. The integrated 0.005 M THAM emission is equivalent to the fluorescence from 2.3 $\times$ 10^{-9} M BNA. Thus, the emission from the analyte at the LLD was only 3% of the blank value.

A Blank Dominated by Scatter. For this study, a 1 × 10^{-5} M solution of one of the substrates used in the bacterial identification scheme, L-alanyl β-naphthylamide, was freshly prepared in 0.005 M THAM buffer at room temperature. At the same time, a 1 × 10^{-5} M substrate solution spiked with 1 × 10^{-9} M BNA was also prepared under the same conditions. For such solutions the blank is dominated by a subnanosecond emission from the unhydrolyzed substrate, which mimics scatter. The blank is also comprised of less intense emission due to THAM impurities and from BNA released by slow self-hydrolysis. The integrated background due to the unspiked solution was equivalent to a 1.7 × 10^{-8} M BNA solution. Immediately after mixing, the decays of both solutions were measured and the signal for BNA in the spiked solution was determined by using the unspiked solution as the blank. The SNR obtained for the initial window was 4, whereas, the SNR for an optimum window where the leading edge has only moved 2.24 ns (3%) toward the trailing edge was 35. These results compare favorably with the model predictions given in Figure 2a.

Rhodamine B in $Ru(bpy)_3^{3+}$. To test the ability of the software to handle a blank with a lifetime that is longer than that of the sample, an alternative chemical system was devised, since the aminopeptidase method has no such interference. The lifetimes of rhodamine B (2.1 ns) and $Ru(bpy)_3^{3+}$ (286 ns) were determined by using 1 × 10^{-5} M solutions of each compound. A solution of 1 × 10^{-8} M rhodamine B in 1 × 10^{-6} M $Ru(bpy)_3^{3+}$ was examined by using a 1 × 10^{-6} M $Ru(bpy)_3^{3+}$ solution as the blank. With no temporal resolution and with time-filtered detection using the initial window, the SNR was <1. A forward search found the optimum SNR to occur when the leading edge was directly on top of the trailing edge, and again gave a SNR <1. When both the leading and trailing edges were allowed to move, an optimum SNR of 7.4 was obtained. For this case the leading edge stayed at its initial position, with the trailing edge being placed such that the window was 1.44 ns wide.

Projected Improvements in Performance. The present laser-based fluorometer has an impulse response of 650 ps. For Gaussian shaped scattering interferences the results presented predict that time filtering can provide significant enhancements in the lower limit of detection for analytes with lifetimes longer than about 6 ns. For analytes with shorter lived decays, the RCA 8850 photomultiplier could be replaced by a channel plate photomultiplier. The temporal resolution, which is limited by the transit time spread of the detector, would drop to a value below 100 ps. This would extend the method to analytes with lifetimes as short as 1 ns.

Since many fluorometric methods have blanks with exponentially shaped interferences (*10*), the above suggested modification may not significantly enhance the performance. Instead the most beneficial change might involve an increase in instrumental sensitivity by operating the TAC in a reverse interactive mode (*7*). As a result, total count rates as high as 160 000 s^{-1} could be possible. For strongly emitting samples, data collection times could be reduced at least a factor of 10 from the present 60-s value. This change would also permit the laser to run at higher repetition rates, increasing the instrumental sensitivity by over a factor of 10.

ACKNOWLEDGMENT

The authors thank Steven Nowak for help with several of the measurements.

LITERATURE CITED

(1) Roach, M. C.; Harmony, M. D. *Anal. Chem.* **1987**, *59*, 411.
(2) Nguyen, D. C.; et al. *Anal. Chem.* **1987**, *59*, 2158.
(3) Cooper, R. S.; et al. *Anal. Chem.* **1988**, *60*, 2692.
(4) Harris, T. D.; Lytle, F. E. In *Ultrasensitive Laser Spectroscopy*; Kliger, D. S., Ed.; Academic Press: New York, 1983; Chapter 7.
(5) Lytle, F. E.; Haugen, G. R. *Anal. Chem.* **1981**, *53*, 1554.
(6) O'Connor, D. V.; Phillips, D. *Time-Correlated Single Photon Counting*; Academic Press: London, 1984.
(7) Lytle, F. E.; Haugen, G. R.; Wallin, B. W. *Rev. Sci. Instrum.* **1979**, *50*, 64.
(8) Poultney, S. K. In *Advances in Electronics and Electron Physics*; Marton, L., Ed.; Academic Press: New York, 1972; Vol. 31, Chapter 2.
(9) Coburn, J. T.; Lytle, F. E.; Huber, D. M. *Anal. Chem.* **1985**, *57*, 1669.
(10) Matthews, T. G.; Lytle, F. E. *Anal. Chem.* **1979**, *51*, 583.

RECEIVED for review September 5, 1989. Accepted September 18, 1989. This research was supported in part by the National Science Foundation Grant CHE-8320158. K.D.H. thanks the Purdue Research Foundation for a David Ross Fellowship.

Supercritical Fluid Chromatography/Flame Photometric Detection: Determination of High Molecular Weight Compounds

Lars A. Pekay and Susan V. Olesik*

Department of Chemistry, The Ohio State University, 120 West 18th Avenue, Columbus, Ohio 43210

The determination of organosulfur compounds by supercritical fluid chromatography/flame photometric detection (SFC/FPD) was further characterized. The noise characteristics of the optimized flame photometric detector were determined. The detection limit was found to be shot-noise-limited for detection of analytes from capillary SFC using supercritical carbon dioxide as the mobile phase. The sensitivity of SFC/FPD was found to be greater than that of SFC/FID (flame ionization detection). The use of highly tapered restrictors substantially lowered the variation of the base line of the FPD during pressure programs. Also, the application of SFC/FPD to the separation and detection of high molecular weight polymers was shown. The detection limit increased slightly with increasing molecular weight of the sample. The effect of replacing carbon atoms in the sample with sulfur atoms on SFC retention was studied. Retention of the organosulfur compounds on a cyano-substituted stationary phase with supercritical carbon dioxide as the mobile phase was similar to that found for normal-phase liquid chromatography. The retention behavior of Lewis bases showed that interactions with free silanol groups on the stationary phase significantly contributed to the retention on the cyano phase.

INTRODUCTION

The applications of supercritical fluid chromatography are multiplying rapidly. Supercritical fluid chromatography (SFC) is not supplanting gas chromatography (GC) or high-performance liquid chromatography (HPLC), but instead SFC is most useful in many applications where neither GC nor HPLC is viable. To further widen the scope of utility of supercritical fluid chromatography, the easy interface of SFC with selective detectors has been successfully demonstrated (*1–3*).

We recently showed that if properly optimized, a single-flame, flame photometric detector (FPD) is a viable SFC detector for selectively determining the presence of sulfur in chromatographed analytes (*4*). In a previous report (*4*), the SFC/FPD technique was found to have some characteristics similar to those of GC/FPD and others that were unique. For example, the optimized SFC/FPD and GC/FPD both have detectivity ranges of 1×10^{-11} to 1×10^{-12} g/s. Also, the slopes of the log–log calibration curves in SFC/FPD and GC/FPD are statistically the same for the same compound. This information was significant evidence that the mechanisms for sulfur dimer formation and chemiluminescence were similar in both SFC/FPD and GC/FPD. Conversely, the quenching effect on the sulfur dimer chemiluminescence caused by the presence of hydrocarbons in the flame was found to be smaller in SFC/FPD than in GC/FPD (*5*) or in HPLC/FPD due to differences in flame conditions (*6*).

This paper includes the further characterization of the SFC/FPD technique. This characterization involved (1) an investigation of possible methods to eliminate the variation in the base line during pressure programming, (2) an analysis of the noise sources that limit sulfur detection, (3) a comparison of the sensitivity of SFC/FPD and SFC/flame ionization detection (FID), (4) a demonstration of possible applications of SFC/FPD such as the determination of pesticides, organosulfur drugs, and model coal compounds, (5) a demonstration that SFC/FPD can be used for the sulfur analysis of high molecular weight compounds, and (6) a study on the effect of sulfur atoms in a molecule on the retention in SFC.

EXPERIMENTAL SECTION

The instrumentation used in this study was described previously (*4*). The flame photometric detector (FPD) was a Hewlett-Packard Model 19256A, which is a single-flame device. For the experiments described in this paper, pressure programming was necessary. Pressure programming was achieved by controlling the syringe pump, an ISCO μ-LC500 (ISCO, Lincoln, NE), with an analog signal that was produced by a digital to analog converter, Model DT2821 (Data Translations, Marlboro, MA), incorporated in the Zenith Z-200 computer system. The data collection from the FPD, data analysis, and pressure programming were accomplished by using original programs written in the ASYST laboratory analysis and programming environment (ASYST Software Technology, Rochester, NY). Frequency domain spectra of the base-line noise on the FPD output were obtained by placing a current amplifier, Model 427 (Keithley Instruments, Cleveland, OH), and a low band-pass filter, Model 3340 (Krohn-Hite Corp., Avon, MA), in series between the photomultiplier's current output signal and an analog to digital converter (Data Translations Model DT2821).

The fuel and oxidant gases for the FPD were instrument-grade hydrogen and oxygen (Matheson Gas Products, Chicago, IL). All analytes in this study were used as delivered and were injected into the supercritical fluid chromatograph as solutes dissolved in either spectrophotometric grade methanol or anhydrous grade acetone (Mallinckrodt Chemical, Inc., Paris, KY). Methyl-*p*-tolyl sulfide, thiophenol, benzo[*b*]thiophene, phenyl sulfide, dibenzothiophene, phenyl disulfide, 1,4,8,11-tetrathiacyclotetradecane, and 1,5,9,13-tetrathiacyclohexadecane were obtained from Aldrich Chemical, Milwaukee, WI. Quinomethionate and Ovex were obtained from Chem Service, West Chester, PA. Carbon disulfide was purchased from Mallinckrodt. Tolbutamide was provided by UpJohn Chemical Co., Kalamazoo, MI. Thiokol LP-3 was obtained from Polysciences, Inc., Warrington, PA.

The chromatographic separations were attained by using a 12 m long, 220 μm i.d. fused silica column coated with 0.25-μm film thickness of 7% cyanopropyl, 7% phenyl methyl siloxane stationary phase, BP-10, (Scientific Glass Engineering, Austin, TX.) This column was further cross-linked with azo-*tert*-butane (*7*) before using it with a supercritical fluid mobile phase. The mobile phase for all separations was supercritical grade carbon dioxide (Scott Specialty Gases). The restrictors used in this study were made in-house with untreated 50 μm i.d. fused silica tubing (Polymicro Technologies). The diameter of the restrictor at its terminus was carefully lowered by heating until the restriction was approximately micrometers in dimension.

RESULTS AND DISCUSSION

I. Analysis of Noise Characteristics of the SFC/FPD System. In ref 4, the detecton limit for the optimized SFC/FPD was found to be approximately nanograms of sample injected into the column with a detectivity of low pg/s. A technique that has even lower detection limits and the capability of measuring the sulfur composition in high mo-

0003-2700/89/0361-2616$01.50/0 © 1989 American Chemical Society

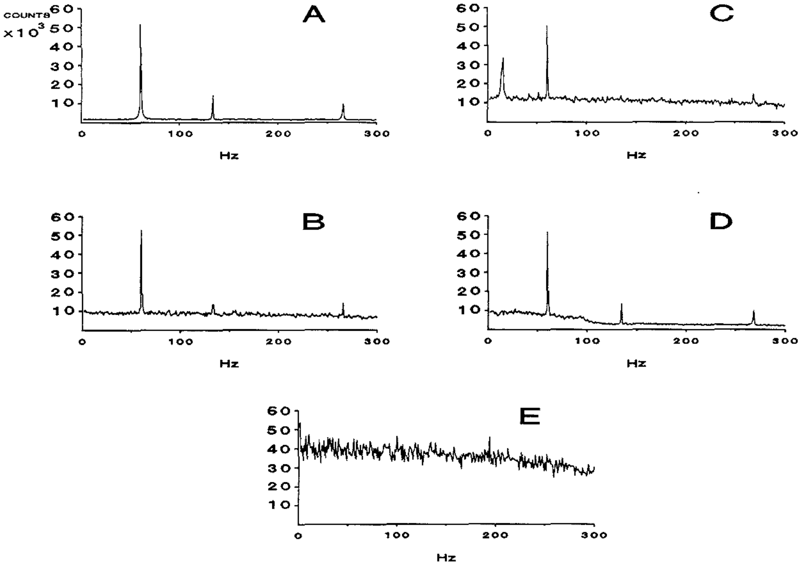

Figure 1. Amplitude noise spectra of SFC/FPD system. Shown is count rate versus frequency (hertz) of the noise. Experimental conditions: (A) flow rate of H_2 270 mL/min, O_2 54 mL/min, flame on, no CO_2 added; (B) flow rate of H_2 167 mL/min, O_2 93 mL/min, flame on, no CO_2 added; (C) same as B but 40 μL/min CO_2 added; (D) same as A but 80 μL/min CO_2 added; (E) same as A with 40 μL/min CO_2 with 5.3 mM CS_2.

lecular weight species would find numerous applications. For example, with the continued growth in the area of biotechnology, new analytical techniques are needed to monitor possible pollutants from the effluent of production plants. Sulfur analysis would be highly useful in detecting bacteria in the water that is exhausted from such a production facility (*8*).

Numerous instrumental and software methods exist for signal-to-noise enhancement (*9*). To apply the most appropriate method of signal-to-noise enhancement to the SFC/FPD technique, more information on the limiting variables was desired. An analysis of the noise characteristics of the SFC/FPD system was undertaken to determine the probability of lowering the detection limit below its present limit. That is, the most important question was: What noise source controls the detection limit of SFC/FPD?

In several studies of GC/FPD with hydrogen/air flames the assumption was made that the most significant type of noise was flicker noise from the flame (*10, 11*). Later, a thorough study of analytical flames showed that in general "high temperature" flames were $1/f$-noise-limited; while "cool" flames such as hydrogen/air flames were shot-noise-limited (*12*). If flame noise has a pure $1/f$ dependence, then no signal-to-noise increase is gained by enhancement techniques such as signal averaging. Alternatively, if the most significant noise is primarily shot noise, then the signal-to-noise ratio improves with the square root of the number of data points taken. Because of the divergent opinions on the noise sources in a hydrogen/air flame and the lack of information of the hydrogen/oxygen flame, which was used in the optimized SFC/FPD, an analysis of the significant noise sources in capillary SFC/FPD was undertaken.

Noise spectra of the capillary SFC/FPD detector were measured under various experimental conditions. The current output from the photomultiplier was amplified with a current amplifier. This signal was filtered with a variable frequency low band-pass filter. The filtered signal was then sampled by a high-speed analog-to-digital converter at a rate approximately 3 times the frequency of the band-pass filter's cutoff to fulfill the Nyquist sampling limit. The frequency domain noise spectrum for each set of conditions was obtained by taking the Fourier transform of the time domain data. The frequency domain spectrum of the FPD detector without the flame lit (dark current measurement) included shot noise with an average current of 1×10^{-9} A and interference noise at 60 Hz. For comparison, the frequency domain spectrum of a constant current supply with an average current of 1×10^{-9} A was measured. Minimal 60-Hz noise was detected under those conditions. Therefore, the 60-Hz interference noise was primarily picked up by the FPD and not the current amplifier and/or the low-pass filter that were used to characterize the noise spectrum of the system. Figure 1A shows the noise spectrum of the FPD system with the flame on, the flame gas (H_2/O_2) flow rates at the optimum conditions for SFC/FPD but without carbon dioxide added, and the photomultiplier on. The strongest characteristic in the spectrum is the interference noise at 60 Hz. Also, additional interference noise was noted at 134 and 266 Hz. The shot noise increased by a factor of 50% over that attributed to the dark current of the photomultiplier dark current.

Next, the noise spectrum of the system under the same conditions as in Figure 1A (good signal-to-noise conditions) was measured with 14 mL/min (STP) carbon dioxide flowing into the flame, which corresponded to 40 μL/min at 170 atm and 60 °C in the column. The frequency spectrum under these conditions was the same as shown in Figure 1A with the type of characteristic noise and the amplitude of the noise being identical. That is, for low flow rates of carbon dioxide and optimum flame gas conditions, the addition of carbon dioxide has no effect on the measured noise. Figure 1B shows the noise spectrum under the same conditions, except the flame gas flow rates were those that provided a poor signal-to-noise ratio in SFC/FPD (*4*). Under these conditions the shot noise level was increased by 164% compared to that observed under the good S/N conditions shown in Figure 1A.

The noise frequency spectrum was also measured for the same carbon dioxide flow but under conditions of H_2/O_2 flame gas flow rates that provided a poor signal-to-noise ratio (same flame gas flow rates as in Figure 1B). Under those conditions the addition of carbon dioxide did have an effect on the noise spectrum (Figure 1C). The random noise increased slightly in this case. Also, a new band at approximately 10 Hz was produced in addition to the 60-Hz interference noise. Similar interference noise has been observed in the flame ionization detector with a hydrogen/air flame (*13*).

The effect of three different types of flow restrictors, integral, reduced diameter, and Lee Scientific frit type, on the flame noise was studied. The type of restrictor had no effect on the measured flame noise amplitude and frequency spectrum when low CO_2 volumetric flow rates such as 14 mL/min (STP) were used.

Figure 1D shows the effect of increasing the flow of carbon dioxide into the flame to a rate of approximately 28 mL/min (STP) for optimum H_2/O_2. At the higher flow rates of carbon dioxide the low-frequency noise components in the frequency spectrum preferentially increased. Finally, Figure 1E shows the noise on the signal that was observed when a continuous flow of carbon disulfide (dissolved in carbon dioxide) was injected into the flame at a rate of 14 mL/min (STP). From these data it is clear that when the signal level is increased above the detection limit, the predominate noise source is white noise.

In summary, the noise in the optimized SFC/FPD at flow rates comparable to those used in capillary SFC/FPD is predominately interference noise at 60 Hz and shot noise. The 60-Hz interference noise can be eliminated by software or hardware filtering. The optimized SFC/FPD would therefore be primarily shot-noise-limited, which is similar to the noise characteristics in H_2/air flames (*12*). Signal-to-noise enhancement can be obtained by signal averaging, with the final limitation on the extent of averaging allowable being controlled by the eventual degradation of the detected resolution of the separation.

II. Possible Methods To Eliminate the Variation in the Base Line of the Chromatogram during Pressure or Density Programming. In ref 4 the variation in the signal intensity and the background intensity of the flame photometric detector was studied as a function of the H_2/O_2 flame gas ratio. A statistical optimization revealed response surfaces for the signal and the background that were practically opposite in behavior. That is, when the H_2/O_2 ratio increased, the signal intensity increased and the background intensity decreased. Under optimum conditions the background intensity could be diminished to levels that corresponded to the dark current of the photomultiplier. In the original statistical optimization the flux of carbon dioxide entering the flame was held constant. Accordingly, carbon dioxide was not used as a variable in the optimization. The primary reason for doing this was that the carbon dioxide flow rate should be primarily controlled by the desired chromatographic efficiency.

A pressure-programmed separation was shown in ref 4. The base line of the FPD increased with increasing quantities of carbon dioxide entering the flame. The hypothesis was made that because the base line and the signal were inversely dependent on flame gas flow rates, then perhaps feedback control between the pressure of carbon dioxide imposed on the column and the flow rate of hydrogen could allow the base line to stay constant with minimal effects on the signal intensity. The following results show a test of this hypothesis.

Under optimum flame gas conditions the calibration curve of carbon disulfide was determined for a column temperature of 60 °C and carbon dioxide pressure of 170 atm, which corresponded to a flow rate of 33 μL/min through the column. Next, the pressure of carbon dioxide in the column was increased to 238 atm, which corresponded to a column flow rate of 41.2 μL/min, and another calibration curve was measured. Then, the hydrogen flow rate was increased until the background counts due to the presence of carbon dioxide in the flame were identical to that found for the case of 170 atm of carbon dioxide in the column. The resulting calibration curves for this experiment are shown in Figure 2. Unfortunately, the results obtained show that when the higher carbon dioxide and hydrogen flow rates were used, the signal intensity was lowered. Feedback of this sort will not achieve the desired goal of allowing easy quantitation of the sulfur signal by eliminating the background because the sulfur signal changes as well.

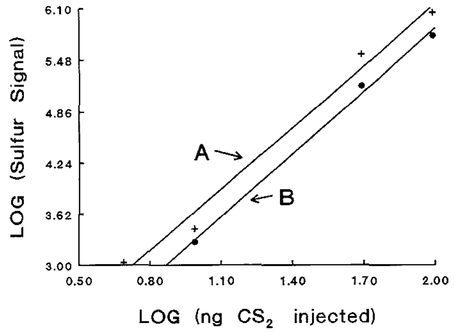

Figure 2. log (sulfur signal) vs log (nanograms of carbon disulfide) injected for two mass flow rates of carbon dioxide. The fuel gas flow rates were changed in B until the base-line background signal was lowered to a value equal to that that found in A. The column was 12 m long, BP-10 with film thickness of 0.25 μm; temperature was 60 °C. For A (+) CO_2 pressure = 170 atm, H_2 flow rate = 240 mL/min, O_2 flow rate = 45 mL/min. For B (●) CO_2 pressure = 238 atm, H_2 flow rate = 280 mL/min, O_2 flow rate = 45 mL/min.

In retrospect, these findings are not surprising. From information in ref 4, a global statement could be made that as the background emission decreased, the signal increased. A closer look at the behavior of both the background emission intensity and the sulfur emission intensity reveals a more complicated interrelationship between background and signal emission. Especially near the optimum conditions for flame gas flow rates, the signal intensity varied considerably as the flame gas flow rates were moved from the optimum conditions. The background emission was not as variant with flame gas conditions. Also, the results in Figure 2 strongly support the two hypotheses purported in ref 4. First, the background emission was predominately controlled by flame temperature; and second, the signal intensity was more strongly affected by the radical reaction chemistry that involved carbon dioxide and hydrogen than by flame temperature (*4*).

Another means of decreasing the base-line variation in pressure programs was, however, discovered. Figure 3A and the other chromatograms in this paper show minimal variation in the base line when the pressure was changed. The base-line variation in Figure 9 of ref 4 was much greater than that found in Figure 3A. No base-line subtraction technique was used to cosmetically improve the appearance of the base lines of the chromatograms in this paper. The attenuation used for the chromatograms in this paper was lower than that in previous studies, which should have made the base-line variation with pressure even more perceptible in this study. Also, the flame gas flow rates in both cases were the same. The only change made in the chromatographic method was that highly tapered restrictors were used to control the flow for the chromatographic analyses in this paper. However, in previous work, short 15 μm i.d. linear restrictors were used. With linear

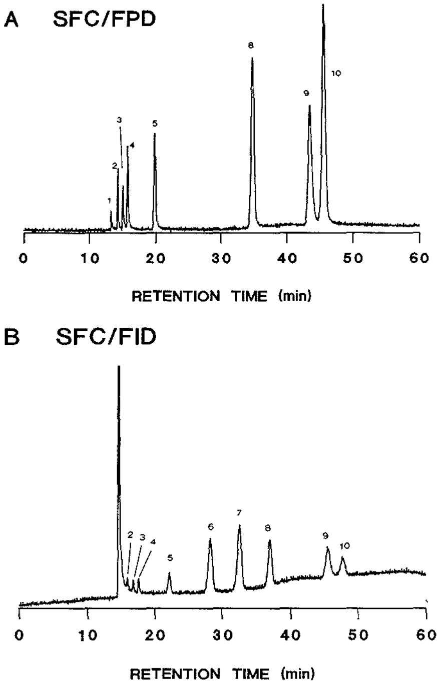

Figure 3. Chromatogram obtained with same column as in Figure 2 at 70 °C, with an initial CO_2 pressure of 102 atm held for 30 min, followed by a ramp of 2.72 atm/min to a final pressure of 129 atm. Chromatogram A used FPD with H_2 = 240 mL/min and O_2 = 5 mL/min. Chromatogram B used FID with H_2 = 130 mL/min and O_2 = 55 mL/min. Compounds were in order of elution: 1, carbon disulfide; 2, tetrahydrothiophene; 3, cyclohexyl mercaptan; 4, thiophenol; 5, benzo[*b*]thiophene; 6, diphenylmethane; 7, dibenzyl; 8, phenyl sulfide; 9, dibenzothiophene; 10, phenyl disulfide.

restrictors both the mass flow rate of the gas and the velocity of the gas increase with pressure (*14*). For highly tapered restrictors the mass flow rate continues to increase with pressure, but the velocity of the gas remains constant at the exit of the restrictor. The variation in speed of the gas with linear restrictors therefore must adversely affect the base-line variation. The need to correct for base-line variation as a function of pressure with steep tapered restriction is clearly not as important as with linear restrictors.

III. Comparison of SFC/FPD and SFC/FID. The flame ionization detector is the most commonly used detector in gas chromatography. For example, 54% of gas chromatographic analyses that were published in 1982 were done with a flame ionization detector (*15*). Flame ionization is also becoming highly important in SFC as well. Accordingly, a comparison of SFC/FPD and SFC/FID was made.

For gas chromatography the advantages of the flame ionization detector are that it (1) responds to almost all organic compounds, (2) has high sensitivity, and (3) has a wide linear dynamic range. In supercritical fluid chromatography similar advantages have been assumed, but not verified.

A comparison was made of the sensitivity of the SFC/FPD and SFC/FID. To make a fair comparison, the flame gas flow rates used in the SFC/FID were optimized by using the Simplex V optimization program (Statistical Programs, Houston, TX). The optimized flame gas conditions were 65 mL/min for hydrogen and 215 mL/min for oxygen at a constant flow of carbon dioxide into the flame of approximately 75 μL/min at 102 atm and 70 °C. These values are different from the suggested values described by the manufacturer of 40 mL/min hydrogen and 400 mL/min for air (which corresponds to a flow rate of 84 mL/min oxygen) for gas chromatographic conditions using helium carrier gas. This initial optimization caused an increase in the signal-to-noise ratio of approximately a factor of 3.

Table I. Comparison of Detection Limits for SFC/FPD and SFC/FID

compound	detection limits,[a] ng FPD	detection limits,[a] ng FID
thiophenol	1.4	3.2
phenyl sulfide	1.3[b]	3.7
dibenzothiophene	1.9[b]	8.4

[a] Based on a signal-to-noise ratio of 3. [b] Taken from ref 4.

Table I shows a comparison of the detection limits for three organosulfur compounds using SFC/FPD and SFC/FID. For all three compounds the detection limits are lower for SFC/FPD than in SFC/FID. For example, for dibenzothiophene, the FPD detection limit is a factor of 4 larger than in FID, and for thiophenol the FPD has a detection limit 2 times lower than that obtained with the FID.

Figure 3A shows the SFC/FPD chromatogram of a test mixture of organosulfur compounds separated on a capillary column coated with BP-10 stationary phase by use of flame gas flow rates that are optimum for the SFC/FPD. With the column still attached to the injector and the restrictor, the same test mixture was separated under identical chromatographic conditions and detected with the flame ionization detector. As mentioned previously, the flow rate for this experiment and all others was controlled by a highly tapered flow restrictor. To separate the test mixture, a pressure program was used. In the pressure program, the pressure was initially held at 102 atm for 30 min and then ramped at a rate of 2.72 atm/min to a final value of 129 atm. The temperature of the separation was 70 °C. The base line increased more significantly over this pressure program in the SFC/FID system than in the SFC/FPD system. For example, for the same pressure program, the background signal in SFC/FID varies from 16 to 127 counts/s (a factor of 8 increase in background noise), while in SFC/FPD the background signal varies from 11 to 27 counts/s (a factor of 2.4). For benzo[*b*]thiophene, a compound that elutes early in the pressure program, the ratio of signal-to-background in FPD to signal-to-background in FID was 5.0. The same ratio for dibenzothiophene, a compound that eluted much later in the pressure program, was 20. Therefore, variation in base line caused by pressure programming was significantly less in the FPD than in the FID when a highly tapered restrictor was used.

In summation, of the two detectors studied, the flame photometric detector was found to be more sensitive than the flame ionization detector. Also, from the aforementioned data, the effect of the base-line variation should have minimal effect on quantitation in SFC/FPD compared to that in SFC/FID. Other workers recently showed preliminary data on a new FID design for SFC with improved detection limits (*16*). In gas chromatography, the flame ionization detector has a lower detection limit compared to that of the FPD. In GC, the FID has a detection limit of 1–100 pg of analyte injected, which is 1–2 orders of magnitude lower than that of FPD (*17*).

The difference in sensitivity of the two detectors for supercritical fluid chromatographic detection is probably due to a diminution of sensitivity for the flame ionization detector when considerable amounts of carbon dioxide are added to the flame. Previous research that studied the effect of carrier gas in GC/FID substantiates this belief. For example, Schafer (*18*) demonstrated decreased sensitivity of flame ionization detection when the carrier gas was carbon dioxide as compared to nitrogen, helium, argon, or hydrogen. The decrease in sensitivity in SFC/FID with carbon dioxide mobile phase may be an amplification of this effect. The lower sensitivity with carbon dioxide as the carrier gas in GC was attributed to the high heat capacity of carbon dioxide. That is, as a noncombustible gas, such as carbon dioxide, is added to the flame, the temperature in the combustion zone decreases. Therefore, a decrease in the extent of ionization also occurs (*18*).

Conclusive evidence identifying the cause of decreased sensitivity when carbon dioxide is the carrier gas is not yet available. However, recent work has substantiated more thoroughly the importance of the flame temperature on the maximum extent of ionization in the FID. For various hydrogen/air flame gas compositions, with different noncombustible gases being added, the maximum extent of ionization always occurred at approximately the same temperature in the reaction zone of the flame (*19*).

IV. Separation of a Disulfide Polymer: Possible Use of SFC/FPD for Sulfur Analysis of High Molecular Weight Compounds. The combination of a chromatographic technique capable of efficiently separating high molecular weight compounds with a sulfur-specific detector is highly desirable. For example, the quantity of and type of sulfur in coal and coal liquefaction products are still not easily determined. Also, in many applications, such as those that are biotechnological, not only is an efficient separation technique needed, but also very small quantities of the material are available. Therefore, a highly sensitive sulfur detector is necessary. The combination of HPLC with a flame photometric detector for sulfur detection is less than ideal for these analyses. For example, the detection limits are considerably higher for HPLC/FPD than for GC/FPD. Also, substantial quenching effects due to the presence of hydrocarbons have been reported in HPLC/FPD (*6*). We report herein a study on the possible use of SFC/FPD for the analysis of sulfur in high molecular weight compounds.

The polymeric system studied was Thiokol LP-3. Thiokol is the trade name for disulfide polymers produced by Morton Thiokol, Inc. Thiokol LP-3 is a polydisulfide elastomer that is used as a sealant and as a feedstock in the polymer industry. The predominant application of these elastomers is based on their high solvent resistance, which is directly proportional to the quantity of sulfur in the elastomer (*20*). Thiokol LP (liquid polymer) elastomers are produced by reacting bis(2-chloroethyl)formal with an inorganic disulfide such as sodium disulfide (*21*) (reaction 1). For Thiokol LP-3, 2% of a trihalide, such as 1,2,3-trichloropropane, is used as a cross-linking reagent (reaction 2) (*21*).

$$ClCH_2CH_2OCH_2OCH_2CH_2Cl + Na_2S_2 \rightarrow (SCH_2CH_2OCH_2OCH_2CH_2S)_n \quad (1)$$

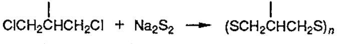

$$ClCH_2\overset{Cl}{C}HCH_2Cl + Na_2S_2 \rightarrow (SCH_2\overset{S}{C}HCH_2S)_n \quad (2)$$

The approximate number-average molecular weight, M_n, and weight-average molecular weight, M_w, of Thiokol LP-3 are 540 and 1500 amu, respectively (*22*). The approximate molecular structure of the polymeric repeating unit is as follows (this structure does not include the subunits from the cross-linking reaction):

$$HS\text{–}(C_2H_4O\text{–}CH_2O\text{–}C_2H_4\text{–}SS)_n\text{–}C_2H_4O\text{–}CH_2O\text{–}C_2H_4\text{–}SH$$

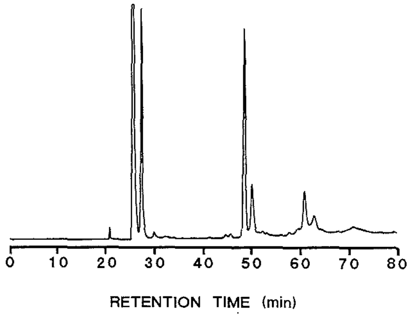

Figure 4. Thiokol LP-3 oligomer separation performed with same column as in Figure 2 at 90 °C using carbon dioxide as the mobile phase. CO_2 pressure was 102 atm for 15 min, followed by a ramp of 3.4 atm/min ending in a final pressure of 306 atm.

Figure 4 shows the chromatographic separation of the oligomers of the Thiokol LP-3 elastomer. This separation is atypical compared to other polymeric separations achieved by HPLC and SFC in that the number of oligomeric units separated was small and the distribution of the oligomers appeared nonrandom. This polymer also has unusual reaction chemistry. Polysulfide polymers that are endcapped with mercaptan linkages undergo a continuous interchange reaction between the mercaptan and the disulfide in the repeating unit. This reaction tends to keep the dispersivity of these polymers low (*23*). Also, the nonrandom distribution may be due to the occurrence of the interchange reaction in the production of the polydisulfide polymer or the extent of the interchange reaction during this process. Considerable debate on the extent and kinetics of the interchange reaction for each of the liquid Thiokols has been published (*24*).

To make certain that the chromatogram was a true representation of the Thiokol LP-3 oligomers, three possible causes of a nonstatistical representation of the elastomer system were considered. First, were the chromatographic conditions degrading the polymer; second, was the injection process causing a mass discrimination effect on some of the higher molecular weight polymers; and third, was some fraction of the polymer permanently adsorbed onto the column?

To test for the possibility of the chromatographic conditions degrading the polymer, the oligomers were separated at temperatures ranging from 40 to 110 °C and pressures from 75 to 276 atm. Over this range the efficiency of the separation changed, but the number of component peaks in the chromatogram did not. The lack of degradation of the Thiokol LP-3 over this temperature range is not surprising. Numerous studies have shown that at least in liquids the elastomer is stable up to temperatures as high as 150 °C (*21*).

To determine if some of the oligomers were irreversibly adsorbed onto the stationary phase, two tests were run. First, after each efficient separation the pressure in the column was ramped to 410 atm to cause further solvation of any adsorbed oligomers. No rise in base line or additional peaks were detected during this process. In the second test the column was replaced by an open tube. A 200-nL aliquot of the same solution used for the chromatogram in Figure 5 was injected into the open tube. The flow rate was also controlled by the same restrictor, and the same pressure program was run. The integration of the resulting sulfur signal from this slug was compared to the integrated sulfur signal of the chromatogram. The integrated areas were found to be statistically the same within 10% error, which is within the reproducibility expected for run-to-run variation for high-pressure injections in SFC (*25*).

The fact that high-pressure injection devices can cause some discrimination in SFC against high molecular weight components of a mixture has been documented (*26*). The most serious discrimination occurs when the valve is cycled between

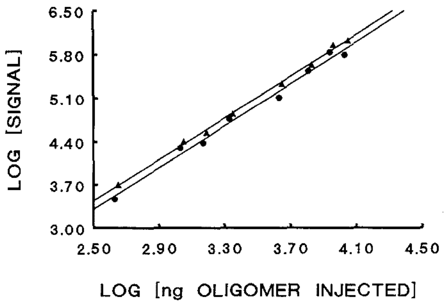

Figure 5. Thiokol LP-3 oligomer calibration curve obtained under chromatographic conditions of Figure 4: (▲) sulfur signal for peak eluting at 25.4 min; (●) sulfur signal for peak eluting at 48.5 min. log (sulfur signal) was plotted vs log (nanograms of Thiokol polymer injected).

the inject and load positions during one injection. Cycling the valve is commonly desirable to provide a symmetric slug injection. During this process in SFC the accompanying pressure drop in the injector also causes precipitation of the high molecular weight component of the mixture. To make certain that minimum error was introduced in the quantitation of these oligomers, the valve was moved to inject and left in that position during the chromatographic run. Also, the injector was operated over the temperature range of 40–90 °C without any change in the measured components in the chromatogram.

From the data obtained in the experiments described above, we felt justified in assuming that all the injected sample had reached the detector during the chromatographic separation. Because the M_n value of Thiokol LP-3 was 540, the chromatographic band with the highest intensity is tentatively assigned to an oligomer with $n = 2$. The subsequent chromatographic bands are probably due to increasingly larger oligomeric units. Also, because the oligomeric system is cross-linked, the cluster of smaller bands around each oligomeric unit is most likely due to different degrees of cross-linking in the oligomers.

The mass spectrum of the Thiokol LP-3 was obtained by using fast atom bombardment (FAB) and laser desorption ionization. Each technique has been used previously to determined the molecular weight distribution of polymers (*27*, *28*).

In the FAB mass spectrum, the largest m/z value detected was 927, but the preponderance of ion signal was found at mass/charge <270 m/z. This behavior is strongly indicative of the sample undergoing substantial fragmentation during the FAB ionization process. In the laser desorption Fourier transform/ion cyclotron resonance (FT/ICR) mass spectrum, the largest m/z value detected was 1391, but again the preponderance of ion signal was found at m/z values <250. Accordingly, the laser desorption technique also caused considerable fragmentation of the polymer. Due to extensive fragmentation of the elastomer for each ionization technique, neither was able to show the oligomeric distribution of the Thiokol LP-3. However, with appropriate standards the supercritical fluid chromatographic analysis may be useful for this purpose.

Calibration curves for chromatographic peaks for the oligomers that had retention times of 25 and 48 min are shown in Figure 5. For sulfur detection the FPD response follows the relationship

$$I = C[S]^n$$

where I is the detected chemiluminescence signal, C is a constant, [S] is the concentration of sulfur, and n is a constant exponent.

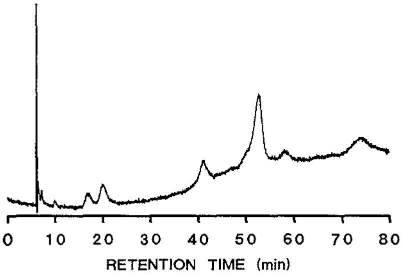

Figure 6. Sulfur cross-linked Thiokol LP-3 oligomer separation under the same chromatographic conditions as in Figure 4.

Calibration curves for sulfur in FPD analysis are always log–log plots such as in Figure 6 with the slope of the plot being the n exponent. The exponent, n, theoretically should have a value of 2 because the detected emission is due to the sulfur dimer which is formed in the flame.

Experimental values of n range from 1.69 to 2.00 (*29*). Burnett et al. (*29*) showed that in GC/FPD the n value was compound dependent. in previous work (*4*), the n value was found to be dependent on the compound in SFC/FPD as well. Also, the n values determined under SFC/FPD conditions were found to be statistically the same as those found for GC/FPD (*4*). Although the variation of the n value with compound type is well documented, not enough information has been collected to date to allow prediction of the n value for a specific compound. For example, information is unavailable on the variation of the exponent, n, for a homologous series of sulfur compounds. The oligomers of an elastomer make up a homologous series. For all the oligomers of the Thiokol LP-3, the n value was the same, $n = 1.69$. The value of n may be constant across a homologous series of sulfur compounds as these data imply, but more homologues must be studied to verify this trend. An extensive study (*30*) of homologues of phosphorus compounds showed that the slope of the calibration curve was invariant across a homologous series for the FPD but only for homologous series.

The detection limits for the first and second oligomers in Figure 6 were determined for a signal-to-noise ratio of 3 (the IUPAC definition of detection limit). For the first oligomeric series, the detection limit was 44 ng of oligomer injected (200-nL injection); and for the second oligomeric series, the detection limit was 54 ng of oligomer injected. These data clearly show that SFC/FPD can sensitively detect sulfur in compounds of moderately high molecular weight (ca. 2000 amu). By comparison, the detection limits for small molecules, such as benzo[*b*]thiophene, were in the nanograms injected range. The percentage of sulfur in a molecule of benzo[*b*]thiophene is approximately 24%. The percentage of sulfur in an oligomer of Thiokol LP-3 is approximately 38%. Therefore, in comparison the detection limit of the polymer was strongly affected by the large molecular weight of the oligomers and is not a simple function of the percentage of sulfur in the sample.

V. Applications of SFC/FPD. One application that is readily suitable to SFC/FPD is the analysis of sulfur vulcanization of polymers. Cross-linking or vulcanization of natural rubbers and synthetic polymers by the interaction of elemental sulfur with the polymers remains a standard method to increase the elasticity of a polymer. Figure 6 illustrates the use of SFC/FPD to monitor the changes in the polymeric structure after the interaction of the polymer with elemental sulfur. The SFC chromatogram in Figure 6 is of the Thiokol

Table II. Effect of Sulfur Atom on Retention

compound	retention time, min	k'^a
cyclohexyl mercaptan	8.62	0.162
methylcyclohexane	7.0	0.038
thiophenol	8.99	0.212
toluene	7.79	0.050
benzo[*b*]thiophene	11.16	0.504
indene	9.18	0.237
phenyl sulfide	19.54	1.633
diphenylmethane	14.76	0.989
dibenzothiophene	26.08	2.515
diphenylethane	19.98	1.693
phenyl disulfide	27.62	2.722
bibenzyl	16.89	1.276

[a] Capacity factor k' calculated with respect to acetone or carbon disulfide, both of which were unretained on the column.

LP-3 elastomer after it was allowed to interact with elemental sulfur for 2 h at a temperature of 110 °C. The resulting cross-linked polymer was not as soluble in the acetone as the original sample of Thiokol LP-3. Accordingly, the chromatographic bands of the oligomers, after vulcanization with sulfur, are shifted to higher retention times compared to those in Figure 4 due to the increased molecular weight of the vulcanized oligomers. Also, a new chromatographic band appeared with a retention time of approximately 74 min. This new band may correspond to a new oligomer unit in the vulcanized polymer.

The characterization of sulfur vulcanization is an application that is uniquely suited to SFC/FPD. The GC/FPD cannot be used for this analysis due to the molecular weight range of the oligomers. HPLC/FPD has numerous problems associated with sulfur detection such as high detection limits and serious quenching interactions of hydrocarbons with the excited sulfur dimer. Sulfur is used to cross-link natural rubber, butyl rubbers, and styrene–butadiene rubber. These polymeric systems are relatively nonpolar. Therefore, except for the possible concern that the polymer molecular weight may be too large to allow solvation in a supercritical fluid, the supercritical solvent and the application seem ideally matched. This type of application also has the potential of contributing to a more thorough understanding of the cross-linking reaction mechanism because the effect of vulcanization on each oligomer unit can be monitored.

Disulfide compounds or polymers are good examples of the types of compounds that are best suited for separation by SFC and detection by a selective detector such as FPD. Disulfide compounds are often typically thermally labile and relatively nonpolar (*31*). These characteristics are ideally suited to SFC analysis. The analysis of disulfides can find use in a broad range of applied chemistries, such as polymer analysis and biochemistry. For example, α-lipoic acid (a disulfide) plays a crucial role in metabolism (*31*). In addition, the S–S linkage is highly important in stabilizing the three-dimensional structure in proteins (*32*).

VI. Effect of Sulfur Atoms in a Molecule on Retention. With the development of new applications comes the desire to provide predictive information on retention behavior of the organosulfur compounds in SFC. Therefore, the effect on retention in SFC of replacing a carbon-bearing subunit of a molecule (methyl, methylene, etc.) with a sulfur atom was studied. Table II shows the results of an experiment in which the retention times of organosulfur compounds were compared to those of the corresponding carbonaceous homologues. The capacity factors were measured for constant pressure and temperature conditions of 70 °C and 102 atm with the BP-10 stationary phase. For each set of homologues, the replacement of a carbon atom with a sulfur atom caused increased retention. This behavior is identical with that found in normal-phase liquid chromatography in which the more polar compound interacts more strongly with the polar sites of the stationary group and therefore is retained longer.

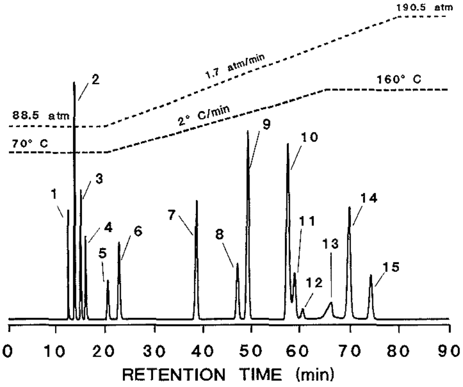

Figure 7. Chromatogram of organosulfur compounds separated on same column as in Figure 2 by using carbon dioxide as the mobile phase with the indicated pressure and temperature programs. Eluted samples are listed in Table III.

Previous studies of the effect of sulfur atoms on retention in isocratic, reverse-phase liquid chromatography showed a mechanism that was much more complicated (*33*). For example, with linear and cyclic alkanes, the replacement of carbon with sulfur caused a decrease in retention. This decrease was attributed to the formation of a solvent "patch" around the sulfur atom in the molecule. Alternatively, the replacement of an aromatic carbon with a sulfur atom had the effect of increasing the retention. The explanation given for this behavior was that the solvent "patch" could not form around the aromatic sulfur atoms due to steric hindrance (*33*).

Thus, for reverse-phase HPLC the solvation sphere around specific types of sulfur moieties was believed to strongly affect the retention of the molecule. In the supercritical state, the number of solvent molecules per sphere is smaller than in the liquid state. But, the interactions between the solute molecules and the solvent sphere may be stronger in the supercritical state than in the liquid state. Also, the size of the solvent sphere is highly variable with the conditions in the supercritical state. It is therefore somewhat surprising that the selective solvation of sulfur atoms does not have a strong effect on the retention of different species in SFC. Our results tend to cast doubt on the assumption in the HPLC studies that the mechanistic differences were totally solvent-controlled.

Figure 7 illustrates other possible applications of SFC/FPD for the determination of molecules such as model coal compounds, pesticides, and organosulfur drugs. In addition, further information on retention behavior of sulfur compounds in normal-phase SFC can be obtained by analyzing the retention behavior in the chromatogram shown in Figure 7. The structures of the model compounds are given in Table III. The retention in this chromatogram can be characterized as typical normal-phase behavior in which the more polar compounds are retained longer, with the exception of three molecules, tetrathiafulvalene (TTF), 1,4,8,11-tetrathiacyclotetradecane, and 1,5,9,13-tetrathiacyclohexadecane. All three of these molecules are retained longer than expected on grounds of substituent polarity alone.

Significant interaction of these three molecules with residual silanol groups is strongly suspected. TTF is a strong Lewis

Table III. Structure of Model Sulfur Compounds

compound[a]	structure
1. carbon disulfide	S=C=S
2. tetrahydrothiophene	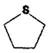
3. cyclohexyl mercaptan	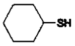
4. thiophenol	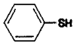
5. methyl *p*-tolyl sulfide	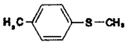
6. benzo[*b*]thiophene	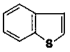
7. phenyl sulfide	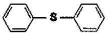
8. dibenzothiophene	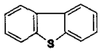
9. phenyl disulfide	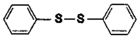
10. quinomethionate	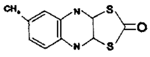
11. Ovex	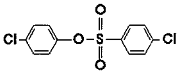
12. tetrathiafulvalene	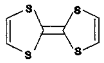
13. tolbutamide	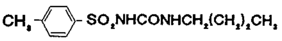
14. 1,4,8,11-tetrathia-cyclotetradecane	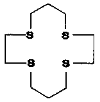
15. 1,5,9,13-tetrathia-cyclohexadecane	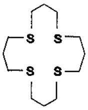

[a] Numbers refer to Figure 7.

base. It readily forms charge-transfer complexes with molecules that can easily accept an electron. The predominate reason for TTF's strong electron-donating behavior is the resonance stabilization of the positive charge. TTF probably interacts with the residual silanol linkages which have Lewis acid character. The large retention time indicates that considerable resonance stabilization of the Lewis acid–base complex must occur.

1,4,8,11-tetrathiacyclotetradecane and 1,5,9,13-tetrathiacyclohexadecane are both macrocyclic thioethers that have characteristics similar to those of macrocyclic ethers, commonly termed crown ethers. These molecules are often used in metal extractions and also serve as ion transport models for porphyrin systems (*34*). Thiacrown ethers are "soft" Lewis bases (*35*) and therefore, like TTF, are expected to interact with Lewis acid sites on the stationary phase such as residual silanol linkages.

The understanding of the interaction of macrocyclic thioethers with ionic species also helps explain their long retention time on a moderately polar stationary phase, as Figure 7 shows. Based on single substituent polarity alone, these molecules should elute with the other cyclic thioethers. Instead, the interaction of the macrocyclic thioethers with the silanol sites must be a cooperative interaction of all the thioether linkages in each ring with individual silanol sites.

The relative retention of the two macrocyclic thioethers further substantiates this belief. 1,4,8,11-Tetrathiacyclotetradecane has a melting point of approximately 118 °C while 1,5,9,13-tetrathiacyclohexadecane has a melting point of 58 °C, yet the lower melting macrocylic thioether is the most strongly retained. The proposed reason for the additional stability is the increased size of the ether ring, which allowed conformational stabilization of the complex with the silanol group. Further studies on the retention of other macrocycles with different basicities and conformation characteristics should provide mechanistic information on the interactions occurring in cyano phases in supercritical fluid chromatography.

VII. Conclusions. In summary, the flame photometric detector was further characterized for use with supercritical fluid chromatography. An analysis of the noise characteristics of the detector showed that random shot noise is the predominate noise source. This characterization will allow further improvements in the signal-to-noise characteristics of this detector for SFC applications.

The use of feedback control of flame gas flow rates to eliminate the variation in the background during pressure programming was found to be an untenable option. However, when a highly tapered restricting capillary was used for flow control, the comparison of the present state-of-the-art SFC/FID to the optimized SFC/FPD showed that the base-line variation in SFC/FPD was insignificant compared to that in SFC/FID. Finally, some of the applications presented here are uniquely suited to SFC separation followed by selective detection, such as FPD. These applications are ones that, for reasons of difficulty of instrumental interface or problems with the thermal stability of the molecules, are not easily implemented by HPLC or GC. These types of applications will certainly become the forte of supercritical fluid chromatography.

ACKNOWLEDGMENT

The authors thank Luther Giddings for contribution work on the SFC/FID optimization. FAB mass spectra were obtained by David Chang at The Ohio State University Chemical Instrumentation Center, by use of a VG 70-250S mass spectrometer. We thank Alan Marshall's research group for obtaining the laser desorption/Fourier transform/ion cyclotron resonance mass spectra. We thank John Olesik at the University of North Carolina for providing the kernel computer program that was used in the noise analysis. Finally, we thank UpJohn Chemical Company for providing pharmaceutical samples for this research.

LITERATURE CITED

(1) Luffer, D. R.; Galante, L. J.; David, P. A.; Novotny, M. V.; Hieftje, G. M. *Anal. Chem.* **1988**, *60*, 1365–1369.
(2) Bornhop, D. J.; Murphy, B. J. *Anal. Chem.* **1989**, *61*, 797–800.
(3) Shaefer, K. H.; Griffiths, P. R. *Anal. Chem.* **1983**, *55*, 1939–1942.
(4) Olesik, S. V.; Pekay, L. A.; Paliwoda, E. A. *Anal. Chem.* **1989**, *61*, 58–65.
(5) Sugiyama, T.; Suzuki, Y.; Takeuchi, T. *J. Chromatogr.* **1973**, *80*, 61–67.
(6) Julin, B. G.; Vanderborn, H. W.; Kirkland, J. J. *J. Chromatogr.* **1975**, *112*, 443–453.
(7) Wright, B. W.; Peaden, P. A.; Lee, M. L.; Stark, T. J. *J. Chromatogr.* **1982**, *248*, 17–34.
(8) Junter, G. A. *Spectra 2000* **1985**, No. 100, Suppl. 21–30.
(9) Hieftje, G. M. *Anal. Chem.* **1972**, *448*, 81A–88A.
(10) Natusch, D. F. S.; Thorpe, T. M. *Anal. Chem.* **1973**, *45*, 1184A–1194A.
(11) Pescar, R. E.; Hartmann, C. H. *J. Chromatogr.* **1973**, *11*, 492–502.
(12) Fujiwara, K.; Ullman, A. H.; Bradshaw, J. D.; Pollard, B. D.; Winefordner, J. D. *Spectrochim. Acta* **1979**, *34B*, 137–150.
(13) Smit, H. C.; Walg, H. L. *Chromatographia* **1975**, *8*, 311–323.

(14) Olesik, S. V.; Pekay, L. A., submitted for publication in *Chromatographia*.
(15) Berezkin, V. G. *CRC Crit. Rev. Anal. Chem.* **1989**, *20*, 291–316.
(16) Richter, B. E.; Bornhop, D. J.; Swanson, J. T.; Wangsgaard, J. G.; Andersen, M. R. *J. Chromatogr. Sci.* **1989**, *27*, 303–308.
(17) Buffington, R.; Wilson, M. K. *Detectors for Gas Chromatography*; Hewlett-Packard: Avondale, PA, 1987.
(18) Schaefer, B. A. *J. Chromatogr. Sci.* **1978**, *16*, 211–217.
(19) Schaefer, B. A. *Combust. Flame* **1983**, *50*, 9–18.
(20) Johnson, R. N. In *Encyclopedia of Polymer Science Technology*; Bikales, N. M., Mark, H. F., Gaylord, N. G., Eds.; Wiley: New York, 1969; Vol. 11, pp 425–447.
(21) Bertozzi, E. R. *Rubber Chem. Technol.* **1968**, *41*, 115–157.
(22) Personal communication with Douglas Doster of Morton Thiokol, Morton Chemicals Division, Woodstock, IL.
(23) Tobolsky, A. V. *The Chemistry of Sulfides*; Interscience Publishers: New York, 1968.
(24) Shlyakhter, R. A.; Ehrenburg, E. G.; Nassonowa, T. P.; Piskarewa, E. P. *J. Appl. Polym. Sci.* **1967**, *11*, 567–574.
(25) Richter, B. E.; Knowles, D. E.; Andersen, M. R.; Porter, N. L.; Campbell, E. R.; Later, D. W. *HRC CC, J. High Resolut. Chromatogr. Chromatogr. Commun.* **1988**, *11*, 29–32.
(26) Richter, B. E. The Pittsburgh Conference and Exposition on Analytical Chemistry and Applied Spectroscopy, February 22–26, 1988, New Orleans, LA, paper 425.
(27) Michael, R.; Stulik, D. *Appl. Surf. Sci.* **1987**, *28*, 367–381.
(28) Marshall, A. G.; Shomo, R. E., II.; Verdun, F. R. *35th ASMS Conference Abstracts*; May 1987, Denver, CO, 938–939.
(29) Burnett, C. H.; Adams, D. F.; Farwell, A. *J. Chromatogr. Sci.* **1978**, *16*, 68–73.
(30) Sass, S.; Parker, G. A. *J. Chromatogr.* **1980**, *189*, 331–349.
(31) Oae, S. *Organic Chemistry of Sulfur*; Plenum Press: New York, 1977.
(32) Harper, H. A. *Review of Physiological Chemistry*, 14th ed.; Lange Medical Publications: California, 1973.
(33) Mockel, H. J. in *Advances in Chromatography*; Giddings, J. C., Grushka, E., Brown, P. R., Eds.; Marcel Dekker: New York, 1987; Vol. 26, pp 1–65.
(34) DeSimone, R. E.; Glick, M. D. *J. Am. Chem. Soc.* **1976**, *98*, 762–767.
(35) Saito, K.; Masuda, Y.; Sekido, E. *Anal. Chim. Acta* **1983**, *151*, 447–455.

RECEIVED for review July 3, 1989. Accepted September 6, 1989. Financial support of this project was provided by the Ohio Coal Development Office, Grant No. R-86-026-01-OH, and the Ohio Mineral and Mining Resource Research Institute, which granted a fellowship to L. Pekay.

Whole Column Detection: Application to High-Performance Liquid Chromatography

Kathy L. Rowlen, Kenneth A. Duell,[1] James P. Avery,[1] and John W. Birks*

Department of Chemistry and Biochemistry and Cooperative Institute for Research in Environmental Sciences (CIRES), University of Colorado, Boulder, Colorado 80309

Whole column detection (WCD) chromatography is implemented for the first time in high-performance liquid chromatography, and several advantages of the technique are demonstrated. The three-dimensional (peak height, position, and time) data set is found to contain significantly more information than conventional postcolumn detection. It is shown that this additional information makes possible (1) significant time savings as a result of peak quantitation at the earliest moment that adequate resolution occurs on column, (2) potential time savings resulting from the ability to predict whether adequate resolution will occur during an on-going chromatographic run, (3) more accurate and precise measurements of capacity factors, (4) a simple solution to the general elution problem, (5) a measure of the rate of equilibration between the mobile and stationary phases, (6) a direct measure of capacity factor versus percent organic modifier behavior during gradient elution, (7) experimental verification of the interconversion between capacity factors determined during a gradient and isocratically determined capacity factors, and (8) simplified method development for process control and other automated analyses.

The purpose of this paper is to explore the potential advantages of continuously monitoring the entire length of a high-performance liquid chromatography (HPLC) column. Several experimental cases in which whole column detection (WCD) offers a unique view of separation and can provide significant time savings are demonstrated. Although presented here as multiple-site UV absorbance detection along a normal-bore HPLC column, WCD could be accomplished with a variety of on-column methods such as photoacoustic (*1*), fluorescence (*2*), refractive index (*3*), and electrochemical (*4*) detection.

In this work we show that WCD produces a three-dimensional data set of peak height, position and time, which can provide significantly more information about the chromatographic process than conventional postcolumn detection. Specifically, we demonstrate that this multidimensional data set provides easy visual access to parameters such as (1) a complete trace of each peak's path through the column, including the location of highly or "permanently" retained peaks, (2) exact exit time from the column, (3) earliest time at which adequate resolution occurs, and (4) column quality. It is also shown that (1) quantitation can be carried out the moment adequate resolution occurs, resulting in relaxed requirements for solvent and time optimization, (2) linear velocities measured along the length of a column provide improved accuracy and precision in capacity factor data, (3) the rate of equilibration between mobile and stationary phases can be measured (in this case due to the limited number of detector sites, 14, an upper limit for the rate is established), (4) capacity factor versus percent organic modifier behavior during gradient elution can be followed directly, and (5) the interconversion between capacity factors determined during a gradient and isocratically determined capacity factors can be experimentally verified. The application of WCD to method development for process control analyses is presented as an example of the versatility and time optimization power of WCD. It is shown that the peak tracing capability of WCD provides unique insight and allows the operator to utilize peak "crossover" information to advantage without the use of mathematical estimation methods (*5*).

In 1968, Brumbaugh and Ackers (*6*) developed a method they titled "scanning gel chromatography" (SGC). Using SGC

---

[1] Department of Electrical and Computer Engineering and CIRES, University of Colorado, Boulder, CO 80309.

© 1989 American Chemical Society

they were able to monitor the absorbance profile of molecular sieve separations throughout the length of a gel column by driving the column past a fixed configuration of light source and detector. In their introductory paper (*6*), the authors stated that "... only a small fraction of the quantitative information obtainable from a given experiment is utilized by conventional procedures of solute zone analysis. This limitation is imposed by the experimental necessity of measuring solute zone configurations at only a single point of the distance coordinate, namely, the point corresponding to the bottom end of the chromatographic column." By scanning the column during soluble zone movement, the authors were able to measure partition coefficients several times during each run, thereby greatly improving the speed and accuracy with which such parameters could be measured. It was observed that analytes within the gel adhered to Beer's law, even under conditions in which the gel was saturated with analyte solution. This linearity in absorbance behavior in the presence of a scattering medium was attributed to "ideal" scattering by the gel, i.e. forward scattering, and column dimensions (*7*). Davis et al. (*7*) reported that a single computer-controlled SGC analysis often required several hours to complete. They noted that such long analysis times were due to the slow rate of migration in gel chromatography and the necessity of scanning slowly in order to obtain reproducible measurements. The limit of detection using ultraviolet light on gels was determined to be in the range of μg/mL or $\cong 10^{-2}$ au (*8*). The usefulness of SGC has been demonstrated in several areas such as the study of zone spreading (*9*) and macromolecule binding studies (*6*).

In an earlier theoretical paper (*10*), we explored the potential advantages of continuously monitoring the entire length of a chromatographic column by using a computer model and advanced the concept that WCD could be used to quantitate any pair of peaks at the earliest moment on the column at which they became sufficiently resolved. Computer simulations also suggested that solvent pulses could be used to selectively separate peaks before they exited the column, thus relaxing the constraint of composing a single optimized mobile phase in order to resolve every peak at one point—the exit of the column. Since a complete map of each peak's progress through the column would be produced by monitoring the separation process, selective separation could be carried out for overlapped peaks without regard to the possible degradation in resolution for previously quantitated peaks. Following our initiative, Gluckman and co-workers (*11*) employed solvent pulses for selective separation of organic dyes. They utilized a transparent column to view the separation of highly colored compounds and suggested that WCD would indeed provide substantially more useful information.

Optimization continues to be of major concern to chromatographers. One may find a large variety of strategies for optimization in the literature (*12–19*). There are graphical approaches, such as the window-diagram method (*13*) and overlapping resolution mapping (*18*), as well as mathematical approaches (*15*). Many of the existing optimization strategies require a large capacity factor data base (developed from several chromatographic runs) and are thus very time-consuming (*16*). For isocratic elution, Quarry and co-workers (*19*) recently presented a method that has attracted much attention. The method involves the use of two or more gradient runs to predict the optimal isocratic mobile phase; however, as the authors pointed out there are a number of potential errors that can limit the accuracy of such a prediction. Sources of error include (*1*) system dwell time, (2) "demixing" of the solvent, (3) nonlinearity in ln k' vs percent organic modifier plots, and (4) interconversion of gradient derived capacity factors and isocratic capacity factors. Despite the numerous strategies available for optimization procedures, in many practical situations experience-based trial-and-error approaches are still employed.

Although the term "optimization" is used quite frequently in the chromatographic literature, there is no single definition of the term which seems appropriate for the wide range of its use (*12*). In this paper, when referring to optimization, we will use two distinct terms, solvent optimization and time optimization, which describe the two steps required for complete optimization of a method. The term solvent optimization will be used to indicate a procedure whose goal is the best possible separation (i.e. base-line resolution, $R = 1.5$) with analysis time only a secondary consideration. The term time optimization will be used to indicate a procedure whose goal is adequate separation (e.g. $R \geq 1.3$) in minimum analysis time.

EXPERIMENTAL SECTION

Instrument. The chromatographic system is composed of a Kratos Spectroflow 400 HPLC pump, a Rheodyne injector with a 1-μL injection loop, a 15-cm glass cartridge column (Alltech Associates, 3-mm i.d.) packed with 5-μm ODS, a Kratos Spectroflow 773 multiple-wavelength absorbance detector, and a Shimadzu CR3A integrating recorder. All of the solvents are Burdick and Jackson HPLC grade and the chemicals Aldrich Reagent grade. The cartridge system is instrumented with 14 UV-sensitive photodiodes (Hamamatsu, 51226-18BQ) mounted within holes at 1-cm intervals along the stainless-steel cartridge holder. The source light entrance holes (1-mm diameter) are located at points directly opposite (180°) of each photodiode along the holder. An 8-W, 25-cm black lamp (Sylvania F8T5, 366 nm) is used as the light source. As an analyte passes through a zone that is illuminated, the amount of light reaching the corresponding photodiode is attenuated. The circuitry that controls diode sampling is similar to that used for diode arrays. All of the diodes are sequentially sampled within $\cong$4 ms resulting in a "snapshot" of peak distribution along the length of the column. Diode integration time is variable between 50 and 1000 ms. To adequately sample a Gaussian peak (base line width $\cong 8\sigma$), a minimum of eight points must be acquired. For an unretained peak (the worst case, peak width $\cong$ 20 s) an integration time of $\leq$400 ms must be used. For most of the studies presented in this work, a 650-ms integration time is employed due to the low light levels reaching the diodes. Since the worst case is rare, typically all of the peaks examined during a run are sufficiently sampled in the time domain.

Calibration. In order to compare peak parameters measured at each point on the column, the signal from every diode must be linear and identical. This is achieved with software through a series of calibration steps. The equation that describes the raw, uncalibrated voltage measured at each diode is given by

$$V_i(k) = C\int_{(k-1)t_0}^{(k)t_0} I_i(t)\,\mathrm{d}t + V_{i,\mathrm{offset}} + V_{0\mathrm{MN}} \tag{1}$$

where $V_i(k)$ is the voltage at diode i as a function of a discrete point in time (k), C is a constant that accounts for capacitor characteristics and diode sensitivity, t_0 is the integration time, $I_i(t)$ is the intensity at diode i as a function of continuous time (t), $V_{i,\mathrm{offset}}$ is the electronic offset of diode i, and $V_{0\mathrm{MN}}$ is the zero mean (or random) noise component of the measurement (e.g., lamp flicker). Ultimately, the goal of calibration is to obtain the pure signal I_i and have each diode respond identically.

The first step in calibrating the system is to remove $V_{i,\mathrm{offset}}$. Since $V_i(k)$ is linearly related to diode integration time, a series of samples are taken ($V_i(k)$ as a function of t_0) prior to a separation run. The resulting line is then extrapolated to zero integration time. At $t_0 = 0$ the integral in eq 1 is equal to zero and $V_i(k) = V_{i,\mathrm{offset}} + V_{0\mathrm{MN}}$. A large number of data points are averaged at each integration time so that $V_{0\mathrm{MN}} \cong 0$ and $V_i(k) \cong V_{i,\mathrm{offset}}$. Thus, $V_{i,\mathrm{offset}}$ may be subtracted directly from the signal. Further noise reduction is then achieved via a digital low pass filter. The next calibration step involves countering peak distortion caused by diode integration time. In practice, peak distortion due to integration time is examined in the frequency domain and removed in the time domain via a digital filter. At this point the blank

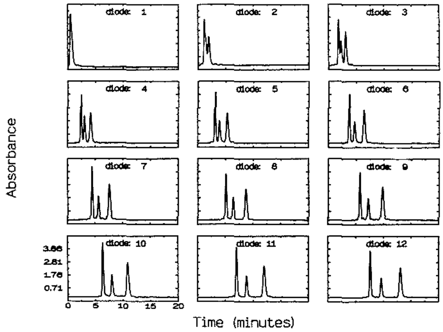

Figure 1. WCD separation of the three isomers of nitroaniline; ≅1.8, 2.6, and 0.75 mg/mL injected concentrations for *o*-, *m*-, and *p*-nitroaniline, respectively: solvent composition of 80/20 water/acetonitrile, 0.4 mL/min flow rate, and 650 ms diode integration time.

intensity (I_0) is ratioed to I (the C term cancels) and the logarithm taken.

As one might expect for light traveling through densely packed particles, the absorbance-vs-concentration response is inherently nonlinear. To determine the degree of nonlinearity an absorbance-vs-concentration plot is obtained and fit with a polynomial function for each diode. The inverse polynomial is then used to reevaluate the data, which in effect linearizes the absorbance-vs-concentration relationship. The slope is multiplied by a constant such that the sensitivity is normalized to that observed at the postcolumn detector.

The last calibration step involves normalizing each detection cell. Since the total mass of an analyte does not change as it progresses along the column, the total peak area at each position must be the same. Areas measured at each position are scaled to the area measured at an arbitrarily chosen reference position (in this case, the last diode) by multiplying each by the correct normalization constant. Peak parameters, such as peak area, width, and height, are measured using a nonlinear least-squares fit to a gamma density function (*20*). The limit of detection, signal to noise (peak-to-peak) ratio of 3, is $\cong 10^{-3}$ absorbance unit. A more detailed description of the WCD absorbance instrument and the calibration procedure will be given in a subsequent paper.

RESULTS AND DISCUSSION

Time Optimization. As mentioned earlier, WCD inherently generates a three-dimensional data set of peak height versus position and time on the column. While 3-D plots of the data are interesting to look at, they are difficult to use for visual information. Figure 1 shows a two-dimensional plot of the separation of the three isomers of nitroaniline. The diode number corresponds to distance along the column; e.g., at diode 1 (Figure 1.1) the mixture has moved 1 cm along the column. Although 14 diodes were employed in this instrument, for clarity only 12 are displayed in Figure 1. At first glance it may be difficult to understand this type of chromatographic display since it is a function of both time and position on the column. It is easiest to think in terms of each diode display being a time-based chromatogram of the separation at that particular position. Thus, looking left to right for each diode one views the fastest peaks first (less retained) and then the slowest (more retained) peaks, just as in conventional chromatograms.

Note that by diode 3 all of the nitroaniline isomers are identifiable and that they are nearly base-line resolved by diode 5. As shown at diode 12, more than adequate resolution is obtained near the exit of the column. In this case, knowing the polarity of the analytes to be separated, the operator chose this particular mobile phase as a starting point for a trial-and-error solvent optimization. It is clear that this separation is not time optimized for exit detection, since time is wasted in "over separating" the analytes. For exit detection then, complete optimization of the method would involve further adjustment of the mobile phase such that adequate resolution occurs at the exit of the column in the shortest possible time. With WCD, time optimization is inherent in the detection process, since any analyte may be quantitated at the earliest position where resolution is deemed sufficient. For the separation shown in Figure 1, each isomer may be quantitated at diode 5, and perhaps at diode 4 if less stringent resolution is acceptable. Thus, complete separation and quantitation are accomplished within 5 min. After this length of time (and possibly earlier), a new sample could be injected, or a pulse of strongly eluting solvent could be introduced to "wash off" the sample, followed by the solvent of choice for the next analysis. Indeed, one can imagine approaching the separation of an unknown mixture by starting off with a high water content isocratic mobile phase (for reversed phase chromatography) in order to assure "over separation" of many if not all components. The problems normally associated with this type of approach, often described as the "general elution problem", simply do not apply to WCD, as will be discussed later in the text. Thus, time savings result from both simplified optimization and reduced analysis time. It is important to note that quantitation early on in the separation process assumes, of course, that the operator has a prior knowledge of how many components there are in the mixture. The same assumption must also be made in postcolumn analysis; i.e., the operator must decide whether or not complete separation has been achieved.

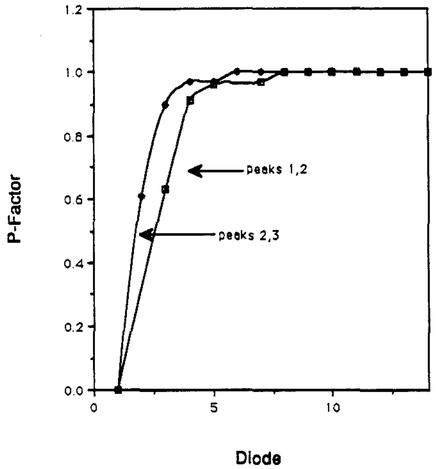

Figure 2. Rate of resolution for separation shown in Figure 1. The rate is defined here as the change in P factor as a function of position on the column. See text for details.

Rate of Resolution. Another time-saving feature of WCD is the ability to predict early in the separation process (assuming real-time display) whether or not adequate resolution will be achieved at a particular position on the column or at the exit of the column. For example, Figure 2 is a plot of the rate at which the analytes in Figure 1 separate. The rate is determined by the change in P factor (*16*). The P factor is a ratio of the height of the valley between two peaks (as determined from the top of the valley to the midpoint of a line drawn between each peak's maximum) and the height of the midpoint (as determined from the midpoint of a line drawn between each peak's maximum to the base line). As shown by the steepness of the slopes for the two sets of peaks, the rate of separation is fast and base-line resolution ($P = 1.0$)

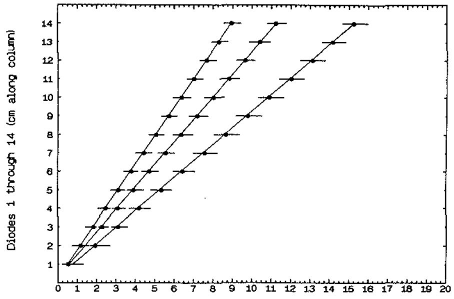

Figure 3. Peak position versus time display for the separation shown in Figure 1. Peak width in the time domain ($\cong 4\sigma$) is represented by horizontal lines drawn through each point.

is achieved by diode 5. This unique information about the rate of separation would allow an operator to make a decision about the suitability of the mobile phase for achieving the desired separation during the initial stages of the analysis. On the basis of the information displayed in Figure 2, one could predict as early as 2–3 min into the separation that adequate resolution will occur on-column. For peaks that do not resolve on-column, a negative prediction could be made early on in the run, the actual time determined by the time required for the partially overlapped peaks to travel past at least two diodes.

Peak Trace. Figure 3 is another type of two-dimensional plot of the separation shown in Figure 1. The absorbance maximum of each observed peak is plotted as a function of time and position on the column. The horizontal lines drawn through each point correspond to the base-line width of the peak ($\cong 4\sigma$ for resolved peaks) in the time domain at a particular diode. One can see from this plot that base-line resolution occurs at diode 5, since there is no overlap between the width lines for adjacent peaks. If one were interested in quantitation at a lesser degree of resolution, the peak width plotted could be redefined accordingly (e.g., 3.5σ).

These plots allow rapid access to capacity factor (k') information. The slope of peak position versus time is the linear velocity of the peak. The capacity factor is related to the velocity (v) by

$$k' = (v_0/v_r) - 1 \qquad (2)$$

where v_0 denotes the linear velocity of an unretained compound and v_r is the linear velocity of the analyte of interest. The determination of capacity factors by WCD measurement of linear velocity is more precise, and potentially more accurate, than the conventional method of retention time measurements

$$k' = (t_r - t_0)/\, t_0 \qquad (3)$$

Since linear velocity is measured as $\Delta d/\Delta t$ between each pair of adjacent diodes, it is not subject to errors resulting from a delay between injection of the sample and recorder start time. The precision of the k' measurement is improved by the use of multiple detection cells along the column, in this case 14. In order to achieve the same precision using conventional methods, several chromatographic runs would be required.

Some of the problems associated with peak crossovers during optimization can be more easily handled with WCD. For example, in optimizing a gradient elution program, the time (gradient time) spent in completing the program is varied. This variation in gradient time often results in unpredictable peak crossovers, such that comparison of postcolumn chromatograms of a mixture obtained by using different gradient times can be difficult. For example, Dolan et al. (*16*) recently reported a case in which extending the gradient time from 5 to 100 min resulted in four peak crossovers. The complete map of retention behavior obtained in WCD chromatography greatly simplifies the assignment of peaks eluted by using different solvent programs.

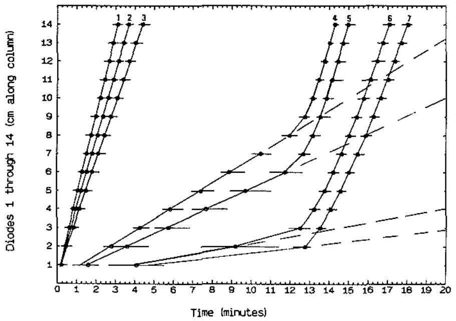

Figure 4. Peak position versus time plot for the separation of nitroaniline isomers (peaks 1–3), dimethylanthraquinone (peak 5), and *tert*-butylanthraquinone (peak 6). Peaks 4 and 7 are impurities from the anthraquinones. Injected concentrations for each analyte are $\cong$0.9, 0.7, 0.3, 0.6, and 2.0 mg/mL for *o*-, *m*-, *p*-nitroaniline, 1,4-dimethylanthraquinone, and 2-*tert*-butylanthraquinone, respectively. The initial solvent (isocratic) was 60/40 water/acetonitrile. Four minutes into the separation the solvent was switched to 100% acetonitrile. Other conditions include 0.4 mL/min flow rate and 650 ms integration time.

The linearity of peak position vs time plots, under isocratic conditions, allows the operator to monitor the quality of the column over long periods of time. For instance, contamination at the head of the column might result in erratic velocities in that region due to poor solute capacity. In addition, contamination would likely result in reduced source intensity reaching the detector.

Isocratic Simplicity. The "general elution problem" is a term generally used to describe the ineffectiveness of isocratic elution for the separation of a mixture composed of compounds with a wide range of retention factors. By use of a constant solvent mixture, early eluting peaks are often poorly resolved while highly retained peaks are broad and greatly extend analysis time. Gradient elution is often chosen as a solution due to its ability to achieve adequate resolution of early eluting peaks while sharpening late eluting peaks and reducing analysis time. However, the problems associated with gradient elution, i.e., (1) the time required to optimize the gradient program, (2) reduced precision of retention time measurements, and (3) detector base-line drift caused by the gradient, make the simplicity and reproducibility of isocratic elution very attractive. Thus, isocratic elution remains the method of choice for many applications (*12*).

WCD offers a simple solution to the general elution problem, in that a complete "movie" of the separation process allows the operator to take advantage of gradient elution benefits under isocratic elution conditions. Figure 4 is an example of a separation of a mixture containing compounds with a wide range in polarity. The initial isocratic mobile phase was selected to ensure that the polar compounds (peaks 1–3) would be separated at some point on the column. As a result, the nonpolar molecules are highly retained (peaks 4–7; dashed lines represent linear velocity if isocratic conditions were maintained throughout the run). The increased analysis time normally associated with highly retained compounds is due to the fact that in conventional detection methods quantitation cannot take place until the peaks exit the column.

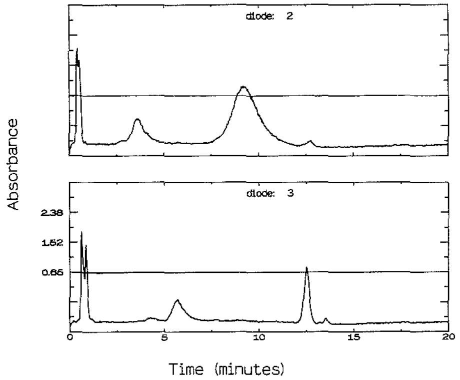

Figure 5. Absorbance vs time plots at diodes 2 and 3 for the separation shown in Figure 4.

As pointed out earlier, with WCD the peaks may be quantitated the moment they become resolved. For the separation shown in Figure 4 the peaks 1–3 are base-line resolved at diode 12 and peaks 4–7 are base-line resolved by diode 3. With confidence that there are only seven components of interest in the mixture, complete quantitation of all components may be completed within 13 min. In the absence of any solvent changes, quantitation of all components at the exit of the column requires ≅66 min. In addition, all of the late eluting peaks are poorly detected postcolumn due to severe band broadening.

Since, in the most simple WCD instrument design, only a single wavelength is used for quantitation, one might wish to utilize postcolumn detection to obtain additional information by using other detectors such as a mass spectrometer or diode array. WCD information can be used to facilitate postcolumn detection (or to simply reduce the time required for the column to clear after analysis is complete). For example, once the desired separation has been achieved on-column, a pulse of strong solvent (organic modifier in this case) may be used to speed up progress toward the exit. For the case demonstrated in Figures 4 and 5 the initial mobile phase is 60/40 H_2O/acetonitrile (ACN). As the separation nears completion, a pulse of 100% ACN is introduced. This pulse serves both to clear the column rapidly, as is shown by the steepness and the curvature of the linear velocity for the nonpolar compounds, and to maintain the degree of separation achieved at the time the new solvent front catches up with each component. The degree of separation is preserved because all of the components are essentially unretained in 100% ACN. Figure 5 shows the chromatogram at diode 2 prior to the new solvent front and at diode 3 after the new solvent has passed over peaks 6 and 7. The peak profile is sharpened considerably by the focusing effect of higher organic modifier content in the mobile phase.

Although not discussed in detail nor quantitated here, it is interesting to note that peak width variation as a function of time spent in a "new" solvent (e.g., isocratic step or gradient) will likely yield important information about both solvent and solute interactions with the stationary phase. As shown in Figure 5, a step to higher percent organic modifier sharpens the peak width in the time domain. A step to lower percent organic modifier (higher percent water) severely broadens the peak width in the time domain.

Rate of Solvent Equilibration. After the solvent composition for isocratic elution has been changed, it is common practice to allow several column volumes to pass through the column in order to achieve complete equilibration between the mobile and stationary phases. When a pump designed only for isocratic elution is used, a change in solvent composition is typically achieved by physically switching the solvent reservoir. For ACN/water mixtures applied in this manner, we note that the number of column volumes required to achieve a stable retention time at the exit of the column is due primarily to the mixing profile of the pump (i.e. how long it takes the pump to deliver "pure" new solvent) and is not due to slow equilibration between the mobile and stationary phases. For example, the linear velocity of 4-nitroaniline in 20/80 ACN/H_2O, is 1.18 cm/min. When an injection of 4-nitroaniline is followed immediately by a true solvent "step" (such a step can be accomplished by pumping several milliliters of the new solvent through the pump prior to connection to the column) to 30/70 ACN/H_2O, the linear velocity, as observed over all of the diodes, is found to correspond to the linear velocity in 30/70 ACN/H_2O under equilibrated conditions (2.17 cm/min). From this and other isocratic step experiments, we estimate the time constant of solvent equilibration, for a step to higher ACN in H_2O, to be ≤10 s. The time constant for a step to higher water (ACN/water) is ≤30 s. These time constants imply that, under the conditions of the system (ACN/water on ODS), the column is equilibrated within a single column volume. For comparison, the time constant for *analyte*/stationary phase equilibrium has been reported by Marshall et al. (*21*) to be ≅10^{-3} s.

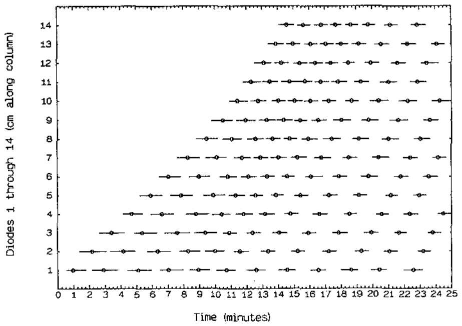

Figure 6. Peak position versus time plot for 2-min-interval injections of 2-nitroaniline (0.9 mg/mL) as mobile phase is changed from 20/80 ACN/H_2O to 30/70 ACN/H_2O.

Capacity Factor Behavior during a Gradient. In order to effectively utilize the sophisticated optimization strategies mentioned in the introduction, such as that developed by Quarry et al. (*19*), it is important to know a priori how the peak capacity factors change as a function of solvent composition. It is also important to verify that capacity factors determined from gradient elution (or during a gradient, as will be shown for WCD) can be accurately related to isocratic capacity factors. With WCD, "instantaneous" capacity factors can be measured at all points during a gradient. Several injections of 2-nitroaniline made at 2-min intervals during a gradient are shown in Figure 6. The gradient used in this case is a result of the mixing profile of our isocratic pump. The profile of solvent delivery (solvent composition vs time) was measured by using the technique described in ref 13 (p 367) with 10^{-5} M anthracene dissolved in the new solvent. The profile is sigmoidal in shape and has a time constant of ≅3.4 min. The solvent change in Figure 6 is from 20/80 ACN/H_2O to 30/70 ACN/H_2O. Each peak trace shown in the figure is fit with a cubic spline function and the derivative taken at each position to produce a plot of velocity as a function of time during the gradient, right vertical axis of Figure 7. By use of the relationship given in eq 2, velocity as a function of time can be converted to instantaneous capacity factor as a function of time, left vertical axis of Figure 7. Since the solvent com-

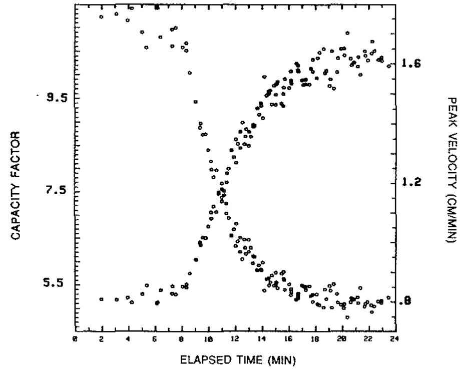

Figure 7. Peak velocity and capacity factor values as a function of elapsed time following a solvent switch. Peak velocity increases from ≅0.8 to 1.6 cm/min, while the capacity factor decreases from ≅11 to 5.2.

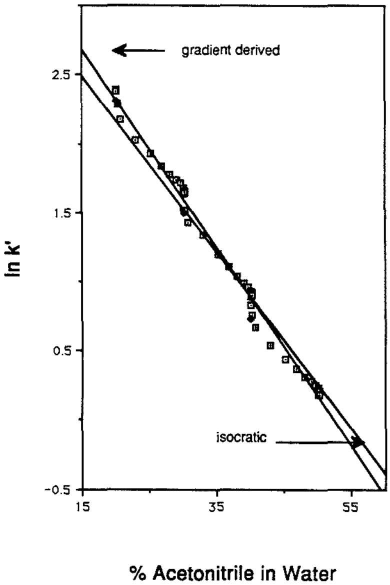

Figure 8. Plot of ln k' vs percent ACN derived from gradient (data points and least-squares line) and isocratic (least-squares line indicated) elution of 2-nitroaniline. Gradient data were obtained for solvent steps of 20–30%, 30–40%, and 40–50% ACN.

position as a function of time and column position is known, a plot of ln k' vs percent organic modifier can be constructed. The linear equation that describes the relationship between ln k' and percent organic modifier is

$$\ln k' = \ln k'_{H_2O} + mx \qquad (4)$$

where the subscript H_2O indicates the capacity factor in water, m is capacity factor sensitivity to changes in the mobile phase, and x is percent organic modifier in water. The equation for 2-nitroaniline, as measured under completely equilibrated isocratic conditions, over the range of 20% ACN to 100% ACN, is ln $k' = 3.44 - 0.0639x$. Figure 8 is a plot of ln k' vs percent ACN for three 10% step gradients. The fit to the above equation for the gradient data is ln $k' = 3.75 - 0.0718x$. The maximum error between the two lines, over the range measured, is ≤12%. The major source of error is believed to be due to inaccuracy in the measurement of the mixing profile of the pump. This systematic error accounts for the curvature in the data at the extreme ends of the three gradient steps. Even so, the relatively good agreement between the two methods of measuring k' as a function of mobile phase composition demonstrates the validity of interconversion of k' data and the usefulness of being able to follow the change in retention behavior as a function of position and time during a solvent gradient. In addition, with WCD the problem of preelution (i.e., solute elutes prior to the arrival of the gradient front, see ref 19) diminishes in importance due to the capability of correlating each peak's trace with time into the gradient.

Effects of Solvent Changes on Quantitation. For the instrument employed in these studies, the blank intensity (I_0) used to calculate absorbance is determined with only solvent on the column prior to the separation run. As long as the solvent composition remains constant, the error associated with this "static" I_0 determination arises principally from the drift and flicker noise of the lamp. However, if the solvent composition is altered during separation, as discussed in the previous section, two additional factors contribute to potential error in quantitation. The extinction coefficient of most analytes has a slight dependence on solvent polarity. For example, the extinction coefficient of 2-nitroaniline, one of the analytes used in characterization of the WCD system, exhibits a ≅3% difference between methanol, acetonitrile, and ethyl acetate (note, however, that the change in peak height shown for peak 6 in Figure 5 is primarily due to a change in refractive index). Extinction-coefficient dependence on microenvironmental polarity raises the question of how the absorption spectrum is affected by a certain fraction of the molecules being partitioned into the stationary phase. [On the other hand, differences in extinction coefficients or fluorescent quantum yields due to dynamic microenvironmental changes may prove to be extremely useful in gaining additional information about retention mechanisms (*22*)]. In addition, the amount of light that reaches each photodiode (with only solvent flowing through the column) depends on the refractive index of the solvent. There is a 12% change measured in I_0 as the solvent is varied from methanol to water and a 11% change between 20% and 60% ACN in water. The maximum value of I_0 is observed to occur at approximately 50/50 organic modifier/water in both cases. These two sources of error could limit the amount of quantitative information obtainable during method development; i.e., when an operator chooses to vary the mobile phase while a separation is in progress. As mentioned previously, both of these sources of error (change in analyte extinction coefficient, change in base line due to variable solvent composition) are also found in gradient elution and contribute to the irreproducibility of quantitative information but are not prohibitive to the use of gradient elution. Since WCD offers many time-saving advantages when operated under fully equilibrated conditions and unique qualitative information under gradient conditions, we do not regard these sources of error to be a major constraint in the application of WCD as implemented here.

Method Development for Process Control. There are many applications in which a mixture is to be sampled at regular intervals in order to follow the progress of a reaction. For example, it has been stated (*23*) that fast HPLC techniques will find wide application in the pharmaceutical industry for "... stability tests, dissolution rates, content uniformity, method development, kinetics, and process control." In many such cases short, "fast" chromatographic columns will serve. The major advantages of these short columns is the speed with which analyses may be carried out. The major

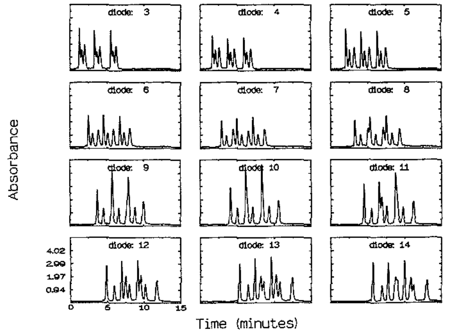

Figure 9. Three injections of nitroaniline isomer mixture (see Figure 1 for concentrations). The time between each injection is 2 min. Other conditions include solvent composition of 70/30 water/acetonitrile, 0.4 mL/min flow rate, and 650 ms integration time.

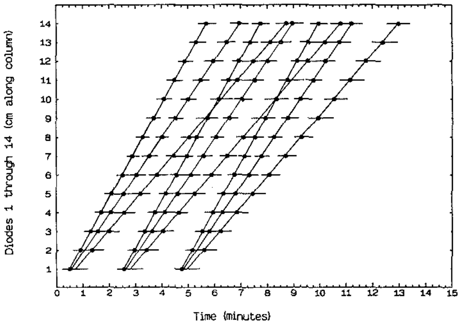

Figure 10. Peak position versus time plot of separation shown in Figure 9.

limitation of such columns is the reduced separation capacity; for complex mixtures it is often necessary to use longer columns in order to achieve the desired separation. WCD offers the advantages of both column types—on a single instrumented column. Figure 9 shows three injections of a mixture made at 2-min intervals. For the solvent mixture used, every peak is adequately resolved at diode 5; thus, a 5-cm column could be used to separate this mixture routinely. However, using WCD an operator can optimize the time interval between injections and the mobile phase composition to suit the length of a fast column while retaining the ability to develop methods for more difficult separations which require longer columns. For example, Figure 10 is a position vs time plot of the separation shown in Figure 9. Note (in both figures) that after complete resolution at diode 5 the peaks begin to merge and then cross one another. In the postcolumn chromatogram several of the peaks are overlapped and it is difficult to identify which peaks are from each injection. If one were to carry out this separation on the same column without WCD, and therefore without the knowledge that each peak is resolved at 5 cm on the column, one might be tempted to simply lengthen the injection interval time until none of the peaks were overlapped at the exit of the column. Such an adjustment would add approximately 2 min to the interval time and extend the total analysis time by $2n$, where n is the number of intervals required to monitor the entire reaction.

Another way in which WCD might be useful in bioanalytical separations is through application to compound stability tests. Very often a newly synthesized compound must be separated from reaction components with little initial information concerning compound stability under chromatographic conditions. As a result, during the first attempt at separation, the compound may be lost, perhaps due to decomposition or permanent retention on the column. The peak tracing capabilities of WCD can provide information about the compound's fate. Indeed, if the analyte is suspected of being unstable, the peak may be stopped (by shutting off the pumps) within a detection cell on-column and the kinetics of decomposition characterized by measuring absorbance decay (assuming absorbance is the detection scheme used) as a function of time. If multiple wavelengths are used, the decay products could be tracked and studied from the point of origin once flow is reinitiated.

Future Trends. In a forthcoming paper we will evaluate the use of WCD chromatography for a true measure of column efficiency without interference from extracolumn contributions to peak width. The width in the time domain can be converted to width in the length domain using the measured linear velocity of the peak. Thus, in WCD, measurements of σ_x^2 can be made at each detection cell on the column and plots of total variance vs position constructed. The result of such a plot is a straight line described by

$$\sigma^2_{\text{total}} = xH + \sigma^2_{\text{extracol}} \qquad (5)$$

where x is position on the column and H is the height equivalent to a theoretical plate. The slope of the plot is equal to H, and the y intercept is the sum of all extracolumn contributions to variance. Thus, WCD can provide a measurement of column efficiency, H, independent of extracolumn variance.

ACKNOWLEDGMENT

We thank Chris Enke for his early contributions to the ideas behind this work. We also thank Dick Henry of Keystone Scientific and Kim Boyce of Alltech Associates for extra effort on our behalf. K.L.R. thanks Procter and Gamble and the American Chemical Society for a Graduate Fellowship.

LITERATURE CITED

(1) Rowlen, K. L.; Birks, J. W.; Duell, K. A.; Avery, J. P. *Anal. Chem.* **1988**, *60*, 311.
(2) Guthrie, E. J.; Jorgenson, J. W. *Anal. Chem.* **1984**, *56*, 483.
(3) Fujimoto, C.; Morita, T.; Jinno, K. *HRC CC, J. High Resolut. Chromatogr. Chromatogr. Commun.* **1986**, *9*, 623.
(4) White, J. G.; St. Claire, R. L.; Jorgenson, J. W. *Anal. Chem.* **1986**, *58*, 293.
(5) Otto, M.; Wegscheider, W.; Lankmayr, E. P. *Anal. Chem.* **1988**, *60*, 517.
(6) Brumbaugh, E. E.; Ackers, G. K. *J. Biol. Chem.* **1968**, *243*, 6315.
(7) Davis, L. C.; Socolofsky, T. J.; Radke, G. A. *Methods Enzymol.* **1985**, *117*, 116.
(8) Jones, M. M.; Harvey, G. A.; Ackers, G. K. *Biophys. Chem.* **1976**, *5*, 327.
(9) Grothusen, J. R.; Zimmerman, J. K. *Biophys. Chem.* **1984**, *20*, 299.
(10) Gelderloos, D. G.; Rowlen, K. L.; Birks, J. W.; Avery, J. P.; Enke, C. G. *Anal. Chem.* **1986**, *54*, 900.
(11) Gluckman, J. C.; Slais, K.; Brinkman, U. A.; Frei, R. W. *Anal. Chem.* **1987**, *59*, 79.
(12) Barth, H. G.; Barber, W. E.; Lochmüller, C. H.; Majors, R. E.; Regnier, F. E. *Anal. Chem.* **1988**, *60*, 387R.
(13) Poole, C. F.; Schutte, S. A. *Contemporary Practive of Chromatography*; Elsevier: Amsterdam, 1984; pp 51, 264.
(14) Dezaro, D. A.; Dvorn, D.; Horn, C.; Hartwick, R. A. *Chromatographia* **1985**, *20*, 87.
(15) Goewie, C. E. *J. Liq. Chromatogr.* **1986**, *9*, 1431.
(16) Quarry, M. A.; Grob, R. L.; Snyder, L. R.; Dolan, J. W.; Rigney, M. P. *J. Chromatogr.* **1987**, *384*, 163.
(17) Dolan, J. W.; Snyder, L. R.; Quarry, M. A. *Chromatographia* **1987**, *24*, 261.
(18) Glajch, J. L.; Kirkland, J. J. *Anal. Chem.* **1983**, *55*, 319A.
(19) Quarry, M. A.; Grob, R. L.; Snyder, L. R. *Anal. Chem.* **1986**, *58*, 907.
(20) Smit, H. C.; Smit, J. C.; Jager, E. M. *Chromatographia* **1986**, *22*, 123.
(21) Marshall, D. B.; Burns, J. W.; Connolly, D. E. *J. Chromatogr.* **1986**, *360*, 13.
(22) Carr, J. W.; Harris, J. M. *Anal. Chem.* **1986**, *58*, 626.
(23) Erni, F. *J. Chromatogr.* **1983**, *282*, 371.

RECEIVED for review June 14, 1989. Accepted September 7, 1989. This work was funded by a grant from the Environmental Protection Agency (Grant No. R-813912-01-1).

Anal. Chem. **1989**, *61*, 2631–2637

Rota-Microspeciation of Aspartic Acid and Asparagine

Béla Noszál*

Department of Inorganic and Analytical Chemistry, L. Eötvös University, Muzeum krt. 4/B, Budapest H-1088, Hungary

Péter Sándor

Central Research Institute of Chemistry, Pf. 17, Budapest H-1575, Hungary

Rotamer analysis and methods for the determination of microspecies concentration were combined. Relationships between the protonation constants of rotational isomers and bulk (macro- and micro-) constants were deduced. Populations for 9 rotamers of asparagine and 15 rotamers of aspartic acid were estimated by using pH dependence of ^1H and ^{13}C NMR coupling constants. The $-COOH$ and $-CONH_2$ groups proved to be practically equivalent in the formation of rotamer populations. A close correlation was found between rotamer population data and other NMR parameters. Protonation constants for each rotational isomer were calculated, including rota-microconstants for the acidic region of aspartic acid, where 12 microforms coexist, six of which are isomers both from protonation and rotational point of view. Such rota-microconstants could not be determined previously, due to their overlapping equilibria.

INTRODUCTION

Aspartic acid and asparagine exist in solution in several forms of protonation and intramolecular rotation. The isomeric products of protonation and rotation always occur in the presence of each other, due to their fast, continuous interconversion. These coexisting species produce composite analytical signals; however they act individually in specific biochemical processes. This is why the determination of their concentration, e.g. an appropriate type of speciation is important, but it needs indirect methods.

Speciation aims at determining not only the total concentration of a given component in the sample but also its distribution among different species. Microspeciation distinguishes between the different isomeric products of protonation (*1*), whereas rota-microspeciation, in addition, must specify the position of the flexible moieties of the molecule.

A sine qua non of the above types of speciation is information on the equilibrium constants. Simple speciation uses thermodynamic macroconstants. Microspeciation is based upon microconstants (microscopic protonation or dissociation constants) or group constants (*1, 2*), whereas rota-microspeciation requires rota-microconstants.

This paper presents the determination of the rotameric and microscopic forms and the relevant equilibrium constants of the title compounds. These closely related amino acids are equally important in biochemical interactions and metal complexation processes (*3*).

Asparagine is one of the best possible examples to study protonation processes of different rotamers. It takes up protons in well-separated steps, but its rotamer populations have not yet been fully elucidated (*4*). The bulky, polar $-CONH_2$ side-chain does not associate with protons but can influence either the proton-binding ability of other groups or the population of the rotamers.

The proton-binding equilibria of aspartic acid are more composite processes. Solutions of aspartic acid contain five protonation microspecies and, thus, 15 rota-microspecies. For the two carboxylates of aspartic acid, which are of similar basicity, protonation constants have been published (*5*) but were derived only from empirical relationships. We therefore performed experiments to evaluate more reliable microconstants. Several valuable contributions have been made toward the characterization of aspartic acid rotamer populations in the basic and neutral pH region (*6–10*). However, no attempt has been made for the rotamer analysis in the most complicated acidic region, where 12 rota-microspecies coexist. We have also estimated the concentration of all these rota-microforms, including the six doubly isomeric (protonation and rotation) species.

EXPERIMENTAL SECTION

Amino acids were of analytical reagent grade (Reanal, Hungary) and used without further purification. All the potentiometric titrations were done with a Radiometer pHM 64 digital research pH meter and ABU 12 automatic buret, attached to an Ingold 1040523059 combined electrode. In all solutions, ionic strength was kept constant at 2.0 mol dm^{-3} by NaCl. This was also the internal filling of the combined electrode. The titrant used was carbonate-free NaOH in 0.1–2.0 mol dm^{-3} concentrations. Amino acids were dissolved in hydrochloric acid solutions. Concentrations were identical with those of the titrants. For pH calibration the following standard solutions were used: 0.01 mol dm^{-3} HCl + 0.09 mol dm^{-3} KCl (declared pH = 2.07); 0.05 mol dm^{-3} potassium acid phthalate (pH = 4.008); 0.01 mol dm^{-3} $Na_2B_4O_7{\cdot}10H_2O$ (pH = 9.180); 0.025 mol dm^{-3} Na_2CO_3 + 0.025 mol dm^{-3} $NaHCO_3$ (pH = 10.012). The temperature was kept at 25.0 ± 0.1 °C by ultrathermostat. The NMR solvent was D_2O. To obtain convertible pH and pD values by means of analytical $\bar{n}_{(pH)}$ and $\bar{n}_{(pD)}$ data (*11*), all potentiometric amino acid titrations were also carried out in D_2O. Most NMR spectra were run on a Varian XL-100/15 spectrometer operating at 100.1 MHz for ^1H and 25.16 MHz for ^{13}C. The proton spectra of the extremely acidic samples (pH = 0.0) were recorded on a Varian XL-400 instrument since the β-methylene protons proved to be magnetically equivalent at 100 MHz. Chemical shifts were measured relative to internal *tert*-butyl alcohol (1.22 ppm for ^1H and 32.50 ppm for ^{13}C).

Accurate NMR data of the ABX type proton spectra were obtained by iterative calculations using the LAOCN3 program (*12*). The rms errors of the calculated "best fit" spectra were less than 0.03 Hz, and the probable errors for individual data points were better than 0.03 Hz.

RESULTS AND DISCUSSION

Protonation Equilibria of Asparagine and Aspartic Acid. Asparagine and aspartic acid have two and three binding sites for protons, respectively. Figures 1 and 2 show their major protonation pathways.

Published values (*13*) for the separately occurring amino and carboxylate protonations of asparagine are $\log K_1 = 8.79$ and $\log K_2 = 2.09$ at $T = 293$ and 1.0 M/dm^3 ionic strength. Our analogous pH-metric stepwise macroconstants at 298 K and 2.0 M/dm^3 ionic strength in H_2O were found to be $\log K_1 = 8.73 \pm 0.02$ and $\log K_2 = 2.02 \pm 0.04$, where uncertainties are standard deviations.

0003-2700/89/0361-2631$01.50/0 © 1989 American Chemical Society

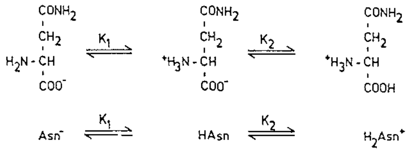

Figure 1. Major protonation processes of asparagine.

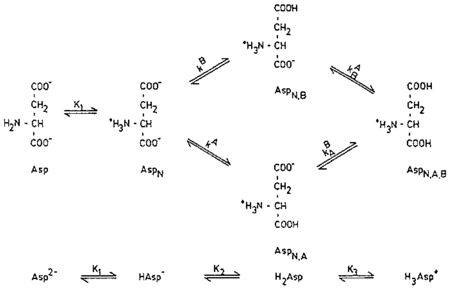

Figure 2. Major protonation processes of aspartic acid.

In the case of aspartic acid, K_2 and K_3 are composites of microconstants (*14*)

$$K_2 = k^A + k^B \tag{1}$$

$$K_2K_3 = k^Ak_A{}^B = k^Bk_B{}^A \tag{2}$$

The superscripts A and B on microconstant k denote the functional group protonating in the given process, while the subscript (if any) indicates the group attached to the proton. Indices A and B denote α- and β-carboxylates, respectively. Two examples of microconstants are given below (see also Figure 2)

$$k^A = \frac{[\mathrm{Asp_{N,A}}]}{[\mathrm{Asp_N}][\mathrm{H^+}]} \tag{3}$$

$$k_A{}^B = \frac{[\mathrm{Asp_{N,A,B}}]}{[\mathrm{Asp_{N,A}}][\mathrm{H^+}]} \tag{4}$$

Several combined pH-metric–spectroscopic methods for the determination of microconstants have been discussed elsewhere (*15–17*). However, no such method could be used for aspartic acid, due to the similar spectroscopic character of the two carboxylates and the small number of intervening atoms between them.

Edsall's early work (*5*) for the estimation of microconstants by using semiquantitative substituent effect data was based on pK values of esters and other derivatives. The utilization of these constants is only recommended with caution (*3*), since the size and the H-bonding characteristics of the ester group are obviously different from those of the carboxyl.

To minimize the ambiguity of the aspartic acid microconstants, we used two further approaches:

(1) Equations 1 and 2 show that in addition to K_2 and K_3, at least one other independent piece of information is necessary in order to evaluate the microconstants. The NMR data of asparagine and aspartic acid in acidic medium are very similar. In fact, their rotamer populations are virtually the same (see Table III), indicating that the $-CONH_2$ group very closely mimics the –COOH. Thus, K_2 of asparagine can be considered a good approximation for $k_B{}^A$ of aspartic acid. Microconstant k^B is calculated from eq 2 as $k^B = K_2K_3/k_B{}^A$. However, note that this treatment provides reliable values only for k^B and $k_B{}^A$. The analogous microconstants for the minor pathway of protonation (k^A and $k_A{}^B$) cannot be determined accurately by this approach, due to the inevitable experimental errors in K_2 and k^B, and the insignificant difference between them.

Table I. Protonation Macroconstants for Amino Acids at 298 K and 2.0 mol dm^{-3} Ionic Strength[a]

	aspartic acid	asparagine	α-alanine	β-alanine
log K_1	9.53 ± 0.02	8.73 ± 0.02	9.74 ± 0.01	10.14 ± 0.03
log K_2	3.65 ± 0.02	2.02 ± 0.04	2.35 ± 0.01	3.60 ± 0.01
log K_3	1.96 ± 0.02			

[a] Uncertainties are standard deviations.

Table II. Protonation Microconstants for Aspartic Acid Given by Edsall et al. (Column I) and Determined in This Work by Method 1 (III) and 2 (II)[a]

	I	II	III
log k^A	2.4	2.37	
log k^B	3.7	3.63	3.59
log $k_B{}^A$	2.0	1.98	2.02
log $k_A{}^B$	3.2	3.24	
reference	5, 3	this work 2	this work 1

[a] For methods see text. Estimated uncertainties are around 0.05 log k units.

(2) Aspartic acid can be regarded either as a β-carboxyl derivative of α-alanine or as an α-carboxyl derivative of β-alanine. In this respect we always denote the N-bound carbon α. When the aspartic acid molecule is "built up" in this way, the absolute value of basicity for both carboxylates changes, but the *ratio* remains equal to 18.1, as in the case of the two alanines. K_2 of eq 1 can be divided into k^A and k^B accordingly. Knowing both k^A and k^B, the other two microconstants $k_B{}^A$ and $k_A{}^B$ can be calculated from eq 2.

The k^A and k^B microconstants derived in this way express the inherent basicity of the unmodified α- and β-carboxylates. Moreover, since they are calculated by using K_2, their values reflect the interaction between the two carboxylates. The effect of protonation on the other group is also reflected in the microconstants (see $k_B{}^A/k^A$ and $k_A{}^B/k^B$ ratios), by using the K_3 macroconstant in the calculations. At present, this is the best approach for determination of aspartic acid microconstants.

In an effort to obtain fully comparable data, we made pH-metric measurements to determine macroconstants for the four relevant amino acids at 298 K and 2.0 mol/dm^3 ionic strength. Table I summarizes the results. The data in Table II indicate that the microconstants for aspartic acid are essentially the same even when different source data and methods are used and despite differences in H-bonding ability of the functional groups in the auxiliary compounds.

Protonation Equilibria of Asparagine Rotamers. Figure 3 shows the staggered rotameric forms of differently protonated asparagine species. The number of theoretically possible species is limited by two factors: (1) the eclipsed rotameric forms essentially do not exist; (2) the concentration of the "inverse" single-proton-containing species, in which the carboxylate holds the proton (–COOH), and the amino group is uncharged ($-NH_2$), is negligible, since the basicity of the amino group is several orders of magnitude greater than that of the carboxylate.

By use of the convention cited previously (*7, 8*) t and g designate the rotamers in which the bulkiest groups are in trans and gauche positions, respectively. In h rotamers, all three carbon-bound hydrogens as well as the three bulky substituents are adjacent. Subscripts N and A occur when

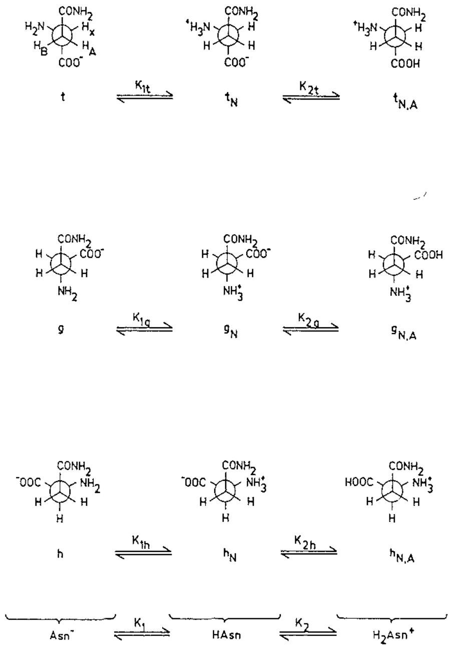

Figure 3. Staggered rotamers of Asn^-, HAsn, and H_2Asn^+.

the amino and α-carboxylate groups are protonated, respectively.

Protonation constants of the individual rotational isomers can then be defined as follows:

$$K_{1t} = \frac{[t_N]}{[t][H^+]} \tag{5}$$

$$K_{1g} = \frac{[g_N]}{[g][H^+]} \tag{6}$$

$$K_{1h} = \frac{[h_N]}{[h][H^+]} \tag{7}$$

$$K_{2t} = \frac{[t_{N,A}]}{[t_N][H^+]} \tag{8}$$

$$K_{2g} = \frac{[g_{N,A}]}{[g_N][H^+]} \tag{9}$$

$$K_{2h} = \frac{[h_{N,A}]}{[h_N][H^+]} \tag{10}$$

The following mass-balance equations are then valid:

$$C_{Asn} = [Asn^-] + [HAsn] + [H_2Asn^+] \tag{11}$$

$$[Asn^-] = [t] + [g] + [h] \tag{12}$$

$$[HAsn] = [t_N] + [g_N] + [h_N] \tag{13}$$

$$[H_2Asn^+] = [t_{N,A}] + [g_{N,A}] + [h_{N,A}] \tag{14}$$

The bulk macroconstants are given as

$$K_1 = \frac{[HAsn]}{[Asn^-][H^+]} \tag{15}$$

$$K_2 = \frac{[H_2Asn^+]}{[HAsn][H^+]} \tag{16}$$

Rotamer mole fractions are designated by using three symbols: F, the concentration of any rota-microspecies relative to the total asparagine concentration (C_{Asn}); f, the concentration of any rota-microspecies relative to the concentration of one of the macrospecies (Asn^-, HAsn, or H_2Asn^+); and Φ, the concentration of a rotameric form, regardless of the protonation stage. (Φ_t, Φ_g, and Φ_h comprise all species in the given t, g, or h rotameric form.)

For example, the mole fraction of g can be written as

$$F_g = [g]/C_{Asn} \tag{17}$$

Examples of partial mole fractions are as follows:

$$f_g = \frac{[g]}{[g] + [t] + [h]} \tag{18}$$

$$f_{g_N} = \frac{[g_N]}{[g_N] + [t_N] + [h_N]} \tag{19}$$

$$f_{g_{N,A}} = \frac{[g_{N,A}]}{[g_{N,A}] + [t_{N,A}] + [h_{N,A}]} \tag{20}$$

Φ values for asparagine can be expressed as

$$\Phi_g = F_g + F_{g_N} + F_{g_{N,A}} \tag{21}$$

$$\Phi_t = F_t + F_{t_N} + F_{t_{N,A}} \tag{22}$$

$$\Phi_h = F_h + F_{h_N} + F_{h_{N,A}} \tag{23}$$

By the introduction of F-type mole fractions not only for rotameric forms but also for macro- (or micro)species, the relation between the f- and F-type rotamer populations can be expressed. The example for Asn^- and g is as follows:

$$F_{Asn^-} = [Asn^-]/C_{Asn} \tag{24}$$

From eq 18, 12, and 24, we derive

$$f_g = \frac{[g]}{[Asn^-]} = \frac{[g]}{F_{Asn^-} C_{Asn^-}} = \frac{F_g}{F_{Asn^-}} \tag{25}$$

F and Φ values depend on the pH; however, f values are pH-independent. From eq 25, it is clear that f_g and F_g are equal when $F_{Asn^-} = 1$. This is the case for asparagine in very basic solutions. In general, rotameric f and F values become practically identical whenever a species in a given state of protonation becomes the overwhelmingly predominant species. In that case, some simplifications become possible.

At very high pH, the concentrations of HAsn and H_2Asn^+ are negligible

$$C_{Asn_{(pH>12)}} = [Asn^-] \tag{26}$$

$$F_{g_{(pH>12)}} = f_g \tag{27}$$

$$F_{t_{(pH>12)}} = f_t \tag{28}$$

$$F_{h_{(pH>12)}} = f_h \tag{29}$$

On the other hand, at neutral pH, HAsn exists almost exclusively

$$C_{Asn_{(8>pH>6)}} = [HAsn] \tag{30}$$

$$F_{g_{N(8>pH>6)}} = f_{g_N} \tag{31}$$

$$F_{t_{N(8>pH>6)}} = f_{t_N} \tag{32}$$

$$F_{h_{N(8>pH>6)}} = f_{h_N} \tag{33}$$

Table III. ^{1}H NMR Data and Calculated Rotamer Populations for Asparagine and Aspartic Acid[a]

		chemical shifts, ppm			obsd three-bond coupling values, Hz		rotamer populations, Φ					
							J_G = 2.4, J_T = 13.3			J_G = 2.56, J_T = 13.6		
compound	pH (pD)	A	B	X	$3J_{AX}$	$3J_{BX}$	t	g	h	t	g	h
asparagine	13.1	3.691	3.849	4.767	8.70	4.96	0.58	0.23	0.19	0.56	0.22	0.23
	7.4	4.109	4.151	5.226	7.27	4.01	0.45	0.15	0.41	0.43	0.13	0.44
	0.0	4.271	4.305	5.613	6.25	4.38	0.35	0.18	0.46	0.33	0.16	0.50
aspartic acid	13.2	3.493	3.815	4.730	9.55	4.06	0.66	0.15	0.19	0.63	0.14	0.23
	7.2	3.914	3.985	5.105	7.94	3.87	0.51	0.14	0.36	0.49	0.12	0.39
	3.87	4.042	4.088	5.179	7.69	3.88	0.49	0.14	0.38	0.47	0.12	0.42
	3.19	4.127	4.155	5.231	7.26	4.13	0.45	0.16	0.40	0.43	0.14	0.43
	0.0	4.358	4.397	5.654	6.34	4.35	0.36	0.18	0.46	0.34	0.16	0.50

[a] The most acidic spectra were recorded at 400 MHz, all others at 100 MHz.

Table IV. Macro- and Rota-Macroconstants of Asparagine in log Units

macroconstants		rota-macroconstants					
		t		g		h	
symbol	value	symbol	value	symbol	value	symbol	value
K_1	8.73	K_{1t}	8.6_2	K_{1g}	8.5_0	K_{1h}	9.0_1
K_2	2.02	K_{2t}	1.9_1	K_{2g}	2.1_1	K_{2h}	2.0_7
β_2	10.75	β_{2t}	10.5_3	β_{2g}	10.6_1	β_{2h}	11.0_8

When the media is very acidic, only the doubly protonated species is present

$$C_{\mathrm{Asn}_{(\mathrm{pH}<1)}} = [\mathrm{H_2Asn^+}] \quad (34)$$

$$F_{\mathrm{g}_{\mathrm{N,A}(\mathrm{pH}<1)}} = f_{\mathrm{g}_{\mathrm{N,A}}} \quad (35)$$

$$F_{\mathrm{t}_{\mathrm{N,A}(\mathrm{pH}<1)}} = f_{\mathrm{t}_{\mathrm{N,A}}} \quad (36)$$

$$F_{\mathrm{h}_{\mathrm{N,A}(\mathrm{pH}<1)}} = f_{\mathrm{h}_{\mathrm{N,A}}} \quad (37)$$

Note, however, that the above simplifications are not valid outside the indicated pH ranges.

Combining and rearranging eq 6, 19, 18, 12, 13, and 15 as well as 9, 20, 19, 14, 13, and 16 gives the rota-macroconstants K_{1g} and K_{2g}, respectively

$$K_{1g} = \frac{f_{\mathrm{g_N}}[\mathrm{HAsn}]}{f_{\mathrm{g}}[\mathrm{Asn^-}][\mathrm{H^+}]} = \frac{f_{\mathrm{g_N}}}{f_{\mathrm{g}}}K_1 \quad (38)$$

$$K_{2g} = \frac{f_{\mathrm{g_{N,A}}}[\mathrm{H_2Asn^+}]}{f_{\mathrm{g_N}}[\mathrm{HAsn}][\mathrm{H^+}]} = \frac{f_{\mathrm{g_{N,A}}}}{f_{\mathrm{g_N}}}k_2 \quad (39)$$

Protonation constants for all other rotational isomers can be expressed in an analogous manner. Equations 38 and 39 show that these parameters are combinations of structure and equilibrium elements and are derived from a bulk protonation constant and two mole fractions. We distinguish the protonation constants as rota-macro- or rota-microconstants. For asparagine, only the former is considered. Due to the overlapping carboxylate protonations, both constants are applicable for aspartic acid.

Mole fractions of rotamers can be elucidated from three-bond coupling constants. Individual rotamers cannot be directly observed, because of their fast interconversion on the NMR time scale. However, their time-averaged signals provide well-established indirect methods (*7–9, 18–22*) for the evaluation of their concentrations. For most α-amino acids, the substituted ethane residue possesses a three-spin ABX pattern, due to the nonequivalent two β- and α-hydrogens. The observed $^3J_{(\mathrm{H_A}-\mathrm{H_X})}$ and $^3J_{(\mathrm{H_B}-\mathrm{H_X})}$ coupling constants are independent only of the magnetic field; but they do depend on pH, because of the change in rotamer populations. In order to extract the rotamer mole fractions from the NMR coupling data, two-parameter formulations (*7, 9, 18–20*) and six-parameter formulations (*21, 22*) have been suggested. As discussed more recently (*8*) the six-parameter treatment may yield results only marginally improved over those obtained with the simpler and more rapid two-parameter method.

The general, two-parameter formulation is as follows:

$$J_{\mathrm{A,X}} = \Phi_t J_G + \Phi_g J_T + \Phi_h J_G \quad (40)$$

$$J_{\mathrm{B,X}} = \Phi_t J_T + \Phi_g J_G + \Phi_h J_G \quad (41)$$

$$\Phi_t + \Phi_g + \Phi_h = 1 \quad (42)$$

where $J_{\mathrm{A,X}}$ and $J_{\mathrm{B,X}}$ are experimental vicinal coupling values and J_G and J_T are coupling parameters for the gauche and trans (anti) positions, respectively.

The NMR aspects of eq 40–42 present the following problems. Since the H_A and H_B assignments are arbitrary, ^{1}H NMR coupling data alone do not provide sufficient evidence for the t and g assignments. This shortcoming can be avoided by using ^{13}C–^{1}H coupling values (*9*). In principle, three-bond ^{13}C–^{1}H couplings can also be used for the numerical evaluation of rotamer populations. However, the limited accuracy of these data restricts their use to assignments only (*8, 9*). An additional difficulty arises in most cases of acidic solution, where the chemical shifts of the two β-methylene protons are very similar. Distinction between these two nuclei is possible only by high-resolution NMR measurements. The most widely accepted J_G and J_T constants for proton–proton couplings are 2.4 and 13.3, as reported by Martin (*8*), and 2.56 and 13.6, reported by Hansen (*9*) et al. Virtually the same values were given in the pioneer works of Pachler (*18*) and Abraham (*19*). Table III gives ^{1}H NMR data and rotamer populations for asparagine and aspartic acid.

An important methodical conclusion can be drawn from Table III. Rotamer populations calculated by Martin's and Hansen's parameters are in good agreement. The estimated uncertainty is approximately 5%. Using rotamer populations, macroconstants, and eq 38 and 39, we calculated protonation constants for rotational isomers. Table IV lists the corresponding bulk constants for comparison. Accuracy of the data is represented by the number and form of decimals.

Protonation Equilibria of Aspartic Acid Rotamers. Figure 2 shows macro- and microequilibria of aspartic acid. All solutions of aspartic acid contain a mixture of rotational isomers. Figure 4 shows structures of these rota-microspecies and the relevant constants. Super- and subscripts of constants indicate first the macro- or microprocess and then the rotameric form. Each of the five protonation stages of aspartic acid is a composite of three rotamers. Thus the total number of rota-microspecies is 15. By choosing appropriate pH values, we can prepare solutions, containing nearly exclusively $\mathrm{Asp^{2-}}$ or $\mathrm{HAsp^-}$ or $\mathrm{H_3Asp^+}$. From the 3-bound coupling data of these systems, rotamer populations of the above species can be determined by the methods discussed for asparagine. How-

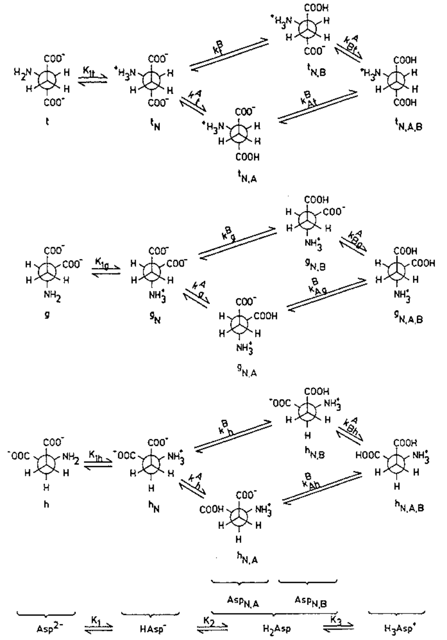

Figure 4. Staggered rotamers of aspartic acid and their protonation equilibria.

ever, the macro-composition of H_2Asp consists of two micro- and accordingly six rota-microspecies. All of these species are isomers either in the stage of protonation or in the form of rotation. Concentrations of such doubly isomeric species have not been previously reported. Calculation of their individual concentrations is not possible even with the knowledge of microconstants and coupling data. Microconstants are useful to calculate only the *sum* of mole fractions for rotamers of protonation isomers

$$\frac{[\mathrm{Asp}_{\mathrm{N,A}}]}{C_{\mathrm{Asp}}} = \frac{k^{\mathrm{A}}[\mathrm{H}^+]}{K_2[\mathrm{H}^+] + K_2K_3[\mathrm{H}^+]^2} = F_{\mathrm{Asp}_{\mathrm{N,A}}} \tag{42}$$

$$F_{\mathrm{Asp}_{\mathrm{N,A}}} = F_{\mathrm{t}_{\mathrm{N,A}}} + F_{\mathrm{g}_{\mathrm{N,A}}} + F_{\mathrm{h}_{\mathrm{N,A}}} \tag{43}$$

$$\frac{[\mathrm{Asp}_{\mathrm{N,B}}]}{C_{\mathrm{Asp}}} = \frac{k^{\mathrm{B}}[\mathrm{H}^+]}{K_2[\mathrm{H}^+] + K_2K_3[\mathrm{H}^+]^2} = F_{\mathrm{Asp}_{\mathrm{N,B}}} \tag{44}$$

$$F_{\mathrm{Asp}_{\mathrm{N,B}}} = F_{\mathrm{t}_{\mathrm{N,B}}} + F_{\mathrm{g}_{\mathrm{N,B}}} + F_{\mathrm{h}_{\mathrm{N,B}}} \tag{45}$$

Similarly, coupling data provide only *sums* for analogous rotamers of isomeric protonation

$$\Phi_{\mathrm{t}} = F_{\mathrm{t}} + F_{\mathrm{t}_{\mathrm{N}}} + F_{\mathrm{t}_{\mathrm{N,A}}} + F_{\mathrm{t}_{\mathrm{N,B}}} + F_{\mathrm{t}_{\mathrm{N,A,B}}} \tag{46}$$

$$\Phi_{\mathrm{g}} = F_{\mathrm{g}} + F_{\mathrm{g}_{\mathrm{N}}} + F_{\mathrm{g}_{\mathrm{N,A}}} + F_{\mathrm{g}_{\mathrm{N,B}}} + F_{\mathrm{g}_{\mathrm{N,A,B}}} \tag{47}$$

$$\Phi_{\mathrm{h}} = F_{\mathrm{h}} + F_{\mathrm{h}_{\mathrm{N}}} + F_{\mathrm{h}_{\mathrm{N,A}}} + F_{\mathrm{h}_{\mathrm{N,B}}} + F_{\mathrm{h}_{\mathrm{N,A,B}}} \tag{48}$$

Populations of the unprotonated rotamers (F_{g}, F_{t}, and F_{h}) are negligible below pH 7. The 12 other rota-microspecies occur in significant concentration. $F_{\mathrm{t}_{\mathrm{N}}}$, $F_{\mathrm{g}_{\mathrm{N}}}$, and $F_{\mathrm{h}_{\mathrm{N}}}$ values are known to form eq 25 type relations as products of $F_{\mathrm{Asp}_{\mathrm{N}}}$ and the respective $f_{\mathrm{t}_{\mathrm{N}}}$, $f_{\mathrm{g}_{\mathrm{N}}}$, and $f_{\mathrm{h}_{\mathrm{N}}}$ data. For example

$$F_{\mathrm{t}_{\mathrm{N}}} = f_{\mathrm{t}_{\mathrm{N}}} F_{\mathrm{Asp}_{\mathrm{N}}} \tag{49}$$

The pH-independent $f_{\mathrm{t}_{\mathrm{N}}}$ value is known from neutral solutions, where $\mathrm{Asp}_{\mathrm{N}}$ is the exclusive protonation form. $F_{\mathrm{Asp}_{\mathrm{N}}}$ can be calculated from macroconstants and pH data by using the appropriate form of an eq 42 type equation. Analogously $F_{\mathrm{t}_{\mathrm{N,A,B}}}$, $F_{\mathrm{g}_{\mathrm{N,A,B}}}$, and $F_{\mathrm{h}_{\mathrm{N,A,B}}}$ can also be calculated for any arbitrarily chosen pH value. Accordingly, Φ_{t}, Φ_{g}, and Φ_{h} can be reduced to forms containing only two terms on the right-hand sides of the equations

$$\Phi_{\mathrm{t}}' = F_{\mathrm{t}_{\mathrm{N,A}}} + F_{\mathrm{t}_{\mathrm{N,B}}} \tag{50}$$

$$\Phi_{\mathrm{g}}' = F_{\mathrm{g}_{\mathrm{N,A}}} + F_{\mathrm{g}_{\mathrm{N,B}}} \tag{51}$$

$$\Phi_{\mathrm{h}}' = F_{\mathrm{h}_{\mathrm{N,A}}} + F_{\mathrm{h}_{\mathrm{N,B}}} \tag{52}$$

Most importantly, eq 43, 45, and 50–52 clearly do not contain sufficient information to elucidate the unknown mole fractions. Evaluation of these rotamer populations needs additional considerations.

Estimation of Rotamer Populations for the Protonation Isomers. Table III shows that in very acidic medium, the rotamer populations of asparagine and aspartic acid are identical. This is not true at other pH values. This observation means that the $-COOH$ and $-CONH_2$ groups have equivalent roles in forming rotamer populations. It follows that natural asparagine is analogous with the $\mathrm{Asp}_{\mathrm{N,B}}$ protonation isomer. Therefore, the populations of their rotamers are practically the same

$$f_{\mathrm{t}_{\mathrm{Asp(N,B)}}} = f_{\mathrm{t}_{\mathrm{Asn(N)}}} \tag{53}$$

$$f_{\mathrm{g}_{\mathrm{Asp(N,B)}}} = f_{\mathrm{g}_{\mathrm{Asn(N)}}} \tag{54}$$

$$f_{\mathrm{h}_{\mathrm{Asp(N,B)}}} = f_{\mathrm{h}_{\mathrm{Asn(N)}}} \tag{55}$$

This provides numerical data for the rotamer populations of the $\mathrm{Asp}_{\mathrm{N,B}}$ major protonation isomer. With the above values, one could now calculate the minor protonation isomer ($\mathrm{Asp}_{\mathrm{N,A}}$) rotamer populations directly, based on eq 50–52. However, the total occurrence probability of these rotamers ($t_{\mathrm{N,A}}$, $g_{\mathrm{N,A}}$, $h_{\mathrm{N,A}}$) does not exceed 5%, even at the most favorable pH. Their contribution to the observed NMR coupling data is commensurable with the uncertainty of the measurement. Thus, we developed an indirect method to estimate the rotamer populations for the minor protonation isomer. This method is based on our data for 18 asparagine and aspartic acid rotamer populations. By definition, the sum of f-type mole fractions is equal to unity. For the rotamers of $\mathrm{Asp}_{\mathrm{N,A}}$ microspecies, this sum takes the following form:

$$1 = f_{\mathrm{t}_{\mathrm{N,A}}} + f_{\mathrm{g}_{\mathrm{N,A}}} + f_{\mathrm{h}_{\mathrm{N,A}}} \tag{56}$$

Evaluation of the quantities on the right-hand side of eq 56 requires two additional relations. The following two ratios could then be estimated:

$$f_{\mathrm{t}_{\mathrm{N,A}}}/f_{\mathrm{h}_{\mathrm{N,A}}} = \mathrm{trans/gauche}_{\mathrm{(C-C)}} \tag{57}$$

$$f_{\mathrm{g}_{\mathrm{N,A}}}/f_{\mathrm{h}_{\mathrm{N,A}}} = \mathrm{trans/gauche}_{\mathrm{(C-N)}} \tag{58}$$

Our explanation of the above relationships is as follows. In the formation of rotamer populations, the role of the substituents of α- and β-carbons is very different. In this perspective, the effect of A, B, and X protons is negligible relative to the bulky groups of high electron density. We therefore tried to find relationships between the relative position of the carboxylate and amino groups with other NMR parameters of the molecule. Comparison of t and h rotamers (Figure 4) shows that the $f_{\mathrm{t}}/f_{\mathrm{h}}$ population ratio measures only the trans/gauche tendency between the two carboxylates, since (1) the amino–β-carboxylate position is equally gauche in both the t and h rotamers and (2) the carbon-bound protons do not significantly influence the populations. Analogous ratios can also be estimated for other stages of protonation (e.g. $f_{\mathrm{t}_{\mathrm{N}}}/f_{\mathrm{h}_{\mathrm{N}}}$, etc.).

As expected, this ratio gradually decreases with the progress of protonation, since uptake of protons is followed by loss of

Table V. Trans/Gauche Tendency Ratios and Sums of Carbonyl ^{13}C NMR Chemical Shifts[a]

	state of group					
symbol of species	β	α	α	t/g$_{(C-C)}$	t/g$_{(C-N)}$	$\sum\delta$, ppm
Asp^{2-}	$-COO^-$	$-COO^-$	$-NH_2$	2.74	0.59	183.91 + 181.26 = 365.17
$HAsp^-$	$-COO^-$	$-COO^-$	$-NH_3^+$	1.24	0.30	178.73 + 175.42 = 354.15
H_3Asp^+	$-COOH$	$-COOH$	$-NH_3^+$	0.66	0.32	174.04 + 171.57 = 345.61
Asn^-	$-CONH_2$	$-COO^-$	$-NH_2$	2.43	0.96	177.80 + 182.63 = 360.43
HAsn	$-CONH_2$	$-COO^-$	$-NH_3^+$	0.98	0.30	174.50 + 175.43 = 349.93
H_2Asn^+	$-CONH_2$	$-COOH$	$-NH_3^+$	0.66	0.32	174.36 + 171.87 = 346.23

[a] For abbreviations see text.

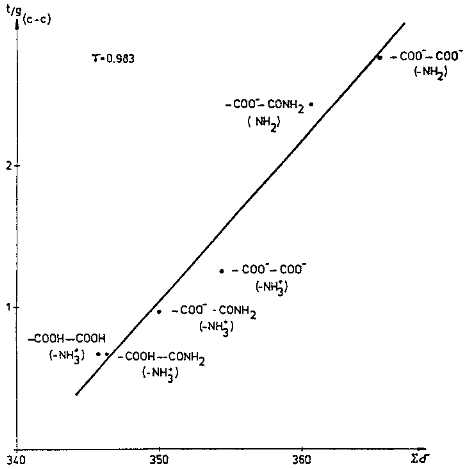

Figure 5. The trans/gauche tendency of the carboxyl(ate) groups plotted against the sum of the carbonyl ^{13}C NMR chemical shifts at different stages of protonation.

Table VI. Macro-, Micro-, Rota-Macro-, and Rota-Microconstants of Aspartic Acid in log Units

macro- or microconstants		rota-macro- or rota-microconstants					
		t		g		h	
symbol	value	symbol	value	symbol	value	symbol	value
K_1	9.53	K_{1t}	9.4_2	K_{1g}	9.4_6	K_{1h}	9.7_6
k^B	3.63	$k^B{}_t$	3.6	$k^B{}_g$	3.7	$k^B{}_h$	3.7
k^A	2.37	$k^A{}_t$	2.3	$k^A{}_g$	2.4	$k^A{}_h$	2.4
$k_A{}^B$	3.24	$k_A{}^B{}_t$	3.1	$k_A{}^B{}_g$	3.3	$k_A{}^B{}_h$	3.3
$k_B{}^A$	1.98	$k_B{}^A{}_t$	1.9	$k_B{}^A{}_g$	2.1	$k_B{}^A{}_h$	2.0
β_2	13.18	β_{2t}	13.0	β_{2g}	13.1	β_{2h}	13.5
β_3	15.14	β_{3t}	14.8_7	β_{3g}	15.1_9	β_{3h}	15.4_8

electron density and basicity at the adjacent groups. This is also manifested in the loss of repulsion between the groups. In Figure 5, f_t/f_h ratios are plotted as a function of the sum of ^{13}C NMR chemical shifts of the α- and β-carbon-bound carbonyl C atoms. Since the chemical shifts are also electron density dependent, the close correlation is not surprising.

Following similar arguments, f_g/f_h, f_{g_N}/f_{h_N}, etc. population ratios characterize the extent to the trans/gauche tendency between the amino and β-carboxylate groups. Table V contains t/g ratios for the case of β-carboxylate–α-carboxylate t/g$_{(C-C)}$ and β-carboxylate–amino t/g$_{(C-N)}$ relations as well as the sum of the two carboxyl carbon ^{13}C chemical shifts ($\sum\delta$).

The t/g$_{(C-N)}$ value is approximately 0.3, wherever the amino group is protonated. Accordingly, this is a good approximation for the $f_{g_{N,A}}/f_{h_{N,A}}$ in eq 53.

On the other hand, the value of the t/g$_{(C-C)}$ ratio is strongly dependent on the protonation state of the groups. Fortunately, the correlation between t/g$_{(C-C)}$ and $\sum\delta$ values is good (Figure 5). If the ^{13}C NMR chemical shift values for the $Asp_{N,A}$ carbonyl carbons are known, the straight line of Figure 5 provides a good approximation for the t/g$_{(C-C)}$ value. The NMR spectrum of $Asp_{N,A}$ species cannot be directly recorded. $Asp_{N,A}$ is a protonation isomer (and only a minor one), so it occurs only in the presence of other species. However, the Sudmeier–Reilley equation (*23*) provides a means to calculate the spectra from appropriate NMR data

$$\Delta\delta_\alpha = f_\alpha C_{\alpha\alpha} + f_\beta C_{\beta\alpha} \qquad (59)$$

$$\Delta\delta_\beta = f_\alpha C_{\alpha\beta} + f_\beta C_{\beta\beta} \qquad (60)$$

where $\Delta\delta_\alpha$ and $\Delta\delta_\beta$ are protonation shifts at a given pH, measured at the α- and β-carbonyl carbons, f_α and f_β are the protonation mole fractions of the α- and β-carboxylates at the same pH, $C_{\alpha\alpha}$ and $C_{\beta\alpha}$ are protonation shift coefficients of the carboxylate at the α- and β-carbonyl, respectively, and so forth. Since the t/g$_{(C-C)}$ values are plotted as a function of the sum of carbonyl chemical shifts, eq 59 and 60 can be combined. Further simplification is possible, since we know the $\Delta\delta_{max} = C_\alpha + C_\beta$ values by acidifying from neutral ($f_\alpha = f_\beta = 0$) to very acidic ($f_\alpha = f_\beta = 1$) medium. The $\sum\delta$ values calculated in this way for the $Asp_{N,A}$ species at pH = 3.19 and 3.87 are 349.6 and 349.4 ppm, respectively. The corresponding t/g$_{(C-C)}$ value is approximately 1.08. Introducing these data as well as t/g$_{(C-N)}$ = 0.3 into eq 56 gives $f_{t_{N,A}} = 0.45$, $f_{g_{N,A}} = 0.13$, and $f_{h_{N,A}} = 0.42$.

The above results and rotamer populations for Asp_N and $Asp_{N,A,B}$ as well as experimental NMR coupling data at pH = 3.19 and 3.87 permitted an independent test calculation for the $Asp_{N,B}$ rotamer populations. The values $f_{tN,B} = 0.42$, $f_{gN,B} = 0.14$, $f_{hN,B} = 0.44$ were obtained. The corresponding data for the neutral asparagine species were $f_{t_N} = 0.43$, $f_{g_N} = 0.13$, and $f_{h_N} = 0.44$.

Considering the number of parameters to be handled, the agreement between these rotamer populations is excellent. This agreement can be interpreted as either evidence of the equivalent role of $-COOH$ and $-CONH_2$ groups forming rotamer populations, or proof of the validity of the evaluation method.

With all the population data and equilibrium constants, rota-macro- and rota-microconstants could be calculated. The values are summarized in Table VI. The number of decimals in the constants is proportional to the accuracy. The uncertainty of rota-microconstants is inevitably greater, since this kind of equilibrium parameter needs more experimental and evaluation methods. The requirements of the thermodynamic relations between the macro- and microconstants are sometimes not absolutely satisfactory, due to roundings.

CONCLUSIONS

Microequilibrium data of aspartic acid have been treated with caution (*3*) thus far. Our studies, however, using different and independent approaches, support Edsall's early statements(*5*). The β-carboxylate basicity is about 18 times greater than that of the α-carboxylate. The interactivity parameter between the two carboxylates is $\Delta \log k = 0.39$; i.e., deprotonation of one of the carboxyl groups causes a 2.5-fold increase in basicity at the other carboxylate group.

Population data of asparagine rotamers indicate that the proportion of rotamer h gradually increases with protonation, at the expense of rotamer t. The repulsing character of bulky groups with high electron density is responsible for the small population of rotamer h, and the predominance of rotamer t at high pH. The enhanced proton binding ability of rotamer h can be explained by the fact that all the basic moieties of the molecule are adjacent. The dominance of rotamer h in acid medium is certainly connected with H bonding and solvation effects. The protonation constants of the rotamers are generally great whenever a basic group in gauche position is situated near the protonation site. For example, the $-CONH_2$ group does not ionize itself in any way but does promote the protonation of other groups in gauche. This gauche effect (E_{gauche}) can be quantified by comparing rota-macroconstants

$$E_{\mathrm{gauche\text{-}NH_2}} = \log K_{1\mathrm{h}} - \log K_{1\mathrm{g}} \simeq 0.5$$

$$E_{\mathrm{gauche\text{-}COO^-}} = \log K_{2\mathrm{h}} - \log K_{2\mathrm{t}} \simeq 0.2$$

In aspartic acid, the decline of rotamer t and the increase of rotamer h can also be observed upon acidifying the solution. Accordingly, protonation constants of h rotamers are always greater, and those of t rotamers are smaller than the corresponding bulk (macro- or micro)constants. In cumulative constants (β), the differences are also accumulated. A difference between the relevant rota-constants of more than 0.2 log k units can be considered significant. The corresponding rotamer populations of the two protonation isomers are nearly equal, suggesting that the formation of a rotational state is essentially independent of which of the carboxylates holds the proton.

The f_t/f_g type ratios for the given states of protonation are also informative, since they measure the different interactions that influence the formation of rotamer populations. In t rotamers, the β-carboxyl(ate)–α-carboxyl(ate) positions are trans, while in g rotamers, the β-carboxyl(ate)–amino(ammonium) positions are trans. This is why the f_t/f_g ratio reflects the relative importance of the β-carboxyl(ate)–α-carboxyl(ate) interaction as compared with the β-carboxyl(ate)–amino(ammonium) interaction in populating the rotamers. The f_g value and its change are always significantly smaller than f_t and its change, indicating that the main governing factor in formation of the rotamer populations is the carboxyl(ate)–carboxyl(ate) interaction. The nonequivalence of rotameric log k values may also imply different receptor- and metal-ion-binding ability for aspartic acid and other biomolecule rotamers.

By means of the appropriate rotamer populations and equilibrium constants the individual concentrations of all rota-microspecies can be calculated at any arbitrarily chosen pH. For example, the relative concentration of $g_{\mathrm{N,B}}$ of aspartic acid ($F_{g_{\mathrm{N,B}}}$) can be given as

$$F_{g_{\mathrm{N,B}}} = F_{\mathrm{Asp_{N,B}}} f_{g_{\mathrm{N,B}}} = \frac{K_1 k^{\mathrm{B}}[\mathrm{H^+}]^2}{1 + K_1[\mathrm{H^+}] + \beta_2[\mathrm{H^+}]^2 + \beta_3[\mathrm{H^+}]^3} f_{g_{\mathrm{N,B}}}$$

$F_{g_{\mathrm{N,B}}}$ can also be expressed by using rota-macro- and rota-microconstants

$$F_{g_{\mathrm{N,B}}} = f_{\mathrm{g}} \frac{K_{1\mathrm{g}} k^{\mathrm{B}}{}_{\mathrm{g}}[\mathrm{H^+}]^2}{1 + K_1[\mathrm{H^+}] + \beta_2[\mathrm{H^+}]^2 + \beta_3[\mathrm{H^+}]^3}$$

The actual values of $F_{g_{\mathrm{N,B}}}$ relative concentrations at pH 7 and 4 are 5.95×10^{-5} and 4.12×10^{-2}, respectively, which are, at the same time, real, absolute concentrations in 1 mol/dm^3 aspartic acid solutions.

LITERATURE CITED

(1) Noszál, B. *J. Phys. Chem.* **1986**, *90*, 6345–6349.
(2) Noszál, B. *J. Phys. Chem.* **1986**, *90*, 4104–4110.
(3) Evans, C. A.; Guevremont, R.; Rabenstein, D. L. In *Metal Ions in Biological Systems*; Sigel, H., Ed.; Marcel Dekker: New York, Basel, 1979; Vol. 9, p 42.
(4) Bartle, K. D.; Jones, D. W.; L'Amie, R. *J. Chem. Soc., Perkin Trans. 2* **1972**, 650–655.
(5) Edsall, J. T.; Blanchard, M. H. *J. Am. Chem. Soc.* **1933**, *55*, 2337–2353.
(6) Fujiwara, S.; Ishizuka, H.; Fundano, S. *Chem. Lett.* **1974**, 1281–1284.
(7) Espersen, W. G.; Martin, R. B. *J. Phys. Chem.* **1976**, *80*, 741–745.
(8) Martin, R. B. *J. Phys. Chem.* **1979**, *83*, 2404–2407.
(9) Hansen, P. E.; Feeney, J.; Roberts, G. C. K. *J. Magn. Res.* **1975**, *17*, 249–261.
(10) Ishizuka, H.; Yamamoto, T.; Arata, Y.; Fujiwara, S. *Bull. Chem. Soc. Jpn.* **1973**, *46*, 468–471.
(11) Noszál, B.; Juhász, M. *Talanta* **1987**, *34*, 397–400.
(12) Bothner-By, A. A.; Castellano, S. M. In *Computer Programs for Chemistry*; Detar, D. F., Ed.; W. A. Benjamin: New York, 1968; pp 10–54.
(13) Perrin, D. D. *J. Chem. Soc.* **1958**, 3125–3128.
(14) Martin, R. B. *Introduction to Biophysical Chemistry*; McGraw-Hill: New York, 1964; p 69.
(15) Martin, R. B. *J. Phys. Chem.* **1971**, *75*, 2657–2661.
(16) Rabenstein, D. L.; Sayer, T. L. *Anal. Chem.* **1976**, *48*, 1141–1146.
(17) Kiss, T.; Tóth, B. *Talanta* **1982**, *29*, 539–544.
(18) Pachler, K. G. R. *Spectrochim. Acta* **1964**, *20*, 581–587.
(19) Abraham, R. J.; McLauchlan, K. A. *Mol. Phys.* **1962**, *5*, 513–523.
(20) Casey, J. P.; Martin, R. B. *J. Am. Chem. Soc.* **1972**, *94*, 6141–6151.
(21) Feeney, J. *J. Magn. Reson.* **1976**, *21*, 473–478.
(22) Bystrov, V. F. *Prog. Nucl. Magn. Reson. Spectrosc.* **1976**, *10*, 41–81.
(23) Sudmeier, J. L.; Reilley, C. N. *Anal. Chem.* **1964**, *36*, 1698–1706.

RECEIVED for review April 3, 1989. Accepted September 7, 1989.

Chemical Acoustic Emission Analysis in the Frequency Domain

Peter D. Wentzell[1] **and Adrian P. Wade***

Laboratory for Automated Chemical Analysis, Department of Chemistry, University of British Columbia, Vancouver, British Columbia, Canada V6T 1Y6

The utility of frequency domain power spectra computed from chemical acoustic emission signals is investigated. Averaged power spectra from eight chemical systems are employed and the frequency range 50 kHz to 1.5 MHz is examined. The chemical processes include aqueous dissolution (NaOH and Na_2CO_3), hydration (silica gel, quicklime), solid–liquid (water) and solid–solid (C_2Cl_6) phase transitions, and carbonated water effervescence. Power spectra for a given chemical system are found to be reproducible for at least several months provided the same acoustic transducer is used in each case. Differences among power spectra indicate differences in the physical processes giving rise to the signal. Bubble release is shown to result in low-frequency signals, while crystal fracture is believed to produce higher frequency signals.

Acoustic emission analysis (AEA), the analysis of acoustic signals from systems undergoing physical change, has been used by engineers and material scientists for many years (*1–3*). Only recently, however, has the area drawn the attention of chemists (*4–11*). Many dynamic chemical systems, particularly those that involve phase transitions, are acoustically active. Chemical changes are normally accompanied by energy transfer and some of the energy released may be in the form of an acoustic wave. Chemical AEA has demonstrated good potential for monitoring industrial processes and chemical systems that are difficult to observe by other means (*10*). Other advantages are the passive, noninvasive nature of the technique and the relatively low cost of the instrumentation.

One reason for the current dearth of applications of AEA to chemistry has been the complex nature of the signals involved. Experimental data are readily obtained, but interpretation has been hampered by the fact that few fundamental studies have been conducted to relate the characteristics of the signals to mechanisms and processes occurring. Much of the previous work has focused on the overall acoustic activity (energy released) as a function of time. Because chemical systems typically emit bursts of acoustic energy, this usually means measuring peak acoustic activity as events occur. Such studies are useful in monitoring the processes that are occurring. Useful information may also be derived through time series analysis as demonstrated by Belchamber et al. (*10, 12*). To distinguish among different mechanisms generating the signals, however, it is necessary to look at the characteristics of the signals themselves. It has been demonstrated that different processes in the hydration of silica gel could be distinguished by using pattern recognition methods (*10*), but little further work has been openly published in this area.

One goal of our current research is to be able to differentiate physical processes occurring in chemical systems by the nature of acoustic signals emitted. One way to study these signals is to obtain the Fourier transform of the signal and examine the characteristics of the resulting power spectrum, i.e. the frequency components of the signal. Power spectra of acoustic emission signals have been reported by several workers (*4, 10, 11*), but little has been done to investigate their utility. Interpretation of the power spectrum is complicated by the fact that the acoustic signal originating in the system is distorted by several factors. First, there are the transmission characteristics of the signal through the medium and across the transducer interface, which are frequency dependent. Also, different frequency components of the signal propagate through the medium with different speeds, adding a dependence on source location. Reflections and the generation of surface waves at the interface are additional complicating factors. Finally, the signal transfer characteristics of the transducer and amplifier system play an important role. Piezoelectric transducers are commonly used for AEA. Simpler types employ a single resonance, which makes frequency domain analysis virtually impossible. We employ broad-band, high-frequency transducers that are composed of multiple resonators. While these have a wide bandwidth, the frequency response is not flat and will affect the appearance of the power spectrum. Typical transducer response functions are shown in Figure 1.

Because of the complicating factors in the frequency analysis of acoustic signals, this study attempted to answer several fundamental questions. The first concerned the reproducibility of power spectra from a given chemical system. Another question was how dependent the power spectra were on the particular transducer used, since each has its own characteristic frequency response. Finally, we wished to consider whether power spectra from different chemical systems contain enough information to distinguish among different processes that might be occurring. To help answer these questions, eight chemical systems, encompassing a variety of processes, were chosen for study with chemical AEA. Frequency components in the range 50 kHz to 1.5 MHz were examined. Since individual power spectra tend to be quite variable due to the nature of the acoustic signals, average power spectra were used in this study.

EXPERIMENTAL SECTION

Instrumentation. The experimental apparatus used in this work is shown in Figure 2. The sample being studied was normally placed on the acoustic transducer in a 30-mL Pyrex beaker, with a thin layer of stopcock grease on the bottom of the beaker to improve acoustic coupling. The exception was the hexachloroethane system, which is more fully described in the section on chemical systems. The transducers used were Bruel and Kjaer Model 8312 broad-band piezoelectric transducers with a built-in 40-dB preamplifier (Bruel and Kjaer, Naerum, Denmark). The frequency responses of the two transducers used in this study are shown in Figure 1. Transducer 1 was used for most studies, with transducer 2 employed for transducer comparisons. The transducer normally rested on a 1-in. foam pad to minimize the influence of laboratory bench vibrations.

The output of the transducer was connected to a Bruel and Kjaer Model 2638 wide band conditioning amplifier, which provides a variety of band-pass filters. A frequency range of 50 kHz to 2 MHz was selected for this work, since ultrasonic frequencies appear to encompass the bulk of acoustic activity (*4, 11*) and monitoring signals in this region avoids audio interference from the laboratory environment (*8*). Although the amplifier is rated to 2 MHz, the upper frequency is limited by the response of the transducer (about 1.2 MHz). The gain of the amplifier is switch

---

[1] Present address: Department of Chemistry, Dalhousie University, Halifax, Nova Scotia, Canada B3H 4J3.

0003-2700/89/0361-2638$01.50/0 © 1989 American Chemical Society

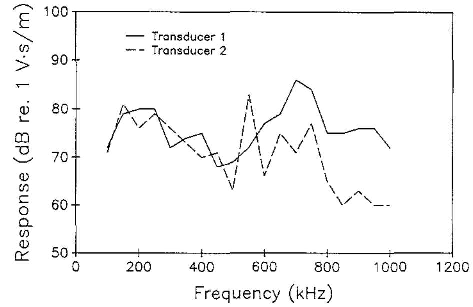

Figure 1. Frequency response of acoustic transducers employed in this study.

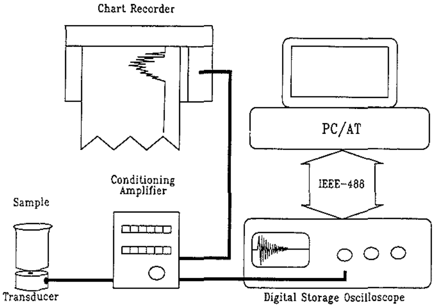

Figure 2. Experimental apparatus for acoustic emission experiments.

selectable over the range 0–60 dB in steps of 1 dB.

The amplifier used has two outputs available, a peak-detect output and a direct output. The peak-detect output responds instantly to the maximum peak amplitude of the signal burst and has a 200-ms decay constant to allow time for a chart recorder to respond. This permits the overall acoustic activity of the system to be monitored with a slow recording device. The direct output is simply the amplified and filtered signal. This was connected to the input of a Tektronix Model 2230 digital storage oscilloscope (Tektronix, Beaverton, OR). For all experiments conducted, a sampling interval of 200-ns was used and 1024 points were acquired per signal. The scope was pretriggered such that about 100 points were collected before the trigger point. The digital data with 8-bit resolution were transferred to a personal computer (12-MHz IBM PC/AT compatible, Nora Systems, Vancouver) via an IEEE-488 bus and stored on a hard disk for later processing. The maximum throughput of this system is approximately 0.5 signals/s.

The number of signals collected and the amplification required varied among systems. Details are given in Table I. The frequency of emissions varied as well, but in all cases the rate of arrival of signals was slow enough to allow individual bursts to be collected. Figure 3 shows the peak amplitudes measured for each set of signals as a function of time. These plots were generated by using data sets collected on the scope and reflect trends that were also observed with the chart recorder. All of the peak amplitudes have been normalized to the maximum for each group. Although common abscissas are shown, each group of signals was collected for a different period of time and does not necessarily represent a complete set of signals for the process. Data acquisition was stopped when (1) no further signals were observed, (2) enough signals had been collected for reliable analysis, or (3) it was felt that a significant change in the mechanism responsible for acoustic signals would occur if the data collection period was extended.

Chemical Systems. Eight chemical systems were examined in this study. These were the melting of ice, the hydration of quicklime, the hydration of silica gel (two cases), a solid–solid phase transition in hexachloroethane, the dissolution of sodium hydroxide and sodium carbonate in water, and effervescence of carbonated water. Each of the systems examined is described in more detail below. For convenience in referencing, each system has been labeled with a letter between A and H.

Table I. Experimental Information on Acoustic Emission Systems Studied

system	no. of signals	measurement period, min	relative intensity
A	44	4.2	1.5
B	35	4.5	1.0
C	24	1.3	710
D	100	4.8	1.4
E	104	7.8	2.0
F	27	1.8	1.1
G	108	10.3	2.0
H	58	2.2	3.9

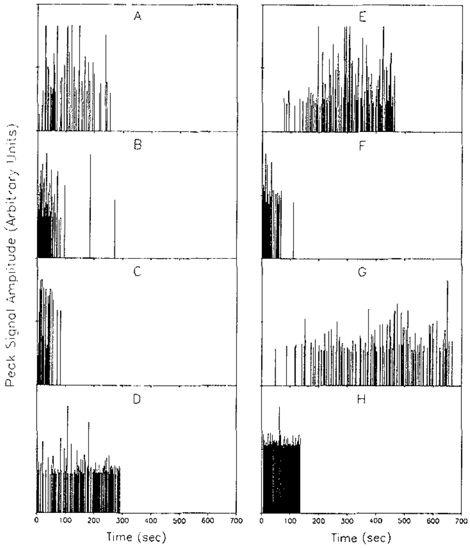

Figure 3. Peak amplitudes of acoustic signals collected for each chemical system studied as a function of time: A, melting ice; B, quicklime hydration; C, silica gel hydration I; D, silica gel hydration II; E, hexachloroethane solid–solid phase transition; F, sodium hydroxide dissolution; G, sodium carbonate dissolution; H, carbonated water. Amplitudes have been normalized to the maximum in each data set to permit comparison.

A. Ice. The melting of ice was used to study the reproducibility of the power spectrum as well as for the comparison of power spectra from different chemical systems. This system was chosen for the reproducibility studies because it was relatively easy to replicate conditions and because the power spectrum was quite broad. In all cases, 10 mL of distilled water was frozen overnight in a 30-mL beaker and then placed on the transducer at room temperature. Signals were collected during the initial stages of the process where signals from crystal fracture are believed to predominate.

B. Lime. The sample in this case was a 1-g pellet (roughly spherical) of reburned lime from a pulp mill (Donohue, St. Felicien, Quebec). The sample consisted primarily of CaO, with small amounts of MgO (0–2.5%) and quartz. The hydration (slaking) produces calcium hydroxide and is accompanied by the crumbling of the relatively hard pellet to form a powder. The reaction is slow unless the temperature is elevated. The sample was placed in a 30-mL beaker and about 15 mL of water just below the boiling point was added to initiate the reaction. Acoustic signals were monitored until the reaction appeared to be complete.

C. Silica Gel I. The hydration of silica gel is one of the most dramatic examples of acoustic emission. Granule fracture is easily audible and constitutes by far the largest signal observed in this study. The bottom of a 30-mL beaker was covered with an even layer of silica gel (6–20 mesh, about 1 g) and 10 mL of distilled water was added to initiate the reaction.

D. Silica Gel II. After the audible fractures described above for the hydration of silica gel have subsided, acoustic activity persists at a much lower level (see Table I). This activity arises from bubble release and (probably) from smaller inaudible fractures. By increasing amplifier gain, a new group of signals can be collected after the audible activity is complete.

E. Hexachloroethane. At a temperature of 43.6 °C, hexachloroethane undergoes a polymorphic phase transition. This transition is acoustically active and was monitored with our system. The sample of hexachloroethane is contained in a sealed tube which is suspended in a temperature bath. In this case, the acoustic transducer was coupled to the tube with a specially designed clamp. To prevent water damage, the transducer was enclosed in a plastic bag and electrical connections were sealed with silicone. Dilatometer readings were also made to monitor the transition. Experimental details of this system will be fully described in a forthcoming paper.

F. Sodium Hydroxide. The dissolution of sodium hydroxide in water is accompanied by the release of small bubbles that are the likely cause of the acoustic activity of the process. In this study, a layer of sodium hydroxide pellets (BDH, Toronto, Ontario) was placed at the bottom of a 30-mL beaker and about 15 mL of distilled water was added. The pellets were allowed to dissolve naturally with no stirring. Acoustic signals were collected during the initial stages of the process.

G. Sodium Carbonate. The dissolution of sodium carbonate, as with sodium hydroxide, is accompanied by the release of bubbles. A thin layer of anhydrous sodium carbonate crystals (BDH, Toronto, Ontario; about 0.5 g) was placed on the bottom of a 30-mL beaker and 10 mL of distilled water was added. Acoustic signals were recorded during the dissolution process.

H. Carbonated Water. A brief experiment was conducted with carbonated water as a system in which the release of bubbles is the only source of acoustic signals. About 15 mL of carbonated water (in the form of a clear soft drink) was added to a 30-mL beaker. Although the primary site of bubble nucleation was near the edge of the beaker and away from the active area of the transducer, adequate signals were obtained.

Data Processing. Oscilloscope signals were stored by Tektronix IEEE-488 driver subroutines as individual files. These files were merged into a single file for each experiment. The power spectrum for each signal was then calculated with a fast Fourier transform algorithm (*13*). Before the Fourier transforms were calculated, a Welch window (*13*) was generally applied to the signals to avoid problems caused by discontinuities at the beginning and end of the signal. Average power spectra were calculated from the individual spectra for each data set. For each of these data sets, individual power spectra were generally on the same order of magnitude.

RESULTS AND DISCUSSION

Effects of Windowing. As noted in the previous section, a Welch window was applied to the signals prior to computing the power spectrum. This was felt necessary since not all signals decayed to the background level by the time all 1024 points were collected. This leads to a discontinuity between the end of the data set and the pretrigger period which can adversely affect the results. The absence of a windowing function is equivalent to applying a square window to the data and this can cause excessive "leakage" among frequencies in the computation of the power spectrum. The use of more smoothly varying windowing functions is generally recommended in such cases (*13*). For the Welch window, each data point in the signal is multiplied by a weight, w_j, given by

$$w_j = 1 - \left(\frac{j - (N-1)/2}{(N+1)/2}\right)^2 \qquad (1)$$

where j is the point number (0 to 1023) and N is the number of points in the data set (1024). As with other window functions, this one rises gradually from zero at the edges of the data to unity at the midpoint.

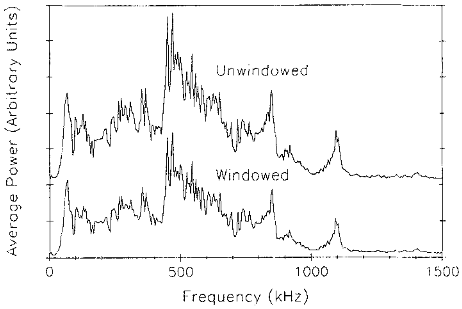

Figure 4. Effect of signal windowing on the average power spectrum of quicklime hydration. The upper spectrum has been offset two units on the ordinate.

To determine the effect that the windowing function was having on the characteristics of the power spectra, Fourier transforms were calculated with and without windowing. It was found that the effects were not significant. Minor changes were noted, especially when individual signals were transformed, but there were no differences in the overall features. There were virtually no differences for averaged power spectra. This is illustrated in Figure 4 which shows average power spectra from the hydration of quicklime computed in both ways. This particular process was used as an illustration since it produces a relatively broad power spectrum. The features of the two spectra in the figure are essentially identical, with a correlation coefficient of 0.996. As expected, the windowed spectrum is attenuated to some extent but the overall shape of the spectrum is unchanged. Although arguments can be made for and against the use of windowing, we have chosen to employ it for the remainder of the spectra presented here because of the nature of the signals.

Reproducibility Studies. In order to assess the utility of the power spectra obtained from the acoustic emission signals, it is first necessary to examine the reproducibility of the power spectra within a given chemical system and among transducers. To this end, four experiments were conducted with the melting ice system. Two experiments were conducted by using each of the two transducers, with the transducers being alternated between experiments. Three of the data sets contained 44 signals, while the other contained 42. The comparison utilized average power spectra rather than individual spectra for two reasons. First, the individual power spectra tend to differ more than the averages due to the variable characteristics of the particular acoustic source and its location. Thus, the average spectra offer a more consistent comparison. Second, a particular chemical system may emit more than one type of signal, making it difficult to compare spectra without knowing a priori the type of signal. In the case of ice, for example, at least two types of signals are suspected. Over the entire process, however, the proportion of signals of each type should be reasonably consistent.

The results of this study are shown in Figure 5. The power spectra in parts a and b of Figure 5 were obtained with transducer 1, while those in parts c and d were obtained with transducer 2. Comparison of the figures indicates that there is good reproducibility for power spectra obtained with the same transducer. The correlation coefficient for Figure 5a,b is 0.85, and that for Figure 5c,d is 0.92. On the other hand, reproducibility between transducers is not as good, although there are some similarities. This is expected since the fre-

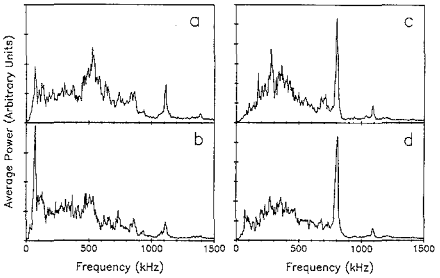

Figure 5. Effect of transducer on power spectra for melting ice. Parts a and b were obtained with transducer 1 and c and d with transducer 2. Spectra for transducer 1 have been scaled up by a factor of 1.5 for comparison.

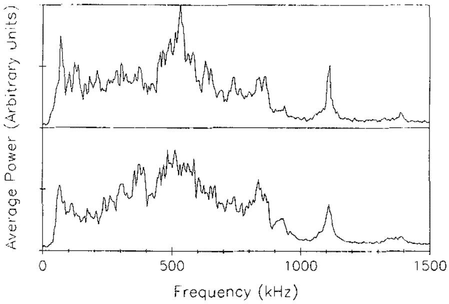

Figure 6. Effect of transducer age on average power spectrum of melting ice. The lower spectrum was obtained about 4 months before the upper one.

quency responses shown in Figure 1 exhibit significant differences. The correlation between parts a and c of Figure 5 is only 0.62, and that between the other pair is 0.61, verifying what can be observed directly.

Another important consideration is the reproducibility of a given transducer over time. As the piezoelectric element ages and is stressed by experimental conditions and general use, one would expect its frequency response to change. If these changes are rapid, the general utility of acoustic power spectra is diminished. To examine the dependence of power spectra on the age of the transducer, the average power spectrum for melting ice (shown in Figure 5a) was compared to one obtained more than 4 months earlier with the same transducer. In the interim, the transducer was routinely employed for a variety of studies. The two spectra, shown in Figure 6, are quite similar, with a correlation coefficient of 0.94. Differences can be attributed to experimental variability, so the transducer response appears to remain fairly constant, at least over a period of several months.

This study shows that the power spectra for a given chemical system can be regarded as reliable if the same transducer is used, but variations can be expected if another transducer is employed. Ideally, it should be possible to compensate for the variable frequency response of transducers mathematically, but in practice this is difficult for several reasons. First, the frequency calibration of a particular transducer is performed by the manufacturer and, while it is a useful guide, it probably lacks sufficient resolution for mathematical corrections. Furthermore, as already noted, the response is expected to change with other variables such as age and temperature. Routine laboratory calibration is difficult, requiring the appropriate apparatus and reference sources. Finally, given the fact that the transducer gain can change by 20 dB or more over the calibrated range, the dynamic range of the current data acquisition system (8 bits) is probably insufficient to permit correction without significant errors arising from quantization.

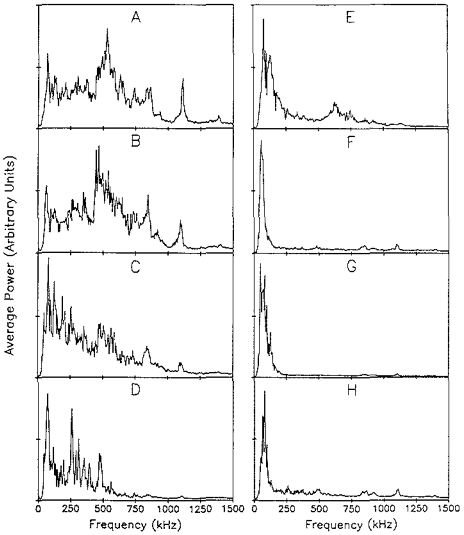

Figure 7. Average power spectra for chemical systems studied: A, melting ice; B, quicklime hydration; C, silica gel hydration I; D, silica gel hydration II; E, hexachloroethane solid–solid phase transition; F, sodium hydroxide dissolution; G, sodium carbonate dissolution; H, carbonated water. Spectra have been independently scaled to permit comparison.

Chemical Systems. Given that the power spectra are sufficiently reproducible, the next concern to be addressed is if there are significant differences among the spectra from different chemical systems. If so, these might be correlated with different processes occurring in those systems. Figure 7 shows the average power spectra from the eight chemical systems used in this study. All of the spectra were obtained with transducer 1 and have been scaled appropriately to allow easy comparison. The relative magnitudes of the signals before scaling are indicated in Table I. It should be noted that there is no particular chronological relationship among the experiments indicated in the figure. The experiments spanned a period of several months.

It is clear that there are significant differences among the spectra in Figure 7, but there also similarities exhibited among several systems. This indicates that the nature of the acoustic signals is associated with fundamental processes occurring within the system, and that these processes may be related in some cases. The most striking similarities are exhibited among systems F, G, and H. These are the dissolution of sodium hydroxide and sodium carbonate and the effervescence of carbonated water, respectively. In systems F and G, bubble release is believed to be the primary source of acoustic emission, and for system H it is known to be the only source. Thus, these low frequencies are believed to result from effervescence. Signals from these systems were obtained over a period of several days, so other sources of the correlation are unlikely. This conclusion is also in agreement with Belchamber et al. (*10*) who attributed low-frequency signals from silica gel to bubble release.

The similarities among spectra for systems F, G, and H are also reflected in the peak amplitude sequences shown in Figure 3. In each case, the peak amplitudes of acoustic signals remain fairly constant, an observation that is consistent with the mechanism of bubble release. For systems F and H (NaOH and carbonated water), bubble nucleation sites are essentially fixed and we would expect a constant peak amplitude. The crystals of sodium carbonate (system G) are smaller and more dispersed than the sodium hydroxide pellets, so bubble nucleation sites will be more spread out around the active area of the transducer. Consequently, a greater variability is observed in peak amplitudes.

All of the remaining power spectra show contributions at higher frequencies. These appear to be related to structural perturbations in the solid matrix. There are strong similarities between the spectra of melting ice (A) and the hydration of quicklime (B), and, to a lesser extent, the silica gel fracture (C). All of these systems involve crystal fracture. The two silica gel spectra (C and D) show similarities, but have some important differences. Although audible fractures are no longer occurring in Figure 7D, crystal fractures are likely still occurring at a lower level. There is also believed to be an important contribution from bubble release (*10*), a hypothesis supported by the dominance of low-frequency bands and the relatively constant peak amplitudes in Figure 3D. The spectrum in Figure 7C shows significant levels at higher frequencies that may arise from the fracture of large granules. This aspect remains to be studied.

The above results suggest that acoustic spectra can indicate important differences among dynamic chemical systems, although our current understanding yields mainly information about physical processes occurring rather than purely chemical interactions. Nevertheless, physical processes are important to chemists, as chemical transformations inextricably manifest themselves in physical form. By examination of the power spectra under different conditions, or as a function of time, important information might be revealed about successive or parallel mechanisms in the process. This capability, and the instrumental simplicity of AEA, indicate a potential for studying chemical processes and for industrial process control applications. Certainly more fundamental and applied studies of acoustic emission are warranted.

ACKNOWLEDGMENT

The authors thank J. T. Wearing and Gilles Dorris of the Pulp and Paper Research Institute of Canada for providing the lime samples and Oliver Lee for the hexachloroethane data.

LITERATURE CITED

(1) Beattie, A. G. *J. Acoust. Emiss.* **1983**, *2*, 95–128.
(2) Betteridge, D.; Connors, P. A.; Lilley, T.; Shoko, N. R.; Cudby, M. E. A.; Wood, D. G. M. *Polymer* **1983**, *24*, 1207–1212.
(3) Belchamber, R. M.; Betteridge, D.; Chow, Y. T.; Sly, T. J.; Wade, A. P. *Anal. Chim. Acta* **1983**, *150*, 115–127.
(4) van Ooijen, J. A. C.; van Tooren, E.; Reedijk, J. *J. Am. Chem. Soc.* **1978**, *100*, 5569–5570.
(5) Clark, G. M.; Garlick, R. *Thermochim. Acta* **1979**, *34*, 365–375.
(6) Howard, A. G.; Greenhalgh, D. A. *Anal. Chim. Acta* **1979**, *106*, 361–364.
(7) Betteridge, D.; Joslin, M. T.; Lilley, T. *Anal. Chem.* **1981**, *53*, 1064–1073.
(8) Sawada, T.; Gohshi, Y.; Abe, C.; Furuya, K. *Anal. Chem.* **1985**, *57*, 366–367.
(9) Sawada, T.; Gohshi, Y.; Abe, C.; Furuya; K. *Anal. Chem.* **1985**, *57*, 1743–1745.
(10) Belchamber, R. M.; Betteridge, D.; Collins, M. P.; Lilley, T.; Marczewski, C. Z.; Wade, A. P. *Anal. Chem.* **1986**, *58*, 1873–1877.
(11) Lonvik, K. *Thermochim. Acta* **1987**, *110*, 253–264.
(12) Belchamber, R. M.; Betteridge, D.; Chow, Y. T.; Hawkes, A. G.; Cudby, M. E. A.; Wood, D. G. M. *J. Comp. Mater.* **1983**, *17*, 420–434.
(13) Press, W. H.; Flannery, B. P.; Teukolsky, S. A.; Vetterling, W. T. *Numerical Recipes*; Cambridge University Press: New York, 1986; Chapter 12.

RECEIVED for review May 22, 1989. Accepted September 7, 1989. This work was funded by the Institute for Chemical Science and Technology (ICST) Grant 5-50886, and by NSERC Grant 5-80246. P.D.W. acknowledges support provided by ICST and by an NSERC Postdoctoral Fellowship.

Anal. Chem. 1989, 61, 2643–2647

Analytical Characteristics of β-Cyclodextrin/Salt Mixtures in Room-Temperature Solid-Surface Luminescence Analysis

Marsha D. Richmond and Robert J. Hurtubise*

Chemistry Department, University of Wyoming, Laramie, Wyoming 82071-3838

β-Cyclodextrin (β-CD)/salt mixtures were investigated as solid matrices for obtaining room-temperature fluorescence (RTF) and room-temperature phosphorescence (RTP) from adsorbed compounds. A 30% β-CD mixture produced strong luminescence signals from adsorbed compounds without the need for a heavy atom. Linear ranges, reproducibility, and limits of detection were obtained for *p*-aminobenzoic acid and phenanthrene. The selectivity demonstrated for the β-CD/NaCl mixtures should prove useful in mixture analysis. Also, it was shown that a saturated solution of β-CD was needed in the sample preparation step and also a matrix packing effect of the dried mixture was important to obtain strong luminescence signals. The spectra obtained with the 30% β-CD/NaCl mixture possessed more fine structure than those obtained with filter paper. The RTF and RTP spectra obtained with the 30% β-CD mixture were practically the same in structural detail as those acquired at low temperature. The powdered β-CD/NaCl mixtures were very easy to handle for low-temperature analysis, conventional luminescence equipment could be used, and only small amounts of analyte were needed to ensure good spectra.

INTRODUCTION

Room-temperature phosphorescence (RTP) analysis has developed into a very effective analytical technique for organic trace analysis. The utility of the approach has been discussed in reviews (*1–3*) as well as books (*4*, *5*). Although filter paper remains the most frequently used solid-surface in RTP analysis, other surfaces and solution media have also proved to yield good RTP signals from phosphors. Hurtubise and co-workers (*6*, *7*) used sodium acetate to determine the luminescence parameters of *p*-aminobenzoic acid (PABA). Su and Winefordner (*8*) used a variety of inorganic substrates to obtain the RTP characteristics of polycyclic aromatic hydrocarbons (PAHs). Femia and Cline Love (*9*) have reported the use of micelle-stabilized solutions to obtain RTP. Donkerbroek et al. (*10*) employed sensitized phosphorescence for obtaining RTP signals. Typical applications for RTP may be found in biological analysis (*11*), drug analysis (*12*), and environmental analysis (*13*).

Recently, the use of cyclodextrins was demonstrated in several areas of analytical chemistry. Cyclodextrins are glucose-containing oligosaccharides joined via α-1,4 linkages into a cone-shaped torus. The more commonly used cyclodextrins are those containing six, seven, and eight glucose units. These cyclodextrins are referred to as α-, β-, and γ-cyclodextrins, respectively. Cyclodextrins have the unique ability to sequester molecules in their hydrophobic cavity (*14*). They have been used as organic modifiers in mobile phases and/or as part of the stationary phase in high-performance liquid chromatography (HPLC) (*15*, *16*). Also, α-cyclodextrin was used as a spray reagent in thin-layer chromatography (TLC) (*17*). Blyshak et al. (*18*) employed cyclodextrins in aqueous solution extraction experiments. Scypinski and Cline Love (*19*) employed cyclodextrins in the presence of heavy atom to induce RTP in solution. Filter paper impregnated with α-cyclodextrin showed an increase in the RTP signal intensity for adsorbed phosphors over untreated filter paper (*20*). Bello and Hurtubise (*21*) demonstrated that an 80% α-cyclodextrin/sodium chloride (α-CD/NaCl) mixture induced RTP from polycyclic aromatics of various size and funtionality.

Bello and Hurtubise (*22*) have reported analytical figures of merit for the RTP and room-temperature fluorescence (RTF) of four model compounds with an 80% α-CD/NaCl mixture. They also investigated interactions responsible for observing RTP on α-CD/NaCl mixtures (*23*, *24*). Recently, it was demonstrated that a 1% α-CD/NaCl mixture could be used instead of an 80% α-CD/NaCl mixture with little loss in the analytical integrity of the signal (*25*). From these investigations, it was believed that β-cyclodextrin should also induce solid-surface RTP. β-Cyclodextrin (β-CD) has a somewhat larger cavity than α-CD, which enables β-CD to accommodate larger molecules than α-CD. The results in this paper illustrate the ability of β-CD/NaCl mixtures to induce RTF and RTP and show the analytically utility of β-CD/NaCl in solid surface luminescence analysis.

EXPERIMENTAL SECTION

Reagents. Benzo[*a*]pyrene, benzo[*f*]quinoline, and benzo[*e*]pyrene were all Aldrich Gold Label reagents and used as received. All other compounds were also purchased from Aldrich and recrystallized from distilled ethanol prior to use. Cyclohexane was Aldrich Gold Label. Ethylene dichloride (1,2-dichloroethane) was reagent grade and was purchased from Mallinkrodt (SpectrAR grade). The methanol and acetone were Photrex grade (J. T. Baker). The 2-propanol and water were HPLC grade and purchased from J. T. Baker. The β-cyclodextrin (Aldrich) was washed with distilled ethanol prior to use. The sodium chloride, sodium bromide, and sodium iodide were all reagent grade from J. T. Baker. All salts were washed with distilled ethanol prior to use. The nitrogen gas was passed through an Oxyclear tube (Alltech Associates, Inc.) to remove any oxygen. The filter paper used in acquiring room temperature spectra was developed in distilled ethanol twice to collect impurities at one end.

Instrumentation. All room temperature fluorescence (RTF) and RTP intensity measurements were obtained by use of a Schoeffel SD 3000 spectrodensitometer with a SD 300 computer. The source was a 200-W Hg–Xe lamp (Canrad-Hanovia, Inc.), and the detector was a R928 PMT (Hamamatsu Corp.). RTF and RTP and low-temperature fluorescene and phosphorescence excitation and emission spectra were collected with a Fluorolog 2+2 spectrofluorometer (Spex Industries). The detector was a water-cooled R928 PMT and a 450-W Xe lamp was used to excite the fluorescence of the samples. The phosphorescence spectra were obtained by using the Spex 1934C phosphorimeter accessory with programmable pulsed source and selectable gated detector. The data were processed with a Spex Datamate computer. The sample holders were previously described (*22*). For low-temperature solid-surface spectra, the dry powder was placed in a quartz tube and slowly submerged in liquid nitrogen, and then the spectra were collected.

Procedures. *Determination of Solubility of β-CD in Various Organic and Organic/Aqueous Solvents.* Saturated solutions of β-CD were prepared and stirred for 1 h. The solution was then filtered and three 25.00-mL aliquots were transferred into weighed beakers, and the solvent was allowed to evaporate at room temperature. After the solvent had evaporated, the beakers were

0003-2700/89/0361-2643$01.50/0 © 1989 American Chemical Society

placed in an oven at 100 °C for 1 h for additional drying. After this, the beakers were placed in a desiccator and allowed to come to room temperature and weighed. The solubilities obtained were the average of six trials except for 50:50 2-propanol/water which was the average of nine runs. The relative standard deviation for all solubility data was between 1.5 and 3.0%.

Preparation of Cyclodextrin Mixture. The β-CD/NaCl mixtures were prepared as follows. Appropriate amounts of β-CD were weighed out and combined with the amount of ground sodium chloride to yield the desired percentage of β-CD/NaCl mixture. The mixture was then stirred in a ball mill for 30 min to ensure a homogeneous mixture of β-CD and NaCl.

Sample Preparation for Intensity Measurements. Sample preparation for intensity measurements was as previously described for α-CD/NaCl (*22*), except for this study a 30% β-CD/NaCl mixture and a 50:50 methanol (MeOH)/water solvent were used.

Sample Preparation for Spectra Collection. Sample preparation for those samples used in the acquisition of excitation and emission spectra was carried out as follows. Into a small test tube, a 0.2-mL aliquot of 50:50 MeOH/H_2O was added along with a 5-μL aliquot of analyte solution and then 100 mg of 30% β-CD/NaCl mixture. The contents of the test tube were then sonicated for 10 s. The slurry was placed in an oven at 110 °C for 40 min. The dried sample was then placed into the sample holder and spectra were obtained. The samples for RTP measurements were degassed with nitrogen for approximately 10 min before their spectra were collected.

RESULTS AND DISCUSSION

Solvent Study. Previously it was believed that inclusion complex formation of cyclodextrins occurred exclusively in aqueous solution. However, Siegel and Breslow (*26*) reported that inclusion complex formation did occur in dimethyl sulfoxide (DMSO) and dimethylformamide (DMF). In 1984, Harada and Takahashi (*27*) reported that β-CD was able to form inclusion complexes in a variety of organic solvents. Recently, Patonay et al. (*28*) proposed a ternary structure for γ-cyclodextrin, pyrene, and 2-methyl-2-propanol (*tert*-butyl alcohol) in aqueous solutions. They reported that not only is size important for inclusion complex formation but hydrogen bonding with 2-methyl-2-propanol and the primary and secondary hydroxy groups of the cyclodextrin increased the effective hydrophobicity of the cyclodextrin cavity. Therefore, the solvent was found to play an active role in complex formation. Also, Patonay et al. (*28*) reported that other alcohols exhibited similar behavior but a less hydrophobic environment was found with these alcohols.

Because the desirable characteristics of a solvent for solid-surface luminescence include a low boiling point and ease of evaporation, water is not a good solvent because of its high boiling point, and many organic compounds are insoluble in water. However, cyclodextrins are only sparingly soluble in organic solvents. Bello and Hurtubise (*22*) reported the effect of various solvents on the luminescent intensity of several compounds with an 80% α-CD/NaCl mixture. They found that for the 80% α-CD/NaCl mixture, more intense signals were obtained by using methanol as a solvent over ethanol, 2-propanol, or other organic solvents such as cyclohexane, dichloroethane, and acetone. The larger solubility of α-CD in methanol compared to the other organic solvents was given as a factor for strong RTP signals. Table I gives the solubility results obtained in this work for β-CD. From Table I, it may be concluded that β-CD is more soluble in alcohol/water solvents. For example, there is a significant increase in the solubility of β-CD with the alcohol/water (50:50) solvents compared to the solubility in the pure alcohol. In fact, for 2-propanol/water, the solubility of β-CD was very high, namely, 3.250 g/100 mL.

Table I. Solubility of β-Cyclodextrin in Various Organic and Aqueous/Organic Solvents

solvent	solubility, g/100 mL
1,2-dichloroethane	0.000
cyclohexane	0.000
acetone	0.024
2-propanol	0.024
2-propanol/water[a]	3.250
ethanol	0.056
ethanol/water[a]	0.878
methanol	0.045
methanol/water[a]	0.295

[a] 50:50 (v/v)

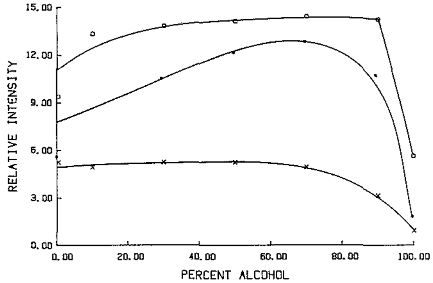

Figure 1. RTP intensity of 4-phenylphenol (100 ng) adsorbed on 30% β-CD/NaCl as a function of water present in methanol (□) ethanol (●), and 2-propanol (X).

Luminescence Characteristics of Compounds Adsorbed on β-CD/NaCl. Bello and Hurtubise (*22*) reported the effects of water content in alcohol solvents on the luminescence properties of compounds adsorbed on 80% α-CD/NaCl mixture. They observed a decrease in luminescence signals for alcohol solvents which had greater than 10% water content. Also, it was demonstrated that little change in intensity was found in the region of 0–10% water content. To determine if an increase in the β-CD solubility would correspond to an increase in luminescence intensity from the adsorbed compound, RTF and RTP intensity measurements were collected by varying the amount of water present in methanol, ethanol, and 2-propanol. These solvents were used to adsorb the compounds on the β-CD/NaCl mixture. For the compounds investigated, there was essentially no change in RTF intensity from 0 to 100% alcohol. For 4-phenylphenol, Figure 1 shows that the RTP intensity did not change much from 10% to 80% water. However, Figure 1 indicates smaller intensities were observed for pure water and pure alcohol. A MeOH/H_2O (50:50) solvent was chosen for future RTF and RTP work with β-CD/NaCl mixtures based on several criteria. This solvent composition was in the plateau region found in Figure 1, thereby allowing for good solubility of β-cyclodextrin without a large increase in drying time for the sample. Also, for most of the compounds studied, the methanol/water solvents gave the largest increase in signal over the other alcohol/water compositions investigated.

Figure 2 is a representative example of RTF and RTP intensity changes with different ratios of millimoles of β-CD to millimoles of analyte in several β-CD/NaCl mixtures. The following discussion pertains to RTP because it showed more dramatic changes in intensity than did RTF. There exists three regions of interest over the range of 0.01–80% β-CD in the β-CD/NaCl mixtures (Figure 2). On the basis of the solubility of β-CD in MeOH/H_2O (50:50), these regions may be defined in reference to the saturation point for β-CD in the solvent. The saturation point is indicated by the arrow in Figure 2. For the mixtures containing amounts of β-CD less than that required for a saturated solution in the sample preparation step, relatively low RTP intensities were observed.

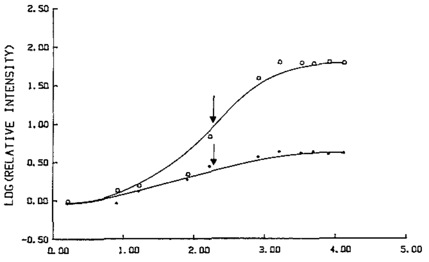

Figure 2. RTF (●) and RTP (□) intensity of PABA (100 ng) as function of β-CD present in β-CD/NaCl mixtures.

Table II. Compounds Examined for RTP and RTF with 30% β-CD/NaCl

compound	solution fluorescence[a]	RTP[b]	RTF[b]
phenanthrene	+	2	1[c]
perylene	+	28	78
tetracene	+	133	43
pyrene	+	16	1133
benzo[*a*]pyrene	+		2597
benzo[*e*]pyrene	+	17	413
4-phenylphenol	+	23	10
1-naphthol	+	166	281
2-naphthol	+	17	812
p-aminobenzoic acid	+	455	255
5,6-benzoquinoline	+	31	7
7,8-benzoquinoline	+	31	7
phenazine	−		
phthalic acid	+	1[d]	2714
terephthalic acid	−	24	5567
isophthalic acid	−	2	5428

[a] Key: +, signal observed; −, signal not observed. [b] 100 ng of analyte adsorbed on 30% β-CD/NaCl. [c] All fluorescence intensities relative to phenanthrene. [d] All phosphorescence intensities relative to phthalic acid.

However, there was a sharp increase in the RTP signal when a saturated solution (1.1% β-CD/NaCl mixture) was used to prepare the sample. The saturation point results in a millimole ratio of β-CD:analyte of 185. With samples prepared with amounts of β-CD greater than the saturation point, the RTP signal continued to increased until 10% β-CD/NaCl mixture corresponding to a millimole ratio of β-CD:analyte of 1680. From 10% to 80% β-CD content, the luminescence signals reached a plateau region and little increase in signal was observed with increasing amounts of β-CD in the β-CD/NaCl mixtures (Figure 2). This is similar to what was reported for α-CD/NaCl (*23*, *24*). In the work with α-CD/NaCl, a maximum RTP signal was almost reached when a saturated solution of α-cyclodextrin was used in the sample preparation step. Figure 2 illustrates that this is not true with β-CD. With β-CD there was a relatively large increase in RTP signal after the saturation point. This implies that not only is it necessary to have a saturated solution, which would ensure maximum complex formation in solution preparation step, but also packing of the dried matrix is important to ensure maximum signal from the phosphors with β-CD/NaCl mixtures. Current studies are underway which should lead to a better understanding of the interactions responsible for the increase in signal beyond the saturation point. A 30% β-CD/NaCl mixture was chosen for further analytical work because this percentage of β-CD was located well within the plateau region in Figure 2, which ensured stable luminescence signals, and because of the relatively small amount of β-CD in the mixture.

Spectral Characteristics. Table II gives a listing of compounds of varying geometry, size, and functionality that were found to give RTP and/or RTF when adsorbed on the 30% β-CD/NaCl mixture. Of the compounds listed in Table II, phthalic acid, terephthalic acid, isophthalic acid, and tetracene did not give RTP and/or RTF in earlier results with an 80% α-CD/NaCl mixture (*21*), but showed both RTF and RTP in this work. The preferential selectivity by α- and β-cyclodextrins for interactions with compounds should be useful for mixture analysis using cyclodextrin solid-surface luminescence analysis. Earlier, Bello and Hurtubise (*29*) showed that considerable selectivity could be obtained with 80% α-CD/NaCl. By using extraction, selective excitation, α-CD/NaCl mixtures and solution fluorescence, they developed a simple method for qualitative analysis of mixtures of polycyclic aromatic hydrocarbons (PAH). With their method, they were able to characterize, at nanogram levels, a nine-component mixture of PAH. It should also be noted that phenazine did not give RTP or RTF with α- and β-cyclodextrin.

Spectra obtained by using the 30% β-CD/NaCl mixture showed somewhat greater fine structure compared to spectra obtained with filter paper, which demonstrated a more homogeneous environment for the phosphor with the 30% β-CD/NaCl matrix. Figure 3 offers a comparison of the RTP spectra of phenanthrene obtained with β-CD/NaCl mixture and on filter paper. It is evident that the spectrum obtained with β-CD/NaCl gave slightly better resolution and somewhat sharper bands compared to the spectrum obtained with filter paper. A comparison of typical RTF and low-temperature fluorescence (LTF) spectra in which both spectra were obtained with the 30% β-CD/NaCl mixture is contained in

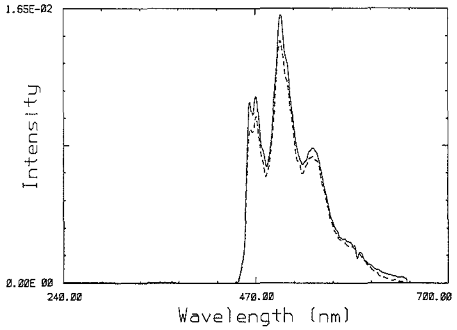

Figure 3. RTP spectrum (——) of 500 ng of phenanthrene with 30% β-CD/NaCl mixture and RTP spectrum (- - -) of 100 ng of phenanthrene on filter paper (0.1 μg/mL ethanol/H_2O (8:2) solution spotted).

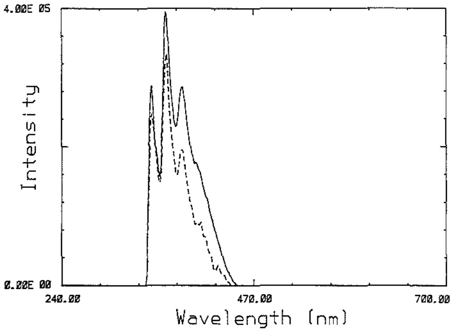

Figure 4. LTF spectrum (——) and RTF spectrum (- - -) of 500 ng of benzo[*f*]quinoline with a 30% β-CD/NaCl mixture.

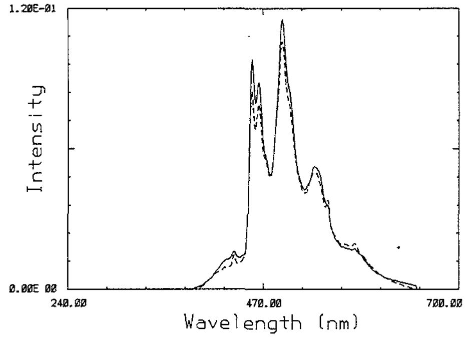

Figure 5. LTP spectrum (——) and RTP spectrum (- - -) of 500 ng of benzo[*f*]quinoline with a 30% β-CD/NaCl mixture.

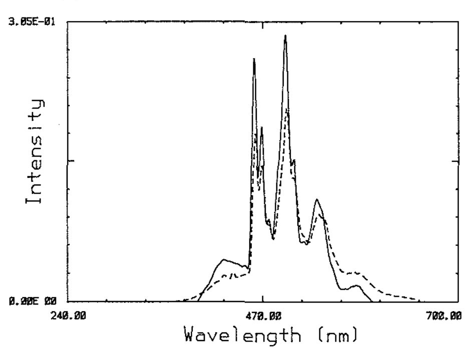

Figure 6. LTP (——) solution spectrum (0.1 μg/mL ethanol) and LTP (- - -) spectrum of 500 ng of phenanthrene with a 30% β-CD/NaCl mixture.

Figure 4. The low-temperature spectrum was obtained at liquid nitrogen temperature. There is only a slight loss in resolution and slight band broadening at room temperature for the fluorescence spectrum. Figure 5 demonstrates that there is also only slight loss in resolution and slight band broadening between RTP and low-temperature phosphorescence (LTP) spectra with β-CD/NaCl. Figures 4 and 5 clearly demonstrate that low temperature is not needed with β-CD/NaCl to obtain well-defined spectra.

In other spectral comparisons, the low-temperature solid-surface and low-temperature solution spectrum of phenanthrene show little loss in band structure with the 30% β-CD/NaCl solid-surface (Figure 6). The results in Figure 6 show that essentially equivalent spectral results were obtained at low temperature with a solid surface as were obtained with a solution at low temperature. It was found that there are other advantages for the β-CD/NaCl mixture over solutions for low-temperature luminescence analysis. For conventional low-temperature solution luminescence, either a solvent that forms a clear glass or special modifications for cracked or snowy solutions are required (*30*). For the 30% β-CD/NaCl mixture, the solvent requirements are somewhat less restrictive. The solvent is used to dissolve the analyte, to adsorb the solute on the surface, and to yield maximum signal intensity. The MeOH/H_2O solvent used with the 30% β-CD/NaCl mixture would not lend itself nicely to low temperature solution luminescence analysis because of snow formation and would require modifications for sample handling, such as those described by Aaron and Winefordner (*30*). The sample holder used with the β-CD/NaCl mixture is the same as for conventional low-temperature solution measurements. Therefore, no instrument modifications were required either for the solid matrix or sample holder. Also, the 30% β-CD/NaCl mixture was easier to handle than a solvent at low temperature. The 30% β-CD/NaCl mixture could be more rapidly placed in the liquid nitrogen, and cracked or snowy solutions were not a problem. The 30% β-CD/NaCl formed a very homogeneous mixture as a result of the sample preparation step; thus well-defined spectra were obtained.

Table III. Analytical Figures of Merit for Model Compounds with 30% β-Cyclodextron/NaCl and -NaBr Mixtures

	linear range, ng		LOD,[a] ng		RSD,[b] %	
compounds	RTF	RTP	RTF	RTP	RTF	RTP
PABA	0–600	0–400	0.60 (0.13)	0.25 (0.14)	3.0	2.6
phenanthrene	0–600	0–600	1.10 (0.60)	0.30 (0.15)	3.0	4.2

[a] LOD, limit of detection. LOD = ks_B/m, k = 3, s_B is the standard deviation of the blank, m = slope. Values for 30% β-CD/NaBr are in parentheses. [b] RSD, relative standard deviation. RSD was determined by using 100-ng samples.

Analytical Parameters for Model Compounds with 30% β-CD/NaCl Mixture. Table III contains the analytical figures of merit for *p*-aminobenzoic acid (PABA) and phenanthrene with 30% β-CD/NaCl mixture. These compounds were chosen on the basis of geometry, size, and functionality. They also represent a strong emitter (PABA) and weak emitter (phenanthrene) observed with the 30% β-CD/NaCl mixture.

The 30% β-CD/NaCl mixture yielded a linear range, reproducibility, and limit of detection comparable to those reported for the α-cyclodextrin/salt mixture (*22*). A 30% β-CD/NaBr mixture was also used to determine analytical figures of merit. The effect of the presence of a heavy atom can be seen in lower RTP limits of detection for both compounds. As shown in Table III, the RTF limits of detection were also lowered with NaBr. This may be due to more effective packing of the matrix; however, additional work would have to be done to prove this. It should be mentioned that with sodium bromide there was an increase in RTP intensity by a factor of approximately 2.5 for both PABA and phenanthrene. Sodium iodide was also investigated but failed to yield a useful dried sample because it reacted with the β-CD.

LITERATURE CITED

(1) Parker, R. T.; Freelander, R. S.; Dunlap, R. B. *Anal. Chim. Acta* **1980**, *119*, 189.
(2) Parker, R. T.; Freelander, R. S.; Dunlap, R. B. *Anal. Chim. Acta* **1980**, *120*, 1.
(3) Vo-Dinh, T.; Winefordner, J. D. *Appl. Spectrosc.* **1977**, *13*, 261.
(4) Hurtubise, R. J. *Solid Surface Luminescence Analysis*; Marcel Dekker: New York, 1981; Chapters 3, 5, and 7.
(5) Vo-Dinh, T. *Room Temperature Phosphorimetry for Chemical Analysis*; John Wiley & Sons: New York, 1984.
(6) von Wandruszka, R. M. A.; Hurtubise, R. J. *Anal. Chem.* **1976**, *48*, 1784.
(7) Ramasamy, S. M.; Senthilnathan, V. P.; Hurtubise, R. J. *Anal. Chem.* **1986**, *58*, 612.
(8) Su, S. Y.; Winefordner, J. D. *Microchem. J.* **1982**, *27*, 151.
(9) Femia, R. A.; Cline Love, L. J. *Anal. Chem.* **1984**, *56*, 327.
(10) Donkerbroek, J. J.; Elzas, J. J.; Gooijer, C.; Frei, R. W.; Velthorst, N. H. *Talanta* **1981**, *28*, 717.
(11) Gaye, M. D.; Aaron, J. J. *Anal. Chim. Acta* **1988**, *205*, 273.
(12) Long, W. J.; Su, S. Y.; Karnes, H. T. *Anal. Chim. Acta* **1988**, *205*, 279.
(13) Vo-Dinh, T.; Bruewer, T. J.; Colovos, G. C.; Wagner, T. J.; Jungers, R. J. *Environ. Sci. Technol.* **1984**, *18*, 477.
(14) Szejtli, J. *Cyclodextrins and Their Inclusion Complexes*; Akademiai Kiado: Budapest, 1982.
(15) Fujimura, K.; Ueda, T.; Kitagawa, M.; Takayanagi, H.; Ando, T. *Anal. Chem.* **1986**, *58*, 2668.
(16) Zukowski, J.; Sybilska, D.; Jurczak, J. *Anal. Chem.* **1985**, *57*, 2215.
(17) Alak, A.; Heilweil, E.; Hinze, W. L.; Oh, H.; Armstrong, D. W. *J. Liq. Chromatogr.* **1984**, *7*, 1273.
(18) Blyshak, L. A.; Rossi, T. M.; Patonay, G.; Warner, I. M. *Anal. Chem.* **1988**, *60*, 2127.
(19) Scypinski, S.; Cline Love, L. J. *Anal. Chem.* **1984**, *56*, 322.

(20) Alak, A. M.; Vo-Dinh, T. *Anal. Chem.* **1988**, *60*, 596.
(21) Bello, J.; Hurtubise, R. J. *Appl. Spectrosc.* **1986**, *40*, 790.
(22) Bello, J. M.; Hurtubise, R. J. *Anal. Lett.* **1986**, *19*, 775.
(23) Bello, J. M.; Hurtubise, R. J. *Anal. Chem.* **1988**, *60*, 1285.
(24) Bello, J. M.; Hurtubise, R. J. *Appl. Spectrosc.* **1988**, *42*, 619.
(25) Richmond, M. D.; Hurtubise, R. J. *Appl. Spectrosc.* **1989**, *43*, 810.
(26) Siegel, B.; Breslow, R. *J. Am. Chem. Soc.* **1975**, *97*, 6869.
(27) Harada, A.; Takahashi, S. *Chem. Lett.* **1984**, 2089.
(28) Patonay, G.; Fowler, K.; Shapira, A.; Nelson, G.; Warner, I. M. *J. Incl. Phenom.* **1987**, *5*, 717.
(29) Bello, J. M.; Hurtubise, R. J. *Anal. Chem.* **1988**, *60*, 1285.
(30) Aaron, J. J.; Winefordner, J. D. *Talanta* **1975**, *22*, 707.

RECEIVED for review July 17, 1989. Accepted September 14, 1989. Financial support for this project was provided by the Department of Energy, Division of Basic Energy Sciences, Grant DE-FG02-86ER13547. Such support does not constitute an endorsement by the Department of Energy of the views expressed in this article.

Evaluation of a Diode Laser/Charge Coupled Device Spectrometer for Near-Infrared Raman Spectroscopy

Yan Wang and Richard L. McCreery*

Department of Chemistry, The Ohio State University, Columbus, Ohio 43210

A charge coupled device (CCD) detector and turnkey diode lasers operating at 782 and 830 nm permit acquisition of Raman spectra in the near-infrared (near-IR) region. With adequate attention to instrumental variables such as filtering and laser characteristics, it was possible to obtain high signal to noise (S/N) spectra from dilute solutions of benzene in CCl_4 and pyridine in water. For the case of benzene in CCl_4, a detection limit of 2 mM and a linear dynamic range of over 900 in concentration were established. The ability of near-IR Raman spectroscopy with the CCD/diode laser spectrometer for reducing fluorescence was demonstrated with fluorescent samples such as nylon and Rhodamine 6G. Although these samples exhibit featureless broad-band fluorescence with a 515-nm laser, excellent Raman spectra were obtained with 782-nm illumination. Although fluorescence suppression may be less effective than that reported for Fourier transform Raman spectroscopy at 1064 nm, the sensitivity was substantially better, with high S/N spectra possible with low laser power and dilute solutions. For example, a spectrum with *S/N* = 74 was obtained for 0.1 M SO_4^{2-} in water with ca. 20 mW of 782-nm laser power at the sample.

INTRODUCTION

The Raman effect has many useful attributes for observing and monitoring solid, liquid, and surface samples, including subpicosecond time resolution, vibrational information without infrared light, surface selectivity, and often resonance enhancement. Accompanying these useful features are some drawbacks, particularly the weakness of the Raman effect and frequent interference from fluorescence, of either the target molecule or other components in the sample. These drawbacks have significantly constrained the breadth of samples that may be examined with Raman spectroscopy, compared to competitive techniques based on IR absorption. Two relatively recent instrumental developments have led to major improvements in Raman spectrometers which promise to greatly enhance its applicability. First, the application of multichannel detectors and accompanying refinement of spectrometer design have led to major signal to noise (S/N) enhancement for visible and UV Raman (*1–5*), with dilute solutions (*6*), surface monolayers (*7, 8*), and weak scatterers (*9*) being observed for the first time. Second, the combination of interferometers and near-IR lasers has resulted in Raman spectrometers capable of greatly suppressing fluorescence (*10–20*). This technique has become known as Fourier transform Raman spectroscopy (FT-Raman) and has extended the utility of Raman spectroscopy to fluorescent samples, mixtures, and other previously intractable analytes.

In a recent communication, we reported a combination of a charge coupled device (CCD) detector with a diode laser to obtain near-IR Raman spectra with a dispersive spectrograph and 782-nm illumination (*21*). Since CCD detectors have high quantum efficiency in the near-IR region compared to PMT's or intensified photodiode arrays (IPDA's) (*9, 22*) and operate at the shot noise limit, the CCD/diode laser Raman spectrometer has high sensitivity compared to FT-Raman. As concluded previously, the shorter laser wavelength required by the CCD photoresponse sacrifices some fluorescence rejection while providing major improvements in detection limits or significant decreases in required laser power, compared to FT-Raman with 1064-nm illumination (*21*). The current report has two objectives related to a more complete examination of the CCD/diode laser Raman spectrometer. First, the sensitivity and detection limits of the spectrometer will be optimized and compared to conventional PMT and IPDA spectrometers. Second, the system will be applied to several difficult samples, including fluorescent solids, mixtures, and dilute solutions.

THEORY

The variables that determine the S/N for a Raman spectrometer depend strongly on the spectrometer design and sample characteristics, so a general expression for S/N as a function of experimental variables would be unwieldy. For the current report, we will consider the common case of a solution illuminated by a beam of constant radius (a, cm) and uniform power density having a total power P_0 (photons s^{-1}). The total Raman scattering (photons sr^{-1} s^{-1}) from the sample is given by

$$I_R = P_0 \beta_s N_d^s d \qquad (1)$$

where β_s is the Raman cross section (cm^2 sr^{-1} molecule^{-1}), N_d^s the number density of analyte (molecules cm^{-3}), and d the length of the laser beam in the sample (cm). It is convenient to define the specific intensity, L (photons cm^{-2} sr^{-1} s^{-1}) by dividing the total Raman signal by the area from which it is

---

*Author to whom correspondence should be addressed.

© 1989 American Chemical Society

radiated (*23*). For the case of 90° observation, L is given by equation 2. Note that L does not depend on the spectrometer

$$L = \frac{P_0\beta_s N_d^s d}{2ad} = \frac{P_0\beta_s N_d^s}{2a} \qquad (2)$$

but rather on laser and sample characteristics. The best case for optimizing S/N is when the Raman scattering just overfills the spectrometer aperture (*6*), and the signal (counts) is given by equation 3. A_D is the area of the laser beam sampled by

$$S = LA_D\Omega TQt \qquad (3)$$

the spectrometer, Ω the collection efficiency (sr), T the spectrometer transmission including collection optics and any filters, Q the detector quantum efficiency (counts/photon), and t the measurement time for each resolution element. A_D is a function of entrance optics and spectrograph magnification but is ultimately limited by the detector or slit area, whichever is smaller. The multichannel advantage, if present, is exhibited in the measurement time t, since an N_c-channel spectrometer will monitor each resolution element N_c times longer than a single-channel scanning system. Stated differently, for a given total measurement time, the signal for a multichannel spectrometer will be N_c times larger than a single-channel system.

Noise in a photodetector has contributions from analyte scattering shot noise, background scattering shot noise, detector readout noise, and dark noise (*22*). For a CCD system monitoring weak scattering from solution, the readout and dark noise are usually negligible and the background scattering shot noise is generally large compared to analyte shot noise. Even with the single-grating spectrograph used here, proper filtering can reduce stray light to the point where inelastic background scattering from the sample solution is the major noise source. Assuming the S/N is background scattering shot noise limited, the noise equals the square root of background scattering (*24*), given by equation 4. The product $\beta_B N_d^B$ refers

$$N = \left(\frac{P_0\beta_B N_d^B}{2a}\Omega TA_D Qt\right)^{1/2} \qquad (4)$$

to all inelastic background scatterers, including solvents, impurities, background fluorescence, etc. Combining eq 2, 3 and 4, the S/N for a background shot noise limited case with 90° observation is given by equation 5. Assuming $\beta_B N_d^B$ is

$$S/N = \frac{\beta_s N_d^s}{(\beta_B N_d^B)^{1/2}}\left(\frac{P_0 A_D\Omega TQt}{2a}\right)^{1/2} \qquad (5)$$

constant for a given solvent, sample matrix, etc., the S/N is linear with analyte concentration (N_d^s), but has a square root dependence on laser power, $A_D\Omega$ product, Q, and t. If analyte rather than background shot noise becomes dominant (e.g. at high analyte concentration), the S/N will depend on $(N_d^s)^{1/2}$ rather than N_d^s. Finally, for a given total measurement time, a single-channel spectrometer spends only t/N_c seconds per spectral resolution element, yielding the $N_c^{1/2}$ improvement in S/N for multichannel systems, assuming all else is equal. The $N_c^{1/2}$ multichannel advantage is not always fully realized due to differences in spectrometer design, including dispersion, A_D, etc. (*6*). For example, a higher dispersion single-channel system may reduce the expected $N_c^{1/2}$ advantage by permitting wider slits than a multichannel system for a given resolution. However, multichannel systems in general lead to a significant, often essential, improvement in S/N.

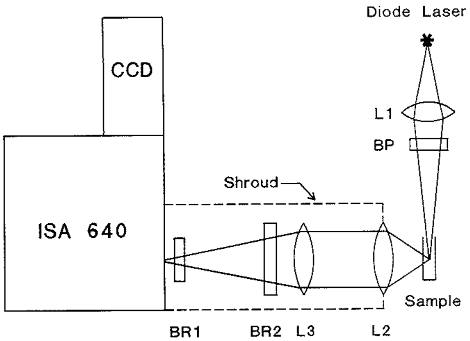

Figure 1. Optical diagram showing filter placement. L1 is a focusing lens built into the diode laser, L2 is a 50 mm *f*/1.4 camera lens, and L3 is a 25 cm *f*/5 biconvex lens. BP, BR1, and BR2 are filters described in the text. The shroud was made from opaque cloth.

EXPERIMENTAL SECTION

The Photometrics PM512 CCD detector was described previously (*21*), as was the Liconix "Diolite" diode laser system. The CCD was maintained at −110 °C in all cases. Both 782-nm (Sharp LT024MD) and 830-nm (Sharp LT015MD) diode lasers were used, both operated at 10 °C. The significantly below ambient operating temperature was recommended by Liconix to maximize temperature stability and reduce drift. At 10 °C, no indication of mode hopping was observed and drift was within the line width of the Raman bands observed. The ISA 640 single-grating spectrograph employed 300 lines/mm (blazed at 1.0 μm) and 150 lines/mm (blazed at 500 nm) classically ruled gratings. The lasers were focused directly into the sample by using their built in focusing lenses, with no additional mirrors or lenses. With the sample approximately 15 cm from the laser head, the beam was about 100 μm in diameter at its waist. The broad-band interference reported earlier (*21*) was reduced but not eliminated by a band-pass filter between the laser and sample, implying that the interference is not due totally to spontaneous emission from the laser, as previously believed. The interference was greatly reduced by carefully preventing stray laser light from entering the spectrometer, mainly by encasing the collection optics in opaque cloth. For minimum interference, it was important to ensure that all light entering the spectrograph passed through both laser line rejection filters as discussed below. The entrance slit width varied from 50 to 150 μm.

Collection optics were oriented at 90° to the laser beam axis, using parallel polarization (Figure 1). An interference band-pass filter BP (special order from Oriel, number 784BP10) was placed after the laser focusing lens and had a peak transmission of 65% at 782 nm. The band-rejection filters BR1 and BR2 (special order from Pomfret research, Orange, VA) were oriented as shown. On the basis of manufacturer's claims and local testing, input angles to BP, BR1, and BR2 deviating from normal by less than 10° degrade filter performance only slightly. BR1 and BR2 each have an optical density of ca. 3.0 at the relevant laser line, with ca. 75% transmission greater than 20 nm away from the rejection wavelength. However, the transmission varies periodically by ±10% due to interference effects in the filters, thus introducing intensity variations discussed below. The product TQ for the optics and detector was determined by recording the spectrum of an ordinary tungsten desk lamp. If one assumes the lamp output is constant over the wavelength region monitored by the spectrometer, a plot of TQ vs $\Delta\bar{\nu}$ was determined and is most useful when normalized to a maximum value of 1.0 as in Figure 2. Correction of a raw spectrum for variations in Q, filter transmission, spectrograph transmission, and collection optics transmission with wavelength were accomplished by dividing the raw spectrum by the normalized TQ vs $\Delta\bar{\nu}$ curve. Separate TQ vs $\Delta\bar{\nu}$ curves were determined for each laser wavelength, as shown in Figure 2. For all spectra, the pixel number of the raw spectrum was converted to $\Delta\bar{\nu}$ after calibration with known Raman peaks from common solvents. Throughout the text and figures, "intensity" refers to the output of the analog to digital (A/D) converter in the CCD system. For all spectra obtained at low concentrations, it was verified that the analyte signal was much smaller than the background level, implying the S/N is background noise limited. Unless stated otherwise, a background spectrum with the laser

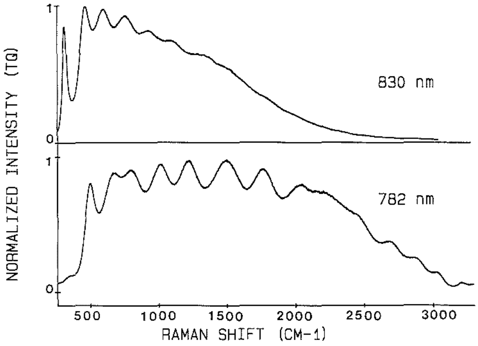

Figure 2. CCD response for a common tungsten desk lamp passing through L2, L3, and BR filters. CCD output was normalized to a maximum value of 1.0 and plotted vs the Raman shift relative to 782 or 830 nm. Each curve is a composite of several spectra covering different portions of the Raman shift range. BR1 and BR2 were chosen to match the corresponding laser. Only BR1 was present for the 830-nm curve, while both BR1 and BR2 were in place at 782 nm.

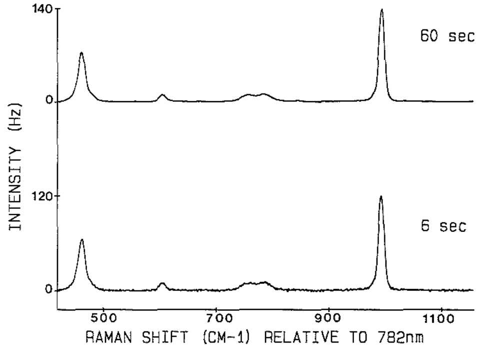

Figure 3. Spectra of 4.0 M benzene in CCl_4 obtained with the 782-nm laser (20 mW at sample), 300 lines/mm grating, 75-μm entrance slit, CCD integration times as shown. BP and BR1 were in place, but not BR2.

off was subtracted from all spectra to correct for CCD bias and dark counts.

Benzene, CCl_4, $(NH_4)_2SO_4$, pyridine, and methanol were reagent grade. Rhodamine 6G was obtained from Lambda Physik (Lambdachrome 5900), and the nylon sample was a common machine screw.

RESULTS AND DISCUSSION

The spectrometer was first evaluated with the 782-nm laser and dilute solution samples, in order to assess sensitivity. Figure 3 shows spectra of 4.0 M (36%) C_6H_6 in CCl_4, in this case with only BP and BR1 in place. Not only are both components easily observed with a 6-s integration time but the S/N of the spectra exhibit the $t^{1/2}$ dependence predicted from eq 5. Figure 4 shows a similar sample, but after dilution of benzene by a factor of 400. It demonstrates a useful S/N even at a concentration as low as 0.01 M (0.1%) benzene in CCl_4. The observation of small bands in the presence of large ones, as shown in Figure 4, is difficult with interferometric detection, because the scattering from the large band is distributed over the entire interferogram, causing noise in transformed spectra near large bands.

$(NH_4)_2SO_4$ in water has been used previously for comparison of multichannel spectrometers (*4*, *6*). Figure 5 shows spectra for three concentrations of aqueous $(NH_4)_2SO_4$ obtained with the CCD/diode system at 782 nm. The 0.1 M spectrum has a S/N which is comparable to that obtained with 100 mW of unfocused 515-nm light and an IPDA detector (*6*). However, this comparison should be considered semiquantitative since the beam focus (*a*, cm) and power were not matched for the two lasers. As N_d^s and t are varied for the three spectra, the S/N varies in accordance with eq 5. The detection limit extrapolated from the 0.01 M spectrum is 0.002 M $(NH_4)_2SO_4$ for a S/N of 2, defined as the average signal height divided by the standard deviation of the background noise. For the case of pyridine in water shown in Figure 6, comparable results were obtained, with a submillimolar detection limit.

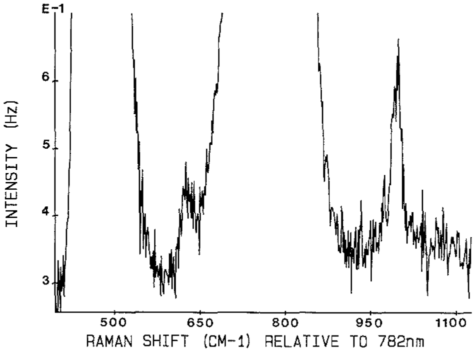

Figure 4. Spectra of 0.01 M benzene in CCl_4. Laser conditions were the same as those given in Figure 3. Intensity expressed as CCD A/D units per second of laser exposure. BP, BR1, BR2 were in place, 30 min integration time; slit width = 125 μm. The large peaks extending off scale at 459 and ~780 cm^{-1} are due to the CCl_4 solvent.

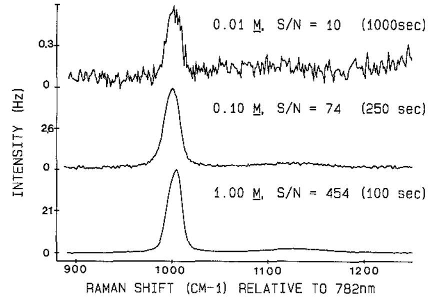

Figure 5. Spectra of various concentrations of $(NH_4)_2SO_4$ in water. Conditions were the same as given in Figure 4, except for integration time, which is shown in parentheses. Solvent background was subtracted after acquiring a spectrum of pure water.

The linearity of signal vs concentration for the benzene/CCl_4 case was determined by measuring the benzene (992 cm^{-1})/CCl_4 (459 cm^{-1}) peak intensity ratio as a function of the molar concentration ratio of benzene to CCl_4. In order to cover a wide range of concentration, the results were plotted in log/log format (Figure 7). Note that the peak ratio is linear (slope of log/log plot = 0.92) over a dynamic range of 900. While the detection limits for benzene, pyridine, and $(NH_4)_2SO_4$ are very good by normal Raman standards, there is substantial room for improvement by using fiber optics and a long sample tube (*25*, *26*). On the basis of results with visible lasers, it should be possible to extend the CCD/diode laser detection limit down to 10^{-5}–10^{-4} M for benzene in CCl_4 (*25*).

Several filter, grating, and laser wavelength combinations were tested with several unconventional samples, some of which are fluorescent. In the absence of any filters, the Stokes

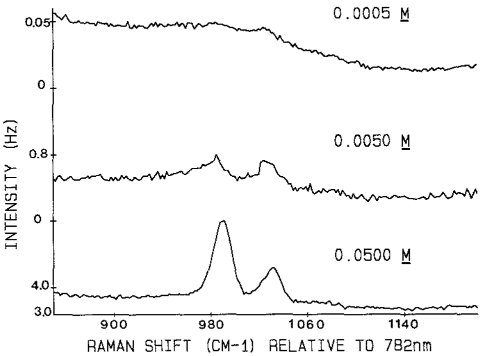

Figure 6. Spectra of pyridine in water: 782-nm laser, 20 mW at sample, 63-μm slit, BP & BR1 in place, 300 lines/mm grating; 100 s integration time for lower spectrum, 1200 s for the remaining two. Solvent background was corrected as in Figure 5.

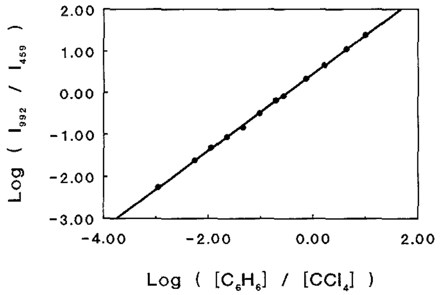

Figure 7. Ratio of the intensity of the 992-cm^{-1} band of benzene to the 459-cm^{-1} band of CCl_4 as a function of the ratio of benzene to CCl_4 concentrations. Conditions were the same given in as Figure 4, except integration time varied from 10 to 100 s.

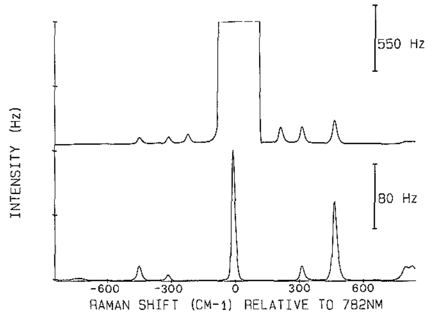

Figure 8. Spectrum of neat CCl_4 obtained with 782-nm laser, 150 grooves/mm grating, and 25-μm slit: upper spectrum, only BP in place, 20 mW at sample, 15-s integration time; lower spectrum, BP and BR1 in place, 20 mW at sample, 60-integration time. Neither spectrum was corrected by dividing by TQ ($\Delta\bar{\nu}$).

and anti-Stokes lines of CCl_4 were easily observed (Figure 8) with a 150 lines/mm grating. Despite the intense, unfiltered Rayleigh scattering, detector blooming or stray Rayleigh light did not interfere with the Raman peaks. Note that BR1 and BR2 have rejection bands ca. 40 nm wide, which affect the Raman shift range of ±500 cm^{-1} relative to a 782-nm laser. Thus the intensities of the CCl_4 peaks between +400 and −400 cm^{-1} are distorted or eliminated if BR1 and/or BR2 are in place (lower spectrum).

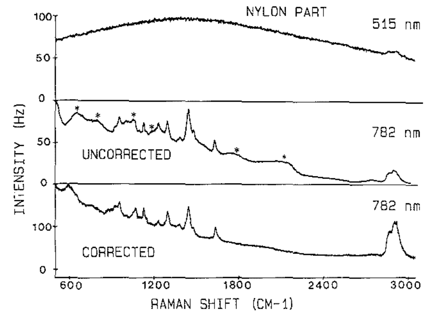

Figure 9. Spectra of nylon obtained with both 515- and 782-nm illumination: 300 grooves/mm grating, upper spectrum recorded with Spex 1403 scanning spectrometer. Second spectrum is a composite of six CCD spectra recorded with BP, BR1, and BR2 in place: 75-μm slit, 20 mW at sample, 60-s integration time. Lower spectrum is same data after division by TQ ($\Delta\bar{\nu}$) spectrum shown in Figure 2. Asterisks indicate artificial peaks caused by transmission of BR1 and BR2, and detector Q.

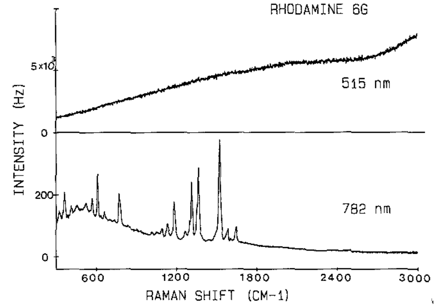

Figure 10. Spectra of Rhodamine 6G powder. Conditions were the same as given in Figure 9 (corrected), except integration time for each spectral segment was 10 s.

Due to the much higher intensity of scattered light, the band rejection filters are indispensable for most solids samples. Figure 9 shows several spectra of nylon which demonstrate the utility of the CCD/diode laser system for a fluorescent sample. The upper spectrum in Figure 9 was obtained with a Spex 1403 double monochromator and 515-nm illumination. Since the 1403 has excellent stray-light performance, the broad spectrum is attributable solely to fluorescence of nylon when illuminated by 515-nm light. The middle plot in Figure 9 is a spectrum of the same sample obtained at 782 nm with BR1 and BR2 in place. While Raman peaks are discernible, they are distorted by variation in filter transmission and detector Q with wavelength. After division by TQ ($\Delta\bar{\nu}$) (from Figure 2), the spectrum is very similar to that for Nylon 66 obtained with FT-Raman instruments (*27*). As apparent from the corrected spectrum, there is residual fluorescence present at 782 nm which was not observed at 1064 nm. This fluorescence is modulated by BR1 and BR2, yielding the artifactual peaks in the uncorrected spectrum. As predicted previously, spectra obtained at 782 nm exhibit less fluorescence reduction than those at 1064 nm. However, the CCD/diode system is operating at very low power (20 mW at sample) compared to most FT-Raman systems and required less than 30 s of integration time. Spectra of nylon were not acquired with 830-nm illumination because the corresponding BR filter was not available at the time the work was carried out. Solid and solution spectra of highly fluorescent Rhodamine 6G are shown in Figures 10 and 11. The spectrum of the solid

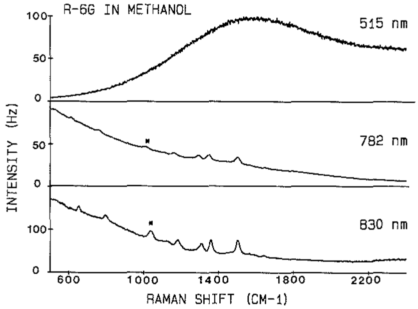

Figure 11. Spectra of Rhodamine 6G in methanol obtained at three laser wavelengths. BR1 was in place for 782- and 830-mm spectra, but BP and BR2 were not. Integration time was 10 s for 782-nm spectrum and 25 s for 830-nm spectrum, 75-μm slit. Laser powers were 30 mW (782 nm) and 40 mW (830 nm) at sample. The 782- and 830-nm spectra are composites of two CCD spectra obtained with 150 grooves/mm grating. Peak marked with an asterisk is due to MeOH.

obtained at 782 nm demonstrates reduction of the broad-band fluorescence observed with 515-nm light. The residual fluorescence is comparable to that observed with 1064-nm excitation (*12*) and is not an impediment to spectral interpretation. Spectra of Rhodamine 6G in methanol permit comparison of 515-, 782-, and 830-nm excitation, as shown in Figure 11. On the basis of Figure 11, the ratio of the 1500-cm^{-1} Raman intensity to the broad-band fluorescence intensity is 27% for the spectrum obtained with the 782-nm laser, while it is 79% with the 830-nm laser. Thus the longer the laser wavelength, the lower the fluorescent background, and this trend should continue as the laser wavelength extends further into the infrared region. With a silicon-based CCD detector, this improvement in fluorescence rejection is accompanied by a trade-off with decreasing the detector *Q*.

The importance of the BR1, BR2, and BP filters was strongly dependent on the sample. For relatively strong Raman scatterers exhibiting relatively weak elastic scattering, such as neat liquids or concentrated (>0.1 M) solutions, no filtering was necessary. A wide range of samples considered "typical" before the advent of multichannel and multiplex spectrometer can be examined with the CCD/diode laser system without filters. For weak scatterers (e.g. dilute solutions) or samples with strong elastic scattering (e.g. solids), filtering is necessary. BR1 and BR2 reduce the elastic scatter at the cost of eliminating the spectrum below 500 cm^{-1}. BP did improve the broad-band background for solid samples, since some of the background is attributable to broad-band spontaneous emission from the diode laser. Although the user must be conscious of this source of background, it is easily eliminated by BP with a 35% reduction in laser power available at the sample. On comparison of the filtering requirements of the CCD/diode laser spectrometer to conventional dispersive spectrometers with ion lasers, BP is analogous to a plasma line rejection filter, and the need for BR1 and BR2 is a strong function of spectrograph type. They were used here in order to exploit the high throughout of a single grating spectrograph but should be unnecessary with double or triple spectrograph designs.

As noted previously (*21*) the useful Raman shift range of the CCD/diode laser system is dictated by the quantum efficiency vs wavelength curve of the CCD. The gradual changes in the *TQ* ($\Delta\bar{\nu}$) curves in Figure 2 above 500 cm^{-1} reflect the CCD photoresponse. With BR1 and BR2 in place, *TQ* is near zero for $\Delta\bar{\nu}$ <500 cm^{-1} and when $\Delta\bar{\nu}$ approaches 3000 cm^{-1}. For the 782-nm laser, Raman shifts above 3000 cm^{-1} are observable, albeit at relatively low *Q*. For the 830-nm laser, it will be difficult to observe Raman shifts above about 2500 cm^{-1}. The restricted Raman shift range available with longer laser wavelength is accompanied by improved fluorescence reduction, so the choice of laser will depend on sample requirements.

CONCLUSIONS

The very high sensitivity, low laser power, solid-state design, short spectral acquisition time, and useful fluorescence reduction make the CCD/diode laser spectrometer a viable alternative to FT-Raman with an interferometer and Nd:YAG laser. For dilute solutions, weak scatterers, thermolabile samples, or dilute components of mixtures, the CCD/diode laser system will usually outperform the FT Raman systems. On the other hand, FT-Raman instruments have better wavelength accuracy and spectral range and should ultimately have lower fluorescence interference when operated at 1064 nm. As noted previously (*21*) the choice of spectrometer type will depend on the sample.

ACKNOWLEDGMENT

The authors thank Bruce Chase, Prabir Dutta, and Terry Gustafson for useful comments and James Williamson for technical assistance.

LITERATURE CITED

(1) Schlotter, N. E.; Schaertel, S. A.; Kelty, S. P.; Howard, R. *Appl. Spectrosc.* **1988**, *42*, 746.
(2) Chang, R. R.; Long, M. B. In *Topics in Applied Physics*; Cardona, M., Guntherodt, G., Eds.; Springer-Verlag: Berlin, 1982; Vol. 50, Chapter 3.
(3) Howard, R.; Maynard, M. *Appl. Spectrosc.* **1986**, *40*, 1245.
(4) Freeman, J. J.; et al. *Appl. Spectrosc.* **1981**, *59*, 1285.
(5) Asher, S. A.; Flaugh, P. L.; Washinger, G. *Spectroscopy (Springfield, Oregon)* **1986**, *1*, 26.
(6) Packard, R. T.; McCreery, R. L. *Anal. Chem.* **1987**, *59*, 2631.
(7) Campion, A.; Brown, J.; Grizzle, W. M. *Surf. Sci.* **1982**, *13*, 38.
(8) Meier, M.; Carron, K. T.; Fluhr, W.; Wokaun, A. *Appl. Spectrosc.* **1989**, *42*, 1066.
(9) Murray, C. A.; Dierker, S. B. *J. Opt. Soc. Am. A* **1986**, *3*, 2151.
(10) Chase, D. B. *J. Am. Chem. Soc.* **1986**, *108*, 7485.
(11) Zimba, C. G.; Hallmark, V. M.; Swalen, J. D.; Rabolt, J. F. *Appl. Spectrosc.* **1987**, *41*, 721.
(12) Chase, D. B. *Anal. Chem.* **1987**, *59*, 881A.
(13) Lewis, E. N.; Kalasinsky, V. F.; Levin, I. W. *Anal. Chem.* **1988**, *60*, 2306.
(14) Parker, S. F.; Williams, K. P.; Mendia, P. J.; Turner, A. J. *Appl. Spectrosc.* **1988**, *42*, 796.
(15) Lewis, N.; Kalasinsky, V. F.; Levin, I. W. *Anal. Chem.* **1988**, *60*, 2658.
(16) Angel, S. M.; Katz, L. W.; Archibald, D. D.; Honigs, D. E. *Appl. Spectrosc.* **1988**, *43*, 367.
(17) Angel, S. M.; Katz, L. W.; Archibald, D. D.; Lin, L. T.; Honigs, D. E. *Appl. Spectrosc.* **1988**, *42*, 1327.
(18) Chase, D. B.; Parkinson, B. A. *Appl. Spectrosc.* **1988**, *42*, 1186.
(19) Lewis, E. N.; Kalasinsky, V. F.; Levin, I. W. *Appl. Spectrosc.* **1988**, *42*, 1188.
(20) Crookell, A.; Fleischmann, M.; Hanniet, M.; Hendra, P. J. *Chem. Phys. Lett.* **1988**, *149*, 123.
(21) Williamson, J. M.; Bowling, R. J.; McCreery, R. L. *Appl. Spectros.* **1989**, *43*, 372.
(22) Bilhorn, R. B.; Sweedler, J. V.; Epperson, P. M.; Denton, M. B. *Appl. Spectrosc.* **1987**, *41*, 1114 and 1125.
(23) Schwab, S. D.; McCreery, R. L.; Gamble, F. T. *Anal. Chem.* **1986**, *58*, 2486.
(24) Ingle, J. D.; Crouch, S. R. *Spectrochemical Analysis*; Prentice-Hall: Englewood Cliffs, NJ, 1988; pp 141–142.
(25) Schwab, S. D.; McCreery, R. L. *Appl. Spectrosc.* **1987**, *41*, 126.
(26) Schwab, S. D.; McCreery, R. L. *Anal. Chem.* **1984**, *56*, 2199.
(27) Purcell, F. J.; Heinz, R. E. *Am. Lab.* **1988**, (August), *34*.

RECEIVED for review July 10, 1989. Accepted September 20, 1989. This work was supported by the Chemical Analysis Division of The National Science Foundation and by Dow Chemical Corporation.

Anal. Chem. **1989**, *61*, 2652-2658

Copper Atomization Mechanisms in Graphite Furnace Atomizers

Pingxin Wang, Vahid Majidi,[1] and James A. Holcombe*

Department of Chemistry, The University of Texas at Austin, Austin, Texas 78712

Cu atomization from a graphite surface has been investigated with the use of thermal desorption mass spectrometry, atomic absorption spectrometry, and computer simulations. The Cu atomization from a sample deposited as an aqueous $Cu(NO_3)_2$ solution is postulated to be a first-order desorption process with the activation energy of 31 ± 2 kcal/mol, suggesting that the desorption of copper atoms from the graphite surface at individual active sites is the rate-limiting step. Powder samples of copper metal and of copper oxide atomize by different mechanisms, but both powders behave similarly and exhibit a measured activation energy between 45 and 60 kcal/mol. The comparison between the powder samples and aqueous solutions revealed that copper oxide molecules are dispersed prior to reduction by carbon for the aqueous solutions. The reactions occurring for aqueous solution samples are $Cu(NO_3)_2(s) \rightarrow CuO(ads) \rightarrow Cu(ads) \rightarrow Cu(g)$. Computer simulations and experimental results have shown that copper dimer may form from gas-phase reactions at higher concentrations, but the gaseous dimer is not generated from the graphite surface. The lower appearance temperatures of the Cu signal under vacuum conditions in comparison with those at atmospheric pressure may be due to the absence of readsorption and unfavorable conditions for copper dimer formation in vacuo.

INTRODUCTION

Cu release from a graphite surface has been studied extensively (*1–12*). Table I summarizes those studies in which a value for the energetics of free-atom formation have been postulated. As illustrated in Table I, there is little agreement either on the process governing atom formation or on the energies involved in the production of gaseous Cu.

By using the tailing portion of the absorbance profile and assuming isothermal conditions, Fuller (*3*) obtained a 33 kcal/mol activation energy value for Cu atomization and suggested that the carbon reduction of copper oxide is the rate-determining step. By using the leading edge of the absorbance profile, Sturgeon et al. (*5*) obtained 77 and 44 kcal/mol for Cu atomization activation energy, E_a, values in the temperature regions below and above 1400 K, respectively. They suggested sublimation of solid Cu takes place in the lower temperature region and decomposition of $Cu_2(g)$ occurs at higher temperatures. Smets (*7*) utilized the initial stage of the atomization signal and suggested that the Cu samples are reduced to the elemental form by carbon, and the subsequent vaporization of the metal would be the rate-determining step. His E_a value of 74 kcal/mol correlates with the reaction enthalpy at the temperature given. By using different models proposed by various researchers (*5–7*), Frech et al. (*9*) compared E_a values for copper atomization and stated that useful information is difficult to extract from energy values obtained with these methods because of the large standard deviations. McNally and Holcombe (*12*) obtained the activation energy of release of 30 ± 2 kcal/mol for Cu by applying the Smets model to the initial stage of Cu atomization and suggested that a relatively strong Cu–graphite interaction exists in the atmospheric pressure system. They further suggested that Cu desorbs from the graphite surface as individual atoms.

Table I. Copper Atomization Mechanisms Proposed and Activation Energy E_a Values Obtained by Different Authors

proposed rate-determining step	E_a, kcal/mol	temp region, K	ref
Cu diffusion in GFA	23	>1540	1
atoms lost from disk nuclei edges (vacuum conditions)	47[a]		2
$Cu_2O + C \rightarrow 2Cu(s/l) + CO$	33	>1720	3
$Cu(s) \rightarrow Cu(g)$	77	<1400	5
$Cu_2(g) \rightarrow Cu(g)$	44	>1400	
Cu_2C_2 forms during atomization	78	<1400	6
	29	>1400	
$Cu(s) \rightarrow Cu(g)$	74		7
$Cu(condensed) \rightarrow Cu(g)$	77		8
$Cu_2(g) \rightarrow Cu(g)$	48	<973[b]	10
$Cu(s) \rightarrow Cu(g)$	81	1372[b]	
$Cu(ads) \rightleftharpoons Cu(g) + C(s)$	29		11
$Cu(ads) \rightleftharpoons Cu(g) + C(s)$	30		12

[a] Obtained under vacuum conditions by using single-crystal graphite with Cu vapor deposition. [b] Pretreatment temperature.

Comparing the results from Monte Carlo simulations to experimental data for graphite furnace atomizers (GFA), Black et al. (*11*) obtained an activation energy of 29 ± 3 kcal/mol and proposed that the release of Cu in a graphite furnace at atmospheric pressure is a first-order desorption process proceeding from submonolayer coverages of Cu atoms dispersed across the surface.

Under a much more controlled set of conditions, Arthur and Cho (*2*) have investigated the Cu desorption process from the (0001) plane of single-crystal graphite by mass spectrometric measurements. The Cu was vapor-deposited onto the basal plane at submonolayer coverages. They concluded that the thermal desorption of Cu has an order of release of $^1/_2$ at low coverage with weak, nonlocalized bonding of metal atoms to the basal plane of graphite. Furthermore, they speculated that two-dimensional nucleation of mobile adsorbed atoms occurs upon adsorption, and the reverse process (i.e., loss of atoms from the edges of disk nuclei) is the rate-limiting step for desorption. For surface coverage below 10^{14} cm^{-2}, the activation energy for the desorption process of Cu on (0001) graphite was reported to be 47 kcal/mol.

Besides the vacuum studies of Arthur and Cho, only a limited number of experimental or theoretical models have focused on the order of release for GFA. Most of the GFA papers have assumed a first-order process (*3, 7, 11*). McNally and Holcombe (*12*) intentionally focused on this issue and reported a first-order release.

In this research the vaporization/atomization behavior of Cu samples is studied in order to elucidate the mechanism

---

* Author to whom correspondence should be addressed.

[1] Present address: Department of Chemistry, University of Kentucky, Lexington, KY 40506.

0003-2700/89/0361-2652$01.50/0 © 1989 American Chemical Society

controlling the production of gaseous Cu atoms both in vacuo and under an atmosphere of inert gas. The samples are initially deposited as an aqueous solution or as powders onto a pyrolytically coated graphite platform.

EXPERIMENTAL SECTION

Apparatus. The atomic absorption/mass spectrometry (AA/MS) vacuum system consisted of a quadrupole mass analyzer (QMA) (Uthe Technology International, Model 100C) with electron impact ionizer (70 eV), a UTI programmable peak selector (PPS), and an Apple II+ microcomputer. This system is described in greater detail elsewhere (*13*, *14*).

A Cu hollow cathode lamp (Perkin-Elmer, Norwalk, CT), operated in direct current (dc) mode at 12 mA, was used as a light source for the vacuum AA measurements. A 0.3-m monochromator (GCA/McPherson Instruments, Model LU700) was used to monitor the 234.7-nm line of Cu. The image-transfer system employed an over-and-under mirror configuration with one-to-one imaging (*15*) with a 1-mm horizontal slit located in the tangential image plane to isolate the region immediately above the graphite surface.

Samples were deposited on a pyrolytically coated graphite flat (1.5 × 0.76 × 0.17 cm, grade FE35, Schunk Carbon Technology, coated by Ringsdorff-Werke GmbH) held between two graphite electrodes on the atomizer assembly. The atomizer was heated with a computer-controlled digital power supply (*16*). A program developed in this laboratory provided a linear temperature ramp (*17*), which was verified by measurements noted in the Procedure section.

Reagents and Chemicals. A Cu stock solution (1000 mg/L) was prepared by dissolving Cu powder in a minimum volume of concentrated HNO_3. The test solutions were prepared by appropriate dilution of the stock solution immediately prior to their use. While the concentrations varied, 4-μL sample aliquots were used in all cases. ACS grade Cu powder and CuO powder were introduced directly onto the platform in some experiments. This was accomplished by touching the water droplet formed on the tip of the sample introduction syringe to the appropriate powder and then transferring this adhering powder to the graphite surface. The Cu powder consisted of particles in the range of 10–50 μm, and all particles passed a 200-mesh sieve (i.e., <75 μm). Analysis of the powder for Cu showed that the CuO and other impurities represented <2% of the sample.

Procedure. The temperature of the graphite flat was calibrated with an optical pyrometer (The Pyrometer Instrument Co., Inc., Northvale, NJ). A hole was drilled in the side of the pyrolytically coated graphite flat with a radius-to-depth of 1:6 to approximate a black body cavity for temperature calibration. The transmission of the windows through which the platform was viewed was also taken into account in the temperature determination. The heating coefficients were then calculated and adjusted by using the software described previously (*17*). The final temperature ramp was linear within ±20 K/s in the detectable range.

The graphite surface was cleaned at $T > 2300$ K for 3 s under vacuum conditions in the prechamber, and the prechamber was then filled with N_2(g). After the atomizer had cooled down, the sample was deposited and dried at 375 K for 40 s. For some experiments a thermal pretreatment under 1 atm of N_2 was employed. Next, the prechamber was evacuated to approximately 10^{-6} Torr, the gate valve that separated the two chambers was then opened, and the atomizer was moved under the QMA ionizer and into the AA light path. When the pressure reached $<2.0 \times 10^{-6}$ Torr, the final atomization cycle was initiated. Following the atomization process, the data were transferred from the PPS to Apple II+ and stored on a floppy disk. Finally, the atomizer was pulled back into the prechamber, the gate value was then closed, and the graphite flat was cleaned for another cycle. The turnaround time was approximately 25 min per sample.

Computer simulations used in studying dimer formation were run on a microcomputer (Turbo PC, PC's Limited) using numerical techniques.

RESULTS AND DISCUSSION

Copper Atomization from $Cu(NO_3)_2$ Aqueous Solutions. Vacuum Studies. $Cu(NO_3)_2$ solutions ranging from 1 to 250 mg/L were used to obtain the mass spectra. The Cu^+ signal was collected at $m/z = 63$ and was verified by monitoring the ratio of Cu^+ isotopes at masses 63 and 65. Figure 1 shows the Cu^+ ($m/z = 63$) signal and the Cu atomic absorbance signal obtained under the same experimental conditions. From Figure 1 it can be seen that the Cu^+ signal has two peaks, but the Cu absorbance signal has only one peak, which coincides with the higher temperature Cu^+ signal. The two signals have been scaled in this figure to illustrate the similarity in peak shape and to emphasize the fact that both signals originate from the same source. Therefore, it can be surmised that the second Cu^+ signal originates from desorbed Cu atoms while the low-temperature peak is a fragmentation pattern of another Cu-containing species. Early in time (ca. 400 K) a CuO^+ peak appears and probably represents the parent ion to the Cu^+ signal observed at this same time interval. Coincident with this peak are signals from NO_2 and O_2, which suggests the decomposition of $Cu(NO_3)_2$ and the accompanying shattering of the nitrate crystal with gaseous release of the oxide thus formed. This has been observed for a number of other metals (*13*, *14*) and does not represent a bona fide loss mechanism.

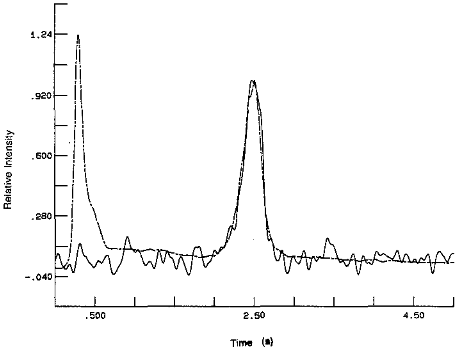

Figure 1. Cu^+ (m/z 63) mass spectral intensity signal (dashed) and Cu absorbance signal (in vacuo) obtained from a 4-μL aliquot of a 100 mg/L $Cu(NO_3)_2$ solution.

When a graphite furnace is used under atmospheric pressure conditions, the multiple collisions between these evolved species and the surface result in condensation of the oxide at that time. This has been verified experimentally by charring the deposited $Cu(NO_3)_2$ solution under 1 atm of N_2 at 523 K. The mass spectral signal detected in vacuo for the low-temperature CuO species is reduced and the high-temperature Cu^+ signal is substantially larger than the case when no atmospheric pressure thermal pretreatment is invoked. This confirms that readsorption of any copper oxide back onto the surface is consistent with the well-behaved "char curves" observed for Cu.

The following classical desorption equation may be used to describe the rate of release of atoms or molecules from the graphite surface (*18*):

$$\frac{\partial \sigma}{\partial t} = -\nu \sigma^n \exp\left(\frac{-E_a}{RT}\right) \tag{1}$$

where σ is the surface coverage at time t, ν is the preexponential factor, n is the order of release, E_a is the activation energy of desorption, R is the gas constant, and T is the time-dependent absolute temperature. This approach is commonly used to describe peak shapes in vacuum desorption experiments.

In the vacuum system at 10^{-6} to 10^{-7} Torr, the mean-free path of the atoms released from the graphite surface is suf-

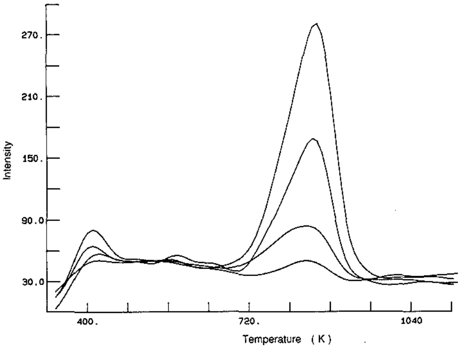

Figure 2. Cu^+ (m/z 63) mass spectral intensity signals as a function of temperature obtained from 4-μL aliquots of $Cu(NO_3)_2$ solutions having concentrations of 1.0 mg/L (4 ng of Cu), 2.5 mg/L (10 ng), 5.0 mg/L (20 ng), and 7.5 mg/L (30 ng).

ficiently large to neglect gas-phase collisions and readsorption back onto the surface, although some readsorption will occur because of large surface morphology disparities in the region of release. This is unlike the tube-type graphite furnace atomizers under atmospheric pressure, where gas-phase collisions and readsorption of gases onto the graphite surface cannot be neglected. In the vacuum system, the rapid removal rate (i.e., pumping speed) makes the recorded intensity signal $I(t)$ proportional to the generation function and the surface coverage σ is proportional to the integral of the intensity signal (*18*).

$$I(t) \propto \frac{-\partial\sigma}{\partial t} \qquad (2)$$

$$\sigma \propto \int_t^\infty I(t)\,\mathrm{d}t \qquad (3)$$

$$\sigma_0 \propto \int_0^\infty I(t)\,\mathrm{d}t \qquad (4)$$

where σ_0 is the initial surface coverage at $t = 0$. Substituting eq 2 and 3 into eq 1 yields

$$\frac{I(t)}{\left[\int_t^\infty I(t)\right]^n} = C\exp\left(\frac{-E_a}{RT}\right) \qquad (5)$$

$$\ln\left(\frac{I(t)}{\left[\int_t^\infty I(t)\right]^n}\right) = \left(\frac{-E_a}{RT}\right) + \ln C \qquad (6)$$

where C is a proportionality constant that is independent of temperature T.

By use of eq 5 and 6, the order of the atomization process and the activation energy can be determined from the intensity profile.

When a linear temperature ramp is used with a starting temperature of T_0 at $t = 0$ and a ramp rate of α, the temperature is described by $T = T_0 + \alpha t$. Assuming that E_a is independent of σ, the temperature, T_p, at which the desorption rate $\partial\sigma/\partial t$ is a maximum can be defined by taking the derivative of eq 1 with respect to t and setting it equal to zero (*18*).

$$\left(\frac{E_a}{RT_p^{\,2}}\right) = \frac{\nu n\sigma^{n-1}}{\alpha\exp\left(\frac{-E_a}{RT_p}\right)} \qquad (7)$$

If we increase the initial amount of sample (and hence σ_0), from eq 7 it can be determined by differentiation that T_p shifts to higher temperatures when $0 \leq n < 1$, T_p remains the same when $n = 1$, and T_p moves to lower temperatures when $n > 1$. Therefore, the desorption order can be determined from the shift of T_p with changing amounts of sample assuming a single release mechanism (i.e., constant E_a and ν). From Figure 2 it can be seen that the peak locations for Cu with different concentrations of Cu are very similar, suggesting that Cu atomization is a first-order process (*12*, *18*). Peak temperatures and the corresponding activation energies for $Cu^+(63)$ signals are given in Table II.

Table II. Peak Temperatures and Calculated Activation Energy Values for Various Concentrations of $Cu(NO_3)_2$ Solutions, 4-μL Sample Injection

mass, ng	T_{max}, K	E_a, kcal/mol
4	833	34.7
10	833	29.1
20	846	30.1
30	856	29.4
40	858	32.4
100	865	30.7
200	869	30.1
300	869	32.4
1000	871	31.6
average	856	31.2 ± 2

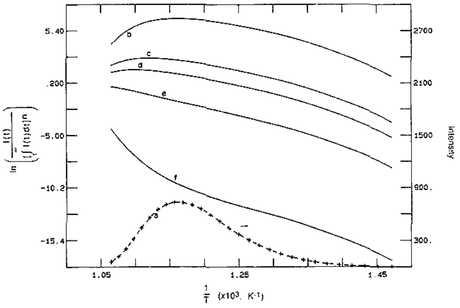

Figure 3. Evaluation of order of release from modified Arrhenius plots using mass intensity data for Cu^+ (m/z 63) and 100 ng of Cu at 2 × 10^{-6} Torr assuming (b) $n = 0$, (c) $n = 1/2$, (d) $n = 2/3$, (e) $n = 1$, and (f) $n = 2$. (For reference, the signal intensity for Cu^+ is shown as a dashed line in curve a.)

Figure 3a shows the atomization profile for 100 ng of Cu. The Arrhenius plots for Cu atomization using eq 6 and orders of release of 0, $1/2$, $2/3$, 1, and 2 are shown in Figure 3b–f, respectively. The best straight line over the region where the signal-to-noise ratio (S/N) is reasonable (i.e., $T > \sim$760 K) corresponds to $n = 1$ and provides additional support to the conclusion that a first-order release is occurring. As shown in Figure 3e, the Arrhenius plot at lower temperatures is approximately linear and seems to have a different E_a value. However, at the beginning of atomization, the signal is weak and it is difficult to extract an accurate value of the base line. Therefore, this region is unusable for postulating the atomization mechanism. This has been demonstrated in more detail by Bass and Holcombe (*19*).

Arrhenius plots for first-order atomization of various amounts of Cu samples are shown in Figure 4. It is interesting to note that in all cases linearity extends from the beginning to the end of the atomization profile, a distinct contrast to results obtained from atmospheric pressure conditions where the finite removal rate perturbs the signal late in the profile (*19*). The E_a values have been calculated by applying a least-squares exponential fit to eq 5 (see Table II). An average activation energy of 31 ± 2 kcal/mol was calculated from these

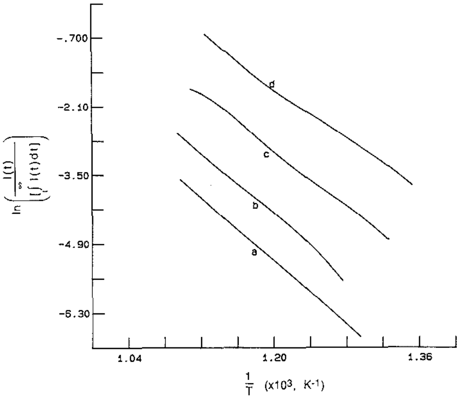

Figure 4. Arrhenius plot for first-order atomization for different initial amounts of Cu: (a) 100, (b) 40, (c) 30, and (d) 10 ng. (Curves have been displaced along the abscissa for display purposes.)

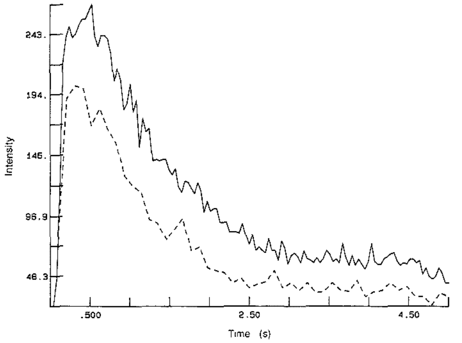

Figure 5. Mass spectral intensities for Cu^+_2 (*m/z* 126) and Cu_2O^+ (*m/z* 142, dashed) obtained from atomization of deposited $Cu(NO_3)_2$ solution (4 μL of 100 mg/L).

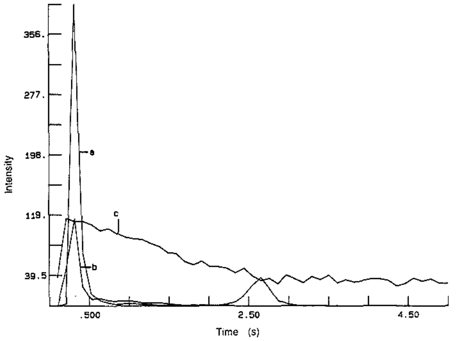

Figure 6. Comparison of mass spectral intensities for (a) Cu^+ (*m/z* 63), (b) CuO^+ (*m/z* 79), and (c) Cu_2^+ (*m/z* 126; ×100). Profiles obtained from a 4-μL aliquot of a 100 mg/L $Cu(NO_3)_2$ solution.

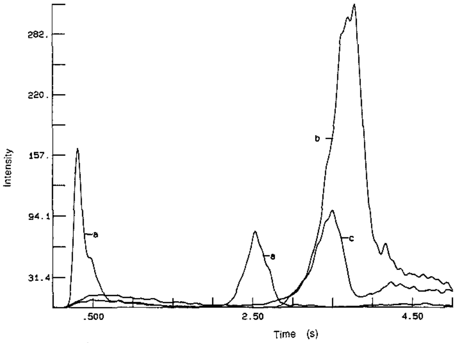

Figure 7. Cu^+ (*m/z* 63) signals obtained from (a) $Cu(NO_3)_2$ solution, (b) Cu powder, and (c) CuO powder atomizations.

data from the vacuum studies. This is in contrast to the value of 47 kcal/mol obtained by Arthur and Cho (*2*) using single-crystal graphite and a vapor-deposited sample.

The differences between our results and those of Arthur and Cho are probably due to the large number of surface imperfections in the typical GFA pyrolytically coated surface and the associated large number of active sites on these surfaces. Thus, the Cu is no longer mobile on the surface and capable of nucleating and forming microdroplets. This is consistent with the 30 kcal/mol value for E_a representing the adsorption of Cu to the surface.

L'vov (*20*) has postulated the existence of a carbide for Cu. A question of semantics thus emerges. While chemisorbed Cu on graphite relies on bonding-type interactions between Cu and C, the bond strengths and accompanying energies needed to break the Cu–C(s) bond are not (and should not be) the same as that found for bulk copper carbide. Thus "adsorbed Cu on graphite" (rather than "copper carbide") is a more accurate description of the chemical/physical state of Cu preceding atomization. During collection of mass spectral data, signals for CuC^+ (*m/z* of 75 and 77) and Cu_2C (*m/z* 138) showed no detectable signal above the noise level.

At higher amplifier gains, Cu_2^+ ($m/z = 126$) and Cu_2O^+ ($m/z = 142$) are observed early in time (Figure 5). A nearly identical peak shape and coincidence in appearance times suggest that these are ions from a common source, most probably Cu_2O, which is a more reduced form of the CuO species that is detected in larger quantities. Figure 6 shows the relative shapes of the peaks for Cu^+, CuO^+, and Cu_2^+. These data confirm the source of the lower temperature (at about 0.5 s, $T \sim 400$ K) peak as CuO with a smaller peak likely due to Cu_2O perhaps being formed at more reactive reducing sites on the surface. It should also be noted that no Cu_2^+ ion signal is detected other than that coincident with Cu_2O^+. This suggests that *the dimer is not a precursor* to atomic Cu in the graphite furnace system operated under vacuum or at atmospheric pressure. However, the dimer may form from gas-phase recombination, and a more detailed discussion of this will be presented in a subsequent section.

Several papers have been presented to support reduction of the oxide to elemental Cu prior to atomization (*5*, *7*, *21*, *22*). Frech et al. (*23*) considered the role of CO(g) in the reduction process and found that Cu was present on the surface and did not require gas-phase reduction. Further, their activation energies agreed with those of this work (i.e., 29–33 kcal). The MS results further show that *surface-adsorbed* Cu (i.e., not droplets or crystallites) is the precursor to Cu(g). It is not clear whether the dispersed, surface-adsorbed species exists during the oxide stage or only once the oxide has decomposed to form Cu. To evaluate this aspect, finely ground powders of elemental Cu and CuO were deposited separately on the graphite and brought through the atomization cycle under vacuum.

CuO and Cu Powder Samples. The Cu^+ signals obtained by depositing the $Cu(NO_3)_2$ aqueous solution, Cu powder, and CuO powder are shown in Figure 7. If one neglects the low-temperature peak for the aqueous solutions (which has been explained earlier), it is readily apparent that the aqueous solution produces a much earlier Cu signal than in the case of either copper oxide or elemental Cu powder. Confirmation that the Cu^+ mass spectral signal was due to evolution of atomic Cu from the surface was obtained by recording the absorbance signal above the surface under vacuum. The atomic absorption signals from both the $Cu(NO_3)_2$ aqueous solution and the CuO and Cu powders were coincident in time with and maintained the general shape of that observed for the mass spectral signal.

These data in Figure 7 strongly suggest two distinct mechanisms for Cu atomization and support the concept that the Cu is adsorbed on the surface in submonolayer amounts and not present as bulk oxide or bulk elemental Cu. The activation energy for the high-temperature desorption from the powders was calculated for several samples. While the powders of CuO and Cu had similar appearance temperatures and shapes, the noise level was sufficiently large that it was difficult to obtain precise measurements for E_a. All values measured fell within the range of 45–60 kcal/mol. This is statistically different from the value obtained for the solution-deposited sample and lies near the value obtained by Arthur and Cho but is significantly smaller than the 75 kcal/mol for the heat of vaporization of bulk Cu(l).

Thus, with the presence of intact bulk amounts initially deposited (i.e., the powders), a mechanism similar to that of Arthur and Cho may be active. This strongly implies that the CuO from the decomposition of the solution-deposited sample exists on the surface as a *dispersed adsorbed species*, rather than as bulk CuO, prior to reduction by graphite. The use of the two powders also confirms the ability of graphite to reduce the oxide even when the CuO is present as relatively large crystallites.

While no definitive evidence has been presented regarding the form of the $Cu(NO_3)_2$ on the surface prior to its decomposition, the significant evolution of CuO(g) suggests that bulk crystallite materials for the nitrate salt may be present since the shattering of these crystals may be responsible for the copious amounts of CuO(g) generated under vacuum conditions. Thus, the atomization processes leading to the formation of Cu gas in the graphite furnace are as follows:

$$Cu(NO_3)_2(s) \rightarrow CuO(ads) \rightarrow Cu(ads) \rightarrow Cu(g) \quad (8)$$

The presence of an atmosphere of an inert gas (e.g., Ar or N_2) should have minimal impact on the surface reactions and release mechanisms proposed above, although, as mentioned previously, it will ensure that the copper oxide that was observed with the vacuum studies will not be lost from the furnace. The other perturbation caused by the presence of atmospheric pressure would be gas-phase reactions that could attenuate the free Cu signal. The formation of the dimer from surface vaporization has been shown to be insignificant from the mass spectral studies presented above. However, the possible formation of the dimer in the gas phase under an atmosphere of pressure must be considered.

Existence and Formation of Copper Dimer, Cu_2. The dimer was shown *not* to vaporize from the graphite surface under vacuum. Additionally, the amount of Cu sample used in routine atmospheric pressure GFA systems (10^{-12} to 10^{-8} g) is less than that used in this experiment (10^{-9} to 10^{-6} g). Thus, if surface nucleation does not form in these vacuum experiments, it is even less likely to form at the lower concentrations in GFA.

However, gas-phase reactions involving Cu(g) may affect the characteristics of the absorbance signal. Because of the long mean free path (~50 m) all gaseous reactions can be neglected. This assumption is not true in an atmospheric pressure system since the collision frequency increases dramatically with pressure. Consider the following reaction:

$$2Cu(g) \rightarrow Cu_2(g) \quad (9)$$

The reaction rate constant of reaction 9, k_f, can be expressed as

$$k_f = \nu_f \exp\left(\frac{-E_a'}{RT}\right) \quad (10)$$

where ν_f is the preexponential factor for the forward reaction shown in eq 9 and E_a' is the activation barrier for dimer formation. The reaction is exothermic, and if one assumes no activation barrier (i.e., $E_a' = 0$), then eq 10 simplifies to $k_f = \nu_f$. Considering the most favorable kinetic conditions, i.e., every collision is "an effective collision", ν_f can be calculated as follows (*24*):

$$\nu_f = \left(\frac{4\pi}{RTM}\right)^{1/2} \phi^2 \text{ atm}^{-1}\cdot\text{s}^{-1} \quad (11)$$

where M is the molecular weight and ϕ is the molecule diameter. Substituting $M = 63$ and $\phi = 2.34 \times 10^{-10}$ m, we obtain $\nu_f = (1.6 \times 10^{10})T^{-1/2}$ $\text{atm}^{-1}\cdot\text{s}^{-1}$. Taking into account the generation by desorption of Cu from the surface, loss by formation of the dimer, and loss by diffusion, the following equation is used to simulate the partial pressure (in atmospheres) of free Cu(g):

$$\frac{\partial P_{Cu}}{\partial t} = k'\nu\sigma \exp\left(\frac{-E_a}{RT}\right) - \nu_f P_{Cu}^2 - k_D D_0 T^{3/2} P_{Cu} \quad (12)$$

where k' is a proportionality constant that accounts for the furnace area, volume, and temperature. D_0 is the diffusion coefficient at 273 K, and k_D is a proportionality constant that accounts for the dependency of the loss rate on furnace geometry. In eq 12, the dimensions of the three items are carefully considered and unit conversion is performed if necessary. Equation 12 was solved numerically, and the results for the P_{Cu}:P_{Cu_2} ratio were checked against the values predicted from equilibrium for reaction 9. If the ratio exceeded this volume, equilibrium concentrations were assumed; i.e., kinetics were not limiting. For all concentrations between 0.001 and 100 ng, the kinetic value was within 99% of the value predicted by equilibrium. Thus, the calculations suggest that equilibrium can be obtained if every collision between two Cu atoms could form $Cu_2(g)$ and the dimer formation is not collision-rate-limited. It should be mentioned that the kinetics for this reaction at these temperatures is not known and *could* reduce the rate of dimer formation, which would only tend to increase the relative amount of free Cu(g).

The assumption of $k_f = \nu_f$ and those used with eq 11 make dimer formation as favorable as possible; and yet, as Figure 8 shows, at low concentrations the formation of the dimer has little effect on the Cu signal simulated by using eq 12. At elevated concentrations, the equilibrium shifts the appearance temperature to higher values and affects only the early time (i.e., low temperature, 800–1200 K) portion of the profile. This may be the reason Fuller (*3*) obtained the 33 kcal/mol E_a value by using the tailing part of absorbance signal. The Cu_2 formation with a large amount of sample may also explain why Cu_2 has been observed in a King furnace (*25*).

Figure 9 shows the Arrhenius plots of the data from Figure 8 and illustrates the deviation from the slope expected for a simple desorption process. However, use of the early portion of the curve provides no assistance in assigning the energetics for desorption or dimer formation. This inability to extract information on gas-phase reaction from GFA Arrhenius plots has been recently discussed elsewhere (*26*).

Thus, dimer formation can occur for higher concentrations that might be used with GFA, although the impact persists only early in time. The presence of the dimer could not be

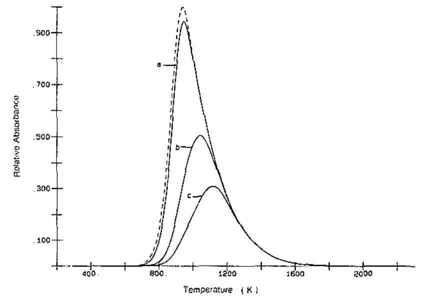

Figure 8. Normalized simulation profiles for Cu atomization under 1 atm of Ar assuming a total Cu mass of (a) 0.04, (b) 4, and (c) 40 ng. The dashed curve represents the profile expected if no dimer were formed. (A furnace volume of 0.7 cm^3 and a heating rate of 1000 K/s are assumed.)

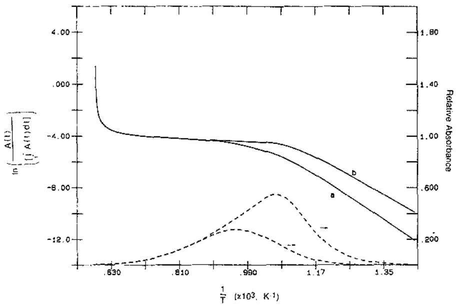

Figure 9. Smets modification of Arrhenius plots of the simulated data shown in Figure 8b assuming (a) dimer formation and (b) no dimer formation in the gas phase. The simulated absorbance profiles are also shown for reference by the dashed lines.

deduced from the Arrhenius plots, and it is possible that misleading conclusions would be drawn in attempting to do so when the dimer exists. The dimer's presence at high partial pressures of Cu and/or low temperatures may explain some of the E_a values obtained by other researchers when high concentrations were being used. Similarly, at very high concentrations, it seems likely that droplet formation with possible vaporization from the edge of disk nuclei or, in the extreme, vaporization from bulk Cu could be observed. However, both instances represent perturbations from the conditions typical of GFA. As will always be the case where the surface plays such a major role in determining the mechanism of release, sample concomitants can alter the behavior of Cu on the surface and lead to a significantly different release process than that reported in this study.

Comparison of Copper Atomization in Vacuum and Atmospheric Pressure Systems. From Figure 1 it can be seen that the appearance temperature of Cu is approximately 720 K, which is lower than that observed in the atmospheric pressure system (ca. 1300 K (e.g. ref 21)). Under vacuum conditions, the mean free path is large enough to neglect the readsorption. However, under 1 atm, the mean free path is approximately 10^{-5} cm. After Cu atoms desorb from the graphite surface, elastic collisions with the inert gas (e.g., Ar) occur, which results in redirection of the Cu and highly probable readsorption of the analyte back onto the surface. The attractive forces between the Cu atoms and the graphite surface have been suggested as a source of peak broadening in the graphite furnace at atmospheric conditions (*12*). When there is an attraction between the analyte and the graphite surface, the appearance temperatures are dependent on the strength of the interaction between the graphite and the element (*11*). The interaction of Cu with the furnace results in multiple collisions at the gas/solid interface with subsequent adsorption and desorption of Cu atoms. This results in an increase in the appearance temperature with 1-atm pressure of inert gas. As noted above, the formation of Cu_2 may also give the impression of an increase in the appearance temperature compared to that of the vacuum system.

The first-order desorption kinetics of $Cu(NO_3)_2$ aqueous solution atomization under vacuum shows that droplets likely do not form before atomization. The E_a value of 31 ± 2 kcal/mol obtained is in good agreement with the 29 ± 3 kcal/mol obtained by Black et al. (*11*) using Monte Carlo simulation and with the E_a values 30 ± 2 of McNally and Holcombe (*12*) using a modified Smets model under atmospheric pressure atomization. Thus, the same atomization mechanism exists under both vacuum and 1 atm. In comparing the atomization of Pb, Bi, and Au in graphite furnace atomic absorption spectrometry (GFAAS) at atmospheric pressure to that under vacuum, Sturgeon and Arlow (*27*) also concluded that there are no significant differences between atmospheric and vacuum vaporization.

CONCLUSIONS

Combined with atmospheric pressure atomic absorption, mass spectrometry is a powerful tool to investigate the atomization mechanism in electrothermal atomizers. Not only can molecular species be detected, but gas-phase reactions and the influence of the dissipation process on the generation profile can be simplified to better isolate the processes occurring. The mass spectral signal intensity is proportional to the rate of generation, and the gas-phase information is a direct reflection of the processes taking place on the graphite surface. Therefore, the atomization mechanism can be investigated without making a large number of assumptions and invoking complicated mathematical data treatment. Some experimental results that cannot be deduced in an atmospheric atomic absorption spectrometry system have been obtained here. For example, the absence of the copper dimer and copper carbide coupled with the strong signal from elemental Cu(g) reliably isolates the mechanism of release. Furthermore, the fact that the values for the activation energies of release obtained in this study are identical with those we have obtained under 1 atm (*11*, *12*) can be combined with the deduced mechanism and the previous work of Arthur and Cho (*2*) to conclude that a large number of active sites exist on the pyrolitically coated graphite surfaces used in GFA. This fact points out the very significant role that these sites play in governing the mechanism of release.

LITERATURE CITED

(1) Sursky, G. A.; Avdeenko, M. A. *Zh. Prikl. Spektrosk.* **1972**, *17*, 564.
(2) Arthur, J. R.; Cho, A. Y. *Surf. Sci.* **1973**, *36*, 641.
(3) Fuller, C. W. *Analyst* **1974**, *99*, 739.
(4) Aggett, J.; Sprott, A. J. *Anal. Chim. Acta* **1974**, *72*, 49.
(5) Sturgeon, R. E.; Chakrabarti, C. L.; Langford, C. H. *Anal. Chem.* **1976**, *48*, 1792.
(6) Katskov, D. A.; Greenstein, I. L. *Zh. Prikl. Spektrosk.* **1979**, *30*, 787.
(7) Smets, B. *Spectrochim. Acta, Part B* **1980**, *35B*, 33.
(8) L'vov, B. V.; Bayunov, P. A.; Ryabchuk, G. N. *Spectrochim. Acta, Part B* **1981**, *36B*, 397.
(9) Frech, W.; Zhou, N. G.; Lundberg, E. *Spectrochim. Acta, Part B* **1982**, *37B*, 691.
(10) Chung, C. *Anal. Chem.* **1984**, *56*, 2714.
(11) Black, S. S.; Riddle, M. R.; Holcombe, J. A. *Appl. Spectrosc.* **1986**, *40*, 925.
(12) McNally, J.; Holcombe, J. A. *Anal. Chem.* **1987**, *59*, 1015.
(13) Bass, D. A.; Holcombe, J. A. *Anal. Chem.* **1987**, *59*, 974.
(14) Droessler, M. S.; Holcombe, J. A. *Spectrochim. Acta, Part B* **1987**, *42B*, 981.
(15) Salmon, S. G.; Holcombe, J. A. *Anal. Chem.* **1978**, *50*, 1714.
(16) Bass, D. A.; Eaton, D. K.; Holcombe, J. A. *Anal. Chem.* **1986**, *58*, 1900.
(17) Christopher, G. F. M. S., III; Holcombe, J. A. *Anal. Instrum.* **1988**, *17*, 235.

(18) Redhead, P. A. *Vacuum* **1962**, *12*, 203.
(19) Bass, D. A.; Holcombe, J. A. *Spectrochim. Acta, Part B* **1988**, *43B*, 1473.
(20) L'vov, B. V. *Analyst* **1987**, *112*, 355.
(21) Wang, P.; Zhang, W.; Xiong, G.; Lin, T. *Spectrochim. Acta, Part B* **1988**, *43B*, 141.
(22) Eklund, R. H.; Holcombe, J. A. *Talanta* **1979**, *26*, 1055.
(23) Frech, W.; Lindberg, A. O.; Lundberg, E.; Cedergren, A. *Fresenius' Z. Anal. Chem.* **1986**, *323*, 716.
(24) Harris, G. M. *Chemical Kinetics*; D. C. Heath and Company: Boston, MA, 1966.
(25) Pearse, R. W. B.; Gaydon, A. G. *The Identification of Molecular Spectra*, 3rd ed.; Chapman and Hall, Ltd.: London, 1963; p 151.
(26) Holcombe, J. A. *Spectrochim. Acta, Part B* **1989**, *44B*, in press.
(27) Sturgeon, R. E.; Arlow, T. S. *J. Anal. At. Spectrom.* **1986**, *1*, 359.

RECEIVED for review July 3, 1989. Accepted September 20, 1989. This work was supported, in part, by grants from the National Science Foundation (CHE-8704024) and the Robert A. Welch Foundation (F-1108).

Simulation of Carbon-13 Nuclear Magnetic Resonance Spectra of Linear Cyclic Aromatic Compounds

Abigail S. Barber and Gary W. Small*

Department of Chemistry, The University of Iowa, Iowa City, Iowa 52242

Hückel molecular orbital theory and molecular mechanics calculations are used to derive structural parameters that allow carbon-13 nuclear magnetic resonance spectra of linear cyclic aromatic compounds to be modeled. With a set of 32 substituted benzenes, naphthalenes, and anthracenes, three models are derived that allow complete spectra to be simulated to an average error of 0.509 ppm. The accuracy of the simulations is keyed by the development of a series of electronic structural parameters based on free valence and autopolarizability, two parameters derived from the molecular orbital calculations. The performance of the computed models is evaluated in detail, and they are subsequently applied to the simulation of spectra of compounds not included in the model development work. The predictive ability of the models is judged to be excellent based on an analysis of these simulated spectra.

INTRODUCTION

In carbon-13 nuclear magnetic resonance spectroscopy (^{13}C NMR), spectrum simulation techniques have come into use as a means to verify chemical shift assignments or to substantiate a proposed structure for an unknown. Aromatic compounds are a challenge to most spectrum simulation methods due to the unique manner in which the aromatic system influences chemical shifts. Unlike carbons in saturated systems, the chemical shifts of aromatic carbons can be influenced by chemical structural effects at large interatomic distances.

Four approaches can be used to simulate or model chemical shifts in aromatic compounds: (1) the direct calculation of chemical shifts based on the theoretical principles of magnetic shielding (*1–8*), (2) the calculation of chemical shifts based on substituent effects (*9*), (3) the derivation of empirical models that relate structural characteristics to chemical shifts (*10–18*), and (4) the retrieval of chemical shifts from a spectral database in which each stored chemical shift is indexed to an encoded representation of the corresponding carbon atom environment (*19*). Each of these methods has limitations. The theoretical methods are computationally intensive, and reported errors between actual and predicted chemical shifts have often exceeded 20 ppm. The approach based on substituent effects is limited in that only short-range inductive effects on chemical shifts are typically encoded. Steric and long-range effects, often important in aromatic systems, are seldom included. Empirical modeling studies have produced highly accurate chemical shift predictions (errors <1 ppm), although the majority of work has focused on saturated systems only. Finally, for the database approaches to be successful in simulating a spectrum, the appropriate chemical shifts must be present in the spectral database.

Recently, work in our laboratory has sought to expand the applicability of the chemical shift modeling approach to more complex chemical systems (*20*, *21*). This work is motivated by the belief that the modeling approach offers the greatest chance for obtaining highly accurate chemical shift predictions without having to build and maintain a large spectral database. In the work reported here, the expansion of this methodology is continued with the introduction of chemical shift modeling procedures for methyl-substituted linear aromatic ring systems. This methodology is keyed by the development of a new series of electronic structural parameters that encode the influence of the aromatic system on ^{13}C NMR chemical shifts. These structural parameters are examined, and the computed chemical shift models are evaluated in terms of their predictive ability.

EXPERIMENTAL SECTION

Thirty-two aromatic compounds were used in the development of the chemical shift models reported here, and six compounds were used in testing the computed models. The broad band decoupled ^{13}C NMR chemical shift values for these compounds were taken from five published studies.

Woolfenden and Grant reported the chemical shifts for the methyl carbons on seven substituted benzenes (*22*). Samples were run neat at room temperature with a Varian V-4311 spectrometer operating at 15.1 MHz. The chemical shifts were reported relative to internal benzene. An offset of 128.6 ppm was used to convert the chemical shifts to a Me_4Si reference. In a later study, the same research group reported chemical shifts for the ring atoms of the benzene compounds, as well as the complete spectra for four tri- and tetramethylnaphthalenes (*23*). Spectra for the methylbenzenes were collected under the same conditions as reported above, while the napthalene spectra were collected by use of a Varian XL-100-15 Fourier transform NMR spectrometer operating at 25.2 MHz. The solvent used was $CDCl_3$. All chemical shifts were reported relative to internal dioxane. An offset of 66.9 ppm was used to convert the shifts to a Me_4Si reference. No concentrations were reported for samples used in either of the studies.

© 1989 American Chemical Society

Thirteen spectra of naphthalene derivatives were reported by Wilson and Stothers (*24*). Samples were prepared as 10–15% (w/v) solutions in $CDCl_3$. Spectra were collected with a Varian XL-100 Fourier transform NMR spectrometer, and chemical shifts were reported relative to internal Me_4Si. The spectra for 12 anthracene derivatives were reported by Caspar, Stothers, and Wilson (*25*). The experimental conditions used were the same as those used for the naphthalene derivatives.

The spectrum of 2,3-dimethylnaphthalene was taken from the work of Gobert et al. (*26*). The sample was prepared as a 0.4 M solution in $CDCl_3$. The spectrum was collected by use of a Varian XL-100-12 WG NMR spectrometer operating at 25.2 MHz. Chemical shifts were reported relative to internal Me_4Si.

All computer software used in this work was written in FORTRAN 77 and implemented on a Prime 9955 interactive computer system operating in the Gerard P. Weeg Computing Center at the University of Iowa. Plots were made by use of the TELLAGRAF interactive graphics system (Integrated Software Systems, Inc., San Diego, CA) and with original software. A Hewlett-Packard 7475A digital plotter was used as the output device.

RESULTS AND DISCUSSION

Overview of Spectrum Simulation Methodology. The spectrum simulation methodology developed here for simple aromatic systems is based upon the empirical chemical shift modeling technique noted above. The developed models have the general form

$$S_j = b_0 + b_1X_1 + b_2X_2 + \dots + b_pX_p \qquad (1)$$

where S_j is the predicted chemical shift for carbon atom j, the b_i values are weighting coefficients, the X_i values are numerical parameters that describe the chemical environment of atom j, and p is the number of terms in the model. A predicted chemical shift for an atom is thus formed from a linear sum of terms that describe the manner in which the surrounding chemical environment determines the shift of that atom. By use of a set of known and correctly assigned chemical shifts, a multiple linear regression analysis is performed to derive the values of the b_i and to select the X_i that are most statistically significant in modeling the chemical shifts. Once the coefficients have been determined, the model can be used to predict the chemical shifts of atoms that were not included in determining the coefficients. A complete simulated spectrum can be formed by assembling the predicted chemical shifts of each unique atom in a structure.

Assembly of Data for Modeling. The 32 compounds used in the development of the chemical shift models are listed in the upper part of Table I, along with the literature reference for the corresponding spectral data. The structures of these compounds were entered into computer disk files by use of a graphical procedure developed by Brügger and Jurs (*27*). To allow steric effects on chemical shifts to be subsequently encoded, force-field molecular mechanics calculations were performed on the structures to generate approximate three-dimensional coordinates for the atoms. A force field described by Stuper et al. (*28*) was used to compute initial atomic coordinates for the structures, and the MMPI procedure of Allinger (*29*) was used to generate final coordinates.

Previous chemical shift modeling studies have indicated that to achieve the highest accuracy of predicted chemical shifts, separate models should be generated for natural structural subgroups of atoms. In this way, each model can be more detailed and thus can achieve a higher prediction accuracy. In the present study, three subgroups of atoms are apparent: group I, methyl carbons; group II, ring carbons; and group III, ring-bridging carbons. For the 32 compounds, groups I, II, and III contain 47, 179, and 50 atoms, respectively. The corresponding chemical shift ranges for the atom groups are 13.7–27.0, 118.0–137.7, and 129.4–135.5 ppm. This assembly of atoms represents the set of 276 topologically unique atoms across the 32 compounds. Atoms in duplicate structural environments were eliminated to ensure that all atoms would be given equal weight in the regression analysis. The selection of the atom groups was performed automatically by use of a procedure developed by Small and Jurs (*30*).

Table I. Compounds Used for Modeling and Testing

no.	name	ref
	modeling	
1	benzene	20
2	1-methylbenzene	19, 20
3	1,2-dimethylbenzene	19, 20
4	1,3-dimethylbenzene	19, 20
5	1,3,5-trimethylbenzene	19, 20
6	1,2,3-trimethylbenzene	19, 20
7	naphthalene	21
8	1-methylnaphthalene	21
9	2-methylnaphthalene	21
10	1,2-dimethylnaphthalene	21
11	1,3-dimethylnaphthalene	21
12	1,4-dimethylnaphthalene	21
13	1,5-dimethylnaphthalene	21
14	1,8-dimethylnaphthalene	21
15	1,6-dimethylnaphthalene	21
16	1,7-dimethylnaphthalene	21
17	2,6-dimethylnaphthalene	21
18	2,3-dimethylnaphthalene	21
19	2,3,6-trimethylnaphthalene	20
20	2,3,5-trimethylnaphthalene	20
21	1,3,5,8-tetramethylnaphthalene	20
22	anthracene	22
23	1-methylanthracene	22
24	2-methylanthracene	22
25	9-methylanthracene	22
26	2,3-dimethylanthracene	23
27	1,4-dimethylanthracene	22
28	9,10-dimethylanthracene	22
29	2,7,9-trimethylanthracene	22
30	1,4,5,8-tetramethylanthracene	22
31	1,4,5,9-tetramethylanthracene	22
32	1,4,5,8,9-pentamethylanthracene	22
	testing	
33	1,4-dimethylbenzene	19, 20
34	1,2,4-trimethylbenzene	19, 20
35	2,7-dimethylnaphthalene	21
36	1,4,6,7-tetramethylnaphthalene	20
37	1,8-dimethylanthracene	22
38	1,4,9-trimethylanthracene	22

Design of Structural Parameters for Aromatic Systems. In our previous studies involving saturated systems, the most useful structural parameters have had the general form

$$X_j = 1/(d_{i,k})^n \qquad (2)$$

where X_j is the computed value of the parameter for atom j (the target atom whose chemical shift is being predicted), $d_{i,k}$ is the interatomic distance between atoms i and k, and n is a weighting exponent (usually 3). The interatomic distances are computed based on the approximate atomic coordinates obtained from molecular mechanics calculations. Individual parameters differ by the criterion used to determine which distances are included in the summation. In some cases, $i = j$, and the k values specify those atoms at a specific topological bond distance from atom j. For example, the summation might be taken over all atoms three bonds from atom j. In this case, the computed parameter would focus on different stereochemical orientations at the distance of three bonds from the target carbon.

The principal difference between the current study and those performed previously lies in the special characteristics of the aromatic system and the manner in which chemical shifts are influenced by these characteristics. In preliminary research, it became evident that the long-range interatomic

Table II. Aromatic Structural Parameters Based on Topological Bond Steps

parameter[a]	description
MXep[b] *n*[c]	maximum value among atoms *n* bonds removed from the target atom
MNep *n*	minimum value among atoms *n* bonds removed from the target atom
TOep *n*	sum of values for atoms *n* bonds removed from the target atom
AVep *n*	average of values for atoms *n* bonds removed from the target atom
NTep *n*	sum of absolute values for atoms *n* bonds removed from the target atom

[a] Structural parameters are identified by a four-character label and a numerical flag. [b] ep, designation for one of the four electronic parameters (AP, autopolarizability; BD, bond order; SD, superdelocalizability; FV, free valence). For example, MXAP designates the maximum autopolarizability. [c] *n*, designation for the number of topological bond steps to be used. For example, $n = 2$ would specify those atoms two bonds removed from the target atom. Thus, MXAP 2 specifies the maximum autopolarizability among atoms two bonds removed from the target atom.

effects seen in many ^{13}C NMR spectra of aromatic compounds could not be fully explained by the parameters used previously. A principal goal for the work was to develop electronic structural parameters that encode information about the π system within the aromatic structures. It was hypothesized that a simple molecular orbital (MO) theory would generate parameters encoding the appropriate information while, at the same time, requiring a minimum of computation time. Hückel molecular orbital (HMO) theory was chosen as it offers a computationally simple approach while encoding information about the π system. The HMO program used in this investigation was formed by combining software modules described individually by Lowe (*31*) and Greenwood (*32*). Additionally, coulomb values and bond integral values defined by Yates (*33*) and Streitwieser (*34*) were used.

In theoretical studies, application of the HMO theory alone to calculate ^{13}C NMR chemical shifts has not been successful (*35*). However, several parameters generated from an HMO calculation (bond order, free valence, and electron density) have been shown to influence chemical shifts (*36*). For the present application, electron density is of no use, as HMO theory calculates an electron density of unity for atoms in alternant aromatic systems. The benzene, naphthalene, and anthracene ring systems employed here are alternant systems.

For our work, four HMO parameters were investigated for their utility in the formation of structural parameters: (1) free valence, (2) autopolarizability, (3) superdelocalizability, and (4) bond order. The first three parameters are computed for each atom in the molecule, while a bond-order parameter is computed for each bond. Free valence and superdelocalizability are both used as potential measures of chemical reactivity. While calculation of the free valence index assumes the initial electronic structure of the molecule is not yet disturbed by the potential reactant, the superdelocalizability index calculation assumes perturbation has occurred. Autopolarizability, as defined by Dewar (*37*), is a measure of the way the π charge density changes with the changing electronegativity of the corresponding atom. The bond order is an arbitrarily defined measure of the bond strength between two atoms.

Given these electronic parameters, a decision had to be made regarding how to formulate the actual structural parameters. To be useful in helping to model chemical shifts, each structural parameter must describe some aspect of the chemical environment of the target carbon. This implies that, in defining the structural parameters, the values produced by the HMO calculation must be selected based on their relationship to the target carbon. Initially, the electronic parameters were evaluated over the atoms at selected topological bond steps removed from the target atom. Table II describes the resulting structural parameters. After the atoms were assembled at a specified bond distance, five different methods were used to combine the values of the chosen electronic parameter.

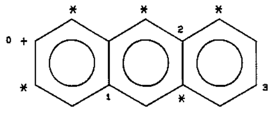

ortho positions

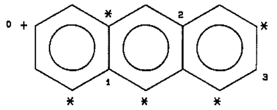

meta positions

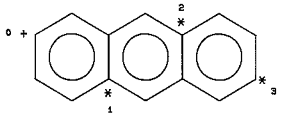

para positions

Figure 1. Asterisks define the atoms residing in the extended ortho (top), meta (middle), and para (bottom) positions in anthracene (compound **22**). The target carbon is designated by a "+", and numbers are used to define the individual para steps radiating outward from this atom.

A preliminary investigation revealed that structural parameters computed at greater than two bond steps from the target carbon were not helpful in modeling chemical shifts. Given that long-range effects on chemical shifts are known to be present in aromatic systems, it was concluded that an alternative scheme must be devised for formulating the structural parameters. On the basis of inspection of many structures and their corresponding ^{13}C NMR spectra, a positional scheme was devised for selecting atoms to be used in constructing the structural parameters. This positional approach is based on an extended definition of the familiar ortho, meta, and para ring designations.

In a given structure, atoms are defined that are para to the target carbon. This procedure is based on "para steps". For example, the target carbon resides at para step 0, while the carbon para to the target carbon resides at para step 1. The carbon para to this atom resides at para step 2. The extended ortho and meta positions are defined based on the para atoms. Ortho atoms are defined as being one bond removed from atoms at even para steps from the target carbon. In this context, para step 0 is considered an even step. Analogously, meta atoms are defined as being one bond removed from atoms at odd para steps. These extended position designations are illustrated in Figure 1 for anthracene (compound **22**). The target carbon is identified by "+", and the individual para steps are designated by number. Atoms meeting the ortho, meta, and para criteria are designated by asterisks.

Table III describes the three types of positional parameters that have been investigated. In each case, the values of the selected electronic parameter are summed over the atoms meeting the positional criterion. In one case, each term in the sum is weighted by the inverse throughspace distance from

Table III. Positional Aromatic Structural Parameters

parameter[a]	description
Aep[b]r[c] 0	average value among atoms meeting the specified positional criterion
Tepr 0	sum of values for atoms meeting the specified positional criterion
Depr n	weighted sum of values for atoms meeting the specified positional criterion. Each value is weighted by $1/d^n$, where d is the throughspace distance from the target atom to the atom whose electronic parameter value is being used. Allowed values of n are 1, 2, and 3

[a] Structural parameters are identified by a four-character label and a numerical flag. [b] ep, designation for one of the four electronic parameters (AP, autopolarizability; BD, bond order; SD, superdelocalizability; FV, free valence). [c] r, positional indicator (O, ortho; M, meta; P, para), where the extended ring positions are defined in the discussion of Figure 1. For example, AFVP specifies the parameter produced by averaging the free valence values for the atoms para to the target atom.

Table IV. Summary of Model Statistics

group	n[a]	p[b]	R[c]	s[d]	F[e]
I	47	5	0.995	0.337	749
II	179	12	0.984	0.747	419
III	50	6	0.911	0.535	34.9

[a] Number of chemical shifts used to define model. [b] Number of parameters in computed model. [c] Correlation coefficient. [d] Standard error of estimate in chemical shift units (ppm). [e] F value for significance of the model.

the target carbon to the corresponding atom. These distances are computed based on the coordinates returned from the molecular mechanics calculations. A weighting exponent can be applied to the inverse distance as discussed previously in relation to eq 2. The distance-based positional parameters allow geometrical information to be coupled with the topologically based HMO parameters.

Computation and Evaluation of Chemical Shift Models. For each of the three atom groups, a combination of stepwise regression and best subset regression (*38*) was used to determine the best sets of parameters for use in modeling the chemical shifts. The many possible models for each group were evaluated based on the statistical diagnostics resulting from the regression computations. In addition, the models were evaluated for the effects of collinearity among the independent variables (*39*). On the basis of this analysis, one model was selected for each atom group. Table IV provides a summary of the overall statistics for each model. Each model is statistically valid, and the standard errors between predicted and observed chemical shifts are significantly less than 1 ppm in each case.

Within each compound, the individual predicted chemical shifts were assembled to form complete simulated spectra. For each of the 32 compounds, the average prediction error across the spectrum was computed. The upper plot in Figure 2 is a bar graph that displays these spectral prediction errors. The mean spectral prediction error is 0.509 ppm.

The simulated spectra were evaluated further by comparing them to each of the experimentally observed spectra. In effect, a library search was performed in which the simulated spectra were treated as "unknowns", and the experimentally observed spectra comprised the "library". Spectral comparisons were performed by use of the ^{13}C NMR library search algorithm described by Carpenter and Small (*40*). In this test, the best possible results would be obtained if the nearest match to each simulated spectrum were the corresponding observed spectrum. This would imply that the simulated spectra are more similar to the corresponding observed spectra than they are to spectra of other similar compounds. In the library search, 30 of the 32 observed spectra were retrieved as the nearest matches to the corresponding simulated spectra. For the two cases in which the correct observed spectrum was not the nearest match, the correct spectrum was found as the second nearest match. These library search results further confirm the high accuracy of the simulated spectra.

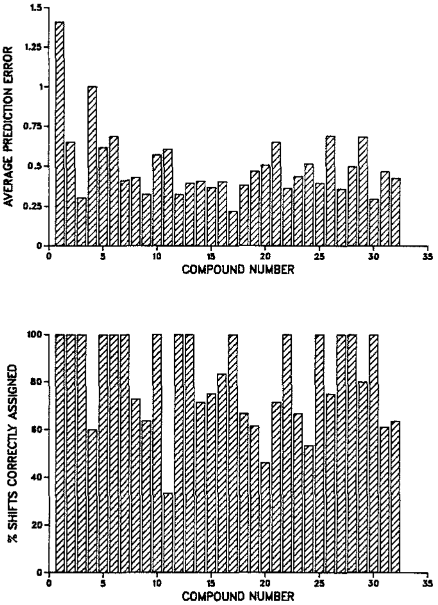

Figure 2. Top: Bar graph depicting the average spectral prediction error (ppm) for compounds **1**–**32**. Bottom: Bar graph depicting the percentage of chemical shifts correctly assigned in compounds **1**–**32** when the predicted spectra were used to assign the shifts.

Perhaps the sternest test of the accuracy of the computed models is an evaluation of their utility for assigning chemical shifts to specific atoms within a structure. To perform shift assignments, the experimental spectrum to be assigned is mapped onto the predicted spectrum. For example, the smallest chemical shift in the experimental spectrum is associated with the atom corresponding to the smallest chemical shift in the predicted spectrum. The other shifts are assigned in a similar manner.

For each of the 32 compounds, the predicted spectra were used to assign the chemical shifts. The percentage of shifts assigned in agreement with the literature shift assignments was taken as an indicator of the success of the models in assigning chemical shifts. The lower plot in Figure 2 is a bar graph that displays these percentages for the 32 compounds.

The success of the spectrum simulation approach to shift assignment is directly dependent on the accuracy of the predicted chemical shifts. An inspection of the lower bar graph in Figure 2 reveals that, for the most part, the models allow a large number of correct assignments to be made. Errors in assignments are caused in every case by the occurrence of several chemical shifts that differ by less than the standard error of the model used to predict the shifts.

Table V. Model for Group III Carbons

no.	coefficient	*t* value[a]	parameter
1	−1.44	1.96	sum of autopolarizabilities for atoms meta to the target carbon (TAPM 0)
2	37.2	7.30	distance-weighted sum of free valences for atoms para to the target carbon (distance exponent 1) (DFVP 1)
3	−8.11	5.26	sum of free valences for atoms para to the target carbon (TFVP 0)
4	−0.404	5.64	count of number of hydrogen atoms attached to carbons two bonds from the target carbon (NNHY 2)
5	−5.08	4.15	maximum free valence among atoms one bond from the target carbon (MXFV 1)
6	54.9	2.99	distance-weighted sum of autopolarizabilities for atoms meta to the target carbon (distance exponent 3) (DAPM 3)
constant	129.17		

[a] *t* value for the significance of the coefficient. A *t* value greater than 4.0 is considered highly significant.

Table VI. Example of Use of the Group III Model with Compound 24

parameter[a]	atom[b] 11 value	atom[b] 11 ppm	atom 12 value	atom 12 ppm	atom 13 value	atom 13 ppm	atom 14 value	atom 14 ppm
TAPM 0	2.05	−2.95	2.33	−3.36	2.29	−3.30	2.14	−3.08
DFVP 1	0.290	10.79	0.141	5.25	0.276	10.27	0.202	7.51
TFVP 0	0.989	−8.02	0.574	−4.66	0.976	−7.92	0.592	−4.80
NNHY 2	2	−0.81	3	−1.21	3	−1.21	3	−1.21
MXFV 1	0.580	−2.95	0.513	−2.61	0.513	−2.61	0.545	−2.77
DAPM 3	0.115	6.31	0.134	7.36	0.129	7.08	0.121	6.64
sum of terms, ppm		2.37		0.77		2.32		2.29
constant, ppm		129.17		129.17		129.17		129.17
predicted shift, ppm		131.54		129.94		131.49		131.46
observed shift, ppm		132.10		130.40		131.30		131.90
residual, ppm		−0.56		−0.46		0.19		−0.44

[a] Parameters correspond to those described in Table V. [b] Atoms refer to those specified in Figure 3.

Examination of Utility of Aromatic Structural Parameters. For the three computed chemical shift models, a total of 23 structural parameters are required. Nine of these are aromatic parameters of the type described in Tables II and III. Nine of the other parameters are distance-based parameters that employ the modeled atomic coordinates, while the remaining five parameters are derived from the topological features of the structures. By themselves, the HMO-based parameters are insufficient to model the chemical shifts accurately. Correspondingly, the distance-based parameters of the type described by eq 2 are also incapable of modeling the shifts when used alone. From this work, it is clear that a combination of steric and electronic structural information is required to allow highly accurate chemical shift models to be formed.

An examination of the nine aromatic structural parameters used reveals three parameters based on topological bond steps (Table II) and six based on our extended definition of ortho, meta, and para positions (Table III). Of the six positional parameters, three are para, two are meta, and one is ortho. Two are weighted by throughspace distances. Of the three parameters based on topological bond steps, only bond steps 1 and 2 are found useful. In addition, each parameter is based on the maximum or minimum value at the selected bond step, rather than on a summation of values. These results confirm that long-range effects are not encoded in a simple manner based on bond distances. The greater utility of the positional parameters supports our definition of the extended ortho, meta, and para positions.

Seven of the nine aromatic parameters are based on computed free valences, and two are based on autopolarizabilities. Throughout the model development work, the parameters based on bond order and superdelocalizability were less useful than those based on free valence and autopolarizability.

To demonstrate the manner in which the computed models work, Table V describes the group III model in detail, and Table VI illustrates the use of this model to predict the chemical shifts of atoms 11, 12, 13, and 14 in 2-methylanthracene (compound **24**). Figure 3 depicts the structure of this compound. The relevant atoms are indicated in the figure.

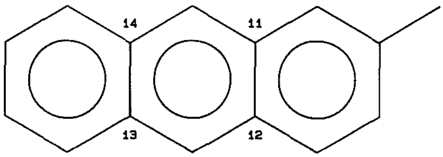

Figure 3. Structure of 2-methylanthracene (compound **24**). The simulation of the chemical shifts of the numbered atoms is detailed in Table VI.

The group III atoms were more difficult to model than the atoms in groups I and II. This is reflected in the lower correlation coefficient and *F* value for this model. The development of the positional aromatic parameters was a key in obtaining a correlation coefficient greater than 0.9. From an inspection of Table V, the only nonaromatic parameter in the model is an indicator variable that identifies the presence of methyl-substituted carbons two bonds from the target carbon. Four of the five aromatic parameters are based on our extended definition of ring position.

Table VI displays the values of the structural parameters used to predict the chemical shifts of the four indicated atoms. These values are multiplied by the corresponding regression coefficients in Table V to obtain the contributions of the parameters in chemical shift units (parts per million). An inspection of the parameter values reveals that the aromatic parameters effectively differentiate among the four target carbons. Each shift is predicted to an accuracy of 0.6 ppm or better. While it is difficult to interpret the function of the parameters in terms of magnetic shielding effects, the models are statistically valid and appear to perform well.

Evaluation of Predictive Ability of Models. The computed models were evaluated further by applying them to the prediction of chemical shifts in six compounds that were not

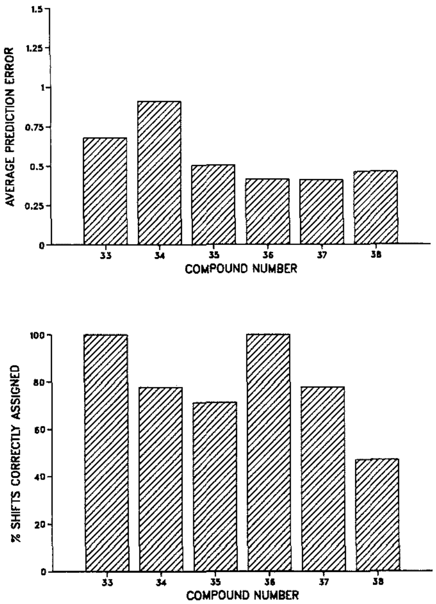

Figure 4. Top: Bar graph depicting the average spectral prediction error (ppm) for compounds **33–38**. Bottom: Bar graph depicting the percentage of chemical shifts correctly assigned in compounds **33–38** when the predicted spectra were used to assign the shifts.

included in the model development work. These compounds, numbered **33–38**, are listed in Table I. Complete simulated spectra were computed for the six compounds. Figure 4 displays the average prediction error for the six compounds, as well as the percentage of chemical shifts that would be correctly assigned by use of the simulated spectra. The two bar graphs in Figure 4 are analogous to those in Figure 2. As before, the models perform extremely well. The mean of the average prediction errors is 0.565 ppm, very close to the value computed for compounds **1–32**. Correspondingly, a majority of the chemical shifts are correctly assigned by use of the simulated spectra. In addition, a library search was performed as before. The library consisted of the experimentally observed spectra of compounds **1–38**. In each case, the observed spectra of compounds **33–38** were retrieved as the nearest matches to the corresponding simulated spectra.

To provide a visual perspective on the quality of the simulated spectra, Figure 5 depicts the simulated and experimentally observed spectra for each of the six compounds. In the figure, lack of plot resolution causes some lines to overlap. Any apparent discrepancies in the number of lines between simulated and observed spectra are a function of the lack of plot resolution. On the basis of each of these evaluations, the chemical shift models are observed to perform in a highly accurate manner.

CONCLUSIONS

The computed chemical shift models allow the ^{13}C NMR spectra of linear cyclic aromatic compounds to be simulated with high accuracy. On the basis of a variety of evaluation criteria, the derived models are judged useful for application to structure elucidation studies and in the confirmation of chemical shift assignments.

We believe the key to the success of this work is the use of a combination of steric and electronic structural parameters. The aromatic parameters derived from HMO calculations are extremely useful when combined with steric parameters based on the approximate atomic coordinates returned from molecular mechanics computations. While molecular mechanics and HMO calculations represent nontraditional tools for analytical chemists, they are both computationally practical. When integrated into a computer-based spectrum simulation system, these techniques can be used efficiently, and simulated spectra can be obtained rapidly. While the methodology described here has been implemented on a large interactive computer system, each of the calculations is compatible with a modern single-user laboratory computer.

The work described here represents a first step toward the

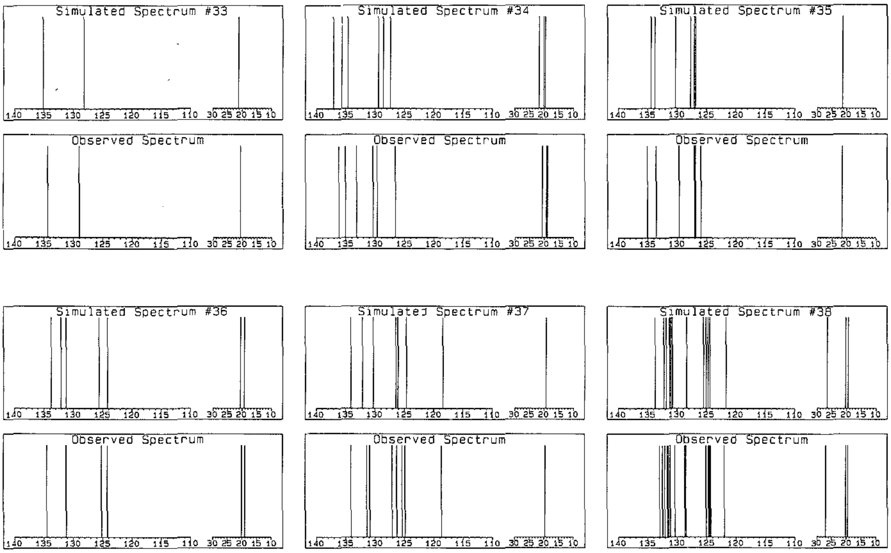

Figure 5. Simulated and observed spectra for compounds **33–38**.

development of a general spectrum simulation methodology for use with aromatic compounds. The key step required to enhance the practicality of the approach is the extension of the methodology to compounds containing heteroatoms and heteroatom-based substituents. This represents the next phase of the research to be performed.

ACKNOWLEDGMENT

Peter C. Jurs and co-workers of the Pennsylvania State University are acknowledged for performing the initial implementation of the HMO software on the Prime computer system.

Registry No. 1, 71-43-2; 2, 108-88-3; 3, 95-47-6; 4, 108-38-3; 5, 108-67-8; 6, 526-73-8; 7, 91-20-3; 8, 90-12-0; 9, 91-57-6; 10, 573-98-8; 11, 575-41-7; 12, 571-58-4; 13, 571-61-9; 14, 569-41-5; 15, 575-43-9; 16, 575-37-1; 17, 581-42-0; 18, 581-40-8; 19, 829-26-5; 20, 2245-38-7; 21, 14558-12-4; 22, 120-12-7; 23, 610-48-0; 24, 613-12-7; 25, 779-02-2; 26, 613-06-9; 27, 781-92-0; 28, 781-43-1; 29, 784-52-1; 30, 2960-97-6; 31, 57380-67-3; 32, 57380-68-4; 33, 106-42-3; 34, 95-63-6; 35, 582-16-1; 36, 13764-18-6; 37, 15815-47-1; 38, 27532-81-6.

LITERATURE CITED

(1) Fukui, H. *Bull. Chem. Soc. Jpn.* **1974**, *47*, 751.
(2) Ando, I.; Nishioka, A.; Kondon, M. *Bull. Chem. Soc. Jpn.* **1974**, *47*, 1097.
(3) Ebraheem, K. A. K.; Webb, G. A. *Prog. Nucl. Magn. Reson.* **1977**, *11*, 149–181.
(4) Solkan, V. N.; Klimenko, V. Yu.; Ustnyuk, Yu. A. *Theor. Exp. Chem.* (*Engl. Transl.*) **1973**, *9*, 254.
(5) Beveridge, D. L. In *Semiempirical Methods of Electronic Structure Calculation, Part B: Applications*; Segal, G. A., Ed.; Plenum: New York, 1977; Vol. 8.
(6) Barfield, M.; Grant, D. M. *J. Chem. Phys.* **1977**, *67*, 3322.
(7) Ditchfield, R.; Miller, D. P.; Pople, J. A. *J. Chem. Phys.* **1971**, *54*, 4186.
(8) Fukui, H.; Yoshida, H.; Muria, K. *J. Chem. Phys* **1981**, *74*, 6988–6989.
(9) Ewing, D. F. *Org. Magn. Reson.* **1979**, *12*, 499–524.
(10) Grant, D. M.; Paul, E. G. *J. Am. Chem. Soc.* **1964**, *86*, 2984–2989.
(11) Lindeman, L. P.; Adams, J. Q. *Anal. Chem.* **1971**, *43*, 1245–1252.
(12) Smith, D. H.; Jurs, P. C. *J. Am. Chem. Soc.* **1978**, *100*, 3316–3321.
(13) Small, G. W.; Jurs, P. C. *Anal. Chem.* **1983**, *55*, 1128–1134.
(14) Small, G. W.; Jurs, P. C. *Anal. Chem.* **1984**, *56*, 2307–2314.
(15) Egolf, D. S.; Jurs, P. C. *Anal. Chem.* **1987**, *59*, 1586–1593.
(16) Sutton, G. P.; Jurs, P. C. *Anal. Chem.* **1989**, *61*, 863–871.
(17) Gasteiger, J.; Marisili, M. *Org. Magn. Reson.* **1981**, *15*, 353.
(18) Gasteiger, J.; Saller, H. *Angew. Chem., Int. Ed. Engl.* **1985**, *24*, 687–689.
(19) Bremser, W. *Anal. Chim. Acta* **1978**, *103*, 355–365.
(20) McIntyre, M. K.; Small, G. W. *Anal. Chem.* **1987**, *59*, 1805–1811.
(21) Small, G. W.; McIntyre, M. K. *Anal. Chem.* **1989**, *61*, 666–674.
(22) Woolfenden, W. D.; Grant, D. M. *J. Am. Chem. Soc.* **1966**, *88*, 1496–1502.
(23) Dalling, D. K.; Ladner, K. H.; Grant, D. M.; Woolfenden, W. R. *J. Am. Chem. Soc.* **1977**, *99*, 7142–7150.
(24) Wilson, N. K.; Stothers, J. B. *J. Magn. Reson.* **1974**, *15*, 31–39.
(25) Caspar, M. L.; Stothers, J. B.; Wilson, N. K. *Can. J. Chem.* **1975**, *53*, 1958–1969.
(26) Gobert, F.; Combrisson, S.; Platzner, N.; Ricard, M. *J. Magn. Reson.* **1976**, *8*, 293–298.
(27) Brügger, W. E.; Jurs, P. C. *Anal. Chem.* **1975**, *47*, 781–784.
(28) Stuper, A. J.; Brugger, W. E.; Jurs, P. C. *Computer Assisted Studies of Chemical Structure and Biological Function*; Wiley-Interscience: New York, 1979; pp 83–90.
(29) Allinger, N. L.; Sprague, J. T. *J. Am. Chem. Soc.* **1973**, *95*, 3893–3907.
(30) Small, G. W.; Jurs, P. C. *Anal. Chem.* **1984**, *56*, 1314–1323.
(31) Lowe, J. P. *Quantum Chemistry*; Academic Press: New York, 1978.
(32) Greenwood, H. H. *Computational Methods In Quantum Chemistry*; Wiley-Interscience: New York, 1972.
(33) Yates, K. *Hückel Molecular Orbital Theory*; Academic Press: New York, 1978.
(34) Streitwieser, A. *Molecular Orbital Theory for Organic Chemists*; Wiley: New York, 1961.
(35) Ducasse, L.; Hoarau, J.; Pesquer, M. *J. Mol. Struc.: THEOCHEM.* **1982**, *88*, 61–70.
(36) Karpus, M.; Pople, J. A. *J. Chem. Phys.* **1963**, *38*, 2803–2807.
(37) Dewar, M. J. S. *The Molecular Orbital Theory of Organic Chemistry*; McGraw-Hill: New York, 1969.
(38) Draper, N. R.; Smith, H. *Applied Regression Analysis*, 2nd ed.; Wiley-Interscience: New York, 1981; Chapter 6.
(39) Belsley, D. A.; Kuh, E.; Welsch, R. E. *Regression Diagnostics: Identifying Influential Data and Sources of Collinearity*; Wiley-Interscience: New York, 1980; Chapter 3.
(40) Carpenter, S. E.; Small, G. W. *Anal. Chem.* **1988**, *60*, 1886–1895.

RECEIVED for review June 27, 1989. Accepted September 19, 1989.

Electrochemical Detection of Peptides

Anne M. Warner[1] **and Stephen G. Weber***

Department of Chemistry, University of Pittsburgh, Pittsburgh, Pennsylvania 15260

A general method of wide applicability for the determination of peptides is described. Peptides longer than dipeptides react in the classical biuret reaction with Cu(II) to yield electroactive Cu(II)-peptide complexes that can be oxidized to the corresponding Cu(III) complexes. This allows the sensitive electrochemical detection of peptides following their separation by reversed-phase liquid chromatography. The reaction chemistry, which is reversible, allows for the determination of peptides that lack an electroactive group or a primary amine. Selectivity for a model peptide is 10^3–10^4 over nonelectroactive amino acids.

The quantitative determination of peptides is an important pursuit in medicine, biology, and the pharmaceutical industry. Two highly selective methods, high-performance liquid chromatography (HPLC)/binding assay (*1, 2*) and HPLC/mass spectrometry (*3–7*), are used when one or a few known peptides are sought. These exacting techniques are less attractive for many tasks that do not require such exquisite selectivity. Unfortunately, there is a lack of reasonably simple and sensitive detectors that are generally useful for peptides. UV absorbance detection at 210 nm (*8–10*) is too general. The techniques that rely on the detection of particular amino acids, such as UV absorbance or fluorescence of the amino acids phenylalanine, tyrosine, and tryptophan (*11*), or electrochemistry of cysteine (*12*), tyrosine, and tryptophan (*13, 14*), lack generality. Procedures that use amine-specific chemistry for derivative formation, such as ninhydrin (*15, 16*), and fluorescamine (*8, 17, 18*), lack specificity. In addition, the amine derivatizing procedures are blind to peptides that lack an amino terminus, such as those that contain pyroglutamate or those that are formylated. The biuret reaction has been used for protein and peptide detection by UV absorbance following HPLC separation; however, the detection limits were a modest 100 pmol (*19*). We describe a simple detection system that uses the biuret reaction and dual electrode amperometric detection. This detection system gives electro-

---

[1] Current address: Eli Lilly & Co., P.O. Box 685, Lafayette, IN 47902.

0003-2700/89/0361-2664$01.50/0 © 1989 American Chemical Society

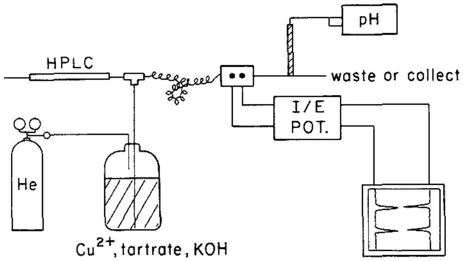

Figure 1. Schematic diagram of the apparatus. A tee mixes the He-pressure-driven stream of biuret reagent with the HPLC effluent. This is mixed in a short piece of knotted Teflon tubing before entering the dual electrode detector. The current from both electrodes is monitored, as is the pH of the effluent.

chemical signals for tripeptides and longer peptides that are not naturally electrochemically active. Thus, it is generally useful and enjoys the selectivity of the electrochemical detector.

The detection system is based on the century-old biuret reaction (*20*). The color of the Cu(II) complex formed in base by peptides and proteins is the basis of its utility in the clinical laboratory. Cu(II)–peptide complexes are also electroactive. The chemistry of these complexes has been studied by Margerum for over a decade, and that work has been reviewed recently (*21*). Cu(II)–peptide complexes, such as Cu(II)–(G_3), (the single-letter abbreviations for the amino acids will be used throughout; Table II defines these abbreviations) undergo a quasireversible oxidation to the Cu(III)–peptide at modest potentials (*21*) (0.6–0.9 V vs a normal hydrogen electrode (NHE)). The ability to be oxidized at modest potentials makes the Cu(II)–peptide complexes suitable for electrochemical detection. Because the electrochemistry is reversible, the more selective dual electrode amperometric detection can be used (*22*). In this scheme an upstream anode (generator) oxidizes Cu(II) to Cu(III), and then the Cu(III) is transported downstream across the surface of a cathode (collector). Current at the cathode from the Cu(III) reduction back to Cu(II) is measured. Investigations have been undertaken to determine both the suitability of this chemistry to electrochemical detection and the suitability of the scheme to peptide determinations.

EXPERIMENTAL SECTION

The electrochemical detector (homemade or BAS, West Lafayette, IN) contains an upstream glassy carbon anode to oxidize Cu(II) to Cu(III) and a downstream glassy carbon cathode to reverse this reaction. (Both electrodes were 3 mm diameter glassy carbon disks; they are separated (center-to-center) by 3.5 mm.) The spacer thickness was 0.013 cm. The current-to-voltage converter and potentiostat consisted of an LC4B from BAS and a homemade current-to-voltage converter for the second electrode.

The mobile phase for reversed-phase liquid chromatography contains water and perhaps either acetonitrile or methanol, phosphate (for buffering near pH 3 or 6 during chromatography), and borate (for buffering near pH 10 for the biuret reaction). The column was a Nova Pak C18 from Waters Associates.

A solution of cupric ion, added as the sulfate or perchlorate, at around millimolar concentration with 3 times that concentration of potassium sodium tartrate and KOH at around 1 M was added to the liquid chromatographic effluent after the column and before the electrochemical detector (see Figure 1). (Actual concentrations are given in the figures and tables.) The postcolumn reagent was pumped from a plastic bottle by using positive He pressure. The pH of the effluent from the electrochemical detector was monitored continuously by using a Fisher "pencil thin" combination pH and reference electrode and a Corning Model 5 or an Orion Model 701 meter. Sufficient pressure was applied to the postcolumn reagent bottle to yield an effluent pH of 9–10. Typically, the anode was held at a potential of 0.8 V and the cathode at 0 or 0.1 V vs Ag/AgCl, 3 M NaCl (which has a measured potential of +0.219 V vs NHE). The currents from both the anode and the cathode were recorded. Cyclic voltammetry was performed with a BAS CV-1B potentiostat. Peptides were obtained from Sigma (St. Louis, MO) and Research Plus (Denville, NJ) (alanine homopolymers only). It is worth noting that even simple peptides vary widely in their stability in solution.

RESULTS AND DISCUSSION

Before electrochemical detection was attempted, cyclic voltammetry at a glassy carbon electrode was used to determine the influence of the matrix on the Cu–peptide chemistry and electrochemistry. Because mobile phases for the reversed-phase liquid chromatography of peptides almost always will contain some organic solvent due to the hydrophobic nature of most peptides (*23*), any detection scheme must be compatible with these solvents. The formation of the Cu(II)–peptide complexes must occur after chromatography if silica-based reversed phases are used because the basic pH required to form the complexes causes hydrolytic destruction of that chromatographic medium. Thus, addition of the reagents in a postcolumn reactor is required. The commonly used solution for the biuret contains a Cu(II) salt, a salt of tartrate, and base. Because chromatography takes place in an acidic to neutral environment, the postcolumn addition of a buffer system and base is required to shift to a basic pH and maintain it. It therefore becomes necessary to determine whether the presence of the organic solvent and the buffer system will perturb the formation and electrochemistry of the complex.

The biuret complex was formed from a basic tartrate solution of copper and the tripeptide AGG. The cyclic voltammetry of this solution at pH 9 (see Figure 2) shows a quasireversible wave (ΔE_p = 80 mV) at 0.70 V vs Ag/AgCl, 3 M NaCl. The ratio of the cathodic to anodic peak currents can be used to infer the lifetime of the Cu(III) product (*24*). If the Cu(III)–peptide is stable on the time scale of the experiment, then the peak current ratio will be 1.0. If the Cu(III) is unstable, the peak current ratio will be less than 1. In aqueous solution at 20 mV s^{-1} the peak current ratio is about 0.5, which indicates that the Cu(III) complex undergoes chemical change to an electrochemically unreactive form on the 10-s time scale. (The experimental time from the half-wave potential to the switching potential is 10 s, and without detailed kinetic analysis, only an order of magnitude estimate is justified.) This decomposition is far more rapid than that observed by Rybka et al. for the G_4 complex (*25*).

Margerum (*21*) has correlated the decomposition rate of Cu(III)–peptides with the E^0 of the Cu(II)/(III) couple. The more positive the E^0, the more rapid the decomposition. The three tripeptides that are somewhat analogous to the AGG (A_3, G_3, L_3) have decomposition rate constants in the 0.5–3-s^{-1} range; thus the cyclic voltammetric determination yields a reasonable value. The rate of the destruction of the Cu(III) complex is faster when 25% (by volume) of the water is replaced by acetonitrile or methanol. The addition of 12.5 mM each of $Na_2B_4O_7$ and K_2HPO_4 (pH 9) in aqueous and mixed organic/aqueous solutions leads to the disappearance of the Cu(III) reduction peak. Voltammetry at 500 mV s^{-1} reveals the Cu(III) reduction wave (see Figure 3). At higher scan rates there is less time for the Cu(III)-consuming reaction to occur, and a voltammetric wave for the reduction is visible. The lifetime of the Cu(III) must be on the order of 100 ms under these conditions. In the mixed solvents of chromatographic relevance no large shift in redox potential is observed.

The cyclic voltammetry indicates that it is possible to detect the peptides by the oxidation of the Cu(II) complex. Cyclic voltammetry of other peptides (GGA, AGGG, A_3, A_4) revealed

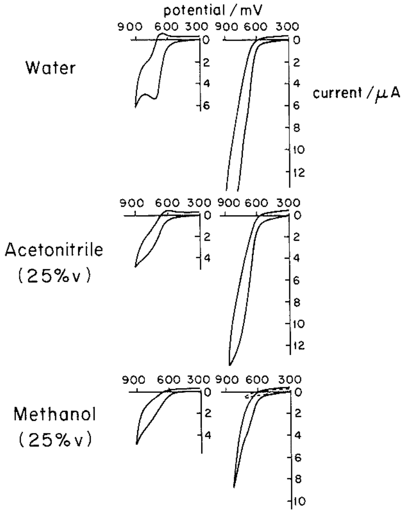

Figure 2. Cyclic voltammetry at a 3 mm diameter glassy carbon disk electrode taken at 0.020 V s^{-1}. In the left column voltammograms of solutions containing 1 mM AGG in an excess of basic copper tartrate are shown (the pH, or apparent pH, of each solution is near 9). The right column contains voltammograms from solutions containing the same solutes, but 12.5 mM phosphate and borate in addition. The top row has voltammograms that are taken in aqueous solution, the middle row is for 25% (v/v) acetonitrile, and the bottom row is for 25% (v/v) methanol. The dashed curve in the lower right panel is a voltammogram of a solution lacking the AGG.

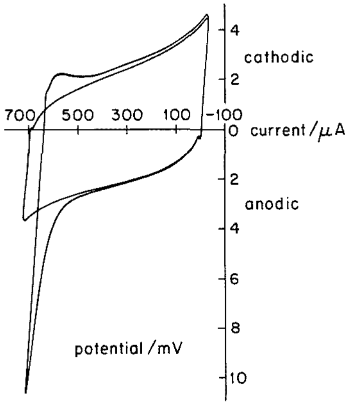

Figure 3. Cyclic voltammetry of AGG in methanolic buffer. Same conditions as in the lower right panel of Figure 2, but at the higher sweep rate of 0.50 V s^{-1}. Note the obvious presence of the Cu(III) → Cu(II) reduction peak, absent in the voltammogram of the solution lacking the AGG (the featureless voltammogram in this figure) and absent in the voltammogram in Figure 2 taken at a slower sweep rate.

longer Cu(III) lifetimes than the one for AGG. Rybka et al. (*25*) mention dramatic effects of borate and carbonate buffers on Cu(III)–G_4 complex stability. It is safe to conclude, from the literature and data presented, that Cu(II)–peptide complexes can be oxidized in an amperometric detector. Whether or not the resulting Cu(III) complex can be reduced at a downstream cathode depends on the transit time between the anode and cathode in the flow cell and the particular peptide involved. This is best determined experimentally.

Table I. Collection Efficiency[a]

solute	aqueous	10% MeOH	40% MeOH	15% AN[c]
A_3	0.28			
A_4	0.19	0.2		
A_5	0.33	0.29		
A_6		0.30		
GGFL			0.16	0.23
Fib-B[b]				0.08

[a] The eluent was 12.5 mM borate, 40 mM phosphate, and the pH was between 3 and 5 (during chromatography) with the indicated volume concentration of solvent. The postcolumn reaction solution was 1.1 mM Cu^{2+}, 3.3 mM tartrate, and 520 mM KOH. [b] Fibrinopeptide B is pEGVNDNEEGFFSAR. [c] Acetonitrile.

The collection efficiency of the detector is defined as the ratio of the current at the collector to the current at the generator (*26*). If the collection efficiency is high, then a Cu(II)–peptide complex that yields a signal by virtue of its oxidation will yield a significant signal at the downstream cathode. When this occurs, there is added selectivity, because the number of compounds giving rise to such signals is smaller than the number giving rise to the oxidation alone. If the collection efficiency is poor, then only the oxidation can be measured. Theoretical efficiencies for completely reversible electrodes have been calculated only for rectangular electrodes (*26*). For the circular electrodes of the dimensions used, the theoretical efficiency for a reversible reaction is about 0.33 if both halves of the redox couple are stable. If, in addition to simple diffusion, chemical processes occur that decrease the concentration of the product in the vicinity of the cathode, then the collection efficiency would be lower, decreasing to zero for a chemically irreversible oxidation. At typical flow rates (1–2 mL min^{-1}) the delay time between Cu(III) production at the upstream anode and Cu(III) reduction at the downstream cathode is on the order of 0.1 s. From the cyclic voltammetry data it can be inferred that the collection efficiency should be greater than zero and dependent on specific experimental conditions. Values obtained in a range of solvent systems are shown in Table I. The collection efficiency, which reflects the stability of the Cu(III)–peptide, is acceptable for analytical work. It reaches nearly the theoretical maximum for several of the alanine oligomers. The fact that the collection efficiency is lower for A_4 than for both A_3 and A_5 is puzzling. While it reinforces the point that the chemistry of the Cu(III)–peptides is sensitive to small alterations in the particular peptide, it is in contradiction with the previously discussed correlation of E^0 and decay rate. It may reflect the fact that the collection efficiency is also sensitive to changes in solvent and buffer composition.

Primary amine groups, and especially amino acids, are the targets of the commonly employed chemical reactions used for peptide derivatization. Because many other amines occur in biological samples, an excessive burden is placed on the chromatography for selectivity. The formation of the biuret complex is more specific because it requires the peptide backbone nitrogen and the molecular geometry of the peptide, but it does, after all, rely on Cu(II) chemistry, and it is well-known that Cu(II) forms complexes with amines. Thus the selectivity of the detector against amino acids was determined by comparing the signal at the anode and cathode for G_3 to that for amino acids. Representative data are shown in Table II. The selectivity at the collector electrode is 10^3–10^4 for G_3 over the nonelectroactive amino acids. Note that the most interfering nonelectroactive species are the basic amino acids, histidine, lysine, and arginine. It is probable that the signal from the amino acids is simply a result of the perturbation of the many complex equilibria in the solution with the result that the background current changes slightly. In

Table II. Sensitivity Ratio[a] for G_3:Analyte at Generator and Collector Electrodes

	electrode	
	generator	collector
Nonelectroactive Analytes		
nonpolar		
alanine (A)	500	4000
phenylalanine (F)	80	1000
glycine (G)	700	4000
isoleucine (I)	300	1000
leucine (L)	300	3000
methionine (M)	700	2000
proline (P)	200	1000
valine (V)	600	8000
polar, not basic		
aspartic acid (D)	2000	2000
glutamic acid (E)	1000	10000
asparagine (N)	500	1000
glutamine (Q)	1000	5000
serine (S)	1000	1000
threonine (T)	2000	2000
basic		
histidine (H)	50	900
lysine (K)	200	800
arginine (R)	1000	800
Electroactive Analytes		
cysteine (C)	2	2
tryptophan (W)	5[b]	200
tyrosine (Y)	2	200
Peptides		
GA	103	3000
G_3	1	1
G_5	2	2
G_6	2	3

[a] The sensitivity ratio is the concentration (μM) of analyte required to yield the same signal as 1.0 μM G_3. Conditions: mobile phase, 12.5 mM borate, 41.2 mM phosphate, pH 3.5; postcolumn phase, 1.1 mM Cu^{2+}, 3.3 mM tartrate, 0.52 M KOH. [b] This datum was taken under slightly different conditions: mobile phase, 50 mM borate, 0.14 M phosphate, pH 3.0; postcolumn solution, 1.1 mM Cu^{2+}, 3.3 mM tartrate, 1.8 M KOH.

fact, the cathodic current response to the amino acids is typically opposite in sign to that for the peptides.

Of the electrochemically active amino acids, only cysteine interferes at the cathode, because it is reversible. Although tyrosine and tryptophan interfere at the anode, their interference at the cathode is minimal because their oxidation products undergo rapid chemical reactions to form species that are difficult to reduce. Within the series of peptides, note the clear demarcation between the dipeptide GA and the tripeptide G_3, a result consistent with the biuret complex chemistry. The higher homologues in the G_n series show good sensitivity, but some signal attenuation occurs.

For many small peptides in both flow injection experiments (i.e., HPLC with no column) and chromatography, the sensitivity is roughly constant. Small peptides of three to six amino acids yield, at the anode, about 8 nA μM^{-1} injected in a 20-μL quantity and about 2 nA μM^{-1} at the cathode. With typical noise values (*27*, *28*) and clean samples this would translate into nanomolar (10 femtomol) detection limits. The experimentally determined detection limit, controlled by pump flow noise, is 12 nM, or 0.25 pmol injected for A_3. This could be improved considerably through the use of a well designed pulse dampener. The dynamic range is not known; however, the relationship between current (at both electrodes) and concentration injected is linear (adjusted $r^2 = 0.9684$ for 34 measurements at the anode; 0.9970 for 31 measurements at the cathode) over the range 86 nM to 86 μM. Most of the scatter in the calibration curves is due to a slow loss in sensitivity. No attempts to minimize the sensitivity loss by electrochemical cleaning were made.

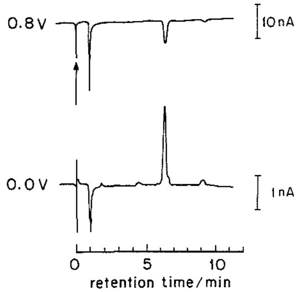

Figure 4. Detection of 54 pmol (20 μL of 2.7 μM) of A_5 using postcolumn addition of basic copper tartrate solution and dual electrode electrochemical detection. The mobile phase is aqueous 10.4 mM potassium dihydrogen phosphate and 12.5 mM sodium borate adjusted to pH 3.2 with phosphoric acid. The postcolumn addition phase is 1.1 mM $CuSO_4$, 3.3 mM potassium sodium tartrate, and 0.52 M KOH. Other conditions: anode, 0.8 V vs Ag/AgCl; cathode, 0.0 V; effluent pH, 9.4. The postcolumn reaction solution is controlled by pressure, not volume, so the mixing ratio is not actually controlled. Measurement showed that the postcolumn reaction volume was typically one-tenth of the column effluent volume.

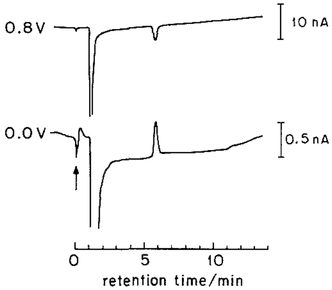

Figure 5. Detection of 8.8 pmol Des-Tyr-leucine-enkephalin (GGFL). Conditions were the same as in Figure 4, except 40% by volume of the water in the mobile phase, but not the postcolumn phase, has been replaced by methanol.

This detection limit compares favorably with the electrochemical detection of tyrosine- and tryptophan-containing peptides (in the 0.1–10-pmol range (*13*, *14*, *29*–*32*)). This detection is poorer than that reported by Mousa (*33*) for β-endorphin: 30 pg or about 0.01 pmol. Fluorescence detection of derivatized peptides, using 9-fluorenylmethyl chloroformate (*34*) and naphthalene-2,3-dicarboxaldehyde (*35*), is accomplished in the 0.2–0.5-pmol range. The current procedure has a selectivity in between the two cited class of procedures, and even though lower detection limits have been reported, this procedure should be useful for a broad spectrum of peptides.

Figures 4–6 show representative chromatograms illustrating the applicability of the detector under a variety of circumstances. The detection of A_5, with 0.30 efficiency at the collector, demonstrates the feasibility of the technique. The electroinactive tetrapeptide fragment of Leu-enkephalin, GGFL, yields a clear response in 40% methanol mobile phase (collection efficiency 0.16) (Figure 5) or in 15% acetonitrile (collection efficiency 0.23). A question that has not been investigated fully is the upper limit of the size for peptides. Certainly, proteins yield the biuret reaction, but whether or not reversible electrochemistry also occurs is not known. The tetradecapeptide fibrinopeptide B yields a signal as well; however, the sensitivity (on a molar basis) is 58 and 180 times

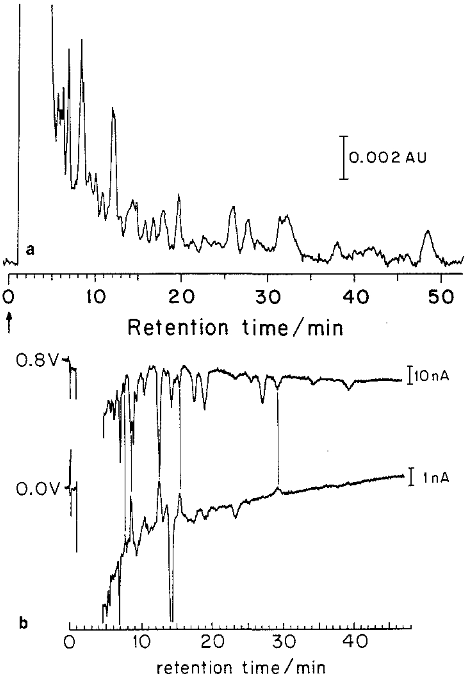

Figure 6. a. Human urine 3000 molecular weight cutoff ultrafiltrate injected onto the column. The mobile phase was as described for Figure 3, except 15% by volume of the water has been replaced by acetonitrile. Detection is UV at 210 nm. b. Same conditions, with postcolumn addition of 1.1 mM $Cu(ClO_4)_2$, 3.3 mM potassium sodium tartrate, and 0.52 M KOH in 15% acetonitrile, and dual electrode electrochemical detection. The five peaks that match the behavior of peptides are marked by vertical lines connecting the anodic and cathodic peaks.

less than for GGFL at the anode and cathode, respectively. Note that the amine terminus in fibrinopeptide B is unreactive toward amine-specific fluorescent reagents because of the cyclization in the pyroglutamate. Other α-amino substituted peptides, such as formylated and acetylated peptides, will also be reactive in this biuret/electrochemical detection system, but not in any amine-specific systems. Chromatograms of urine and canine CSF that have been treated only by ultrafiltration through a 3000 molecular weight cutoff filter are remarkably simple. Figure 6 compares the chromatograms of urine obtained by UV detection and the current method. The number of compounds yielding signals that are consistent with the component being a peptide is much smaller in Figure 6b than in Figure 6a. The selectivity advantage is clear.

It is not expected that this procedure will supplant the existing highly specific methods such as LC/binding assay (*1*, *2*) or LC/MS (*3–7*). However, the inherent simplicity, generality, selectivity, and sensitivity combine well to recommend it highly for determining peptides in such circumstances as screening or monitoring protein degradation. Whether the components that give peptide-like peaks are, in fact, peptides is currently being investigated by mass spectrometry on collected effluent. Further work toward increasing the selectivity toward peptides is underway.

LITERATURE CITED

(1) Venn, R. F. *J. Chromatogr.* **1987**, *423*, 93.
(2) Clement-Jones, V.; Lowry, P. J.; Rees, L. H.; Besser, G. M. *Nature* **1980**, *283*, 295.
(3) Desiderio, D. M.; Yamada, S. *J. Chromatogr.* **1982**, *239*, 87.
(4) Desiderio, D. M.; Kai, M.; Tanzer, F. S.; Trimble, J.; Wakelyn, C. *J. Chromatogr.* **1984**, *342*, 245.
(5) Fridland, G. H.; Desiderio, D. M. *J. Chromatogr.* **1986**, *379*, 251.
(6) Desiderio, D. M.; Dass, C. *Anal. Lett.* **1986**, *19*, 1963.
(7) Liu, D.; Desiderio, D. M. *J. Chromatogr.* **1987**, *422*, 61.
(8) Spatola, A. F.; Benovitz, D. E. *J. Chromatogr.* **1985**, *327*, 165.
(9) Richardson, W. S., III; Burns, L. *J. Chem. Educ.* **1988**, *65*, 162.
(10) Tellerova, K.; Spaced, P.; Adam, M. *J. Chromatogr.* **1983**, *273*, 197.
(11) Haschemeyer, R. H.; Haschemeyer, A. D. V. *Proteins, A Guide to Study by Physical and Chemical Methods*; Wiley & Sons: New York, 1973; Chapter 9, p 217.
(12) Allison, L.; Shoup, R. E. *Anal. Chem.* **1983**, *55*, 8.
(13) Fleming, L. H.; Reynolds, N. C., Jr. *J. Chromatogr.* **1986**, *375*, 65.
(14) Bretz, J. T.; Brown, P. R. *J. Chromatogr. Sci.* **1988**, *26*, 310.
(15) Molnar, I.; Horváth, C. *J. Chromatogr.* **1977**, *142*, 623.
(16) Hirago, Y.; Kinoshita, T. *J. Chromatogr.* **1981**, *226*, 43.
(17) Frei, R. W.; Lawrence, J. F. *Chemical Derivatization in Analytical Chemistry*; Plenum Press: New York, 1981; Vol. 1, Chapter 3, p 127.
(18) Udenfriend, S.; Stein, S.; Böhlen, P.; Dairman, W.; Leimgruber, W.; Weigele, M. *Science* **1972**, *178*, 871.
(19) Schlabach, T. D. *Anal. Biochem.* **1984**, *139*, 309.
(20) Mehl, J. W.; Pacovska, E.; Winzler, R. J. *J. Biol. Chem.* **1949**, *177*, 13.
(21) Margerum, D. W. *Pure Appl. Chem.* **1983**, *55*, 23–34.
(22) Roston, D. A.; Shoup, R. E.; Kissinger, P. T. *Anal. Chem.* **1982**, *54*, 1417A.
(23) Meek, J. L. *Proc. Natl. Acad. Sci.* (*USA*) **1980**, *77*, 1632.
(24) Bard, A. J.; Faulkner, L. R. *Electrochemical Methods*; Wiley; New York, 1980; p 429.
(25) Rybka, J. S.; Kurtz, J. L.; Neubecker, T. A.; Margerum, D. W. *Inorg. Chem.* **1980**, *19*, 2791.
(26) Matsuda, H. *J. Electroanal. Chem. Interfacial Electrochem.* **1968**, *16*, 153.
(27) Morgan, D. M.; Weber, S. G. *Anal. Chem.* **1984**, *56*, 2560.
(28) Weber, S. G. *Anal. Chem.* **1989**, *61*, 295.
(29) Bennett, G. W.; Johnson, J. V.; Marsden, C. A. *IBRO Handb. Ser.* (*Neuropeptides*) **1989**, *11*, 125.
(30) Drumheller, A. L.; Bachelard, H.; St.-Pierre, S.; Jolicoeur, F. B. *J. Liq. Chromatogr.* **1985**, *8*, 1829.
(31) Sauter, A.; Frick, W. *J. Chromatogr.* **1984**, *297*, 215.
(32) White, M. W. *J. Chromatogr.* **1983**, *262*, 420.
(33) Mousa, S.; Couri, D. *J. Chromatogr.* **1983**, *267*, 191.
(34) Vogt, W.; Egeler, E.; Sommer, W.; Eisenbeiss, F.; Meyer, H. D. *J. Chromatogr.* **1987**, *400*, 83.
(35) deMontigny, P.; Stobaugh, T. F.; Givens, R. S.; Carlson, R. G.; Srinivasachar, K.; Sternson, L. A.; Higuchi, T. *Anal. Chem.* **1987**, *59*, 1096.

RECEIVED for review July 10, 1989. Accepted September 7, 1989. Helpful discussions with Dominic Desiderio are gratefully acknowledged. Support of this research through Grant GM 28112 from the National Institutes of Health is also gratefully acknowledged.

Anal. Chem. **1989,** *61,* 2669-2673

Determination of Polycyclic Aromatic Hydrocarbons Using Gas Chromatography/Laser Ionization Mass Spectrometry with Picosecond and Nanosecond Light Pulses

Charles W. Wilkerson, Jr., Steven M. Colby, and James P. Reilly*

Department of Chemistry, Indiana University, Bloomington, Indiana 47405

The effect of laser pulse duration on the ionization efficiency of a variety of polycyclic aromatic hydrocarbons is studied by use of laser ionization gas chromatography/mass spectrometry. For compounds that undergo rapid excited-state relaxation, the use of ultrashort (picosecond) light pulses increases the probability of ionization relative to relaxation, resulting in improved ionization efficiency for these species.

INTRODUCTION

Laser multiphoton ionization has been employed as an effective ion source for the mass spectrometric determination of many compounds (*1–10*). In this technique, which offers some unique advantages compared to other ionization methods, analyte molecules are first excited by a UV laser to a low-lying electronic state, and then a second UV photon is absorbed to generate the ion. Under appropriate experimental conditions, laser ionization can be a very efficient process, and when combined with the high ion transmission of a time-of-flight mass spectrometer, excellent sensitivity can be achieved (*2, 4*). The time-of-flight instrument records an entire mass spectrum with each laser pulse. This eliminates the need to scan a mass analyzer and provides a multiplex advantage that also enhances sensitivity. High sensitivity is particularly useful when the analyte is present in small concentration or is in the ion source for only a short period of time, such as in gas chromatography/mass spectrometry (GC/MS). A gas chromatograph is used for sample introduction in our experiments to ensure that trace impurities, which can drastically alter observed ionization yields (*11, 12*), are separated from the compounds of interest. The GC also provides a quantitative and reproducible method for introducing multiple analytes into the ion source, thereby enabling a direct measurement of their relative ionization efficiencies under nearly identical conditions. In addition to the mass selectivity obtained in GC/MS, laser ionization can provide an additional degree of molecular selectivity, since the laser wavelength can be tuned so that certain analytes produce very strong ion signals, while other species may show little or no ionization (*2, 3*).

A number of previous investigations have explored the influence of laser conditions on the ionization yields of various species (*1–3, 13–15*). In the course of these studies it has been observed that ionization efficiencies can vary dramatically from compound to compound. Some of the reasons for this behavior are obvious. Molecules have different absorption characteristics and different ionization potentials. It is therefore not surprising that changing the laser wavelength would result in significant changes in relative ionization yields. Other reasons are more subtle. For example, the neutral precursor molecules can undergo dissociation after the absorption of the first photon. The resulting fragments may or may not be laser ionizable. Benzaldehyde is an example of a molecule that shows this kind of behavior, and its multiphoton ionization characteristics have been studied in detail (*11, 14, 15*). Excited neutral molecules can also undergo nonradiative relaxation. If an electronically excited molecule relaxes to a lower-lying state before it absorbs a second, ionizing photon, a loss of ionization efficiency may be observed. Some relaxation phenomena, such as internal conversion and intersystem crossing, can occur on very rapid, subnanosecond, time scales (*1, 16, 17*). In theory, one could overcome this problem by increasing the intensity of the laser pulse, thereby increasing the rate of photoionization relative to the rate of spontaneous relaxation. However, in practice this has not been of great utility. Previous experiments have shown that as the pulse intensity is increased, dissociation of both neutrals and ions becomes a dominant process (*13*). On the other hand, if the laser pulse is short compared to the time scale of these relaxation events, the use of high intensities is not necessary. In this case, photoionization should be favored compared to excited-state relaxation, and the ionization efficiency of a molecule with a very short excited-state lifetime should improve. The goal of the current study is to use both nanosecond and picosecond laser pulses to investigate the effect of laser pulse duration on the ionization efficiency of several polycyclic aromatic hydrocarbons. The measurements undertaken here employ species that have been studied in the past (*2, 4, 7*) but involve the use of different light wavelengths and pulse durations.

Table I. Selected Properties of the PAH Analytes Studied

molecule	MW, amu	IP,[a] eV	ϵ (240 nm)	ϵ (266 nm)	ϵ (299 nm)
naphthalene	128	8.12	2600	7000	200
biphenyl	154	8.27	15400	3000	≈0
acenaphthene	154	7.66	1000	5500	1500
fluorene	166	7.78	11500	12000	4000
phenanthrene	178	8.03	87000	16000	150
anthracene	178	7.43	40000	1500	200
fluoranthene	202	7.72	11000	10000	3600
pyrene	202	7.53	8500	20000	7000

[a] Values from Murov, S. L. *Handbook of Photochemistry*; Marcel Dekker: New York, 1973.

EXPERIMENTAL SECTION

Naphthalene (Eastman), biphenyl (MCB), acenaphthene (MCB), fluorene (MCB), phenanthrene (New England Nuclear), anthracene (MCB), fluoranthene (City Chemical Co.), and pyrene (Aldrich) are all used as received. For some experiments, stock solutions of the various analytes are prepared in methylene chloride (Fischer, Spectranalyzed), and these solutions are combined and diluted to give a final sample containing ≈7 ng/μL of each component. In other experiments, a standard polycyclic aromatic hydrocarbon sample (Accu-Standard M-610), containing all of the desired analytes except biphenyl, is used, and biphenyl is spiked into this sample to give a final concentration of 10 ng/μL of each component. A summary of selected properties of the molecules studied is given in Table I. The analytes are separated, using a Varian 3700 GC with on-column injection, on a 30 m/250 μm i.d. fused silica capillary column (Supelco SPB-1). The nitrogen carrier gas flows at a rate of ≈0.6 mL/min. A heated interface, which is held at a constant temperature of 250 or 320 °C (depending on the sample used), connects the GC to the mass spectrometer. The end of the column is positioned between the

0003-2700/89/0361-2669$01.50/0 © 1989 American Chemical Society

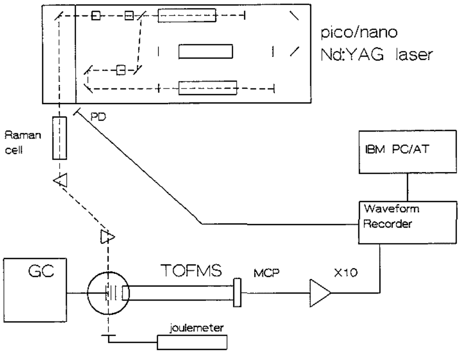

Figure 1. Schematic layout of experimental apparatus. The dotted line shows the path of the picosecond light pulse.

first two accelerating grids of a linear time-of-flight mass spectrometer that has been described earlier (2). A schematic drawing of the experimental apparatus is shown in Figure 1. The mass spectrometer is evacuated by a liquid-nitrogen-trapped Varian VHS-6 diffusion pump. Spectrometer pressure during the experimental runs is 4.6 × 10^{-5} Torr. Dual microchannel plates (Varian) configured in tandem are used for ion detection. The detector signal is amplified (LeCroy VV101ATB) and then digitized by using a high-speed waveform recorder (Biomation 6500). The digital signal is stored in a microcomputer for data display and analysis. A pico/nano pulsed Nd:YAG laser (Quantel YG-571-C) is used as the light source in all experiments. Conversion of the 1.06-μm Nd:YAG fundamental to the UV fourth harmonic at 266 nm is accomplished by two steps of frequency doubling (in KD*P and KDP). In nanosecond mode, the laser produces $\approx$10 ns (fwhm) Q-switched pulses. When operated in picosecond mode, the active/passive mode-locked system produces pulses of 18 picosecond (fwhm) duration at 1.06 μm. We estimate that the pulse duration at 266 nm is $\approx$10 ps, although this has not been directly measured. Stimulated Raman shifting in hydrogen gas (*18*) is used to obtain additional UV wavelengths, specifically, the first anti-Stokes (240 nm) and first Stokes (299 nm) lines of the fourth harmonic of the Nd:YAG. This technique for generating multiple wavelengths of coherent UV light from a fixed frequency pump laser offers the advantages of simplicity, ease of operation, and ruggedness compared to tunable dye lasers, and may be more suitable for routine analysis than a dye laser. The details of our Raman shifting technique will be presented in a separate publication (*19*). A 250 mm focal length lens is used to focus the beam into the ionization region of the mass spectrometer, and the focal point is positioned to intersect the analytes as they elute from the GC. The diameter of the beam at the point of ionization is $\approx$800 μm. The laser pulse energy is measured with a Laser Precision RjP-735 joulemeter mounted on the instrument so as to intercept the beam as it exits the spectrometer.

RESULTS

It is important to bear in mind that the purpose of the current study is to observe the effect of laser pulse duration on the *relative* ionization efficiencies of different molecules. With our current laser system, the amount of light produced in nanosecond mode is considerably greater than in picosecond mode. As a result, the absolute ion signal is invariably larger, and the signal to noise ratio tends to be better, in the longer pulse measurements. Nevertheless, the purpose of the short-pulse experiment is to improve our understanding of why ionization efficiencies vary as they do from one molecule to the next.

240-nm Wavelength. Figure 2 shows laser ionization chromatograms of the polycyclic aromatic hydrocarbon sample recorded by using the 240-nm first anti-Stokes line of the Nd:YAG fourth harmonic. Figure 2A displays the chromatogram obtained with nanosecond light having an average pulse energy of 100 μJ. Figure 2B shows the chromatogram recorded by using picosecond light at the same wavelength but at a significantly lower pulse energy of 2 μJ. Some loss of chromatographic resolution is observed in the picosecond experiment, this being due to a larger injection volume (2.0 μL compared to 0.6 μL in the nano experiment). Note that in the nanosecond chromatogram the area of the biphenyl peak is $\approx$4 times smaller than the area of the naphthalene peak. The picosecond result is dramatically different, the biphenyl signal being $\approx$13 times larger than the naphthalene response. Fluorene and anthracene also exhibit enhanced ionization efficiency with the picosecond pulses in comparison with naphthalene.

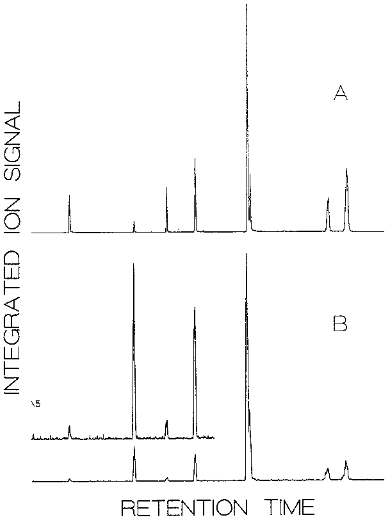

Figure 2. Chromatograms of polycyclic aromatic hydrocarbon sample at 240-nm wavelength: (A) nanosecond laser ionization, 100 μJ/pulse, 0.6-μL injection volume ($\approx$7 ng/component); (B) picosecond laser ionization, 2 μJ/pulse, 2-μL injection volume. Elution order is naphthalene, biphenyl, acenaphthene, fluorene, phenanthrene, anthracene, fluoranthene, pyrene.

299-nm Wavelength. The laser ionization chromatograms of the polycyclic aromatic hydrocarbon sample obtained by using the Stokes Raman shifted light at 299 nm are shown in Figure 3. Again, Figure 3A gives the nanosecond data acquired by using a laser pulse energy of 616 μJ, while Figure 3B shows the chromatogram obtained in the picosecond experiment at an average pulse energy of 52 μJ. Note that the chromatograms at this wavelength appear completely different from those recorded with the 240-nm light, demonstrating that molecular selectivity can be obtained by prudent selection of laser wavelength, even without using supersonic beam sample introduction to reduce spectral congestion. Phenanthrene and anthracene, both of which ionize well at 240 nm, yield very small ion signals for both picosecond and nanosecond pulse durations at this wavelength, as do both naphthalene and biphenyl. By comparison with naphthalene, fluorene and fluoranthene appear to ionize much more efficiently with picosecond light. The relative ionization efficiencies of acenaphthene and fluorene seem to reverse on going from nanosecond to picosecond conditions, and this observation will be discussed in the following section.

266-nm Wavelength. Chromatograms obtained by using the fourth harmonic of the Nd:YAG laser at 266 nm are presented in Figure 4. The nanosecond result, with an average pulse energy of 710 μJ, is shown in Figure 4A, while the pi-

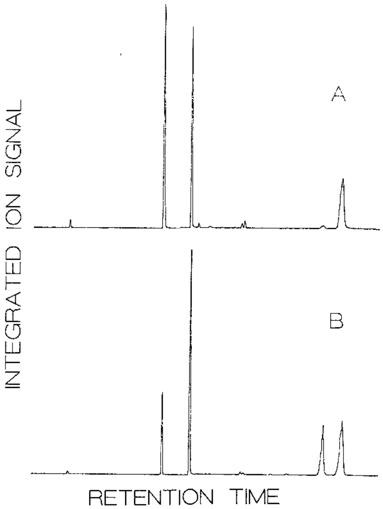

Figure 3. Chromatograms of polycyclic aromatic hydrocarbon sample at 299-nm wavelength: (A) nanosecond laser ionization, 616 μJ/pulse, 0.6-μL injection volume; (B) picosecond laser ionization, 52 μJ/pulse, 0.6-μL injection volume. The elution order is the same as in Figure 2.

cosecond chromatogram, recorded by using 410 μJ/pulse laser energy, is shown in Figure 4B. The nanosecond results presented here are somewhat different than those reported by Gross for a few of these analytes (*7*). It is not clear why this is the case. While the nanosecond and picosecond results are quite similar at this wavelength, one noteworthy exception is the improvement in fluoranthene ionization yield with shorter light pulses.

Since the primary goal of this work was to determine the ionization yield for these molecules as a function of laser pulse width, the full capability of the mass spectrometric detection system was not exploited. Single ion monitoring to improve both sensitivity and selectivity has been demonstrated using laser ionization MS (*5, 6*), but was not employed in this study. Ion signals with flight times corresponding to a mass range of 1–210 amu were integrated to obtain the data presented above. This time window discriminated against scattered laser light and high mass background, although very little of the latter was observed and it was not necessary to perform background subtraction. The amount of ion fragmentation was found to be strongly dependent on the laser intensity. In these experiments, the lowest light intensities were at 240 nm, and in this case fragment ions were responsible for less than 10% of the total ion signal. However, at the 266- and 299-nm wavelengths, more energetic pulses of light were available, particularly under nanosecond conditions, and fragment ions made up 30–90% of the ion yield. Since the fragments are believed to result from photofragmentation of parent ions, it is appropriate to include them in the total ion sum.

DISCUSSION

In order to understand the significance of the data presented in the previous section, it is first necessary to discuss those molecular characteristics that lead to efficient laser ionization. Clearly, in order for a resonant ionization process to occur, it is necessary for the molecules of interest to absorb the incident light. Therefore, investigating the UV absorption properties of the various analytes should give an initial indication as to their expected laser ionization propensities. Unfortunately, while solution-phase UV absorption spectra of the analytes involved in this study are well-known (*17*), gas-phase spectra for most have not been published. To measure accurate molar extinction coefficients of large gas-phase molecules generally requires a heated gas absorption cell. The higher temperatures needed to attain sufficient vapor pressure for such determinations typically lead to a significant amount of thermal congestion. This results in spectra that are not much better resolved than they are in solution. Furthermore, without accurate knowledge of the vapor pressure curve for a compound, information about the temperature of a heated cell is not sufficient to determine the sample concentration. In order to determine gas-phase extinction coefficients for the species in our experiment, we employ a hybrid approach. We have recorded low-resolution ($\approx$1 Å) gas-phase absorption spectra for each of the eight polycyclic aromatic hydrocarbons. The general appearance of these spectra is very similar to the published solution spectra; that is, the bands are of approximately the same width and shape. However, all are shifted by 6 to 18 nm from their solution counterparts. For this reason, we use the measured liquid phase extinction coefficients in conjunction with the shifted gas phase wavelength measurements.

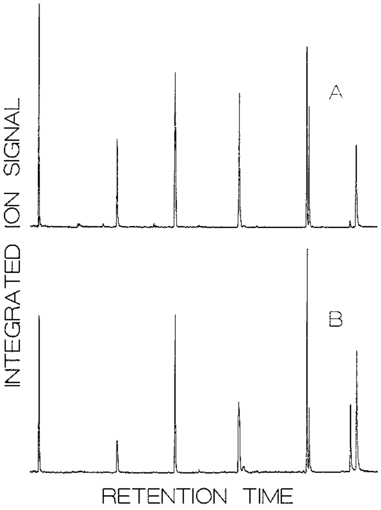

Figure 4. Chromatograms of polycyclic aromatic hydrocarbon sample at 266-nm wavelength: (A) nanosecond laser ionization, 71 μJ/pulse, 0.6-μL injection volume; (B) picosecond laser ionization, 41 μJ/pulse, 0.6-μL injection volume. Elution order is the same as in Figure 2, although retention times are not identical due to use of a different GC temperature program.

From the 240-nm data, it is clear that the picosecond result is dramatically different than the nanosecond result. In particular, we focus on biphenyl. In the nanosecond experiment, biphenyl ionizes poorly compared to naphthalene, while with the shorter light pulse biphenyl ionizes very well compared to naphthalene. The current nanosecond result is similar to earlier data obtained by using a 10-ns pulse KrF excimer laser (*2, 4*) whose wavelength is 248 nm. Using the method outlined above for determining gas-phase extinction coefficients, we find that biphenyl absorbs about 10 times more strongly than naphthalene at both the KrF wavelength and 240 nm. This number correlates well with the observed chromatographic peak ratios in Figure 2B. We therefore believe that biphenyl's poor ionization efficiency in the nanosecond experiment is the result of rapid excited-state relaxation. There are several additional pieces of data to support this interpretation. It is well-known to physical organic chemists that molecules with "floppy" substituent groups, that is, groups that are free to rotate and vibrate with respect to the rest of the molecule, often display fast relaxation characteristics (*20*). The quantum yield of fluorescence for biphenyl is 0.13, which also suggests rapid nonradiative decay (*21*). In additon, although the radiative lifetime of biphenyl in solution is on the order of several nanoseconds (*17*), lifetime measurements in the gas phase using a 2-ns dye laser pulse suggest that the lifetime is much shorter, perhaps on the order of hundreds of picoseconds (*22*). The fact that biphenyl ionizes well with picosecond light pulses establishes a lower bound on the lifetime of 10 ps. Other molecules, including fluorene and anthracene, also show improved ionization efficiency relative to naphthalene using the shorter light pulses. These species also have short radiative lifetimes in solution and are therefore also likely to be experiencing rapid excited-state relaxation.

The 299-nm data also exhibit some interesting effects. Phenanthrene and anthracene, both of which ionize very well at 240 nm, ionize only sparingly at 299 nm due to their small extinction coefficients in this region of the spectrum. This observation is true for both nanosecond and picosecond experiments. The exceptional case, fluoranthene, has a short fluorescence lifetime in solution and has a nonradiative relaxation rate that is 4 times greater than its radiative rate (*16*). Its ionization characteristics should be quite analogous to those of biphenyl as described above. The dramatic change in relative ion yields for acenaphthene and fluorene on going from nanosecond to picosecond conditions merits further comment. In the picosecond experiment, the ratio of the chromatographic peak areas is the same as the ratio of the extinction coefficients, as one might most simply predict. It is noteworthy that in this case the laser pulse energy is rather small (52 μJ). In the nanosecond experiment, the pulse energy is substantially higher (616 μJ), and the reversal of the peak heights may be indicative of transition saturation effects. When saturation occurs, all of the strongly absorbing molecules irradiated by the laser beam are converted to ions, and the relative ionization efficiencies for all of the other species change, complicating the interpretation of the data.

The analytical utility of this technique would be improved if a quantitative model could predict laser ionization efficiencies of various compounds. An initial formulation will now be presented, in which we assume that the ionization efficiency of a molecule depends primarily on four factors: [1] σ_1, the cross section for absorption of the first photon which excites the molecule from the ground electronic state into an electronically excited intermediate state; [2] σ_2, the cross section for absorption of the second photon which pumps the excited molecule into the ionization continuum; [3] τ, the lifetime of the electronically excited intermediate state; and [4] the laser fluence, which affects the rate of stimulated absorption. We assume that the time for the absorption of both excitation and ionization photons, which is less than or equal to the temporal profile of the laser pulse (τ_{las}), is short compared to the lifetime of the resonant excited state ($\tau_{las} < \tau$). This should be a valid assumption under *picosecond* laser conditions but is not generally true under *nanosecond* conditions. While the excitation cross-section σ_1 can be obtained directly from the molar extinction coefficients, we must assume that the excited-state photoionization cross-section σ_2 is approximately the same for all molecules under study. Finally, to ensure that ion yield will directly depend on σ_1, we assume that the first absorption step is not saturated. This model allows us to estimate the photoionization yield of compound i in the picosecond experiment based on the following equation:

$$\#\mathrm{Ions}(i) = k*n(i)*\sigma_1(i)$$

where #Ions(i) is the number of ions produced by laser ionization of $n(i)$ neutral molecules and k is a constant that is proportional to the laser fluence and the ionization cross section (σ_2). The number of neutral precursors in the laser focal volume, $n(i)$, is proportional to the mass of each component injected and inversely proportional to its molecular weight.

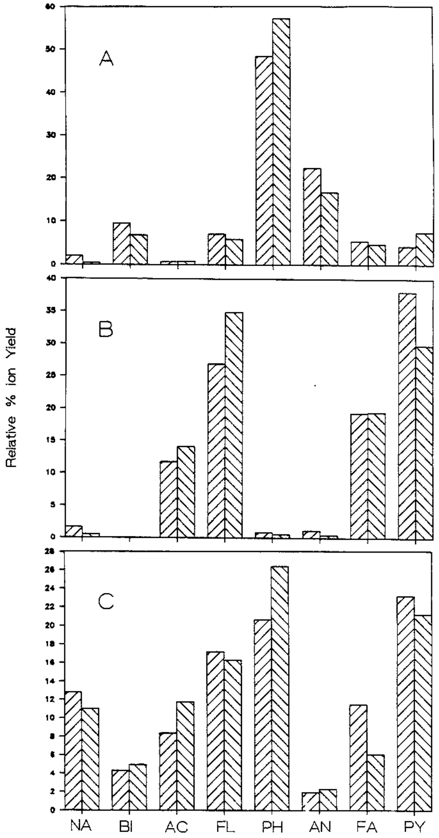

Figure 5. Comparison of picosecond experimental results to results from model described in text: (A) 240-nm laser wavelength, (B) 299-nm laser wavelength, (C) 266-nm laser wavelength; (left bar) calculated value, (right bar) experimental value; NA, naphthalene; BI, biphenyl; AC, acenaphthene; FL, fluorene; PH, phenanthrene; AN, anthracene; FA, fluoranthene; PY, pyrene. Experimental results represent total ion chromatogram peak areas.

Figure 5 presents a series of bar graphs that compare the picosecond experimental chromatographic peak areas to results predicted from the above model. Part A corresponds to the 240-nm case. There is a strong correlation between the experimental and calculated values; where we predict good ionization efficiency we observe it, and where we predict poor ion yield we also observe that. This encouraging agreement is also found at the 299-nm wavelength, as evident in Figure 5B. At 266 nm the correspondence between calculation and experiment is also quite good, with the exception of fluoranthene (FL). Its experimental response is about a factor of 2 lower than the model predicts, and the errors in both the experimental measurement and in the data incorporated into the model are small compared to this difference. The most likely explanation for this discrepancy is that fluoranthene has a significantly different excited-state photoionization cross section (σ_2) compared to the other analytes at this wavelength. We are currently pursuing experiments to investigate the nature of this unexpected result.

In the earlier discussion on biphenyl ionization efficiency, the difference between the fluorescence lifetime measured in solution and that measured in the gas phase was mentioned. Recent work in our laboratory indicates that for some molecules the fluorescence lifetime in the gas phase is longer than that in solution, while for other molecules the opposite is true. Certainly the interaction between the excited molecule and the solvent critically affects the excited-state dynamics. In some cases, such as biphenyl, the presence of a solvent cage around the molecule may inhibit free rotation about the inter-ring bond, and without this free rotation, the rate of relaxation should be diminished. Even in some rigid molecules, following the initial excitation of high-lying electronic states, internal conversion can lead to substantial population in vibrationally excited levels of the first excited singlet state, S_1. Vibrational relaxation by solvent collisions can populate lower vibrational levels of S_1. In this case the solvent's effect is to increase both the observed lifetime and the quantum yield of fluorescence. However, for other molecules, the presence of the solvent may provide other pathways for rapid collisional deactivation leading to shorter excited-state lifetimes and smaller amounts of fluorescence. Understanding such differences in gas-phase vs liquid-phase excited-state relaxation is a problem of general interest, and laser ionization can help provide some of this information. Picosecond pump–probe ionization experiments can be used to determine the lifetimes of various molecules in the gas phase, while picosecond time-resolved fluorescence can be applied to measure solution lifetimes.

CONCLUSIONS

Interpretation of the results obtained in the current study has allowed us to more clearly understand previous experimental observations (*2*, *4*, *7*). The analytical benefit gained from this understanding is the potential for an increase in detection sensitivity when ultrashort light pulses are used to photoionize species that undergo rapid nonradiative processes. This potential will only be realized when high-energy coherent picosecond light sources are available. The good agreement between the experimental data and calculated "chromatograms" suggests that it should be possible to predict with semiquantitative accuracy the behavior of other species on the basis of our simple model. Also, these measurements have demonstrated that an additional degree of selectivity can be gained by controlling the laser pulse duration. Future experiments will be directed at determining effective ionization cross sections by performing intensity-dependent measurements of ion yield (*1*). In addition, we will continue to investigate the application of picosecond pulse laser ionization to improving the detection sensitivity of other species, such as nitro-containing molecules, phenols, and chlorinated aromatics, some of which also ionize poorly with nanosecond radiation (*5*, *6*, *23*). These applications may impact environmental analysis, due to the ubiquity of these types of compounds. Numerous molecules undergo efficient intersystem crossing as a result of heavy atom substitution (*16*). It is likely that excited-state relaxation effects will adversely affect the ionization efficiencies of these species, and the use of picosecond light pulses may improve their detection sensitivity.

Registry No. Naphthalene, 91-20-3; biphenyl, 92-52-4; acenaphthene, 83-32-9; fluorene, 86-73-7; phenanthrene, 85-01-8; anthracene, 120-12-7; fluoranthene, 206-44-0; pyrene, 129-00-0.

LITERATURE CITED

(1) Reilly, J. P.; Kompa, K. L. *J. Chem. Phys.* **1980**, *73*, 5468.
(2) Rhodes, G.; Opsal, R. B.; Meek, J. T.; Reilly, J. P. *Anal. Chem.* **1983**, *53*, 280.
(3) Lubman, D. M. *Anal. Chem.* **1987**, *59*, 31A.
(4) Opsal, R. B.; Reilly, J. P. *Optics News* **1986**, (June), 18.
(5) Opsal, R. B.; Reilly, J. P. *Anal. Chem.* **1986**, *58*, 2919.
(6) Opsal, R. B.; Reilly, J. P. *Anal. Chem.* **1988**, *60*, 1060.
(7) Sack, T. M.; McCrery, M. A.; Gross, M. L. *Anal. Chem.* **1985**, *57*, 1290.
(8) Lubman, D. M.; Naaman, R.; Zare, R. N. *J. Chem. Phys.* **1980**, *72*, 3034.
(9) Sin, C. H.; Tembreull, R.; Lubman, D. M. *Anal. Chem.* **1984**, *56*, 2776.
(10) Lubman, D. M.; Tembreull, R.; Sin, C. H. *Anal. Chem.* **1985**, *57*, 1084.
(11) Long, S. R.; Meek, J. T.; Harrington, P. J.; Reilly, J. P. *J. Chem. Phys.* **1983**, *78*, 3341.
(12) Rockwood, S.; Reilly, J. P.; Hohla, K.; Kompa, K. L. *Opt. Commun.* **1979**, *28*, 175.
(13) Sekreta, E.; Owens, K. G.; Reilly, J. P. *Chem. Phys. Lett.* **1986**, *132*, 450.
(14) Yang, J. J.; Gobeli, D. A.; Pandolfi, R. S.; El-Sayed, M. A. *J. Phys. Chem.* **1983**, *87*, 2255.
(15) Yang, J. J.; Gobeli, D. A.; El-Sayed, M. A. *J. Phys. Chem.* **1985**, *89*, 3426.
(16) Birks, J. B. *Photophysics of Aromatic Molecules*; Wiley-Interscience: London, 1970.
(17) Berlman, I. B. *Handbook of Fluorescence Spectra of Aromatic Molecules*, 2nd ed.; Academic Press: New York, 1971.
(18) Brink, D. H.; Proch, D.; Basting, D.; Hohla, K.; Lokai, P. *Laser Optoelektron.* **1982**, 41.
(19) Wilkerson, C. W., Jr.; Sekreta, E.; Reilly, J. P., manuscript in preparation.
(20) Drexhage, K. H. In *Dye Lasers*; Schäfer, F. P., Ed.; Springer: Berlin, 1977; Springer Topics in Applied Physics 1, Chapter 4.
(21) Li, R.; Lim, E. C. *J. Chem. Phys.* **1972**, *57*, 605.
(22) Wilkerson, C. W., Jr.; Reilly, J. P., unpublished results, 1988.
(23) Opsal, R. B. Ph.D. Thesis, Indiana University, Bloomington, IN, 1985.

RECEIVED for review May 12, 1989. Accepted August 4, 1989. This work has been supported by grants from the National Science Foundation and the U.S. Environmental Protection Agency. The picosecond laser system was acquired through an equipment grant from the Army Research Office. C.W.W. acknowledges fellowship support from Proctor & Gamble and Upjohn.

Anal. Chem. **1989**, *61*, 2674–2682

Influence of the Ratio of Matrix to Analyte on the Fast Atom Bombardment Mass Spectrometric Response of Peptides Sampled from Aqueous Glycerol

C. E. Heine,[1] **J. F. Holland,**[2] **and J. T. Watson***[,1,2]

Departments of Chemistry and Biochemistry, Michigan State University, East Lansing, Michigan 48824

Fast atom bombardment mass spectrometry (FAB-MS) studies of the nonapeptide bradykinin sampled from aqueous glycerol illustrate the importance of the matrix to analyte ratio in the FAB experiment. Enhanced mass spectral results (in conventional direct probe FAB analyses) are characterized by increased ionization efficiency of the analyte together with a substantial reduction in the glycerol background signal. Replicate analyses of different bradykinin/glycerol/water mixtures show this improvement to depend upon the glycerol/bradykinin relationship and not the water/bradykinin relationship in sampling 4 nmol of bradykinin from 1% to 56% aqueous glycerol (2 μL initial sample volumes). The optimum desorption ionization occurs when the molar ratio of glycerol to bradykinin is approximately 300:1. A model emphasizing the importance of the analyte surface concentration in the matrix (with water being simply a convenient vehicle for the deposition of minute portions of glycerol) is proposed to account for the spectral enhancement. The FAB-MS enhancement behavior of four other peptides, selected for their differences in hydrophobicity (and hence, surface activity in glycerol), is compared to that of bradykinin.

INTRODUCTION

Since its advent in 1981 (*1*), fast atom bombardment (FAB) has become the dominant mode in desorption ionization mass spectrometry. This technique provides molecular weight information from sustained and reproducible ion signals for many nonvolatile, thermally labile analytes. The innovative feature of FAB-MS involves the use of a liquid support compound, or matrix, to provide an environment conducive to sustained desorption ionization under conditions of kiloelectronvolt particle bombardment. Although persistent questions concerning the mechanism still remain, much has been learned regarding the desorption ionization process in FAB as many of the parameters and conditions in the experiment have been optimized (*2*). One factor that has been shown to exert considerable influence over the mass spectral results is the concentration of the analyte at the surface of the matrix (*3–13*).

Unfortunately, the matrix compound itself provides a mass spectrum that can interfere with and complicate spectral interpretation for the analyte. The mass spectrometrist would prefer to maximize the signal from the analyte and minimize the interfering matrix spectrum. Various strategies in sample preparation have evolved to accomplish these goals. Many workers add acidic or cationic modifiers to their samples to enhance the analyte ion abundance in the positive ion mode; however, this method also increases the abundance or complexity of the matrix spectrum in many cases (*13, 14*). Some laboratories apply the matrix from a solution of a particular concentration (e.g., 50% aqueous glycerol), while others deposit a portion of neat matrix on the sample pedestal.

Our work originated with the observation that application of the glycerol matrix in a dilute aqueous solution (rather than neat) allows a significant enhancement in the spectral quality of conventional direct probe FAB analyses. This observation prompted a systematic study regarding the effects of analyte, glycerol, and water quantity upon the FAB-MS results for five peptides. The experimental findings suggest that the molar ratio of glycerol to analyte is critical in optimizing the desorption ionization behavior of the sample. The optimum occurs at the point where the formation and detection of analyte ions are differentially favored over that of the matrix ions.

EXPERIMENTAL SECTION

Mass Spectrometry. All experiments were performed upon a double focusing (EB geometry) JEOL HX-110 mass spectrometer. This instrument is equipped with a FAB gun which produces a 6-keV xenon beam that was used for this work. The source pressure with the xenon beam operating was approximately 3×10^{-6} Torr. A resolving power of 3000 was employed at an acceleration potential of 8 or 10 kV. For the comparisons strictly involving bradykinin, scans were collected over a mass interval from 30 to 1200 u, in a period of 10.1 s, allowing 2.8 s between consecutive scans. For those runs utilized in the comparison of results from the five peptides, a mass range of 0–1300 u was scanned in 11.1 s, allowing 2.1 s between scans. All data were acquired, stored, and processed with the JEOL DA5000 data system.

Materials. The five peptides ([val^4]-angiotensin III, proenkephalin, bradykinin, fibronectin related peptide, and NPNANPNANPNA) were purchased from Sigma Chemical Co. and glycerol was obtained from Mallinckrodt, Inc. Aqueous matrix solutions were prepared in terms of weight percentage glycerol.

Sample Preparation and Analysis. All aqueous solutions of matrix and analyte were applied with Hamilton syringes. Sample application began by depositing the glycerol matrix upon the probe tip. The analyte portion was then added and the sample stirred with the syringe needle for approximately 15 s. All sample compositions reported below describe the sample prior to exposure to the vacuum. The probe was introduced into the source of the mass spectrometer immediately after evacuating the vacuum lock. At this point, the FAB beam, acceleration potential, repeller potential, and lens potentials were adjusted to optimize the peak shape and intensity at a selected m/z value (e.g., m/z 185). Only minor adjustments were needed for each parameter because of prior focusing, and the entire process, from probe insertion to initiation of the scan, was accomplished in approximately 1 min. Due to the transient desorptive behavior of some samples, on occasions when extensive focusing (requiring longer than one minute) was necessary, the probe was removed from the source without the acquisition of data and a new sample was applied. For this reason, also, the first scan of each run was utilized for data comparison.

Ion abundances represented in the figures were divided by the full-scale value of the output device; hence, they are intended to be interpreted in an absolute sense. Appropriate peaks in the bradykinin spectrum have been labeled according to the nomenclature suggested by Roepstorff and Fohlman (*15*) and modified by Biemann (*16*). Figures illustrating bradykinin ion response under various conditions are based on a representative

---

[1] Department of Chemistry.
[2] Department of Biochemistry.

0003-2700/89/0361-2674$01.50/0 © 1989 American Chemical Society

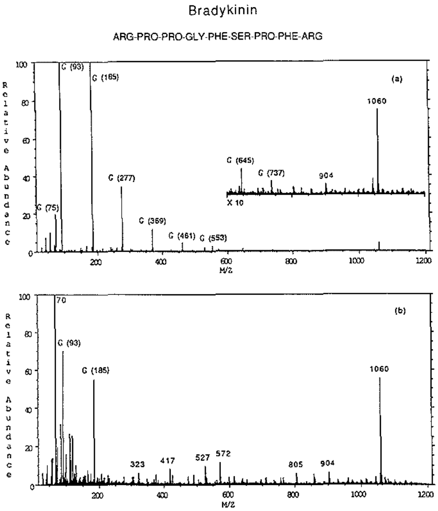

Figure 1. (a) FAB mass spectrum of 1.0 μL of aqueous bradykinin solution (4 nmol/μL) added to 1 μL of glycerol. Major peaks derived from the glycerol matrix are labeled with a "G". (b) FAB mass spectrum of 1.0 μL of bradykinin solution added to 1.0 μL of 10% glycerol.

cross section of the mass spectrum: one ion of low mass (e.g., m/z 70), another of intermediate mass (e.g., m/z 527), and the $[M + H]^+$ ion (m/z 1060); other significant bradykinin ions (m/z 120, 491, 572, 805, 903) in each spectral region usually behaved in an analogous manner. Comparison of results (absolute peak intensity values) was limited to those data collected from an individual session on the mass spectrometer. Results from different days were not compared because of differences in instrumental conditions (e.g., source cleanliness and settings of detection electronics).

RESULTS AND DISCUSSION

Figure 1a shows a spectrum of 4 nmol of bradykinin dispersed in 56% (w/w) glycerol in water (prior to exposure to the vacuum). This sample was prepared by adding 1.0 μL of an aqueous bradykinin solution (4 nmol/μL) to 1 μL of glycerol. Those peaks denoted by a "G" correspond to glycerol matrix ions. Figure 1b shows a spectrum of 4 nmol of bradykinin dispersed in an environment of 5% (w/w) glycerol in water. This sample was obtained by adding 1.0 μL of the aqueous bradykinin solution to 1.0 μL of 10% glycerol in water. Interestingly, the spectra display significant differences. The spectrum taken from the sample containing less glycerol and more water (Figure 1b) shows a much better visibility of analyte peaks over matrix peaks, although both samples contained the same amount of bradykinin. This improvement occurs from the $[M + H]^+$ signal at m/z 1060, through peaks corresponding to structurally significant fragment ions, to lower mass immonium ions.

To more carefully characterize this effect, mass spectral results from samples composed of 1%, 2%, 5%, 21%, and 56% glycerol in water were compared. Each sample contained 4 nmol of bradykinin and the total sample volume in each case was initially 2 μL. Figure 2 shows peak intensities for selected analyte ions (divided by the full-scale signal of the output device) plotted against weight percent of glycerol. Each point represents the mean of three separate runs (the first scan was evaluated from each run) and the error bars correspond to one standard deviation of these data. For all analyte ions there is a significant increase in abundance as the sample consists of more water and less glycerol. This enhancement reaches a maximum followed by a decline in abundance as the glycerol becomes scarce. Interestingly, the optimum matrix composition does not appear to be identical for all analyte ions. While the higher mass analyte ion abundances maximize at 5% glycerol (as viewed in Figure 2), the ion abundances for m/z 70 maximize at 2% glycerol. The peak at m/z 70 corresponds to an immonium ion which is indicative of the proline amino acid residue. For bradykinin and the other four peptides investigated in this work, peak intensities for the immonium ions and other especially low mass fragment ions optimized at slightly lower proportions of glycerol in water than the peak intensities for other analyte ions. This trend, which may appear subtle given the precision of results obtained from the two sample compositions shown in Figure 2, is nonetheless reproducible in the repeated formulation of these curves.

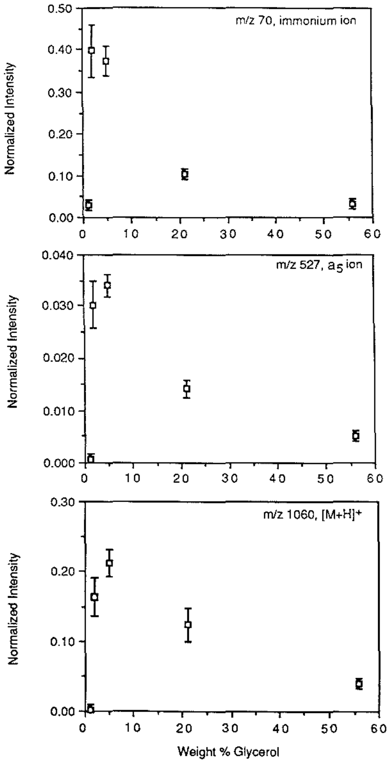

Figure 2. Plots of peak intensity for selected bradykinin ions (m/z 70 (top), m/z 527 (middle), and m/z 1060) versus weight percentage glycerol. Each sample contained 4 nmol of bradykinin and the total sample volume in each case was 2 μL.

Figure 3 shows the corresponding data for selected matrix ions. Quite clearly, the glycerol peak intensities decrease substantially as the amount of glycerol in the sample declines. Accordingly, the net effect observed in Figure 1 is due to two complementary factors. Increasing the amount of water and decreasing the amount of glycerol in the sample appear to bolster analyte ion abundances and diminish matrix ion abundances significantly. This result is analogous to the observations of Caprioli while using the continuous flow FAB probe (*17*).

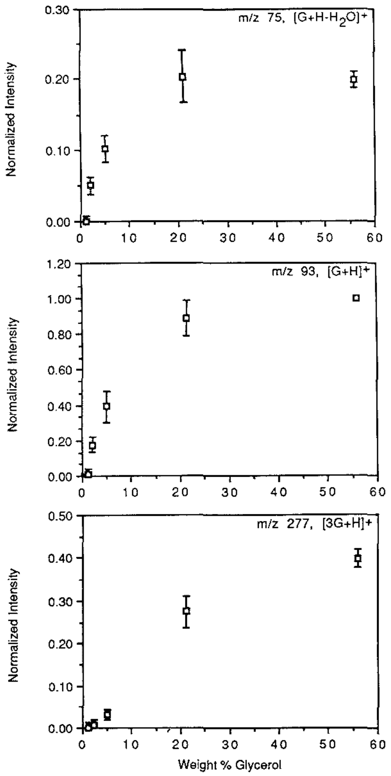

Figure 3. Plots of peak intensity for selected glycerol ions (*m/z* 75 (top), *m/z* 93 (middle), and *m/z* 277) versus weight percentage glycerol. Each sample contained 4 nmol of bradykinin and the total sample volume in each case was 2 μL.

Another difference in results obtained from the two sample compositions represented in Figure 1 involves the time dependence of the experiment. While the sample containing more glycerol maintains a signal over a relatively long period of time, the signal from the sample containing less glycerol is more transient. The ion abundances produced from the latter environment tend to diminish comparatively rapidly; consequently, the first spectrum obtained under these circumstances is often the most useful. This observation suggested a comparison of ionization efficiency of the analyte as a function of matrix composition. An assessment of ionization efficiency was accomplished by integrating the ion current for several analyte ions while analyzing samples containing the same amount of bradykinin, but different concentrations of matrix, namely, 2-μL portions of 56% and 5% glycerol in water (the same two sample compositions represented in Figure 1). Accordingly, spectra from both these sample compositions were collected continuously until the $[M + H]^+$ signal (*m/z* 1060) could no longer be distinguished from detector noise (this required approximately 30–40 min for the samples containing more glycerol and approximately 10–15 min for the samples containing less glycerol). The signal areas under the mass chronograms for analyte ions at *m/z* 70, 120, 417, 527, 572, 805, and 1060 were then integrated. This comparison was carried out 3 times (on three separate days). The data indicate that analyte in the 5% aqueous glycerol sample experiences enhanced desorption ionization (more ions detected) in comparison to that in the 56% aqueous glycerol sample. The increase in ionization efficiency is by a factor of 2. This trend was observed for all analyte ions that were examined.

Table I

Part 1 (4 nmol of Bradykinin (B) in Each)

sample	% glycerol	amt of glycerol (G), mg (mmol)	molar G/B	amt of water (W), mg (mmol)	molar W/B
1	56	1.3 (0.014)	4000	1.00 (0.056)	10 000
2	21	0.44 (0.0048)	1000	1.65 (0.092)	20 000
3	5	0.10 (0.0011)	300	1.92 (0.11)	30 000
4	2	0.05 (0.0005)	100	1.96 (0.11)	30 000
5	1	0.02 (0.0002)	50	1.98 (0.11)	30 000

Part 2 (4 nmol of Bradykinin (B) in Each)

sample	% glycerol	amt of glycerol (G), mg (mmol)	molar G/B	amt of water (W), mg (mmol)	molar W/B
A	8	0.11 (0.0012)	300	1.16 (0.064)	20 000
B	7	0.10 (0.0011)	300	1.42 (0.079)	20 000
C	3	0.10 (0.0011)	300	2.92 (0.16)	40 000
D	8	0.41 (0.0044)	1000	4.68 (0.26)	60 000

The phenomenon described in Figures 1, 2, and 3 raises interesting questions. For instance, does the increased water or the decreased glycerol content account for the greater analyte signal observed when analyzing samples of lower weight percentage glycerol as shown in Figure 2? Is water a reagent responsible for the spectral enhancement or merely a passive carrier which supplies variable quantities of matrix for the analyte? We conducted a series of experiments designed to definitively answer these questions. Part 1 of Table I breaks down the samples represented in Figures 2 and 3 into their individual components. The molar ratios of glycerol and water, respectively, to the analyte are also included. The amount of bradykinin present in each case was constant (4 nmol). From inspection of Figures 2 and 3, the composition of sample 3 was chosen as that providing the optimum results for this quantity of analyte. Sample 3 initially contained 0.10 mg of glycerol and 1.92 mg of water, along with the 4 nmol of bradykinin. Experiments were performed to determine whether this particular level of glycerol or this particular level of water was responsible for the observed effect.

Sample compositions A, B, and C listed in part 2 of Table I were prepared from the optimal amount of glycerol used in sample 3, but widely varying amounts of water. The range of water quantities incorporated into samples A–C is quite large with respect to the range of water quantities used in samples 1–5 (part 1 of Table I) within which the relatively sharp optimization was observed in Figure 2. Samples A–C also contained 4 nmol of bradykinin and each sample was analyzed in triplicate. These results are compared to those obtained from the optimal sample composition (sample 3) in Figure 4 for selected analyte ions and in Figure 5 for selected matrix ions. These data indicate a correlation of the FAB response to the glycerol/analyte relationship and not the water/analyte relationship. Note the good agreement between the data (Figures 4 and 5) collected from samples A, B, and C and that obtained from the designated optimum sample (sample 3).

Finally, sample D is included to demonstrate that the effect cannot be attributed to the weight percentage of glycerol in water present in the original sample. Both samples A and D initially contain 8% glycerol in water, but sample D shows significantly inferior results in Figures 4 and 5 because it contains more than the optimum ratio of glycerol to brady-

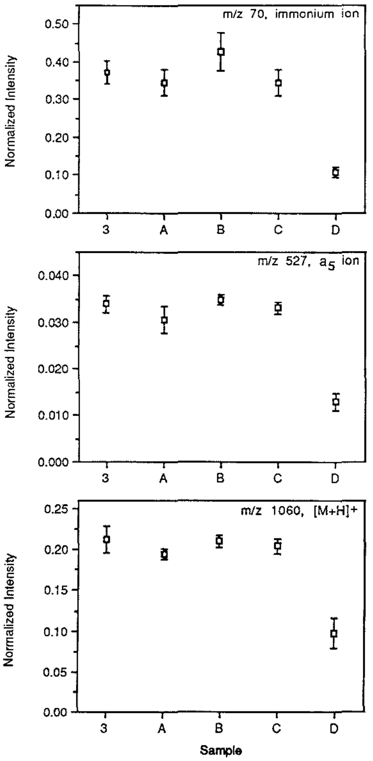

Figure 4. Peak intensity for selected bradykinin ions (*m/z* 70 (top), *m/z* 527 (middle), and *m/z* (1060) plotted against sample composition (described in Table I). Samples A, B, and C contain the same amount of glycerol, but significantly different amounts of water than the optimum composition (sample 3, Table I). Sample D contains more than the optimum amount of glycerol and water but the same weight percentage of glycerol in water as sample A.

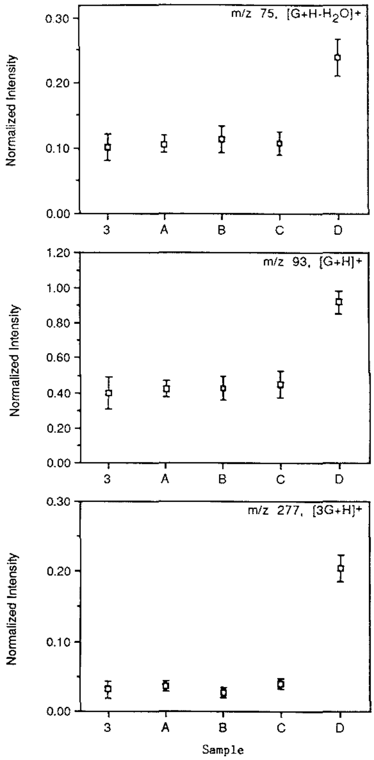

Figure 5. Peak intensity for selected glycerol ions (*m/z* 75 (top), *m/z* 93 (middle), and *m/z* 277) plotted against sample composition (described in Table I). Samples A, B, and C contain the same amount of glycerol but significantly different amounts of water than the optimum composition (sample 3, Table I). Sample D contains more than the optimum amount of glycerol and water but the same weight percentage of glycerol in water as sample A.

kinin. Indeed, the results from sample D much more closely resemble those from sample 2 (part 1 of Table I) which is composed of a similar ratio of glycerol to bradykinin.

These data indicate that macroscopic amounts of water play no role in the enhancement mechanism within the range of water quantities employed in this study. This conclusion prompted a series of simplistic measurements to ascertain how much water the optimal portion of the hygroscopic glycerol might hold under the influence of the vacuum. Therefore, gravimetric measurements were made of the optimal sample composition both before and after exposure to the vacuum lock. Assuming that the vacuum removes only water from the sample and not glycerol, it was determined that virtually 100% of the water is gone by the time the probe is inserted into the source. It is important to note that these results do not preclude the participation of trace levels of water in determining the spectral results. Greater than trace levels of water, however, are definitely not involved in the mass spectral enhancement. We therefore began viewing this system, which was tertiary in sample preparation, as a binary one (simply a mixture of analyte in glycerol) by the time the analysis by FAB-MS had begun.

Up to this point, a constant amount of bradykinin had been used in all the experiments; thus the actual ratio of glycerol to bradykinin had varied according to the quantity of glycerol used. Once attention focused on the glycerol/analyte relationship in the sample, it was decided to manipulate the glycerol to bradykinin molar ratio by varying the amount of bradykinin in a constant amount of glycerol. Therefore, calibration curves were constructed for bradykinin sampled from the larger, 1.3-mg portion of glycerol and also the optimal, 0.10-mg portion.

Results obtained with the larger amount of glycerol (1.3 mg) are plotted in Figure 6 for various bradykinin ions as a function of bradykinin quantity. Data points correspond to 1, 4, 8, and 12 nmol of bradykinin dispersed in approximately 1.3 mg of glycerol. Ion current at each *m/z* value shows a roughly linear response within the range of bradykinin quantities employed. Figure 7 shows the response for various glycerol ions as a function of bradykinin amount. In general, these plots show little change in glycerol ion response as 1 to 12 nmol of bradykinin are mixed into the constant amount (1.3 mg) of glycerol, with the exception of some higher mass cluster ions (e.g., *m/z* 369) which seem to fall off in abundance with increasing bradykinin concentration. A possible explanation for this latter observation is discussed below.

Results obtained with the smaller amount of glycerol (0.10 mg) are presented in Figures 8 and 9. These figures correspond to experiments analogous to those represented in Figures 6 and 7, respectively. The analyte ion current in

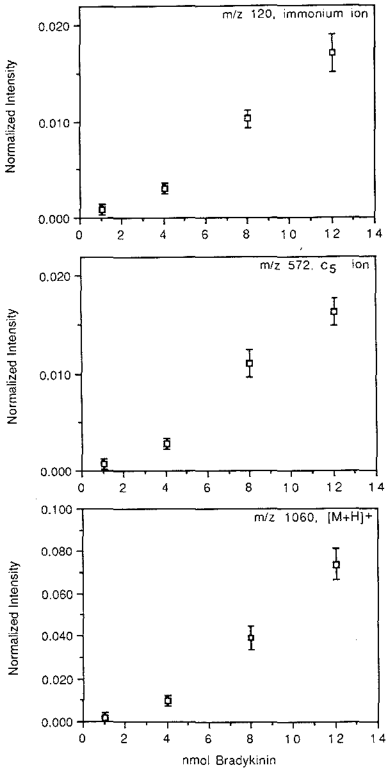

Figure 6. Response for selected bradykinin ions (*m/z* 120 (top), *m/z* 572 (middle), and *m/z* 1060) produced from samples composed of the indicated amount of bradykinin in 1.3 mg of glycerol.

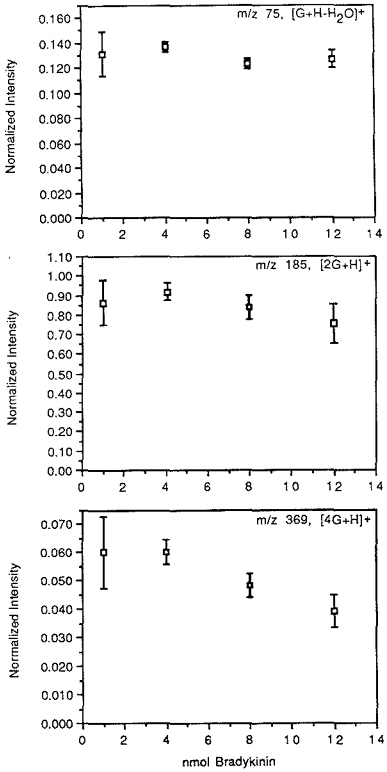

Figure 7. Response for selected glycerol ions (*m/z* 75 (top), *m/z* 185 (middle), and *m/z* 369) produced from samples composed of the indicated amount of bradykinin in 1.3 mg of glycerol.

Figure 8 shows little linearity and a tendency to "plateau", or even decrease, with increasing bradykinin concentration. Analyte response curves of this shape have been observed by others using FAB-MS (*13*, *18–21*). This behavior is believed to result from optimizing the concentration of the analyte at the matrix surface; once this optimal surface concentration is achieved, further increases in analyte sample quantity yield no improvement in analyte ion response.

Figure 9 shows the matrix ion response for the 0.10-mg glycerol samples. These data provide an even more striking contrast with the curves in Figure 7 (from the 1.3-mg glycerol samples). Small additional increments of bradykinin substantially reduce matrix ion abundances detected from the 0.10-mg glycerol samples (Figure 9), where they had very little effect during analyses of samples containing 1.3 mg of glycerol (Figure 7). This behavior can also be interpreted as a surface effect, in which small additional increments of analyte begin to dominate the surface of the matrix and strongly suppress desorption ionization of the more abundant glycerol molecules.

The onset of this surface coverage effect is also apparent in Figure 7 (1.3-mg glycerol samples) in the response profile of the largest glycerol cluster shown (*m/z* 369); for higher concentrations of bradykinin fewer glycerol cluster ions are produced. The diminished response at *m/z* 369 may indicate sufficient analyte surface population to interfere with the creation of these larger cluster ions. This interpretation is consistent with that from a previous discussion regarding the effect of surface coverage on glycerol cluster ion detection (*22*).

These results stimulated consideration of the following model to explain the mass spectral enhancement. In the last several years the collective efforts of many workers (*3–13*, *18*, *20–23*) have clearly established the tendency of FAB mass spectra to reflect the surface composition of the sample. Formation of surface-active derivatives of many analytes has successfully increased signal intensity for those species while suppressing ion current from other sample components (*8*, *9*, *12*). Surfactants have been shown to dramatically diminish matrix ion signals by preferentially occupying surface sites (*4*). We postulate that concentrating a certain amount of analyte into a smaller portion of glycerol facilitates surface population of the glycerol by the analyte. When 4 nmol of bradykinin is mixed with 1.3 mg of glycerol, the ratio of glycerol to bradykinin molecules is approximately 4000 to 1. Samples of this composition did not show pronounced evidence of surface effects. In the samples containing the 0.10-mg portions of glycerol, however, the ratio of glycerol to bradykinin molecules is approximately 300 to 1. Pronounced evidence of surface effects did result from analysis of samples containing this smaller portion of matrix. The smaller glycerol volume will decrease dispersion of the analyte and provide an increased surface area to volume ratio. The increased surface concentration will be driven by a higher bulk concentration, resulting in significant analytical advantages.

In this process water is considered primarily as a convenient vehicle for depositing minute portions of glycerol on the sample probe tip. Microscopic examination of the optimal

Table II

peptide	sequence	$[M + H]^+$	Bull and Breese hydrophobicity index[a]
[Val[4]]-angiotensin III	Arg-Val-Tyr-Val-His-Pro-Phe	917	−463
proenkephalin	Tyr-Gly-Gly-Phe-Met-Arg-Gly-Leu	900	−268
bradykinin	Arg-Pro-Pro-Gly-Phe-Ser-Pro-Phe-Arg	1060	−104
fibronectin related peptide	Cys-Gln-Asp-Ser-Glu-Thr-Arg-Thr-Phe-Tyr	1249	+119
NPNANPNANPNA	Asn-Pro-Asn-Ala-Asn-Pro-Asn-Ala-Asn-Pro-Asn-Ala	1207	+555

[a] Hydrophobicity increases from bottom to top.

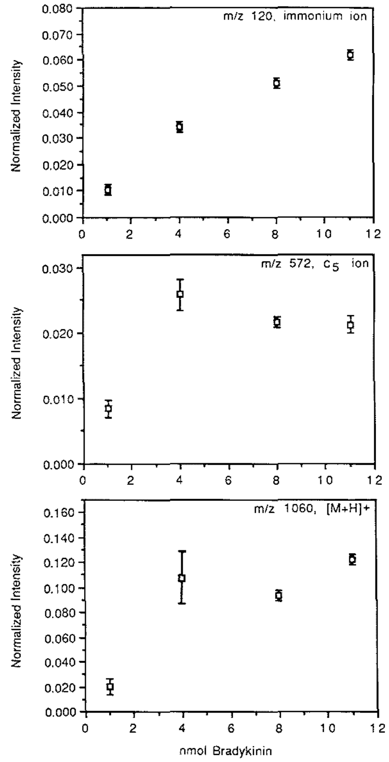

Figure 8. Response for selected bradykinin ions (*m/z* 120 (top), *m/z* 572 (middle), and *m/z* 1060) produced from samples composed of the indicated amount of bradykinin in 0.10 mg of glycerol.

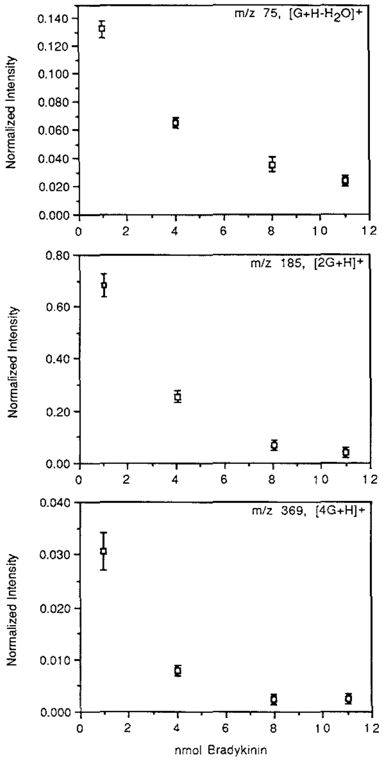

Figure 9. Response for selected glycerol ions (*m/z* 75 (top), *m/z* 185 (middle), and *m/z* 369) produced from samples composed of the indicated amount of bradykinin in 0.10 mg of glycerol.

sample composition (0.10 mg of glycerol and 1.92 mg of water) after exposure to the vacuum lock revealed a very thin layer of viscous material uniformly distributed over the sample stage. In view of the high precision of results obtained from these samples, evaporation of the water seems to be involved in providing a relatively specialized sample preparation.

In considering a model which emphasizes surface effects, one might expect differences in the enhancement behavior for analytes which possess different surface activities in glycerol. To address this question, a comparison study was undertaken for five peptides (including bradykinin) of comparable size, but widely differing values of the Bull and Breese Hydrophobicity Index (*24*). These peptides are listed in Table II along with their amino acid sequences, the mass of each protonated molecule, and the appropriate Bull and Breese index. It should be noted that the most negative values of the Bull and Breese index correspond to the most hydrophobic peptides.

Figure 10 displays the mass spectral response for the $[M + H]^+$ ion of three of the peptides listed in Table II as a function of sample composition. The peptides represented include the most hydrophobic ([val[4]]-angiotensin III), the peptide of intermediate hydrophobicity (bradykinin), and the least hydrophobic (NPNANPNANPNA). These curves are analogous to those shown in Figure 2 (as evidenced by the similar shape of the bradykinin curve) but contain two important differences. The first pertains to the sample composition axis, which was changed from weight percent glycerol to absolute amount of glycerol. The second change regards the addition of a sample composition (2.3 μmol of glycerol) to provide greater resolution of these curves and facilitate the

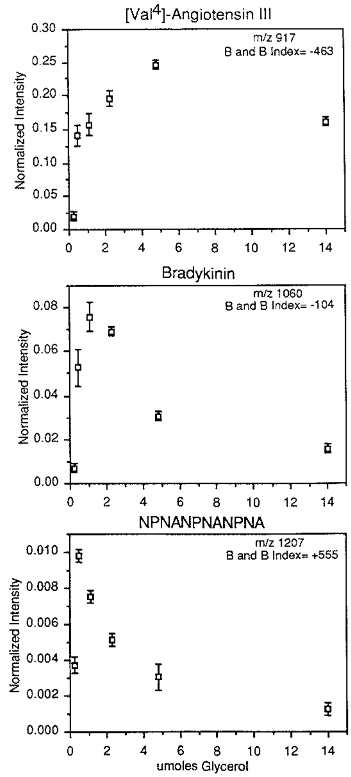

Figure 10. Plots of $[M + H]^+$ peak intensity for three peptides versus the absolute amount of glycerol in sample. All samples contain 4 nmol of analyte.

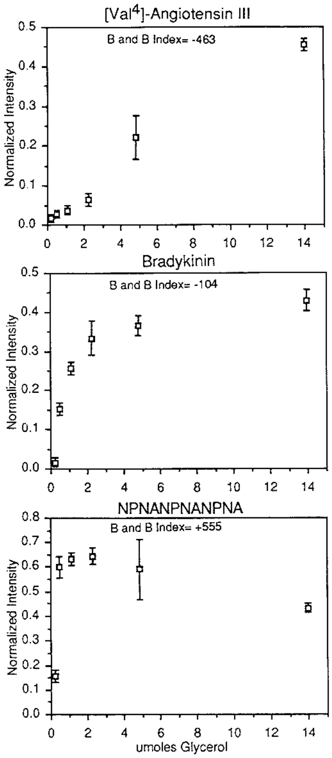

Figure 11. Plots of $[\text{glycerol} + H]^+$ peak intensity (at m/z 93) versus absolute amount of glycerol present in samples containing 4 nmol of the indicated peptide.

Table III. Sample Compositions Represented in Figures 12 and 13[a]

µmol of glycerol	nmol of bradykinin
0.55	2
1.1	4
2.2	8
3.4	12

[a] Molar ratio of glycerol to bradykinin = 300:1.

identification of a trend among them. All samples represented in Figure 10 contained 4 nmol of analyte. A trend is indeed apparent as the $[M + H]^+$ peak intensity for the most hydrophobic peptide ([Val^4]-angiotensin III) is maximized in a larger portion of glycerol than is the $[M + H]^+$ peak intensity for bradykinin. Likewise, the ion abundances of the least hydrophobic peptide (NPNANPNANPNA) are maximized in smaller portions of glycerol than are those of bradykinin. Curves generated for other important peaks throughout the mass spectrum of each of the three peptides showed close agreement with those displayed in Figure 10 (with the exception of those corresponding to immonium ions). These results are consistent with a model emphasizing surface effects because the most hydrophobic peptide, which has the greatest tendency to reside at the glycerol surface, would be expected to tolerate larger portions of glycerol in establishing its optimal surface concentration. In contrast, the least hydrophobic peptide would require the smallest portions of glycerol before it is forced toward the surface and the enhancement is observed. Data from samples containing the other two peptides in Table II (proenkephalin and fibronectin related peptide) also fit into this trend in optimization as a function of hydrophobicity.

A related trend is also apparent for the glycerol ion response in this set of experiments. Figure 11 shows peak intensities for m/z 93 ($[\text{glycerol} + H]^+$) plotted in a manner similar to that in Figure 10. Samples containing the most hydrophobic peptide show significant suppression of the glycerol peak in relatively large portions of glycerol, whereas samples containing the least hydrophobic peptide show no substantial diminution of glycerol peak intensity until the smallest portions of glycerol are used. It is interesting to note that the segments of these curves where the glycerol peaks are strongly suppressed correspond to the segments in which the accompanying analyte signals are strongly enhanced (in Figure 10). This fact implies the existence of a competition between analyte and matrix, which is also consistent with a model emphasizing surface effects.

In pursuit of the importance of the ratio of glycerol to analyte in the FAB experiment, a study was designed to analyze a series of samples in which the glycerol to bradykinin ratio was maintained at a constant value while adjusting the absolute quantities of each component. The ratio chosen was approximately 300 glycerol molecules for each bradykinin molecule (a ratio similar to that in the designated optimum sample 3 of Table I), and the experiments encompassed a range from 2 to 12 nmol of bradykinin. The compositions of

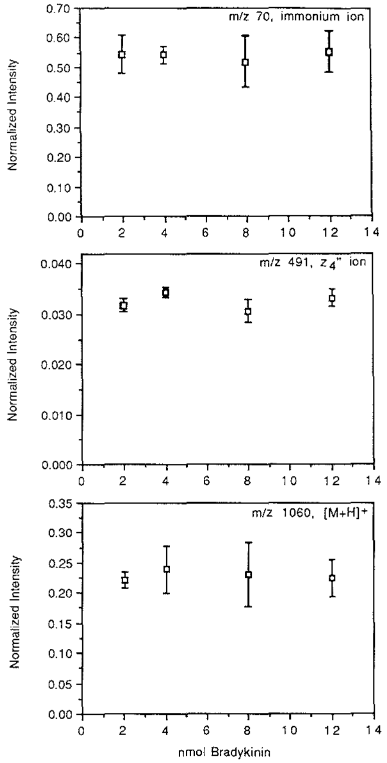

Figure 12. Plots of abundance of selected bradykinin ions (*m/z* 70 (top), *m/z* 491 (middle), and *m/z* 1060) versus nanomoles of bradykinin in sample. All samples possess a constant ratio (300:1) of glycerol molecules to bradykinin molecules although the absolute quantities of each vary.

these samples are listed in Table III. Figure 12 shows the abundance of selected analyte ions plotted against the amount of bradykinin present in the sample. One observes little effect of increased analyte sample quantity upon analyte ion response. Likewise, little change in results is observed when glycerol ion response is plotted against glycerol sample quantity (Figure 13). Despite an increase in the levels of all sample components by some 600%, the greatest variation observed in the abundance of any ion was 38%; besides those plotted in Figures 12 and 13, peak intensities at *m/z* 120, 527, 572, 805, 903, 277, and 369 were examined. Spectra from all samples described in Table III are qualitatively similar. This consistency of spectral results after significant manipulation of sample composition suggests that the ratio of glycerol to bradykinin molecules can be a useful factor in approximating the optimal mass spectral response.

As previously mentioned, acidic modifiers have commonly been included in FAB-MS sample preparations to increase analyte ion abundances in the positive ion mode. A limited comparison of the spectral enhancement resulting from addition of acidic modifiers with that due to manipulation of the ratio of glycerol to analyte was conducted. Samples composed of 1.3 mg of glycerol and 4 nmol of bradykinin (sample 1 in part 1 of Table I) were analyzed by FAB-MS and the results compared to those from similar samples which also contained 100 nmol of HCl. Addition of the acid increased the abundances of the six bradykinin ions which were evaluated (*m/z* 70, 120, 417, 572, 903, and 1060) by an average of 34%. These acidified samples also displayed increased glycerol ion abundances; the five glycerol ions evaluated (*m/z* 75, 93, 185, 277, and 369) showed an average increase in abundance of 6%. The optimal sample 3 composition in part 1 of Table I (4 nmol of bradykinin and 0.10 mg of glycerol) was also analyzed with and without the addition of 100 nmol of HCl. The added acid increased the abundances of the six specified bradykinin ions by an average of 7%. At the same time, the five designated glycerol ions were increased in abundance by an average of 9%. Mass spectra obtained from the optimal sample composition with and without the HCl were indistinguishable in a qualitative sense. For the sake of reference, the abundance of the six bradykinin ions was enhanced by 690% on average by optimizing the ratio of glycerol to bradykinin (nonacidified samples), while the abundance of the five glycerol ions was decreased by an average of 64%. A separate study undertaken with bradykinin, glycerol, and tartaric acid also showed that any spectral enhancement gained by adding the acidic modifier was insignificant to that gained through optimization of the glycerol to analyte ratio.

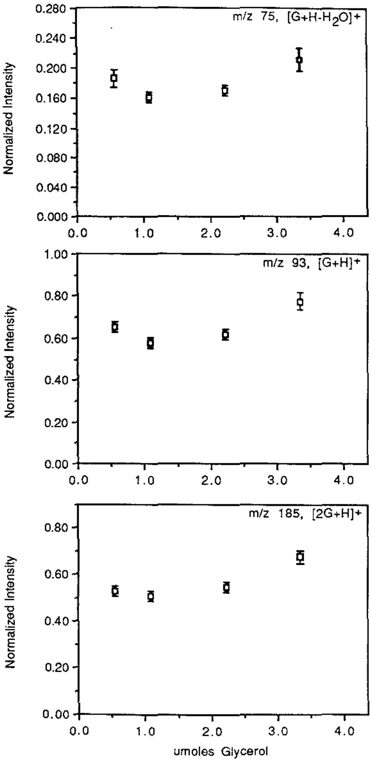

Figure 13. Plots of abundance of selected glycerol ions (*m/z* 75 (top), *m/z* 93 (middle), and *m/z* 185) versus micromoles of glycerol in sample. All samples possess a constant ratio (300:1) of glycerol molecules to bradykinin molecules although the absolute quantities of each vary.

CONCLUSION

It has been shown that the matrix to analyte ratio profoundly affects the quality of FAB-MS results. Although the qualitative information regarding the analyte is maximized when using the smaller portions of glycerol, it is interesting to note that a wider linear response for the analyte results from the use of larger amounts of glycerol. This would indicate that the larger glycerol portions are better suited for quantitative purposes where dynamic range is important.

The spectral enhancement can be realized simply by mixing the analyte with a 1-μL portion of 10% (w/w) aqueous glycerol. By introducing less glycerol into the mass spectrometer source, one can also reasonably expect less rapid contamination of the ion lenses. The only disadvantage encountered by this approach regards ion signals of decreased temporal duration in comparison to those measured from samples introduced in larger amounts of the glycerol matrix. However, for the many applications of FAB-MS which do not require extremely long-lived ion currents, this method provides substantial analytical advantages.

LITERATURE CITED

(1) Barber, M.; Bordoli, R. S.; Sedgwick, R. D.; Tyler, A. N. *J. Chem. Soc., Chem. Commun.* **1981**, 325.
(2) Martin, S. A.; Costello, C. E.; Biemann, K. *Anal. Chem.* **1982**, *54*, 2362.
(3) Ligon, W. V.; Dorn, S. B. *Int. J. Mass Spectrom. Ion Processes* **1984**, *57*, 75.
(4) Ligon, W. V.; Dorn, S. B. *Int. J. Mass Spectrom. Ion Processes* **1984**, *61*, 113.
(5) Ligon, W. V.; Dorn, S. B. *Anal. Chem.* **1985**, *57*, 1993.
(6) Ligon, W. V.; Dorn, S. B. *Int. J. Mass Spectrom. Ion Processes* **1985**, *63*, 315.
(7) Ligon, W. V.; Dorn, S. B. *Int. J. Mass Spectrom. Ion. Processes* **1986**, *68*, 337.
(8) Ligon, W. V.; Dorn, S. B. *Anal. Chem.* **1986**, *58*, 1889.
(9) Ligon, W. V. *Anal. Chem.* **1986**, *58*, 485.
(10) Ligon, W. V.; Dorn, S. B. *Int. J. Mass Spectrom. Ion Processes* **1986**, *78*, 99.
(11) Barber, M.; Bordoli, R. S.; Elliott, G. J.; Sedgwick, R. D.; Tyler, A. N. *Anal. Chem.* **1982**, *54*, 645A.
(12) Naylor, S.; Findeis, A. F.; Gibson, B. W.; Williams, D. H. *J. Am. Chem. Soc.* **1986**, *108*, 6359.
(13) DePauw, E. *Mass Spectrom. Rev.* **1986**, *5*, 191.
(14) Fenselau, C.; Cotter, R. J. *Chem. Rev.* **1987**, *87*, 501.
(15) Roepstorff, P.; Fohlman, J. *Biomed. Mass Spectrom.* **1984**, *11*, 601.
(16) Biemann, K. *Biomed. Environ. Mass Spectrom.* **1988**, *16*, 99.
(17) Caprioli, R. M.; Fan, T. *Biochem. Biophys. Res. Commun.* **1986**, *141*, 1058.
(18) Beckner, C. F.; Caprioli, R. M. *Biomed. Mass Spectrom.* **1984**, *11*, 60.
(19) Clay, K. L; Stene, D. O.; Murphy, R. C. *Biomed. Mass Spectrom.* **1984**, *11*, 47.
(20) Beckner, C. F.; Caprioli, R. M. *Anal. Biochem.* **1983**, *130*, 328.
(21) Allmaier, G. M. *Rapid Commun. Mass Spectrom.* **1988**, *2*, 74.
(22) Barber, M.; Bordoli, R. S.; Elliott, G. J.; Sedgwick, R. D.; Tyler, A. N. *J. Chem. Soc., Faraday Trans. 1* **1983**, *79*, 1249.
(23) Clench, M. R.; Garner, G. V.; Gordon, D. B.; Barber, M. *Biomed. Mass Spectrom.* **1985**, *12*, 355.
(24) Bull, H. B.; Breese, K. *Arch. Biochem. Biophys.* **1974**, *161*, 665.

RECEIVED for review February 27, 1989. Accepted September 7, 1989. This work was supported by the National Institutes of Health (NIH Grant No. DRR-00480 administered through the Biomedical Research Technology Program).

Comparison of Screening Techniques for Polychlorinated Biphenyls in Waste Oils

Carol R. Sutcliffe, Ernest S. Gladney,* Deanna M. Seitz, and George H. Brooks

Health and Environmental Chemistry, Group HSE-9, Mail Stop K-484, Los Alamos National Laboratory, Los Alamos, New Mexico 87545

A commercial colorimetric field screening kit for the detection of polychlorinated biphenyls (PCBs) is compared to instrumental thermal neutron activation analysis as a screening tool in a variety of oil matrices. The precision of these two methods was compared to an accepted method of analysis, gas chromatography with electron capture detection, and interferences of each screening technique were investigated. The colorimetric test was shown to be less reliable and more prone to interferences than neutron activation analysis. The advantages and limitations of each method are discussed.

INTRODUCTION

With polychlorinated biphenyls (PCBs) becoming a widely recognized regulatory problem, accurate and simple screening techniques applicable to large numbers of environmental samples are highly desirable. The major source of PCB introduction into the environment has been through the disposal of contaminated oils. PCBs were routinely used into the 1970s in dielectric fluids in capacitors and transformers, heat transfer fluids, hydraulic fluids, and lubricating and cutting oils. Enactment of the Toxic Substances Control Act (PL 94-469) in 1978 and subsequent amendments in 1981 (PL 97-129) established regulations for disposal of existing PCBs and severely restricted future production and use of these compounds. A review providing an excellent overview of PCBs and their analysis by gas chromatography and mass spectrometry can be found in ref 1.

Several screening methods for PCBs have been developed or proposed. The use of simplified chromatographic procedures (gas, thin layer, or high pressure), of total organic halide (TOX) methods, of X-ray fluorescence, and of chemical determination for total chlorine have been reviewed by Erickson (*2*). The latter is the basis for the many commercial colorimetric kits that provide a field test to determine if the PCB concentration in oils are within the EPA disposal limits. These kits usually provide semiquantitative results of greater than 50 ppm or greater than 500 ppm depending upon which kit is used. There has been some uncertainty about the accuracy of these results for actual field samples, especially at the lower regulatory limit of 50 ppm. These considerations led us to investigate the use of instrumental thermal neutron activation analysis (ITNA) as a screening technique for PCBs. Since EPA has approved this method for TOX analysis (*3*), it could be an acceptable screening methodology for PCBs. When ITNA is available, it is a rapid, simple, reliable, and almost interference-free technique that can significantly reduce the number of samples requiring the more time-consuming EPA approved methods employing gas chromatography and electron capture detection (GC/ECD).

Another important reason for having a reliable screening method is the high sensitivity of electron capture detectors (ECD). The ECD is easily saturated with analyte and can take several days to restabilize when high concentration samples are inadvertantly injected without proper dilution. This may

0003-2700/89/0361-2682$01.50/0 © 1989 American Chemical Society

also lead to eventual loss of sensitivity and necessitate detector replacement. To protect against these possibilities, unknown samples are highly diluted initially and rediluted as necessary to achieve the proper analytical range, often requiring several analytical runs before the correct range for measuring PCBs is found. Due to the time involved in analysis, data reduction, and the need for experienced analysts, GC/ECD analysis is not desirable for routine screening of large numbers of samples. While other screening techniques sacrifice the specificity of the GC/ECD analysis, the advantages are speed, low cost, simplicity, and the ability to significantly reduce the number of samples requiring more sophisticated and time-consuming analysis.

EXPERIMENTAL SECTION

Preparation of Standards. Aroclor 1242 and 1260 standards were prepared by dissolving known amounts of the neat PCB (99%, Chem Service) in 1 mL of hexane and adding to a halogen-free hydrocarbon oil. All prepared standards were placed in an ultrasonic bath overnight to promote homogeneity. Homogeneity was confirmed by gas chromatographic analysis.

Other halogenated compounds were used to investigate the potential interference from non-chlorinated halocarbon compounds dissolved in the oils. The compounds that were liquids at room temperture were gravimetrically added directly to the halogen-free blank oil. The compounds that were solids were first dissolved in hexane, and this solution was gravimetrically diluted with the blank oil. Serial dilution was then used to provide a range of concentrations. Mixtures were produced by combining several of the concentrated stock oil solutions and diluting this mixture with blank oil.

All ITNA analyses were standardized against solutions prepared by dissolving high-purity NaCl, NaF, NaBr, and KIO_3 in deionized, distilled water. The neutron moderating properties of oil and water are similar, thus eliminating the need for exact matrix matching for samples and standards.

Standard Reference Materials for total chlorine in oil and PCBs in oil were obtained from the National Institute for Standards and Technology (NIST, formerly the National Bureau of Standards). A large variety of PCB in oil quality assurance materials were also obtained from EPA, Cincinnati, OH. The small quantities of each oil reference material prevented their use for colorimetric evaluation.

Colorimetric Kits. Several kits are produced commercially to test oils for PCBs in the field. Most work on the principle of total chlorine detection. A widely used product is the Clor-N-Oil kit, which the manufacturer clearly labels as "A PCB screening test for transformer oil" and states in the instructions that "This test is intended for use only with transformer oil of petroleum origin. It may not be useful for other fluids." (*4*). This kit was selected for further investigation since we have observed that the manufacturer's advice may be widely ignored and in the hope that its applicability could be extended to oils of unknown origin (including waste oils). We used two different Clor-N-Oil kits, one that detects levels of PCBs greater than 50 ppm and another which detects PCBs greater than 500 ppm. Both kits consist of two capped polyethylene tubes containing glass ampules of reagents. The tube with the black cap is the tube in which the oil is added and the tube with the white cap is the second tube where the positive or negative result of the test is determined.

To screen a sample with these kits, a 5-mL aliquot of the oil sample is placed into the first tube and an ampule containing a 3:1 mixture of diglyme (or diethylene glycol methyl ether)/naphthalene catalyst is broken and the tube shaken. An ampule containing sodium dispersed in oil is then broken and any organic chlorine in the sample is stripped out forming sodium chloride. A buffer solution (0.18 M NaH_2PO_4 + 0.3 N HNO_3) from the second tube is added to the first tube and shaken, neutralizing any excess sodium and extracting the sodium chloride into the aqueous phase. The aqueous phase is permitted to separate for 2 min and then transferred to the second tube. The ampule of premeasured mercuric nitrate is broken and mixed with the aqueous phase, forming a complex with the chloride ions. The final step is the breaking of the ampule of 0.1% diphenylcarbazone indicator in the tube. If no excess chlorine is present in the sample, the solution turns pink to purple. A yellow solution indicates excess chlorine and the possible presence of PCBs, necessitating a GC/ECD analysis. The amount of mercuric nitrate present in the 50 ppm kits is set to react with 21 ppm chlorine. This corresponds to 50 ppm Aroclor 1242 which is the PCB containing the least amount of chlorine normally found in oil samples. Other common Aroclors found in oils would therefore give a positive result below 50 ppm. The kits were thus developed with the idea of erring on the side of false positives as opposed to false negatives.

Instrumental Neutron Activation Analysis. Small aliquots (1 mL) of potentially contaminated oils are encapsulated in polyethylene containers and irradiated individually in the manually operated, pneumatic transfer, thermal neutron irradiation facility of the Los Alamos Omega West Reactor for 1 min in a neutron flux of 1×10^{13} $(n/cm^2)/s$. Induced γ-ray activity of the sample is observed with a large, high-resolution Ge(Li) detector coupled to a 4096-channel pulse-height analyzer. The following γ-rays are used for quantitative determination of total elemental halogen content of the oil: 1633 keV from 11.0 s ^{20}F, 2167 keV from 37.2 min ^{38}Cl, 617 keV from 17.7 min ^{80}Br, and 442 keV from 25.0 min ^{128}I. Two separate counts are required. The first, for 60 s, following only 20 s of decay, permits the observation of fluorine. If the system dead time exceeds 10%, these fluorine data must be discarded, since there is insufficient time to change counting geometry to reduce dead time. At the end of the initial count, a counting geometry is selected that results in a counting system dead time of less than 10%. At a total decay time of 2.0 min, the remaining induced γ-ray activities are counted for 200 s. Spectral data are integrated on the CRT display of the pulse-height analyzer or transferred to magnetic tape for off-line reduction on a Digital Equipment Corp. VAX 11/730 computing system. Quantitative data are obtained by comparison of net peak areas of the samples with those of known elemental standards irradiated and counted in the same fashion. The total time required for an analysis is about 10 min, equally divided between sample preparation and neutron activation. Detection limits of 5 ppm F, 0.5 ppm Cl, 0.3 ppm Br, and 0.2 ppm I have been demonstrated. Additional details may be found in Gladney et al. (*5*).

Gas Chromatography/Electron Capture Detection Analysis. Approximately 0.1 mL of contaminated oil is weighed and diluted to 1 mL with pesticide grade hexane. Serial dilutions of factors of 10 (up to 10000) are made to the sample depending upon the expected PCB concentration levels as revealed by a screening technique. An attempt is made to limit detector loading to less than 50 ng of total chlorine. One microgram per milliliter of lindane is spiked into the sample before analysis for use as an internal standard. A 1-μL splitless injection is made onto a 30 m × 0.25 mm DB-5 fused silica capillary column. The oven temperature is programmed to start at 120 °C to trap the PCBs, rise to 220 °C at 15 deg/min, and finish by increasing to 280 °C at 4 deg/min. All PCBs are eluted from the column within 35 min. Calibration standards are prepared from dilutions of EPA certified PCBs in oil. Each commercially produced PCB gives approximately 40–50 resolved peaks and specific PCBs can be identified from a unique fingerprint pattern. Six well-resolved peaks are chosen for quantitation, and a calibration curve plotting normalized area versus concentration is developed for each peak. The concentrations determined from each calibration curve are averaged to give an indication of the match of the sample PCB to the standard PCB and the potential uncertainty involved in the analysis. Additional information on this analysis is available from ref 6.

RESULTS AND DISCUSSION

PCBs are actually made up of a mixture of congeners of a polychlorinated biphenyl ring. The various compositions and the percent weight chlorine present in commercial Aroclors can be found in ref 1, 2, and 7. Most screening techniques use this percent weight chlorine to calculate a potential PCB value from the measured chlorine value. Erickson (*2*) indicates that most PCBs found in oils will be Aroclors 1242, 1254, and 1260. Assuming that Aroclor 1242 will be the least chlorinated PCB found in oils, a potential PCB value can be determined by dividing the concentration of chlorine measured

Table I. Screening Results from Aroclor 1242 and 1260 in Oils Prepared In-House (μg/g)

		ITNA			calculated	
Aroclor	GC/ECD	Cl	potential PCB	kit	Cl	PCB
1242	91 ± 11	42 ± 4	100 ± 9	<50	44	105
	71 ± 7	33 ± 3	79 ± 7	<50	33	79
	57 ± 6	25 ± 3	60 ± 7	<50	26	63
	46 ± 5	21 ± 2	50 ± 5	<50	22	52
	39 ± 4	19 ± 2	45 ± 5	<50	18	42
1260	75 ± 8	45 ± 5	107 ± 12	>50	48	79
	54 ± 5	34 ± 3	81 ± 7	>50	36	60
	42 ± 4	27 ± 3	64 ± 7	<50	29	48
	34 ± 3	25 ± 3	60 ± 7	<50	24	40
	26 ± 3	19 ± 2	45 ± 5	<50	19	32

in unknown samples by 0.42. This will give a conservative number for possible PCB concentration, because the actual PCB value would be lower for the more highly chlorinated PCBs. When the total chlorine content of the sample is less than 21 ppm, the maximum PCB content is less than the EPA control limit of 50 ppm and the oil may be disposed of without further analysis.

Colorimetric screening kits use the principle of measuring total chlorine in oils and have been used extensively in the field to determine PCB disposal requirements. There are several problems that can arise in administering these kits. These products are frequently used for applications that the developers clearly indicate as inappropriate. We also found the results of the kits to be dependent on the training and experience of the user. When the kits are used for the analysis of Askarels (pure PCBs or high concentrations of PCBs mixed with trichlorobenzene) an inversion occurs, causing the oil layer instead of the aqueous layer to be transferred to the second tube. Unless the user is alert, a negative test result will occur, when in fact the sample contains percent levels of PCBs. This could mean that those samples with the highest amounts of PCBs would be judged to be below the 50 ppm EPA concern limit. This problem is clearly documented in the product literature (*4*). Another problem commonly seen is the attempt to screen water samples with these kits. Since water reacts with the sodium dispersion, erroneous conclusions could easily be drawn.

To investigate the accuracy of colorimetric kits, we tested them with PCB standards in oil made up in our laboratory. Erickson (*2*) characterizes transformer oil as containing mineral oil with 20–30% aromatics and the balance as hydrocarbons. This type material was selected for preparation of our spiked samples. NIST or EPA standards were not used because they are available in only 1-mL aliquots while the kits require 5 mL of oil. Representative results (expressed as potential PCBs) are shown in Table I for Aroclors 1242 and 1260 as determined by the kits, ITNA, and GC/ECD. The difference between the GC/ECD results and the calculated spike concentrations were all less than 2 times the experimental uncertainty of the GC/ECD data. The differences between the ITNA results and the calculated spike concentrations were all less than one experimental uncertainty of the ITNA data. As expected, the potential PCBs are higher than the calculated PCBs in every sample containing Aroclor 1260, erring on the side of false positives. No false negatives were observed by ITNA. The kit results were highly variable, sometimes giving false negatives even at the 100 μg/g level. Studies conducted by the Electric Power Research Institute (*8*) indicated a much higher accuracy than we were able to obtain. The kits gave instances of false negatives that could have led to incorrect disposal action, while the ITNA values would not have led to any incorrect disposal actions. Our results support the conclusion of Bertram (*9*) that these kits could not be applied to PCB determination in many waste oils.

Table II. Chlorine Concentrations in NIST Chlorine in Oil Standard Reference Materials

SRM	ITNA, μg/g	certified, μg/g
1818-I	26.8 ± 1.4	29 ± 5
1818-II	62.2 ± 2.5	63 ± 4
1818-III	79.7 ± 2.8	78 ± 4
1818-IV	226 ± 4	231 ± 6
1818-V	549 ± 16	558 ± 11

Table III. ITNA Screening of PCB Content of NIST and EPA Transformer Oil Reference Materials (μg/g)

		ITNA		
agency	Aroclor	Cl	potential PCB	certified PCB
NIST	1242	41.0 ± 0.7	97 ± 2	100 ±1
NIST	1260	58 ± 4	138 ± 9	100 ± 3
EPA	1016	4.5 ± 0.2	10.7 ± 0.4	10.1
EPA	1016	19.5 ± 0.9	47 ± 2	50.1 ± 11
EPA	1016	201 ± 4	478 ± 11	501 ± 100
EPA	1242	5.2 ± 1.3	12.4 ± 3.1	10.1
EPA	1242	20 ± 1	48 ± 3	50.2 ± 7.7
EPA	1242	206 ± 5	490 ± 12	501 ± 55
EPA	1254	6.0 ± 1.4	14.3 ± 3.5	10.0
EPA	1254	24.3 ± 0.7	58 ± 2	50.0 ± 8.2
EPA	1254	263 ± 6	627 ± 14	500 ± 60
EPA	1260	7.2 ± 0.5	17.2 ± 1.1	10.1
EPA	1260	27 ± 3	64 ± 6	50.0 ± 7.0
EPA	1260	284 ± 2	677 ± 5	499 ± 60

Table IV. ITNA Screening of PCB Content of EPA Capacitor Oil Reference Materials (μg/g)

	ITNA		
Aroclor	Cl	potential PCB	certified PCB
1016	2.8 ± 0.8	6.6 ± 1.9	11.8
1016	19.9 ± 1.8	48 ± 4	51.2 ± 11
1016	200 ± 1	475 ± 2	507 ± 101
1242	223 ± 13	531 ± 30	514
1242	20.2 ± 1.7	48 ± 4	51.4
1242	3.7 ± 1.1	8.8 ± 2.5	10.4
1254	7.1 ± 0.5	16.8 ± 1.3	12.7
1254	25 ± 1	60 ± 3	50 ± 10
1254	259 ± 2	616 ± 4	500 ± 60
1254	257 ± 16	612 ± 38	512
1254	26 ± 2.2	62 ± 5	51.2
1254	5.6 ± 1.4	12.6 ± 3.3	10.4

Table V. ITNA Screening of PCB Content of NIST Motor Oil Standard Reference Materials (μg/g)

	ITNA		
Aroclor	Cl	potential PCB	certified PCB
1242	46.2 ± 2.7	108 ± 4	100 ± 1
1260	58.6 ± 2.0	140 ± 5	100 ± 2

The precision and accuracy of ITNA determination of chlorine in oil are shown in Table II using NIST SRM 1818 Chlorine in Oil. Five replicate analyses are summarized for each chlorine level. All experimental mean values are within one NIST standard deviation of the NIST certified value. The relative standard deviations for our determinations range from 1.8% to 5.2%.

Data for ITNA screening of a variety of certified EPA and NIST PCB in Oil reference materials are shown in Tables

Table VI. ITNA Screening of PCB Content of EPA Hydraulic Oil Reference Materials (μg/g)

Aroclor	ITNA Cl	ITNA potential PCB	certified PCB
1016	52 ± 1	124 ± 4	11.4
1016	76 ± 3	179 ± 6	57.1 ± 12
1016	286 ± 6	681 ± 14	576 ± 115
1254	183 ± 5	434 ± 13	11.5
1254	80 ± 3	192 ± 8	57.6 ± 9.0
1260	55 ± 2	131 ± 4	11.7
1260	376 ± 21	894 ± 49	576 ± 67
1260	151 ± 5	360 ± 12	57.4 ± 8.2

Table VII. Halogen Standards in Oil Screened by ITNA and Colorimetric Kits (μg/g)

compound	element	calcd concn	ITNA	kit
fluorobenzene	F	1100	980 ± 200	
	Cl	0	<3	<50
	F	110	100 ± 25	
	Cl	0	<3	<50
	F	13	10 ± 4	
	Cl	0	<3	<50
fluorobiphenyl	F	880	810 ± 160	
	Cl	0	<3	>50, <500
	F	97	70 ± 25	
	Cl	0	<3	<50
	F	10	7 ± 4	
	Cl	0	<3	<50
bromobenzene	Br	1500	1300 ± 100	
	Cl	0	<3	>50, >500
	Br	100	86 ± 8	
	Cl	0	<3	>50, <500
	Br	10.5	8.7 ± 0.8	
	Cl	0	<3	<50
2,4-tribromobiphenyl	Br	550	540 ± 30	
	Cl	0	<3	>50, >500
	Br	91	80 ± 6	
	Cl	0	<3	>50, <500
	Br	9.3	8.0 ± 0.9	
	Cl	0	<3	<50
iodobenzene	I	1700	1600 ± 100	
	Cl	0	<3	>50, >500
	I	100	96 ± 8	
	Cl	0	<3	<50
	I	11	10 ± 1	
	Cl	0	<3	<50
diiodopentane	I	2400	2300 ± 200	
	Cl	0	<3	>50, >500
	I	85	80 ± 8	
	Cl	0	<3	<50
	I	8.1	7.4 ± 0.8	
	Cl	0	<3	<50
iodopropane	I	1800	1300 ± 90	
	Cl	0	<3	>50, >500
	I	83	53 ± 5	
	Cl	0	<3	<50
	I	8.5	5.0 ± 0.7	
	Cl	0	<3	<50
combination-I	F	600	350 ± 70	
	Cl	660	620 ± 40	>50, >500
	Br	2450	2100 ± 200	
	I	1740	1600 ± 200	
combination-II	F	90		
	Cl	98	100 ± 9	>50, <500
	Br	360	300 ± 30	
	I	260	230 ± 20	
combination-III	F	9.2		
	Cl	10	11 ± 3	>50, <500
	Br	37	29 ± 3	
	I	26	24 ± 2	

III–V. The data shown represent the mean ± one standard deviation among five replicate analyses. The chlorine contents measured by ITNA are converted to potential PCBs according to the screening assumption stated above. In only one case (1016 in capacitor oil at 12 μg/g) did the ITNA potential PCB value fall more than one experimental standard deviation below the certified PCB concentration.

The data for hydraulic oil reference materials shown in Table VI (the mean ± one standard deviation among five replicates) illustrate the inability of the ITNA screening method to differentiate between PCBs and other chlorinated organic compounds. The potential PCBs derived from ITNA data are consistently above the certified PCB concentration in every sample.

For chlorine concentrations of over 20 ppm, precision of ~10% can be obtained by ITNA. The uncertainty increases to ~100% at 3 ppm due to variability of the chlorine blank in the plastic of the irradiation containers. The blank problem can be overcome by rapidly transferring the oil to a clean (nonirradiated) container immediately after the neutron irradiation and before counting. With this transfer, precisions of ~10% can be obtained at chlorine concentrations of 1 ppm with detection limits of 0.1 ppm. Additional operator time and radiation exposure are required for this sample transfer.

An advantage of the manual ITNA method over completely automated neutron activation systems (*10, 11*) is the analyst's ability to change counting geometry at will to accommodate high activity samples (usually due to high chlorine concentration). The analyst can maintain counting system dead times below 10% but must calibrate each geometry used. In this fashion, quantitative chlorine concentrations may be obtained even for pure solvents or PCBs. Most automated activation systems operate at a fixed geometry and will usually have an upper limit to the analyte concentration they can handle quantitatively.

We wanted to determine the performance of these screening procedures on actual field samples, since laboratory-prepared spikes often fail to include the uncontrolled interferences sometimes seen in real samples. We analyzed 43 samples by all three methods and an additional 67 samples by ITNA and GC/ECD alone. GC/ECD analyses were assumed to be correct in this study. At the regulation level of 50 ppm, false positives were observed for 23% of the samples analyzed by ITNA and 42% of the samples screened by the kits. This disparity between ITNA and kit results would greatly impact the number of samples needing the more time-consuming GC/ECD confirmation if one were depending exclusively on kit results for screening decisions. We observed earlier that the number of false negatives for the kits with laboratory-prepared spiked standards was disconcertingly high and this trend continued into actual field samples. Of the samples screened with the kits, 9.3% showed below 50 ppm PCB while GC/ECD analysis showed them to be above this regulation level. ITNA has not yet shown a confirmed false negative over several hundred samples. The trend for false positives was similar at the 500 ppm regulation limit with the kits being much higher than for ITNA. Insufficient data have been collected to date to permit the evaluation of the false negative rates of the kits at the higher concentration level. No confirmed false negatives have been encountered for ITNA at this level.

A comparison of screening measurements on halogen-free oils spiked with up to four different organohalogen compounds at a number of different concentrations is shown in Table VII. These data demonstrate an important limitation of the colorimetric kits. They are not specific to chlorine in oil. They consistently yielded positive results for organobromine and high levels of organoiodine compounds, while organofluorine compounds seemed to have little effect on their performance. The errors were on the conservative side of false positives, with no false negatives observed in this particular test. The ITNA method is not only consistently accurate about chlorine levels in the face of all potential organohalogen interferences but also provides quantitative information about the levels of these other elements. The low bias of the data on some compounds is believed to be due to impure standards used to spike the blank oil. None of the concentrated organohalogen compounds were checked for purity.

CONCLUSIONS

The kits are low cost (approximately $5) and quick and can be easily utilized in the field. We have shown, however, that using these results as a definitive analysis could lead to disposal violations. Furthermore, they are unable to distinguish between inorganic and organic chlorine or PCBs and other chlorinated organics. The kits also give false positives due to several interferences such as water, organobromine, and organoiodine compounds.

The data for chlorine via ITNA are quantitative, in contrast to those produced by the colorimetric PCB kits, which are semiquantitative with only 50 and 500 ppm level detection. Both procedures respond to any chlorine-containing compound (organic or inorganic). Inorganic chlorides are relatively insoluble in organic solvents and oils, so ITNA is an effective method for screening these matrices for organochlorine compounds. Although ITNA is still nonspecific for different sources of chlorine, it is not prone to false positives from interferences such as other halogens and can simultaneously provide data on bromine and iodine content of the oil as well. These additional elemental measurements are often required by disposal facilities depending upon the specific requirements of their EPA permits. ITNA is also much more sensitive, giving a very high probability of being able to observe PCBs at the regulatory level. By use of our irradiation-decay-counting scheme, 10 samples per reactor-hour may be analyzed at a cost of approximately $5–$10 each. Even though an ITNA analysis is inexpensive, it requires access to a reactor and trained personnel.

The great solubility of inorganic chlorides and relatively insolubility of organochlorine compounds in aqueous media render ITNA ineffective as a screening method for PCBs in water without some type of chemical separation. The usefulness of ITNA for screening soils and sediments for organochlorine is limited by the intense induced activity in aluminum, a major element in these materials. The use of longer periods prior to counting would reduce this interference and might prove effective for the identification of highly contaminated materials. Potential organochlorine contaminants are more effectively removed by organic solvent extraction, followed by ITNA screening of the extract.

The actual presence of PCBs must be determined with a more definitive method such as GC/ECD analysis. The GC/ECD method is very accurate (routinely ~10%) with detection limits of 10 ppb. However, the analysis is time-consuming, typically 35 min/run in addition to sample preparation. Using the ITNA data to determine dilution requirements can greatly decrease the time involved in this analysis. Trained personnel are required to run GC/ECD and experience in matching PCB standards to the sample matrix is needed. As a result, GC/ECD analysis can be moderately expensive.

ACKNOWLEDGMENT

We thank Roger Ferenbaugh for his assistance in locating regulations, the staff of the Omega West Reactor for their assistance with the neutron irradiations, Barbara Hemberger and David Dogruel for their assistance with the sample preparation and GC/ECD measurements, and Pete Del Mar for his referee analyses on Chem Service PCB chemicals.

LITERATURE CITED

(1) Alford-Stevens, A. L. *Environ. Sci. Technol.* **1986**, *20*, 1194.
(2) Erickson, M. D. *Analytical Chemistry of PCBs*; Butterworth Publishers: Boston, MA, 1986; pp 259–264.
(3) *Test Methods for Evaluating Solid Waste*, *SW-846*, 3rd ed.; U.S. Environmental Protection Agency, U.S. Government Printing Office: Washington, DC, 1986; Vol.1, Method 9022.
(4) Product insert Sheet, Clor-N-Oil 50 PCB Screening Kit; Dexsil Corp.: Hamden, CT.
(5) Gladney, E. S.; Curtis, D. B.; Perrin, D. R.; Owens, J. W.; Goode, W. E. "Nuclear Techniques for the Chemical Analysis of Environmental Materials"; Los Alamos Scientific Laboratory Report LA-8192-MS; Los Alamos Scientific Laboratory: Los Alamos, NM, 1980.
(6) Gautier, M. A., Gladney, E. S., Eds. "Health and Environmental Chemistry: Analytical Techniques, Data Management, and Quality Assurance"; Los Alamos National Laboratory Report LA-10300-M; Los Alamos National Laboratory: Los Alamos, NM, 1986.
(7) Hutzinger, O.; Safe, S.; Zitko, V. *The Chemistry of PCBs*; CRC Press: Boca Raton, FL, 1974.
(8) Fisher, D. J.; Rouse, T. O. "Field Determination of PCB is Transformer Oil, Volume 2: Clor-N-Oil PCB Screening Test"; Electric Power Research Institute, Report EL-3766, Vol. 2, 1984.
(9) Bertram, F. J. "A Study of Clor-N-Oil 50 PCB Screening Kits on Waste Oil Samples"; Goodyear Atomic Corporation Report GAT-T-3372, 1985.
(10) Minor, M. M.; Hensley, W. K.; Denton, M. M.; Garcia, S. R. *J. Radioanal. Chem.* **1982**, *70*, 459.
(11) Attas, M.; Chen, J. D.; Hildebrandt, E. A. *J. Radioanal. Chem.* **1987**, *109*, 55.

RECEIVED for review June 12, 1989. Accepted September 12, 1989. This work was performed under the auspices of the U.S. Department of Energy.

CORRESPONDENCE

Assessing Heterogeneity of the High-Mannose Glycopeptide gp432 on the Variant Surface Glycoprotein of Trypanosomes: A Comparison of Plasma Desorption Mass Spectrometry and Radiolabeling Techniques

Sir: African trypanosomes are parasitic protozoa that have evolved an effective mechanism for protection against the immune system of their mammalian hosts known as *antigenic variation*. The essential molecule for this process is the *variant surface glycoprotein* (VSG), a polypeptide of around 500 amino acids that is roughly 10% carbohydrate by weight. The VSG of the IlTat 1.3 variant of *Trypanosoma brucei* has two asparagine-linked glycan moieties, as well as a glycosylphosphatidylinositol membrane anchor (*1*). The complete structure of the glycosylphosphatidylinositol anchor has been

0003-2700/89/0361-2686$01.50/0 © 1989 American Chemical Society

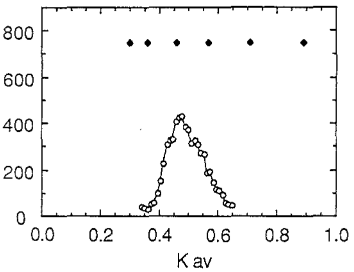

Figure 1. Fractionation of free oligosaccharide from EndoH-treated gp432 obtained from [^{3}H]mannose-labeled VSG. Elution positions (◆) of GlcNAc$_{1-6}$ standards. Adapted with permission from ref 3.

reported recently by Ferguson et al. (*2*). The two N-linked sites of this protein contain markedly different types of oligosaccharides. Those at Asn-419 are almost exclusively complex biantennary, while those at Asn-432 are high-mannose species. In previous studies (*1*), carbohydrate analysis of the tryptic glycopeptide gp432 (which contains the latter site) indicated 2.1 mol of GlcNAc and 6.2 mol of mannose per mole of peptide. [^{3}H]Mannose-labeled gp432 was then isolated from metabolically labeled trypanosomes, the oligosaccharides were released by endo-β-*N*-acetylglucosaminidase H (EndoH) treatment, and size fractionation indicated 4–7 mannosyl residues per molecule.

Plasma desorption mass spectrometry (PDMS), developed by Macfarlane and Torgerson (*3*), has been used previously in our laboratory to determine the structures of tryptic glycopeptides of bovine fetuin (*4*) and the carbohydrate heterogeneity of glycosylated ovomucoids (*5, 6*). We thus perceived an opportunity to determine the mannose heterogeneity of gp432 directly, using a technique that would not involve in vivo labeling and cleavage of the oligosaccharide from the glycopeptide.

EXPERIMENTAL SECTION

The purification of VSG and preparation of the glycopeptide, gp432, have been described in detail previously (*1*). In brief, homogeneous VSG was digested with trypsin/chymotrypsin, and the gp432 was initially purified on a preparative C_{18} column, with elution by a CH_3CN gradient. It was then further purified by lectin affinity chromatography. Amino acid and carbohydrate analysis resulted in the following molar concentrations: Asx (1.1), Glx (1.3), Lys (0.8), Phe (0.7), Thr (1.0), GlcNAc (2.1), and Man (6.2) (*1*). The gp432 sequence, based upon a previously published cDNA sequence (*7*), is Phe-Asn-Glu-Thr-Lys.

For size evaluation, the gp432 oligosaccharide was labeled in vivo and then released from peptide by EndoH, an enzyme that cleaves between the two GlcNAc residues of certain N-linked oligosaccharides (*1*). The resulting material was analyzed by P4 gel filtration and comparison with GlcNAc$_n$ standards.

Plasma desorption mass spectral measurements of purified and nonradiolabeled gp432 glycopeptide from 59-kDa VSG were carried out on a BIO-ION Nordic (Uppsala, Sweden) Model BIN-10K time-of-flight mass spectrometer. Samples were dissolved in a solution of acetic acid/glutathione at an approximate concentration of 1 mol/L, and the solution was electrosprayed onto an aluminized Mylar sample foil. The secondary ion count was then accumulated for a preset primary ion count of 7×10^6 counts.

RESULTS AND DISCUSSION

Results of the size fractionation of the free oligosaccharide from EndoH-treated gp432 from [^{3}H]mannose-labeled VSG are shown in Figure 1. The elution positions of GlcNAc$_{1-6}$ standards are also included in the figure, from which it was estimated that the oligosaccharides on Asn-432 from mature VSG are Man$_{4-7}$GlcNAc moieties (*1*).

Table I

species	monoisotopic mass	av mass
Phe-Asn(GlcNAc$_2$Man$_4$)-Glu-Thr-Lys	1692.68	1693.80
Phe-Asn(GlcNAc$_2$Man$_5$)-Glu-Thr-Lys	1854.73	1855.96
Phe-Asn(GlcNAc$_2$Man$_6$)-Glu-Thr-Lys	2016.78	2018.12
Phe-Asn(GlcNAc$_2$Man$_7$)-Glu-Thr-Lys	2178.84	2180.27
Phe-Asn(GlcNAc$_2$Man$_8$)-Glu-Thr-Lys	2340.89	2342.43
Phe-Asn(GlcNAc$_2$Man$_9$)-Glu-Thr-Lys	2502.94	2504.59

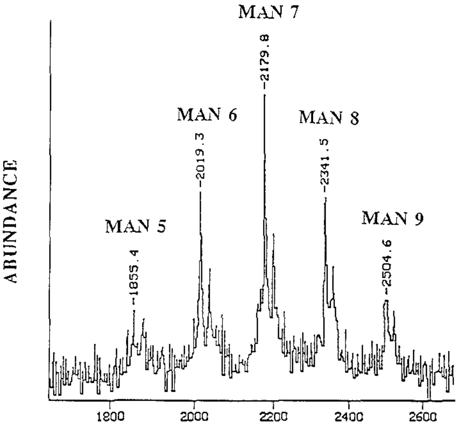

Figure 2. Positive ion plasma desorption mass spectrum of the intact, nonradiolabeled gp432 glycopeptide from the 59-kDa VSG obtained from *T. brucei*.

The general structure of the gp432 glycopeptide from the VSG of the IITat 1.3 variant of *T. brucei* is

Phe-Asn(GlcNAc-GlcNAc-Man$_n$)-Glu-Thr-Lys

Plasma desorption mass spectrometry provides a means for determining the molecular weights of peptides, glycopeptides, and other large, nonvolatile molecules by recording their protonated (MH$^+$) or cationized (M + Na$^+$) ions. Thus, the MH$^+$ ions for gp432 containing from 4 to 9 mannose residues can be calculated (Table I). Figure 2 shows the positive ion, plasma desorption mass spectrum of the intact, nonradiolabeled gp432 glycopeptide. The size and heterogeneity is clearly revealed, and the ions correspond to structures containing from 5 to 9 mannose units. In general, masses of the ions measured by this technique lie between the predicted monoisotopic and average masses for MH$^+$ ions, reflecting the fact that the unresolved isotopic distributions (due to ^{13}C, ^{2}H, etc.) are not symmetrical at this mass (*8*). For each of the oligomers, a lower intensity M + Na$^+$ ion is also observed, 22 amu higher than the MH$^+$ ion.

CONCLUSIONS

The determination of the size (and hence the number of mannose residues) of the oligosaccharide attached to Asn-432 is quite obviously different for the radiolabeling (4–7 mannose) and the plasma desorption (5–9 mannose) techniques. It should be noted, however, that the gp432 glycopeptide used for the plasma desorption measurement was purified from the VSG of trypanosomes obtained directly from the bloodstream of the rat. For the size fractionation measurement, the gp432 was obtained from trypanosomes cultured in a low-glucose medium for 1 h with [^{3}H]mannose prior to purification of the VSG (*3*). The gel filtration data is based on the analysis of radioactivity, rather than mass. Therefore, these data reflect oligosaccharides synthesized only during the culture period. This population may differ from the bulk VSG due to altered metabolic conditions.

The PDMS technique has several distinct advantages for the structural analysis of oligosaccharides. First, it provides a direct measurement of molecular weights. By contrast, gel filtration is based on comparison with standards. Second, the PDMS technique unambiguously reveals oligosaccharide microheterogeneity. While the size fractionation of free oligosaccharides shows a definite distribution, it cannot separate the oligomers. In contrast, plasma desorption produces several peaks spaced 162 mass units apart. In addition, plasma desorption provides a direct measurement that obviates the need for radiolabeling and processing by EndoH prior to analysis. Thus, it would appear that plasma desorption mass spectral measurements offer a distinct advantage for measurements of this kind.

LITERATURE CITED

(1) Bangs, J. D.; Doering, T. L.; Englund, P. T.; Hart, G. W. *J. Biol. Chem.* **1988**, *263*, 17697–17705.
(2) Ferguson, M. A. J.; Homans, S. W.; Dwek, R. A.; Rademacher, T. W. *Science* **1988**, *239*, 743–759.
(3) Macfarlane, R. D.; Torgerson, D. F. *Science* **1976**, *191*, 920.
(4) Townsend, R. R.; Alai, M.; Hardy, M. R.; Fenselau, C. *Anal. Biochem.* **1988**, *171*, 180.
(5) Wang, R.; Cotter, R. J.; Lin, T.-Y.; Laskowski, M. *Rapid Commun. Mass. Spectrom.* **1988**, 71–73.
(6) Cotter, R. J. *Anal. Chem.* **1988**, *60*, 781A–790A.
(7) Rice-Ficht, A. C.; Chen, K. K.; Donelson, J. E. *Nature* **1981**, *294*, 53–57.
(8) Yergey, J.; Heller, D.; Hansen, G.; Cotter, R. J.; Fenselau, C. *Anal. Chem.* **1983**, *55*, 353.

[1] Department of Pharmacology and Molecular Sciences.
[2] Department of Biological Chemistry.
[3] Current address: Smith Kline & French Laboratories, Department of Physical and Structural Chemistry, King of Prussia, PA 19406.
[4] Current address: Department of Microbiology and Immunology, Stanford University School of Medicine, Fairchild Bldg., Stanford, CA 94305.
[5] Current address: Department of Chemistry, University of Maryland Baltimore County, Baltimore, MD 21228.

Mark F. Bean[1,3]
James D. Bangs[2,4]
Tamara L. Doering[2]
Paul T. Englund[2]
Gerald W. Hart[2]
Catherine Fenselau[1,5]
Robert J. Cotter*[,1]

Department of Pharmacology and Molecular Sciences
and Department of Biological Chemistry
Johns Hopkins University School of Medicine
Baltimore, Maryland 21205

RECEIVED for review July 17, 1989. Accepted September 27, 1989. This work was supported by grants to P.T.E. and G.W.H. from the National Institutes of Health (AI 21334) and from the MacArthur Foundation, and to R.J.C. from the National Science Foundation (BBS 85-15390). T.L.D. was supported by a Medical Scientist Training Grant (5T32GM07309). M.F.B. and C.C.F. were supported by the National Science Foundation (DCB 85-09638). Mass spectral analyses were carried out at the Middle Atlantic Mass Spectrometry Laboratory, an NSF Shared Instrumentation Facility.

CORRECTION

Effect of Apolar Diluents on the Behavior of Chiral Stationary Phases in Gas Chromatography. Binary Mixtures of *N*-Lauroyl-L-valine-*tert*-butylamide with Squalane and *n*-Tetracosane

Katsunori Watabe, Emanuel Gil-Av, Toshiyuki Hobo, and Shigetaka Suzuki (*Anal. Chem.* **1989**, *61*, 126–132).

Equation 2 on p 127 should read

$$V_{\mathrm{mix}}^{x} = V_{\mathrm{g}}^{\mathrm{a}}(1 - x) + V_{\mathrm{g}}^{\mathrm{c}}(x)$$

Also, on page 131, the sentence in the second paragraph under the heading Relevance of the Results to Polymeric Phases should read as follows: ..., when an average of about six dimethylsiloxane units separated two selector groups (*20*).

When you're confronted with a specific "need to know"...

Analytical CHEMISTRY

Every chemist knows, having the most up to date information is essential for success. And, in the vital field of measurement science, ANALYTICAL CHEMISTRY is the one publication you cannot do without. For over sixty years, ANALYTICAL CHEMISTRY has proven to be a useful problem-solving resource, no matter what your specialty. And now, it covers methods used in the biotechnology field.

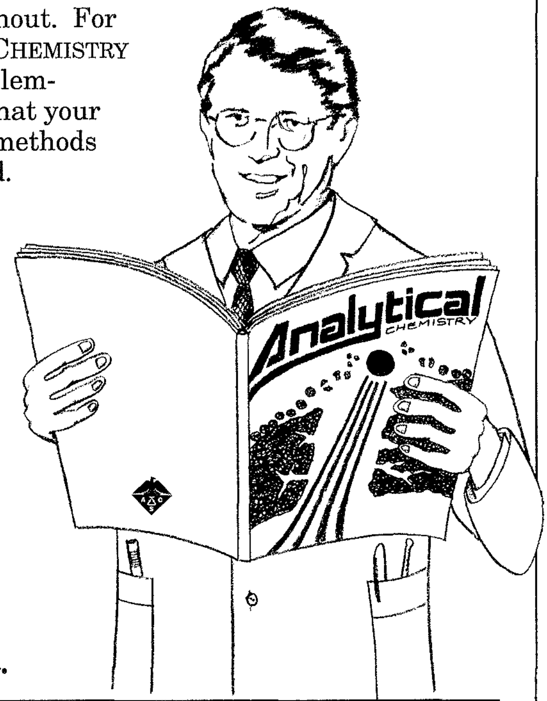

Publishing information that will help you deal more skillfully with problems such as sampling, data analysis and methodology— the papers in today's twice monthly ANALYTICAL CHEMISTRY cover real world problems involving trace analysis of air, water, soil, materials, drugs, and biopolymers.

Call now and reserve your own personal subscription.

Volume 61 (1989)	U.S.	Canada and Mexico	Europe Air-Service Included	All Other Countries Air-Service Included
ACS Member - 1 year	$ 27	$ 56	$ 83	$120
2 years	$ 45	$103	$157	$231
Nonmember	$ 49	$ 78	$155	$192

Member rates are for personal use only. Subscriptions may start any month of the year and expire one year later. Foreign payment must be made in U.S. currency by international money order, UNESCO coupons, or U.S. bank draft, or order through your subscription agency. For nonmember rates in Japan, contact Maruzen Co., Ltd. This publication is available on microfilm, microfiche, and the full text is available online on STN International.

Call Toll-Free
1-800/227-5558
for credit card orders
or write:
American Chemical Society
Marketing Communication Dept.
1155 Sixteenth Street N.W.
Washington D.C. 20036

Determine Hydrogen in Refractory Metals Efficiently with the *LECO*® RH-404 Hydrogen Determinator

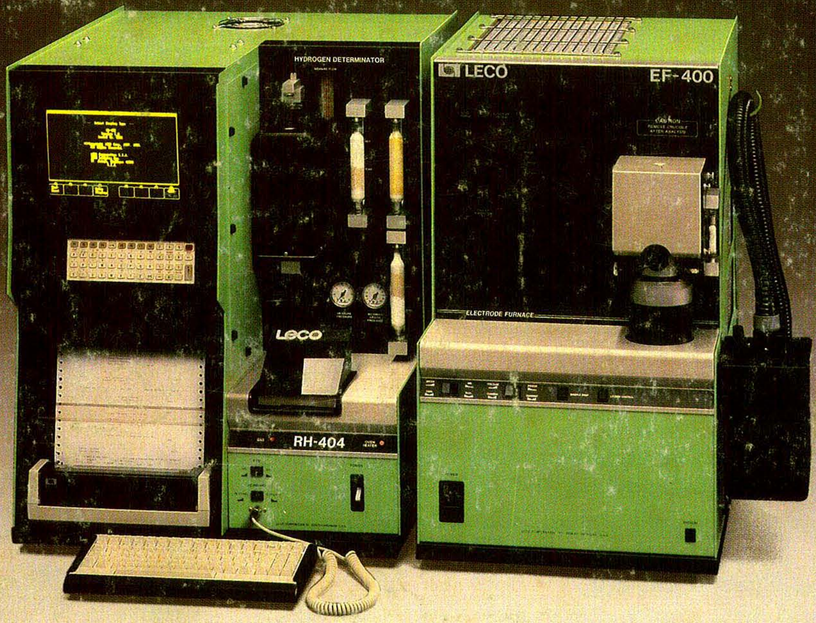

- **Range: 0.3 to 250 ppm**
- **1 gram nominal sample size**
- **Furnace Temperatures to 3000°C**

The LECO® RH-404 Hydrogen Determinator provides today's analyst with the accuracy (±0.05 ppm) and sensitivity (±0.01 ppm) of a thermal conductivity detection system combined with the operational ease of menu-driven software. The powerful 6.5 kw electrode impulse furnace permits complete fusion of refractory metals. For a nominal 1 gram sample, hydrogen contents from 0.3 to 250 ppm are determined within 3 minutes.

LECO® Corporation 3000 Lakeview Avenue
St. Joseph, MI 49085-2396 U.S.A. Phone: (616) 983-5531

leco®

CIRCLE 90 ON READER SERVICE CARD

1380